Studies on Development of Bio-based Biodegradable Polymers and Their Efficacy as Biomaterials

Thesis Submitted in Partial Fulfilment of the Requirements

for the Degree of

DOCTOR OF PHILOSOPHY

By

Chethana M

DEPARTMENT OF CHEMICAL ENGINEERING

INDIAN INSTITUTE OF TECHNOLOGY GUWAHATI

October 2022

Dedicated to

My Beloved Parents

Department of Chemical Engineering

Indian Institute of Technology Guwahati

CERTIFICATE

This is to certify that the research work in the thesis entitled **"Studies on Development of Bio-based Biodegradable Polymers and Their Efficacy as Biomaterials"** is carried out by me at the Department of Chemical Engineering, Indian Institute of Technology Guwahati, under the supervision of Prof. Vimal Katiyar and Dr. Amit Kumar. The results documented in this thesis are achieved by me and have not been submitted to any other University or Institute for the award of any degree or diploma.

Chethana M
Roll no.: 166107103
Department of Chemical Engineering
Indian Institute of Technology Guwahati
Guwahati -781 039, India.

Department of Chemical Engineering
Indian Institute of Technology Guwahati

CERTIFICATE

This is to certify that the thesis entitled **"Studies on Development of Bio-based Biodegradable Polymers and Their Efficacy as Biomaterials"**, is being submitted by **Chethana M** for the award of Ph.D. The research work has been carried out by her at the Department of Chemical Engineering, Indian Institute of Technology Guwahati, under our guidance and supervision. The work documented in this thesis has not been submitted to any other University or Institute for the award of any degree or diploma.

Dr. Vimal Katiyar
Professor
Department of Chemical Engineering
Indian Institute of Technology Guwahati
Guwahati-781 039, India

Dr. Amit Kumar
Associate Professor
Department of Chemical Engineering
Indian Institute of Technology Guwahati
Guwahati-781 039, India

Acknowledgement

I sincerely express my deepest sense of gratitude to my learned mentor and thesis supervisors Prof. Vimal Katiyar and Dr. Amit Kumar for their valuable guidance and advice throughout my research period. Their true scientific spirit, encouragement, and self-reliance have helped me immensely to develop the quality of my research work. I am extremely fortunate to be involved in challenging research work supported by them. It has enriched my life. This work initiated many new thoughts and ideas which enhanced my scientific temperament. I experienced a feeling of self-satisfaction after the completion of my work and without their continual guidance, this would not have materialized. I shall remain grateful to them forever.

I would also like to thank my doctoral committee members Prof. Mihir Kumar Purkait, Prof. Ramgopal V S Uppaluri, and Prof. Senthil Kumar Sivaprakasam for their valuable suggestions, comments, encouragement, and valuable criticism during the assessments of my Ph.D. program. I would like to thank the Centre of Excellence for Sustainable Polymers (CoE-SusPol), the Centre for Sustainable Polymers, Central Instruments Facility (CIF), and IIT Guwahati for research and analytical facilities. I would also like to thank the head and all the authorities of the Department of Chemical Engineering for providing me with all research and analytical facilities required for my work. I am extremely thankful to the technical and non-technical staff of the Department of Chemical Engineering for their help and assistance in the successful completion of my work.

I express my sincere thanks to Prof. Shinichi Sakurai, Prof. Sono Sasaki, and Prof. Yuji Aso of the department of Biobased Material Science, Kyoto Institute of Technology, Japan for providing the opportunity to work in their laboratories. I am also thankful to Ms. Sano for her help during my stay at KIT Japan.

I owe my sincere gratitude to Dr. Akhilesh Kumar Pal, Dr. Surendra Singh Gaur, Dr. Rahul Patwa, Dr. Prodyut Dhar, Dr. Gourhari Chakraborty, Dr. Monika, Dr. Narendren S, Dr. Shasanka Sekhar Borkotoky, Dr. Melakuu Tesfaye, Dr. Siddhartha Mohan Bhasney, Dr. Naba Kumar Kalita, Dr. Neha Mulchandani, Dr. Kiran Kumar Gali, Dr. Prasanna, Pankaj, Arjun Sankla, Doli, Munmi, Kona, Bhanupriya and the members of CoE-SusPol for helping me in every way they could and for making my stay more delightful along with their moral support in the laboratory. Finally, I would like to convey my sincere gratitude to my parents for their unconditional love and encouragement and their countless sacrifices, which have made it possible for me to reach this stage in my life. In the end, I owe it all to the Almighty for being all in all and enabling me to the completion of the doctoral work. Blessings of the Almighty are always solicited.

Chethana M

ABSTRACT

Exhaustion of non-renewable resources and increasing concern towards the non-biodegradability of conventional polymers demands research for alternative, bio-based and biodegradable polymers having comparable properties. Recently, research in the field of sustainable polymers is highly focused on the use of renewable wastes generated from agriculture, food, and the meat industry for the development of biodegradable biomaterials. The biomaterials prepared from these renewable wastes find their applications in the field of medicine and help to restore biological functions. Polyhydroxybutyrate (PHB) is a biodegradable biomaterial of bacterial origin produced intracellularly as an energy reserve in a stress-induced condition which has a potential application in drug delivery. Poly(latic acid) (PLA) is another class of bio-based polymer produced by the polymerization of lactide predominantly used in biomedical applications and packaging. Prodigiosin is a bacterial pigment used as a remedy for cancer treatment, and nanocellulose is a bionanomaterial suitable for high-performance applications. In this perspective, the current study extensively deals with the utilization of waste sorghum stalks consisting of fermentable sugars, cellulose, and hemicellulose for the production of biomaterials such as PHB and nanocellulose. Prodigiosin is produced from *Serratia nematodiphila* isolated from river water, and metal-free PLA is synthesized using prodigiosin as a metal-free catalyst.

Over the assessment, the juice from agricultural waste sorghum stalks consisting of ~60 g/L of fermentable sugar is used as an inexpensive carbon source for the production of PHB. The minimal media supplemented with sorghum juice is used for the optimization and production of PHB. The optimized conditions yielded the maximum productivity of ~8.2 g/L of PHB within 24 h of cultivation. The fed-batch operation with dO_2 controlled strategy maximized the productivity four-folds in comparison to the batch operation. It was able to obtain PHB with a

molecular weight of ~400 KDa and recovery of ~94% using solvent extraction. The characterization of the produced PHB exhibited improved crystallization temperature (T_c) from 101 to 105 °C, glass transition temperature (T_g) from -8 to -10 °C, melting temperature (T_m) from 162 to 175 °C, maximum degradation temperature (T_{max}) of 318 °C, and wettability from 79 to 93 °C which are comparable to commercial PHB. Based on this assessment, the produced PHB is utilized for the preparation of microspheres using the solvent evaporation method. The morphology and size of the microsphere could be tuned from 7-300 µm by varying the stirring speed. To check its efficacy as an embolizing agent for minimally invasive treatments, a low-cost 3D printed PLA-based hepatic phantom costing 221 INR was developed and evaluated for its suitability as an *in vitro* model for simulating the right hepatic artery. Further, the unique setup has been developed to mimic the systolic and diastolic blood pressures with a flow rate ranging from 60 to 120 mL/min. The inline microscopic setup helps in the tracking of the flow of the microsphere inside the channels and at the junctions. The study also confirmed the embolization effect for the 0.9 mm channel based on the microsphere size.

Another objective of this thesis is focused on the production of organic small-molecule prodigiosin (PG). A detailed study on the production of prodigiosin revealed a maximum yield of ~0.37 ± 0.04 g/g of cell biomass at optimum conditions with a molecular mass of (m/z) 323.6 Da, and a characteristic absorption wavelength λ_{max} of 535 nm. Further, the antibacterial test conducted with prodigiosin against *Staphylococcus aureus* confirmed its antibacterial ability. The produced prodigiosin is also utilized as an organocatalyst for ring-opening polymerization (ROP) of L-lactide to produce a metal-free PLA of molecular weight of ~5000 Da. This range of molecular weight is more suitable for drug delivery applications. However, commercial PLA is susceptible for bacterial adhesion which in turn leads to infections. This remains an obstacle in implementing PLA-based implants. To tackle this issue, prodigiosin incorporated PLA has been developed, which possesses an improved hydrophobicity with a contact angle of

111±1.5°. The degradation temperature of the prodigiosin is 215 °C, which is more than the melting temperature of PLA supports the processability and sterilization of the PLA-based implants without any toxic gases. Further, the prodigiosin improved the transparency of the PLA and acted as a nucleation site. The *in vitro* study on biofilm formation shows excellent inhibition activity against implant-associated pathogens such as *Klebsiella aerogenes* and *Staphylococcus aureus*. On the other hand, leftover sorghum bagasse after extraction of juice is utilized for the fabrication of nanocellulose using alkaline hydroxide peroxide treatment. The current method utilized the high-pressure treatment at 15 lb and it could remove ~97% of the lignin. Further, the obtained cellulose was hydrolyzed with sulfuric acid at different time intervals to produce the nanocellulose of 33 ± 4 nm to 560 ± 126 nm in size. This process also yielded ~50 g/L of xylose and 7 g/L of glucose, indicating the breakdown of hemicellulose as well as cellulose, respectively.

The cytotoxicity test performed on baby hamster kidney fibroblast cells (BHK-21) confirmed the non-toxicity of all the developed biomaterials. Overall the developed materials such as PHB, PLA, and prodigiosin successfully demonstrated their ability as potential drug carriers, organic catalysts, biocompatible materials, antibiofilm-forming agents, and embolizing agents for hepatic cancers.

Table of Content

List of Figures

List of Tables

Abbreviations

[L]/[PG]	[Lactide]/[Prodigiosin]
^{13}C NMR	Carbon nuclear magnetic resonance
^{1}H NMR	Proton nuclear magnetic resonance
3D	3-dimensional
3D-HVFM	3D printed hepatic vascular flow model
AHL	Acyl homoserine lactone
AHP	Alkaline hydrogen peroxide
AK	Amikacin
BHK-21	Baby hamster kidney fibroblast cells
Bio-PA	Bio-polyamide
Bio-PE	Bio-based polyethylene
Bio-PET	Bio-polyethylene terephthalate
BnOH	Benzyl alcohol
C	Chloramphenicol
CAD	Computer-aided design
CCD	Central composite design
CDW	Cell dry weight
CEP	Cephalothin
CFU	Colony forming unit
DCM	Dichloromethane
DHB	2,5-dihydroxybenzoic acid
DMAP	4-dimethylaminopyridine
DMEM	Dulbecco's modified Eagle's medium
DO_2	Dissolved oxygen
DRDO	Defense Research and Development Organization

DSC	Differential scanning calorimetry
Exo-SAP	Exonuclease I Shrimp Alkaline Phosphatase
FDM	Fused Deposition Modeling
FESEM	Field emission scanning electron microscopy
FESEM-EDX	Field emission scanning electron microscopy-energy dispersive x-ray spectroscopy
FETEM	Field emission transmission electron microscopy
FTIR	Fourier transform infrared spectroscopy
GEN	Gentamicin
GPC	Gel permeation chromatography
HBV	Hepatitis B virus
HCC	Hepatocellular carcinoma
MALDI-TOF-MS	Matrix-assisted laser desorption ionization-time-of-flight mass spectrometry
MAR	Multiple antibiotic resistance
mcl-PHA	Medium chain length PHAs
M_n	Number average molecular weight
MTT	3-(4,5-dimethylthiazol-2-yl)-2,5-diphenyltetrazolium bromide reagent
M_w	Weight average molecular weight
NCBI	National Center for Biotechnology Information
NMR	Nuclear magnetic resonance
nPLA	Neat Poly(lactic acid)
P(HB-co-HV	Poly(beta-hydroxybutyric-co-beta-hydroxyvaleric acid)
P3HB	Poly (3-hydroxybutyrate)
PBAT	Polybutylene adipate terephthalate
PCL	Poly(ε-caprolactone)

PDI	Poly dispersity index
PDP	4-pyrrolidono-pyridine
PE	Polyethylene
PET	Polyethylene terephthalate
PG	Prodigiosin
PGA	Polyglycolide
PHAs	Polyhydroxyalkanoates
PLA	Poly(lactic acid)
PLA-PG-C	Poly(lactic acid)-Prodigiosin-Crude
PLA-PG-P	Poly(lactic acid)-Prodigiosin-Pure
POM	Polarizing optical microscopy
PP	Polypropylene
PVA	Poly(vinyl alcohol)
RHA	Right hepatic artery
ROP	Ring-opening polymerization
ROP	Ring-opening polymerization
rRNA	Ribosomal ribonucleic acid
SBF	Simulated body fluid
SCADA	Supervisory control and data acquisition
scl-PHA	Short-chain length PHAs
TE	Tetracyclin
TGA	Thermogravimetric analysis
TG-FTIR	Thermogravimetric analysis hyphenated with Fourier transform infrared spectroscopy
TMS	Tetramethylsilane
UHPLC	Ultra-high-performance liquid chromatography
USFDA	U.S Food and Drug Administration

UV-Vis	UV-Vis spectroscopy
WHO	World Health Organization
XRD	X-ray diffraction

CHAPTER 1

Introduction and Literature Review

This chapter presents a brief preamble of the fundamentals and terminologies of biomaterials, their origin, and various process involved in the synthesis or fabrication of biomaterials. The emphasis has been made on agricultural waste biomass, polyhydroxybutyrate (PHB), poly(lactic acid) (PLA), prodigiosin, prodigiosin-loaded PLA, nanocellulose, and their properties. The chapter extensively covers the various processes, carbon sources, and microorganisms used for the production of biomaterials. Moving on, the chapter enlightens the industrial production of PHAs. The chapter also covers the current status of biodegradable plastics in India. Further, the objectives of the thesis are summarized, followed by the organization of the thesis.

Publications:

Chethana Mudenur, Tabli Ghosh, and Vimal Katiyar, 2021, Nanodelivery system of bioactive compounds in edible food packaging, Springer Singapore. pp 273-298.

Chethana Mudenur, Prodyut Dhar and Vimal Katiyar, 2020, Nanocellulose: surface modification strategies, cellulose nanocrystals: an emerging nanocellulose for numerous chemical processes, Walter de Gruyter GmbH. pp 81-118.

Chethana Mudenur, Kona Mondal, Urvashi Singh, and Vimal Katiyar, 2019, Production of polyhydroxybutyrate and its potential applications, Advances in sustainable polymers., Springer, pp 131-164

1.1 Introduction

Plastics are used for various purposes due to their light weight, durability, and flexibility, which have become an integral part of daily life. There is a family of hundreds of different polymers with a wide range of properties and applications [1]. These materials are designed to encounter the needs of every single application cost-effectively. The versatility, along with its inexpensiveness, has resulted in high production worldwide, exceeding more than 300 million tons. The single-use plastics are creating more waste in the environment due to their non-recyclability, and more than 50% of such plastics are thrown away into the environment after their use [2]. A considerable amount of plastics is also leaked into the environment as litter, and such single-use products made up of non-degradable plastics constitute a high proportion of the garbage found in the aquatic and terrestrial environments [3]. The accumulation of non-degradable plastics in the aquatic environment has been considered a global issue by the United Nations Environment Assembly [4], leading to the generation of microplastics. A few years ago, microplastics started turning up in the guts of fish and other aquatic animals, which created a huge concern about the use and safety of seafood. In 2019 the research reported on the microplastic contamination in gudgeon fish enlightened that ~9% of the microplastics are common in an investigated group of fish that ingested seven types of plastics. These include the ethylene vinyl acetate copolymer used in the food packaging films, polypropylene, polyethylene terephthalate, polyvinyl chloride used in the water bottles and caps, and cellophane used in the food packaging films, polyvinyl acetate used in the adhesive formulations and coatings [5].

The petrochemical sources used in plastic production are non-renewable and are contributing to the huge leaps of plastic waste in the environment [6]. Non-renewable fossil resources include oil, natural gas, and coal. Their degradation takes thousands of years in the soil conditions. Since the 20th century, the world population has been increasing, and there has been

a huge change in oil supplies. It is time to move forward by promoting more sustainable technologies to save the integrity of the ecosystem.

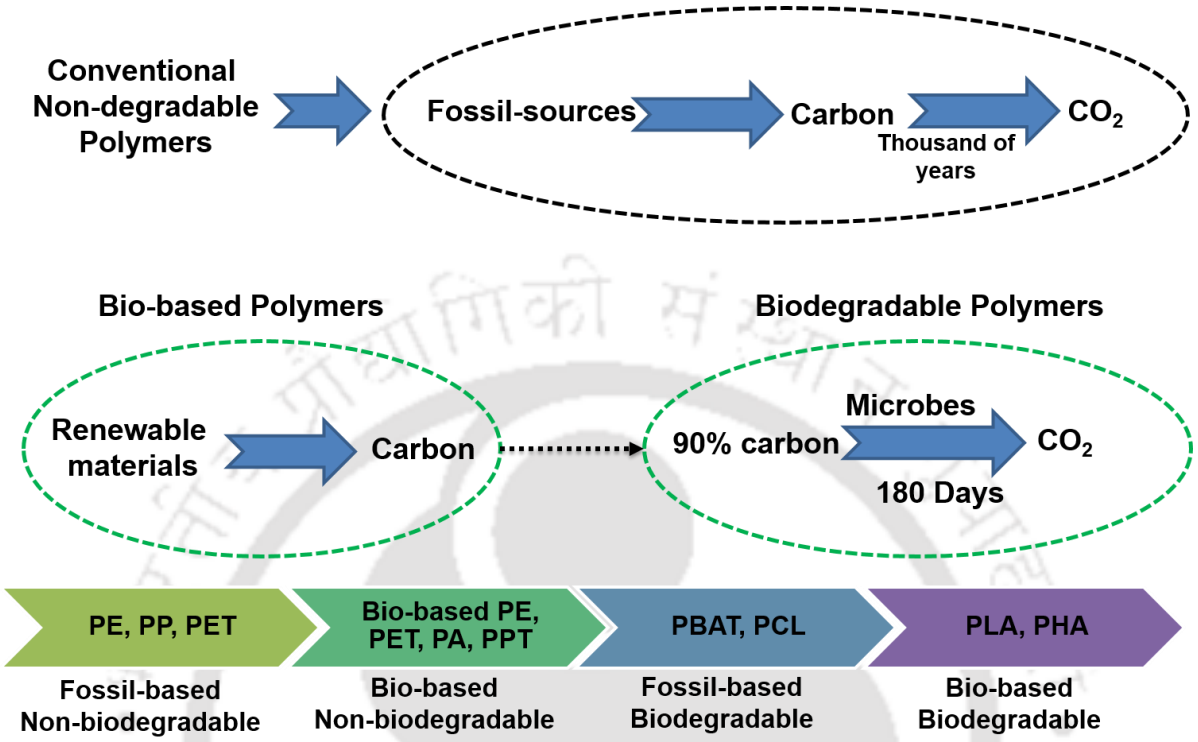

Figure 1.1. Classification of polymers based on the origin and biodegradability.

The polymers are classified based on their origin and biodegradability. Figure 1.1 illustrates the classification of plastics into four categories. The first category includes fossil-based non-biodegradable plastics such as polyethylene (PE), polypropylene (PP), and polyethylene terephthalate (PET). The second category is bio-based non-biodegradable plastics which includes bio-based polyethylene (Bio-PE) polyethylene terephthalate (Bio-PET), polyamide (Bio-PA), and polypropylene terephthalate (Bio-PPT). The third category is the fossil-based biodegradable plastics including polybutylene adipate terephthalate (PBAT) and poly(ε-caprolactone) (PCL). The fourth category involves bio-based biodegradable plastics, which include poly(lactic acid) and polyhydroxyalkanoates (PHAs).

The fourth category, including PHAs and PLA, is seeking more attention due to their biocompatibility and biodegradability properties. These polymers are produced using renewable feedstocks. The PLA is a bio-based polymer produced from lactic acid. Whereas the PHAs are thermoplastic biocompatible polyesters found as intracellular granules in the cytoplasm of the cells. Both polymers are derived from renewable bio-based carbon sources using the different synthetic pathways as shown in Figure 1.2. The process of PHB production and the microorganisms used is discussed further.

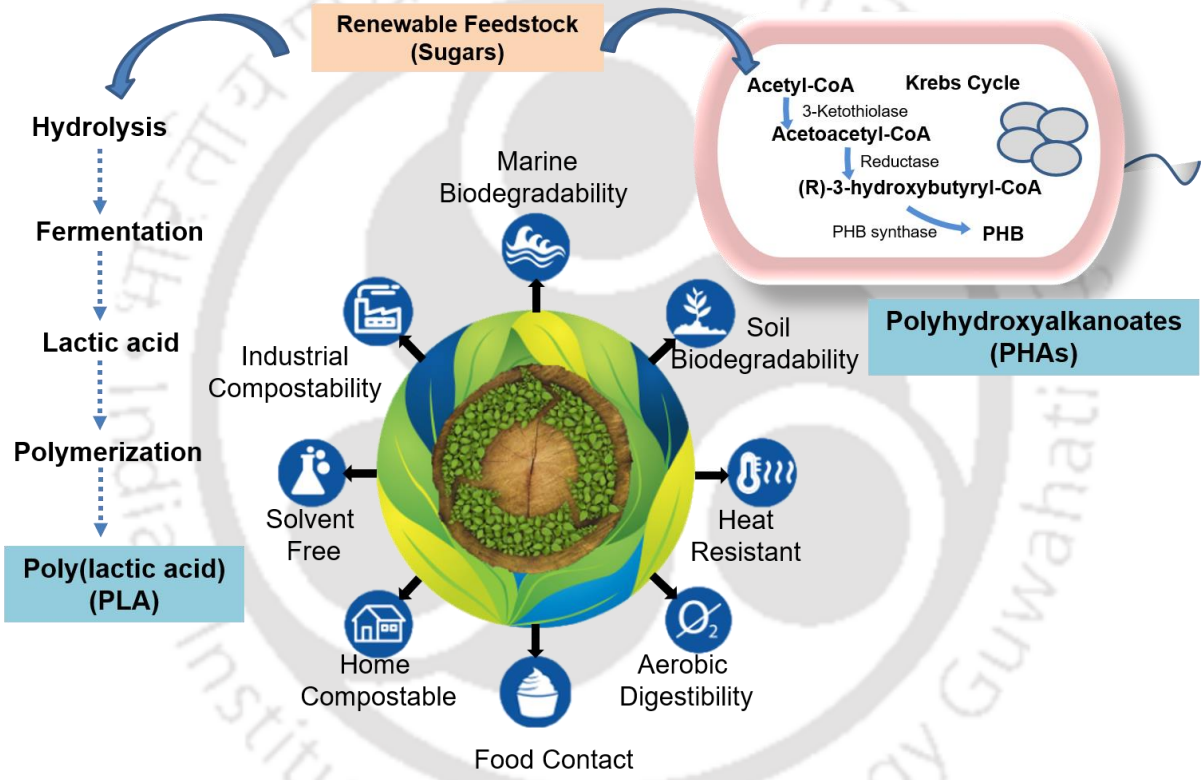

Figure 1.2. The process of PHB and PLA production from renewable feedstocks and their characteristic properties**.**

1.2 Biosynthesis of polyhydroxyalkanoates (PHAs)

The PHAs are promising alternatives to various conventional non-degradable plastics. These are produced by microorganisms and are biocompatible as they do not hamper the biological system [7]. These are synthesized by ~75 bacterial genera in the presence of excess carbon

when other nutrients are limiting. Their molecular mass varies from 50,000 to 1,000,000 Da based on the microbe used [8].

The term PHA describes the class of polyesters synthesized in the form of energy and carbon storage in bacterial cells. PHB is a member of PHA family. The general structure of the PHAs and their types based on the functional group is shown in Figure 1.3. The general formula for homopolyesters is shown in Figure 1.3 (A), where x=1; R=methyl is poly(3-hydroxybutyrate), R=ethyl is poly(3-hydroxyvalerate), R=propyl is poly(3-hydroxyhexanoates), R=pentyl is poly(3-hydroxyoctanoate), R=nonyl is poly(3-hydroxydodecanoate); for x=2; R=hydrogen is poly(4-hydroxybutyrate), R=methyl is poly(3-hydroxyvalerate);for x=3; R=hydrogen is poly(5-hydroxyvalerate), R=methyl is poly(5-hydroxyhexanoates) for x=4; R=hexyl is poly(6-hydroxydodecanoate). Figure 1.3 (B) corresponds to the general formula for copolyesters, where R= $(CH_2)_2$ represents PHBV, R= $(CH_2)_3$ represents PHBH.

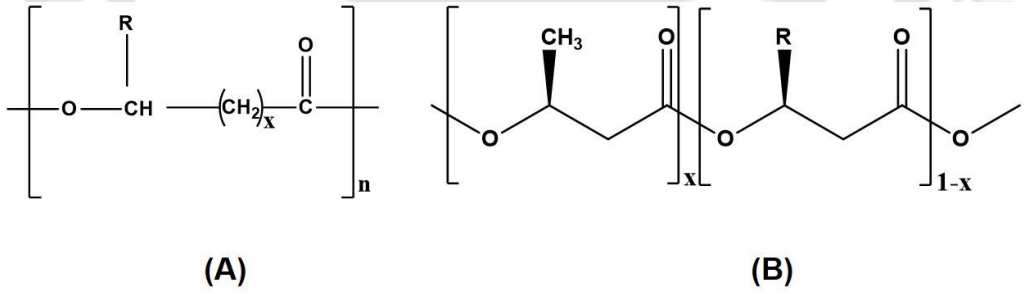

Figure 1.3. The general formula of PHA.

PHAs are further categorized into short chain length and medium chain length based on structures. The classification is mainly based on the number of carbon atoms in the branching polymer chain, which ranges from 3-14 carbon atoms [9]. Short chain lengths consist of 3-5 carbon atoms, while medium chain lengths consist of 6-14 or even more carbon atoms. Examples of short-chain length PHAs (scl-PHA) include poly (3-hydroxybutyrate) (P3HB), poly (4-hydroxybutyrate), and poly (3-hydroxyvalerate). The medium chain length PHAs (mcl-

PHA) include poly (3-hydroxyhexanoate) and poly (3-hydroxyacanoates). The scl-PHAs are stiff, brittle, and highly crystalline, whereas mcl-PHAs are flexible and elastic materials with low crystallinity.

1.3 Microorganisms and carbon sources used for the biosynthesis of PHB

The hydrocarbon degraders belonging to the genera *Pseudomonas, Sphingobacterium, Acinetobacter, Brochothrix, Caulobacter, Burkholderia, Ralstonia,* and *Yokenella* [10] are capable of degrading hydrocarbons to produce PHB. Halophile *Haloferax mediterranei* grows in high salt conditions and produces 65% PHA of its cell dry weight (CDW) using glucose as the carbon source [11]. *H. boliviensis* utilizes starch hydrolysate to produce PHB of ~56% of CDW [12]. Photosynthetic bacteria such as *Synechocystis sp.* and *Synehcystis sp.* accumulate PHB under nitrogen and phosphate-limiting conditions [13]. The overall class of microorganisms used for the economical production of PHAs and their copolymers, such as wild and recombinant strains of *Ralstonia eutropha, Wautersia eutropha* [14], *Azotobacter sp.*[15], *bacillus sp.*[16], *Halomonas sp.*[17],[18], *Haloferax sp.*[19], *Aeromonas sp.*[20], *Methylobacterium sp.*[21], *Thermus thermophillus* [22], *Sacchrophagus degradans* [23], *Chromobacterium sp.*[24], *Recombinant E.coli* [25] etc.

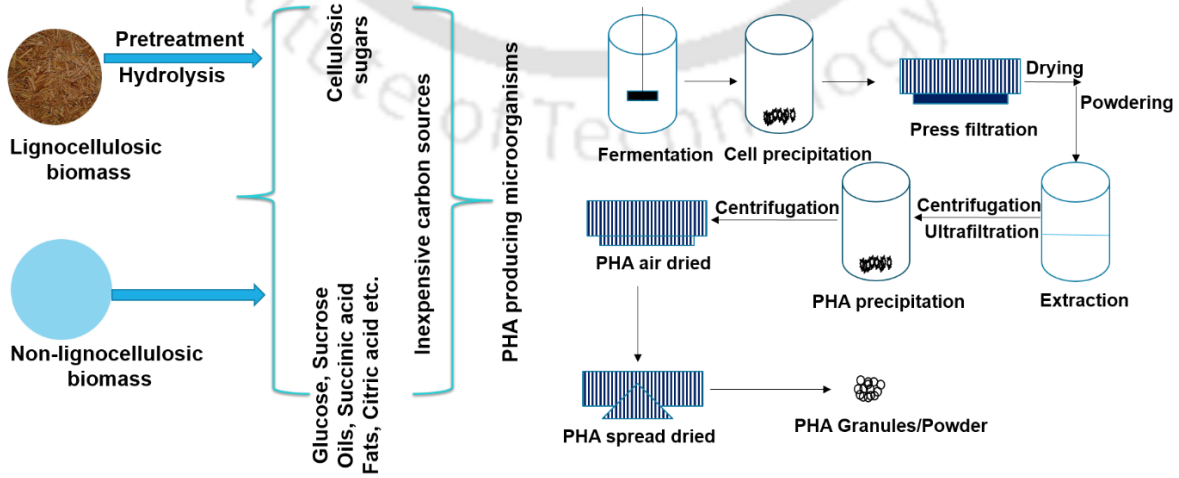

Figure 1.4. The general process of production and extraction of PHB.

The PHAs producers utilize a variety of substrates, including plant oils, D-glucose, camelina seeds, CO_2, sugar beet, sugar cane, sludge, glucose, carob pod, and acetate and the general process of PHB production is shown in Figure 1.4.

1.4 Fermentation strategies used for the production of PHAs

The production of PHAs is carried out using various fermentation strategies. The batch, fed-batch, and continuous operations are prominent in the production of PHB. All the processes are having its advantages and disadvantages for cell growth and product formation.

1.4.1 Batch fermentation

Batch systems are closed systems in which the substrate and the inoculum are added to the fermenter in a batch. This process is the most popular and also a simple process with added advantages such as simple operations, control systems, less cost and, easy to maintain the sterilized conditions, easy to measure the yield [26]. These are also associated with certain disadvantages, which include a slower growth rate because of nutrient depletion with time and less efficient due to the discontinuity in the production process to yield particular products [27], [28]. The batch culture of the *Azotobacter beijerinckii* grown on a glucose media free from ammonia and supply of glucose, oxygen, and molecular nitrogen in limited quantity could yield poly-beta-hydroxybutyrate accumulation of more than 70% at the end of an exponential phase [29]. The batch culture of *Alcaligenes eutropha* can yield 24 g/L of poly-beta-hydroxybutyric acid with ammonia limitation. It can also produce ~17 g/L of poly(beta-hydroxybutyric-co-beta-hydroxyvaleric acid) [P(HB-co-HV)] when there is an addition of propionic acid along with glucose [30].

1.4.2 Fed-batch fermentation

The fed-batch process is more applicable when the concentration of substrate present in the fermentation broth is toxic to microbial growth. To reduce such effects, a substrate is added gradually when it is consumed by the culture. The process is stopped only when the reaction volume reaches 75% of the fermenter volume [31]. But the major drawback associated with this type of process is the increase in the fermentation volume due to the repeated addition of the feeding solution, which further causes the dilution of the fermentation broth [32]. P3HB by *Alcaligenes latus* in the fed-batch fermentation can yield the maximum PHB concentration of more than 4 g/L/h after 16 h of growth with nitrogen limitation [33]. The recombinant *E.coli* was developed by harboring the *Alcaligenes latus* genes responsible for P(3HB-co-3HV) production by utilizing the chemically defined medium with high production yield [34].

1.4.3 Continuous fermentation

It is an open system where the exponential growth rate is maintained in a reactor for a long duration by adding fresh media at regular intervals of time. These are having advantages such as lower installation cost, less fermenter volume, heat exchangers number can be reduced, and lower cost with automation. The disadvantages such as difficulty in evaluating the yield because of the variable volumes and more contamination risks [28]. The nitrogen limitation in the chemostat can yield a very less amount of the poly-beta-hydroxybutyrate, but the oxygen limitation can yield up to 50% of poly-beta-hydroxybutyrate of the dry cell weight, but the carbon limitation yields not more than 3% [29]. In *Alcaligenes eutrophus*, the variation in the carbon and nitrogen ratio yields ~33% (wt/wt) of PHB [30]. The various carbon sources reported in the literature for the production of PHA are tabulated in Table 1.1. The commercially available PHB using various carbon sources and their brand name are mentioned in Table 1.2.

1.5 Characteristics of PHAs

PHAs are thermoplastic in nature and vary in their property depending on the chemical compositions. They are resistant to moisture and possess aroma barrier properties. They are also brittle and stiff, which are insoluble in water and soluble in chloroform, resistant to hydrolytic degradation, have good ultraviolet resistance, poor resistance to acid and bases, comparatively less sticky than traditional polymers, and most importantly they are biocompatible and non-toxic, therefore used in medical industries. Though the characteristics of the PHAs produced by the pure cultures are studied widely, there is less data available for the PHAs produced by the mixed cultures. The homopolymer of PHB has a crystallinity of ~55-80% with low impact strength and high brittleness [35]. These have the glass transition temperature (T_g), melting temperature (T_m), and cold crystallization temperature (T_c) of -1 to 10 °C [36], [37], 175 °C, 63.4 °C, respectively. The elongation to break is ~5% [38]. In contrast, industrial copolymers such as poly (3HB-co-3HV) have better properties such as improved mechanical properties because of the improved toughness, impact strength, and flexibility changes that occurred due to the incorporation of the hydroxyvalerate units in the hydroxybutyrate polymeric chain [39]. Similarly, the crystallinity of the poly(3HB-*co*-3HP) decreases with increasing the fraction of the 3HP units [40]. The weight average molecular weight of the PHAs ranges from 253 to 696 kDa, and they are produced using whey and glycerol, with a polydispersity index (PDI) of 2.2 and 2.7 [37], and the molecular weight can vary up to ~1000 kDa. The crystallinity of scl-PHAs and mcl-PHAs are 40-80% and 20-40% [41].

The mechanical properties of the PHAs are determined by monomer components, chain length, the distance between side groups, and ester linkages [42]. However, P(4HB) is a flexible material with high elongation at break and low Young's modulus of 0.1-0.15GPa than P(3HB). These polymers possess an equal number of carbon atoms. However, their mechanical

properties are completely different. The key difference between them is the position of the methyl group in the polymer backbone. This leads to a change in polymer crystallinity, 3D structure, and mechanical properties of the polymer [43]. Nevertheless, the drawbacks associated with PHB could be overcome by mixing the PHB with other PHA units leading to improved material properties with a reduction in process temperature and brittleness. The most studied copolymer is P(3HB-*co*-3HV), in which the increase in P(3HV) content decreases the melting point as a result of a significant increase in flexibility, a low melting point of ~97 °C could be achieved in the presence of 34 mol% of HV [44]. The increase in HV fraction increases flexibility. The combination of other polymers including 3HHx, and 4HB leads to the copolymer composition with improved properties suitable for packaging applications [45]. Fermentation is an efficient process useful in the production of such homopolymers and copolymers with properties suitable for packaging and other plastic applications.

Table 1.1. Production of polyhydroxyalkanoates using various carbon sources and the respective properties.

Type of PHA	Type of Fermentation/ Reaction time	Microbe used	Feedstock used	Yield (g/L)	Properties	Reference
PHB	Batch	*Bacillus aryabhattai* PKV01	Sweet sorghum	4	T_g:1 °C, Tm: 167 °C	[46]
PHB	Fed-batch/38 h	*Azohydromonas australica*	Sucrose/Ammonium sulfate	22.6	T_g:6 °C	[47]
PHBV	Batch/8 days	*Thauera sp.*	Sludge	1.4	NA	[48]
PHBV	Batch/48 h	*Bacillus sp.*	Glucose	1.6	NA	[49]
PHB	Batch/72 h	*Haloferax mediterranei*	Microalgal biomass/Peptone	2.2	T_d:241 °C, Tm: 150 °C	[50]
PHB	Batch/72 h	*Bacillus megaterium*	Carob pod/Yeast extract	6.6	T_m: 172 °C	[51]
PHB	Electrosynthesis/72 h	*Ralstonia eutropha*	Acetate	0.4	NA	[52]
PHB	Batch and Fed-Batch	*Bacillus megaterium*	Grain sorghum stalk juice	8	**T_g:-8 to -10 °C**, **T_m: 170 °C** **T_c: 87-105 °C**	Current study

Table 1.2. The carbon sources and the microorganisms used for the production of PHAs at a commercial scale.

PHA producers	Microbe used	Feedstock used	Production (MT/Year)	Products	Applications
Danimer Scientific, (Georgia), Nodax™	Soil bacteria	Canola oil, Soybean oil	9000	Dental flosser, barrier coatings, straw	Food & Beverage Personal care, Toys
Kaneka, (Japan), Green Planet™	Soil bacteria	Plant oils	5000	Straw & Bags	Food Packaging
TianAn Biologic Materials Co.Ltd, (China), ENMAT™	*Cupravidus necator*	D-glucose	2000	Films, Fiber & Nonwovens	Packaging & Other
Yield 10 Bioscience, (United States)	N/A	Camelina seeds	50	Resin	N/A
Bio-on (Bologna), MinervPHA™	*Cupravidus necator*	CO_2, sugar beet, sugar cane	10	Nanocapsule	Chemotherapy Biocosmetics

1.6 Applications of PHAs

With these production strategies and the characteristic properties, the subsequent section deals with a detailed description of the applications of the PHAs for various applications.

The property of PHAs that makes them compatible with living cells is their biodegradability. The studies have demonstrated the biodegradation of P(3HB), poly(3-hydroxybutyrate-co-3-hydroxyvalerate) P(3HB-co-3HV), poly(3-hydroxybutyrate-co-3-hydroxyhexanoate) P(3HB-co-3HHx) with the help of lipase and other hydrolytic enzymes. This degradation will form the degradation products such as oligomers of hydroxyl acids [53]. The blend of 60 wt.% PHBHHx with PHB can induce and improve the cell growth and proliferation of chondrocytes [53], [54]. Some studies demonstrated the biodegradable and biocompatible trileaflet heart valve scaffolds using porous PHAs with a pore size of 180-240 μm. The blending of P(3HHx-co-3HO) with Polyglycolide (PGA) can result in non-progressive heart valve regurgitation after implanting the material. Polymer composites can be used that replicates the structure and function of musculoskeletal tissues [55]. PRP-enriched PGA-hyaluronan scaffolds and commercially available Hyaff-11 (hyaluronan-based scaffold by Fida Advanced Biopolymers, Italy), BioSeed-C, a synthetic polymer scaffold made up of fibrin, polyglycolic/PLA and polydioxane (by BioTissue, Switzerland) can be used for the treatment of the chondral defects [56]. PHAs are suitable for soft tissue repair, viscosupplementation, and in augmentation [57]. Poly(4-hydroxybutyrate-co-hydroxyalkanoate) copolymers with a molecular weight of 10-10000 KDa are used for the development of meniscus regeneration devices, cell encapsulation devices, controlled release devices, etc.[58].

Nevertheless, commercialization is still facing difficulty due to the unavailability of huge quantities of raw materials for production scale. Proceeding further, there is a need to explore

inexpensive and waste resources for the production of PHAs, and hence, agricultural wastes are promising alternatives due to their availability and no cost.

1.7 Agricultural waste and its utilization

India is known for its agro-based economy, with more than 70% of the population still dependent primarily on agriculture for their livelihood. However, agriculture generates a huge amount of waste; part of it is used as fodder, and the rest is burnt. This lead to the emission of greenhouse gases into the environment. The current scenario associated with plastic waste generation and agro-waste is a major concern, and suitable alternatives are needed to solve such global issues [59]. India alone generates 500 million tons/year of agricultural waste, out of which 360 million tons are used for fodder and the rest 140 million tons are burnt [60], leading to the emission of toxic greenhouse gases such as CO_2, CO, NH_3, NOX, SOX, VOCs. Sorghum (Figure 1.5) is an energy crop produced in 107 countries [61][62]; the gross production is shown in Figure 1.6, in which the USA, Nigeria, and India are the major producers contributing to the gross production value of 38%, 40%, and 22%. The United States is the leading exporter of sorghum, contributing to ~75% of the trade worldwide. Besides food, sorghum is also used for animal feed and ethanol production. In India, the major producers are Karnataka (KA), Maharashtra (MH), Andhra Pradesh (AP), Gujarat (GJ), Madhya Pradesh (MP), and Rajasthan (RJ).

This crop yields 10-25% of sugars based on the breeds [63], with 1/3rd of the water required to grow corn and sugarcane. The competitive sugar content and the presence of cellulose and hemicellulose make sorghum waste an ideal candidate for producing bio-based and biodegradable polymers. Sorghum is a bioenergy crop and helps to mitigate greenhouse gas emissions to the environment.

Figure 1.5. (A) The crop sorghum with grain and stalks and (B) Heap of agricultural waste after crop harvest.

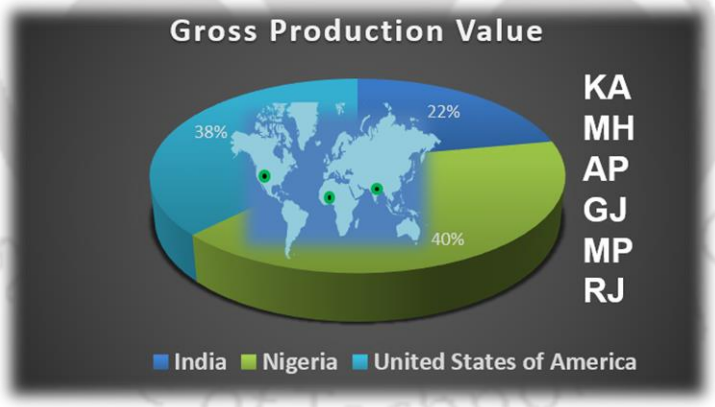

Figure 1.6. Gross production value of sorghum production in major sorghum producers.

1.8 Poly(lactic acid) and its applications

PLA is another class of bio-based polymer that exhibits excellent properties compared to fossil-based polymers. It is a bio-based aliphatic polymer produced by the condensation polymerization of lactic acid [64] and the ring-opening polymerization (ROP) of cyclic lactide [65]. These lactone-based polymers polymerize on heating in the presence of catalysts or initiators. A wide range of metallic and organometallic catalysts are explored to date for the ROP of lactide and are tabulated in Table 1.3. These catalysts are alkoxides, oxides, carboxylates, tin, zinc, aluminum, etc. Tin(II) 2-ethyl hexanoate is the most widely used catalyst in the ROP of lactide. Despite its high activity, removing a tin component from the produced product is practically impossible, which leads to toxic end products [66]. This is the foremost concern that limits its applications in the field of medicine and implant fixation devices. Therefore, there is a need to develop environment-friendly processes and products to tackle such challenging issues. There are some inves

Furthermore, the commercially available PLA used in the production of internal fixation devices is prone to bacterial attack [67] and biofilm formation, which accounts for a greater portion of hospital-acquired infections. These infections are caused by various opportunistic pathogens, depending on the implant site, material composition, and properties. The main reason behind the infection is the surface interactions between the biomaterial and the pathogen in the presence of the immune response of the host [68]. Bacterial adhesion on the internal fixation devices is the first and most critical period of bacterial colonization [69], leading to infection at the site of implants.

Table 1.3. The ring-opening polymerization of the L-lactide using organic and metal-based catalysts.

Polymer	Synthetic method	Catalyst	Characteristics	Cytotoxicity	Applications	Reference
PLA	ROP of L-lactide	2-methyl-pyridine Pyridine Pyrrole	M_n=880 Da M_n=280 Da M_n=780 Da	NA	Carrier drug complex for drug delivery	[70]
PLA	ROP of L-lactide	Nicotine Nicorandil	M_n=6900 Da M_n=4800 Da	NA	Drug delivery	[71]
PLA	ROP of L-lactide	Tin(II) Octoate, Zirconium, Titanium	M_n=50 KDa	Allergic	NA	[72]
PLA	ROP of L-lactide	Bismuth subsalicylate	M_n=2500 Da	Low toxicity	Biomedical applications	[73]
PLA	ROP of L-lactide	Prodigiosin	**M_n=5000 Da**	Non-cytotoxic	Drug delivery	Current study

1.9 Synthetic colorants

There is a growing concern about the toxicity and safety of the synthetic colorants used internally to color the polymer resin [74]. However, the leaching of toxic heavy metals and cyanine compounds from consumer products penetrates deep inside the body leading to gastrointestinal problems, skin allergies, neurotoxicity [75], and psychotoxicity (Allura red AC) [76].

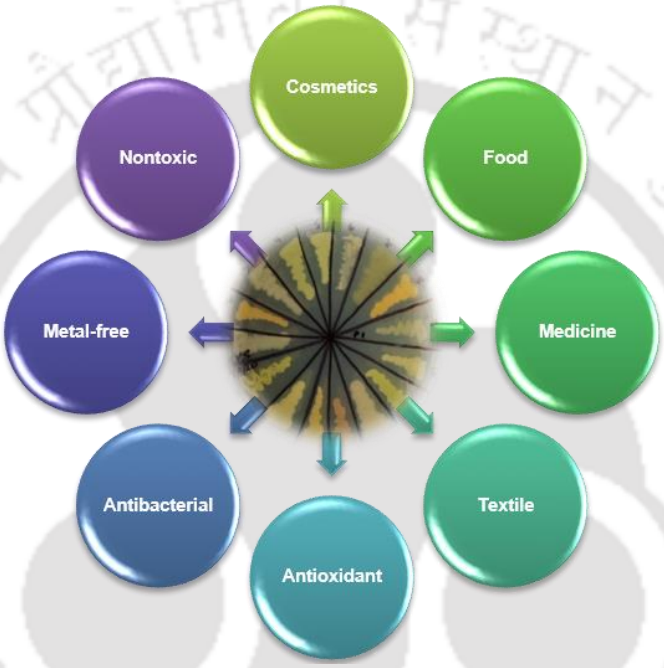

Figure 1.7. Properties of the bacterial pigments.

Considering all the adverse effects of colors, the U.S Food and Drug Administration (U.S FDA) [77], World Health Organization (WHO) [78], and European Food Standard Authority (EFSA) [79] excluded the use of synthetic dyes and pigment in food ingredients, medicine, and packaging applications. Emphasis has been made on natural colors of plant and microbial origin because they not only add color but also have anticancer, antioxidant, and better anti-inflammatory properties [80]. The various bacterial pigments and their characteristic properties are tabulated in Table 1.4. The current research details the production of bio-based biodegradable polymers such as PHB, PLA, and nanocellulose and an organic small molecule prodigiosin and their effective utilization as biomaterials for various applications.

Table 1.4. The methods of production of bacterial pigments and their characteristic properties.

Type of Pigment	Production method	Microbe used	Characteristics	Yield	Applications	Reference
Prodigiosin analogues	Chemical synthesis	NA	Antimalarial	65%	*P. Yoelii* Murin infection	[81]
Prodigiosin	Fermentation	*Pseudomonas putida* KT2440	Antibacterial	NA	Breast cancer	[82]
Violacein	Fermentation	*Janthinobacterium lividum*	Antiviral	3.5 g/L	Dyeing polyamide fabric	[83]
Prodigiosin	Solid-state Fermentation	*Serratia marcescens* FZSF02	Anticancer	1.5 g/L	Lung carcinoma cell lines	[84]
Prodigiosin	Solid-state Fermentation	*Serratia nematodiphila* CoE-SusPol1	Antibacterial	0.37 g/g of CDW	**Metal-Free Catalyst Biofilm Inhibition**	Current study

1.10 Action on the development of alternatives for conventional plastics: Global v/s India

Various agencies and governments across the world have worked and come up with policies to alleviate the threat of plastics on the environment. Globally, various governments have started replacing conventional plastics with biodegradable plastics since 2004. The government of Luxemburg and Valorlux has enforced the usage of eco-sac reusable bags, which impacted the reduction in plastic usage by 85%. Costa Rica has selected renewable materials such as cassava bags, and wooden coffee stirrers. The government of California and Mexico have passed the law to reduce conventional plastics and encourage the usage of cutlery made of corn starch, cups made from plants, and bamboo fiber coated with PLA. Indonesian company Evoware produced biodegradable cups made up of seaweed in 2016 [85], and Edinburgh-based firm CHOOSE has invented completely paper-based bottles [86]. London-based startup Notpla makes sustainable packaging from seaweed [87].

The Indian government has taken steps to ban the manufacture, import, and creation of stock, sale, and distribution of single-use plastics from 1st July 2022. This major step helps in reducing the adverse effects of single-use plastics on the environment, including aquatic and terrestrial ecosystems. The list of banned items includes plastic plates, cups, glasses, cutlery, banners, etc. The Ministry of Environment, Forest and Climate Change formulated the plastic waste management amendment rule on 16 February 2022. These guidelines outline the circular economy and plastic waste. Further, the government of India is promoting the inventions and providing platforms for accelerated implementation of the alternatives [88]. Defense Research and Development Organization (DRDO), DFRL has developed natural fiber-reinforced biodegradable cutlery using injection or compression molding.

1.11 Research gap

The major drawback associated with the production of biodegradable polymers such as PHB is the cost of raw materials used to develop an efficient aerobic fermentation process. Further, to tackle the problem associated with raw materials, there is a need to explore an inexpensive and bio-based renewable material rejected from agricultural activity and to optimize the process for maximum yield. The second drawback associated with another biodegradable polymer PLA is the use of the metal catalyst for the polymerization of lactide, which retains in the synthesized polymer, and removal of such component is impossible. Moreover, the PLA available in the market is prone to bacterial adhesion leading to biofilm formation on the surface. This poses a high risk for the products used for intended implant applications. Therefore, this research attempts to synthesize and fabricate the biomaterials in an environmentally friendly manner.

1.12 Aim and objectives

The main aim of the current work is to produce bio-based and biodegradable polymers such as polyhydroxybutyrate using a renewable agricultural feedstock and poly(lactic acid) using non-toxic metal-free catalyst prodigiosin. Here the sorghum juice from the stalks is used as a carbon source for the production of PHB, and the rest bagasse is utilized for the production of nanocellulose without producing any residues. The production of PHB is performed by *Bacillus megaterium.* Further, the products have been explored for their applicability as biomaterials for embolizing and antibacterial applications.

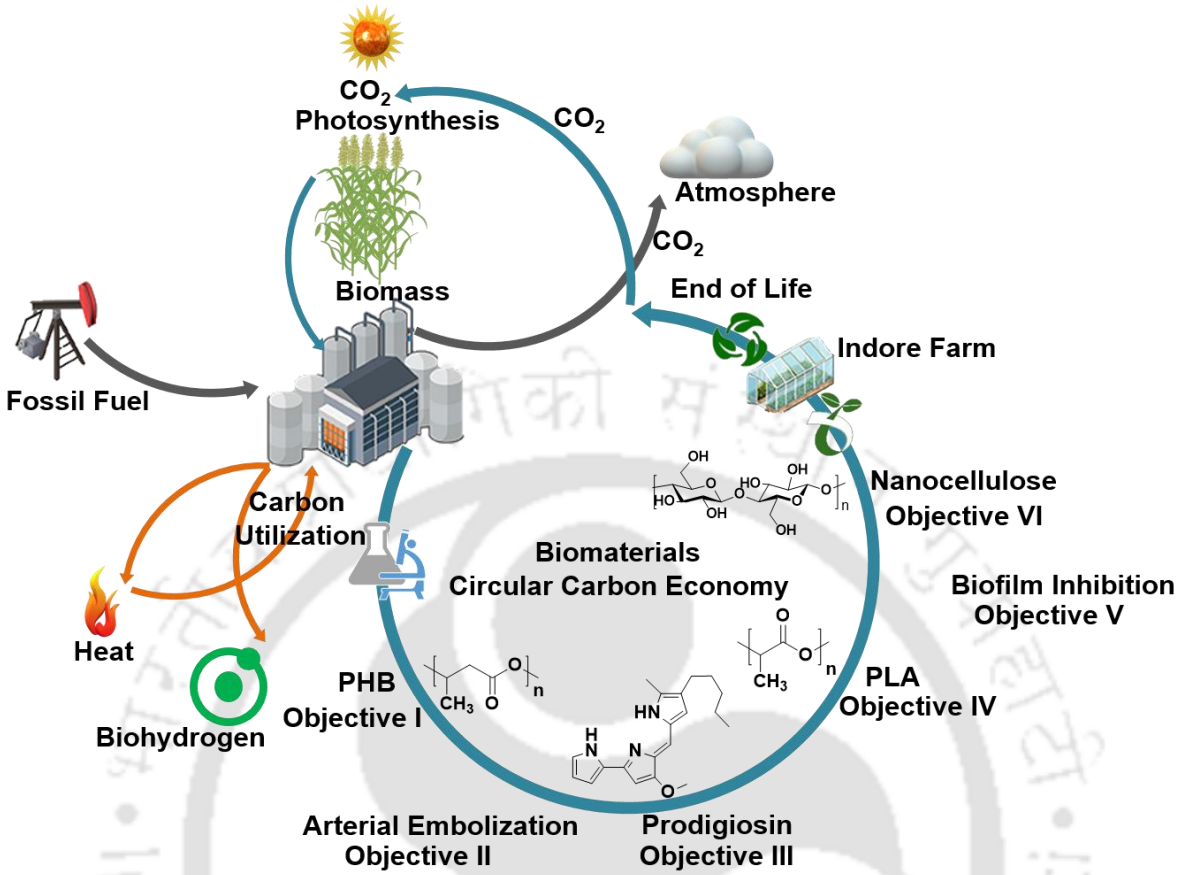

Figure 1.8. The overall scheme of production of biomaterials in a sustainable route.

1. **Development of a strategy for PHB production involving the upstream and downstream processing**
    - Extraction of juice rich in fermentable sugars from sorghum stalks
    - Screening of process parameters using central composite design for PHB production using *Bacillus megaterium*.
    - Extraction of PHB from bacterial cell biomass using solvent extraction
2. **Development of PHB microspheres and low-cost PLA-based 3D printed vascular phantom for *in vitro* embolization studies**
    - Preparation of PHB microspheres using solvent evaporation technique
    - Development of hepatic vascular phantom using 3D printing and post-processing using epoxy resin

- Study of embolization effect of the PHB microspheres by using a developed vascular model

3. **Biosynthesis of prodigiosin using *Serratia nematodiphila* isolated from river water**
    - Isolation of *Serratia nematodiphila* from Brahmaputra river water
    - Study on the effect of nitrogen sources on the production of prodigiosin
    - Extraction of prodigiosin from cell biomass using ethanol as a solvent and its characterization
    - Application of prodigiosin as an antibacterial agent against *Staphylococcus aureus*
4. **Application of prodigiosin as a metal-free organic catalyst for the synthesis of bio-based PLA**
    - Study on the effect of prodigiosin concentration on the molecular weight of PLA
    - End group analysis using the MALDI-TOF analysis
    - In vitro cytotoxicity study on the developed polymer on BHK-21 cells
5. **Development of prodigiosin-loaded PLA and its application as an antibiofilm-forming agent**
    - Preparation of the prodigiosin-loaded PLA using a solvent casting method
    - *In vitro* study on the inhibition effect of prodigiosin-loaded PLA films
    - Inhibition activity against implant-associated pathogens such as *Klebsiella aerogenes* and *Staphylococcus aureus*
6. **Production of nanocellulose from waste sorghum biomass**
    - Compositional analysis and chemical pretreatment of waste sorghum biomass left over after the extraction of juice

- Effect of alkaline hydrogen peroxide treatment on the removal of lignin and defibrillation
- Fabrication of nanocellulose using acid hydrolysis and morphological analysis

1.13 Organization of thesis

The present work is divided into nine chapters. The outline of the information discussed in each chapter is given below.

Chapter 1: Introduction and Literature Review

This chapter explains the role and importance of waste agricultural biomass and its utilization for the production of bio-based and biodegradable polymers such as polyhydroxyalkanoates through various types of fermentation strategies. Also, the types of bacterial pigments and their applications are discussed along with the different methodologies used for the fabrication of nanocellulose.

Chapter 2: Materials and Methods

This chapter explains the methodologies involved in the production of the PHB, PLA, prodigiosin, synthesis of microspheres, development of 3D printed vascular phantom, fabrication of nanocellulose, development of prodigiosin-loaded PLA films, and their applications.

Chapter 3: Production of Polyhydroxybutyrate [PHB] from Waste Sorghum Stalks as Raw Material

The basic requirement for the synthesis of PHB is a carbon source. In this chapter, emphasis has been made on the utilization of sorghum juice from waste sorghum stalks using *Bacillus megaterium*. The optimization of the media and process parameters are discussed along with

the extraction and purification of PHB. The analysis of characteristic properties of the synthesized PHB is also discussed.

Chapter 4: Preparation of PHB Microspheres for Embolization: In vitro Study Using PLA-Based 3D-Printed Hepatic Vascular Phantom

PHB is known for its biocompatible and biodegradable properties, and PLA is biodegradable. In this chapter, it has been emphasized on the fabrication of microspheres from the obtained PHB. The development of a low-cost PLA-based hepatic phantom to study the distribution of the PHB microspheres in the hepatic vasculature.

Chapter 5: Biosynthesis of Prodigiosin from Serratia nematodiphila for the Synthesis of Poly(lactic acid)

Prodigiosin is a small organic molecule produced by bacteria having inherent anticancer properties. This chapter discusses the isolation of the *Serratia nematodiphila* from the river water, biosynthesis, and extraction of prodigiosin and its application as a pH indicator.

Chapter 6: Synthesis of Metal-Free Poly(lactic acid) (PLA) using Prodigiosin as a Catalyst

The metallic and organometallic catalysts used in the synthesis of the PLA are unable to remove from the synthesized polymers, which poses a toxic side effect. In this chapter, the prodigiosin synthesized by *Serratia nematodiphila* is used as an organic metal-free catalyst with varying [lactide]/[prodigiosin] concentrations resulting in variable molecular weight.

Chapter 7: Prodigiosin-Loaded Poly(lactic acid) to Combat the Biofilm-Associated Infections

The biofilm-associated infections are the major reasons for implant failure posing life-threatening events. This chapter enlightens the loading of prodigiosin into the PLA to get surface functionalized PLA with all the inherent properties in addition to an anti-biofilm forming capability.

Chapter 8: Fabrication of Nanocellulose from Waste Sorghum Bagasse

The juice from the sorghum stalks has been utilized for the synthesis of PHB, whereas the bagasse is of waste. This chapter describes the utilization of waste sorghum bagasse for the synthesis of nanocellulose by using alkaline hydrogen peroxide pretreatment followed by hydrolysis.

Chapter 9: Conclusions and Future Perspectives

This chapter summarizes the research work which has been carried out and briefly presents possible future studies.

CHAPTER 2

Materials and Methods

Graphical Overview

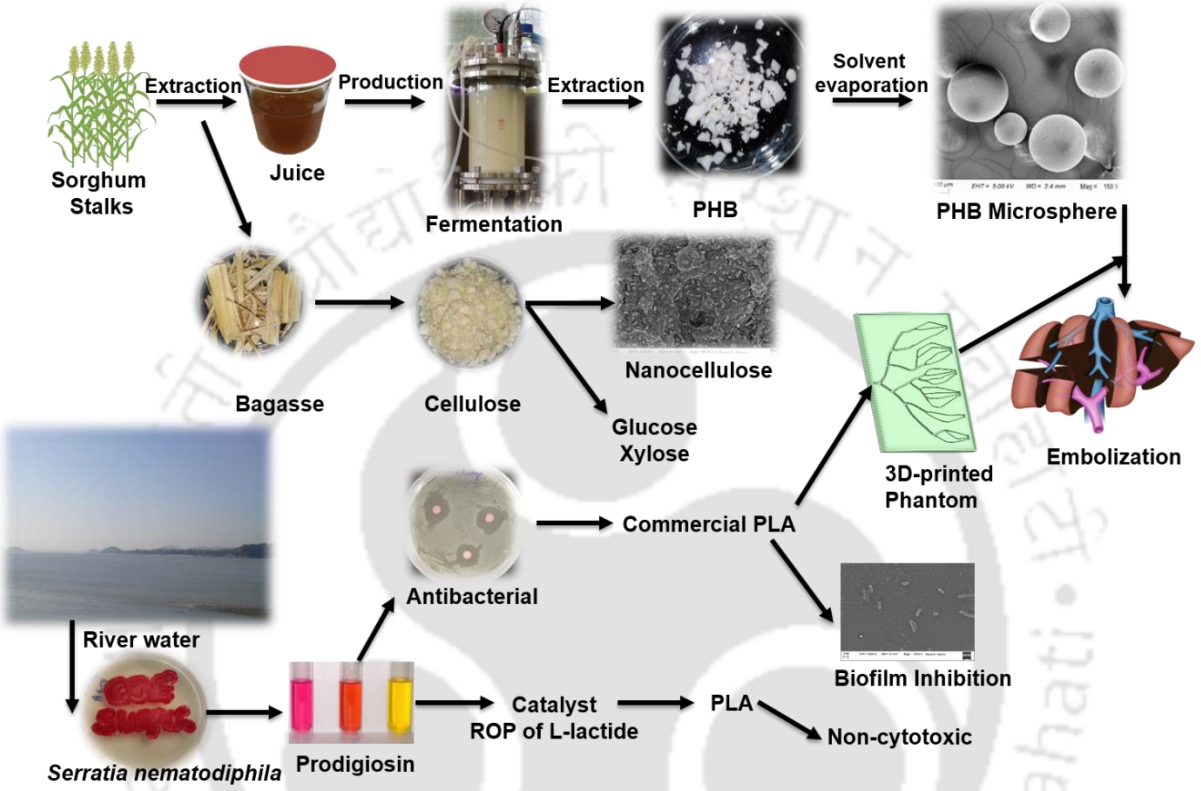

This chapter aims to present the materials used, methods of preparation of materials, process conditions, methodologies, and characterization techniques.

Waste sorghum stalks were collected from the Vijayanagara district of the state of Karnataka, India. The juice was extracted and supplemented with a nitrogen source and other media components. Further, it was used for the production of PHB using fermentation by *Bacillus megaterium*. Media screening was performed using a central composite design. Fed-batch operations were performed using dissolved oxygen (DO, 30-60%) control strategy to reduce the production time from 72 h to 24 h. Further, PHB was extracted using the reflux method. Leftover sorghum bagasse was used for the preparation of nanocellulose by following the

alkaline hydrogen peroxide (AHP) pretreatment. Further, the cellulose obtained from AHP pretreatment (pH 11.5) was used for the acid hydrolysis at different time intervals between 5-60 min to get different morphologies. The same cellulose was subjected to enzyme hydrolysis using cellulase enzyme blend Cellic CTec2 with enzyme loading from 0.2-1.0 g/g of biomass to get fermentable sugars. The produced PHB (20 mg/mL of dichloromethane) from the above process is used for the preparation of microspheres using oil in water emulsion with 1% w/v of polyvinyl alcohol (PVA) solution followed by solvent evaporation with stirring speed from 500-1000 rpm to get different sizes. These microspheres were further utilized for embolization of the right hepatic artery using PLA-based 3D printed hepatic phantom developed at a feed rate of 30 mm/s with 0.1 mm layer height for precision. The nozzle temperature and bed temperature were set to 200 °C and 45 °C, respectively. Furthermore, the prodigiosin was biosynthesized at 30 °C for 48 h with 1-4 g/L peptone using *Serratia nematodiphila*. Prodigiosin was extracted using ethanol, purified using column chromatography, and used as a metal-free organic catalyst for ring-opening polymerization of L-lactide with a [Lactide]/[Prodigiosin]=100-10000 in the presence of benzyl alcohol at 180 °C. In addition, the prodigiosin was studied for its application as a colorant, and antibiofilm forming agent for PLA (Nature Works PLA 2003D) films developed using the solvent casting technique. The produced samples were characterized using analytical techniques such as X-ray diffraction, Fourier transform infrared spectroscopy, gel permeation chromatography, thermogravimetry, differential scanning calorimetry, field emission scanning electron microscopy, wettability, UV-vis spectroscopy, high-performance liquid chromatography, viscometry, color spectrophotometry, polarizing optical microscopy, density, matrix-assisted laser desorption ionization-time of flight mass spectrometry, nuclear magnetic resonance spectroscopy.

2.1 Production of polyhydroxybutyrate (PHB) from waste sorghum stalks

2.1.1 Materials

Sorghum stalks were obtained from the Vijayanagara district of the state of Karnataka, *Bacillus megaterium* (NCIM-5472) was obtained from CSIR-NCIM, ammonium sodium phosphate dibasic tetrahydrate ($NaNH_4HPO_4.4H_2O$), potassium dihydrogen phosphate (KH_2PO_4), dipotassium hydrogen phosphate (K_2HPO_4), magnesium sulfate ($MgSO_4$), ferric chloride ($FeCl_3$), calcium chloride ($CaCl_2$), Manganese(II) sulfate ($MnSO_4$), cobalt(II) chloride hexahydrate ($CoCl_2.6H_2O$), copper(II) chloride ($CuCl_2$), zinc sulfate heptahydrate ($ZnSO_4.7H_2O$), nutrient agar, Luria Bertani agar, hydrochloric acid (HCl) and sodium hydroxide (NaOH) were procured from HiMedia Laboratories, India. Chloroform ($CHCl_3$) was from Spectrochem Pvt Ltd, India, acetone (CH_3COCH_3), methanol (CH_3OH) were procured from Merck Specialties Pvt. Ltd. Chloroform-d (99.8%), and 2,5-Dihydroxybenzoic acid (>99.0%) matrix purchased from Sigma Aldrich, India. 96-well plates (Nunclon Delta Surface) were procured from Thermo Fisher Scientific, India. Baby hamster kidney fibroblast cells (BHK-21) were obtained from National Centre for Cell Science (Pune, India). Dimethyl sulfoxide (DMSO, ≥99.9%) was from Sigma Aldrich, India, Dulbecco's modified Eagle's medium (DMEM, Gibco^{TM}), trypan blue stain (0.4%, Gibco^{TM}), 96-well cell culture plates (Nunclon^{TM} Delta Surface), 3-(4,5-dimethylthiazol-2-yl)-2,5-diphenyltetrazolium bromide reagent (MTT, Invitrogen^{TM}) were procured from ThermoFisher Scientific, India. Commercial PHB was purchased from Sigma Aldrich, India

2.1.2 Extraction of sorghum juice and its characterization

Sorghum stalks devoid of grains and leaves were collected and washed thrice with water to remove soil or residual material present on the surface. The stalks were then crushed using a crusher to extract the juice. The complete process of extraction is shown in Figure 2.1. Then

pH of the obtained juice was adjusted to 7 using 2 N NaOH and 1 N HCl, sterilized in an autoclave at 121 °C for 20 min, and used as a carbon source in a subsequent process. The sugar content of juice was quantified by UHPLC using glucose and fructose as standards. The residual bagasse was dried at 60 °C for 48 h to remove the moisture completely and stored in an air-tight container, and used for the production of nanocellulose later.

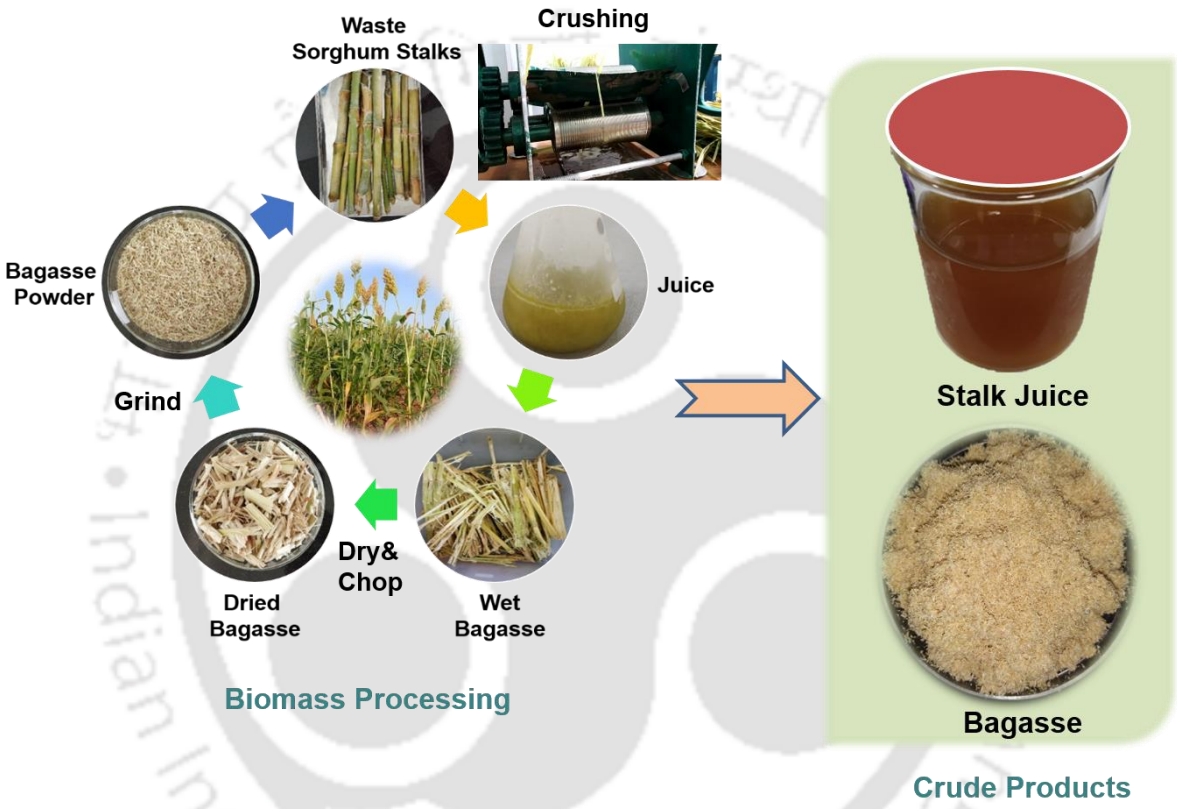

Figure 2.1. Schematic representation of the collection and extraction of the sorghum juice from waste stalks and leftover bagasse for further utilization in nanocellulose production.

2.1.3 Optimization of PHB production using the central composite design (CCD)

Screening and optimization of media components were performed for PHB production using sorghum juice as a carbon source by employing the central composite design. The experimental design matrix comprising of 16 experimental runs with the following parameters: concentration of carbon source (sorghum juice, 10, 30, and 50 g/L), the concentration of nitrogen source (2,

6, and 10 g/L), and Inoculum size (5, 7.5, and 10%). All the mentioned parameters were tested at three different levels, which are shown in Table 2.1. Lower and upper parameters were chosen based on the initial experimental runs. The design was developed using the JMP® Pro v.14 by SAS. All the experiments were carried out in a 500 mL conical flask consisting of 200 mL media.

Bacillus megaterium cultures were grown and maintained on nutrient agar plates at 4 °C and subcultured at regular intervals of time. PHB biosynthesis using sorghum juice extract was studied in the shake flasks by adding the raw sorghum juice to the minimal media with the following composition: 2-10 g/L of ammonium sodium phosphate dibasic tetrahydrate ($NaNH_4HPO_4.4H_2O$) as nitrogen source, sorghum juice consisting of 10-50 g/L of sugars as carbon source, KH_2PO_4 3.7 g/L, K_2HPO_4 7.5 g/L, $MgSO_4$ 250 g/L (1 mL/L), and 1 mL/L of trace element solution consisting of $FeCl_3$ 2.78 g/L, $CaCl_2$ 1.47 g/L, $MnSO_4$ 1.98 g/L, $CoCl_2.6H_2O$ 2.38 g/L, $CuCl_2$ 0.17 g/L, $ZnSO_4.7H_2O$ 0.29 g/L. The initial pH was adjusted to 7 by the addition of HCl and NaOH. Then it was incubated at 120 rpm for 72 h for the accumulation of PHB granules.

Table 2.1. Statistical optimization of PHB production using sorghum juice as a carbon source.

Run No.	Pattern	Sorghum Juice (g/L)	Nitrogen (g/L)	Inoculum (%)	Response	
					Dry cell weight (g/L)	PHB concentration (g/L)
1	+++	50	10	10	1.72	0.49
2	A00	50	6	7.5	1.47	0.48
3	0A0	30	10	7.5	1.614	0.78
4	+−−	50	2	5	1.8	1.09
5	00a	30	6	5	1.52	0.45
6	+−+	50	2	10	1.728	0.63
7	00A	30	6	10	1.64	0.41
8	000	30	6	7.5	1.54	0.58
9	−−+	10	2	10	1.686	0.61
10	0a0	30	2	7.5	1.784	1.20
11	−++	10	10	10	1.84	0.52
12	−−−	10	2	5	1.52	0.59
13	−+−	10	10	5	1.474	0.37
14	000	30	6	7.5	1.54	0.58
15	++−	50	10	5	1.56	0.66
16	a00	10	6	7.5	1.454	0.36

The batch and fed-batch experiments were performed using a 3.5 L bottom-driven in-situ sterilizable bioreactor (Biojenik Engineering, Chennai, India), shown in Figure 2.2. The operating variables such as pH, temperature, dissolved oxygen (dO_2), and agitation rates were controlled using supervisory control and data acquisition (SCADA) (SIMATIC S7-1200 controller and SIMATIC WinCC explorer software, Siemens). The reactor was sterilized in situ for 20 min at 121 °C and cooled before every batch started. pH was measured using electrode InPro® 3030, and dO_2 was measured using InPro® 6000 probe (Mettler Toledo, Switzerland). The temperature was maintained at 37 ± 1 °C, and the foam was controlled by the addition of non-ionic silicon antifoaming agent (Loba Chemie, India).

Batch Strategy: The dissolved oxygen (dO_2) concentration was set at 100% saturation at the beginning of the batch fermentation process. When the dO_2 reached 20%, the regulation of dO_2 was started using a cascade control strategy with varying agitation speeds from 200 to 1200 rpm and airflow from 1 to 2 L/min to maintain the final set dO_2 concentration. The pH was maintained at 7.0 ± 0.2 by the addition of 1 N HCl and 2 N NaOH. The culture was withdrawn periodically during the fermentation for the quantification of the sugars, cell biomass, and PHB.

Fed-batch Strategy: Fed-batch fermentations were performed by applying a three-stage procedure

Stage 1: Batch culture: A cell growth phase

Stage 2: Fed-batch culture with carbon and nitrogen supply: Cell growth and PHB accumulation phase.

Stage 3: Fed-batch culture without nitrogen supply: PHB accumulation phase.

The fed-batch strategy was employed by feeding sorghum juice regulated by dO_2 with a cut-off level of 20%, 40%, and 60% saturation.

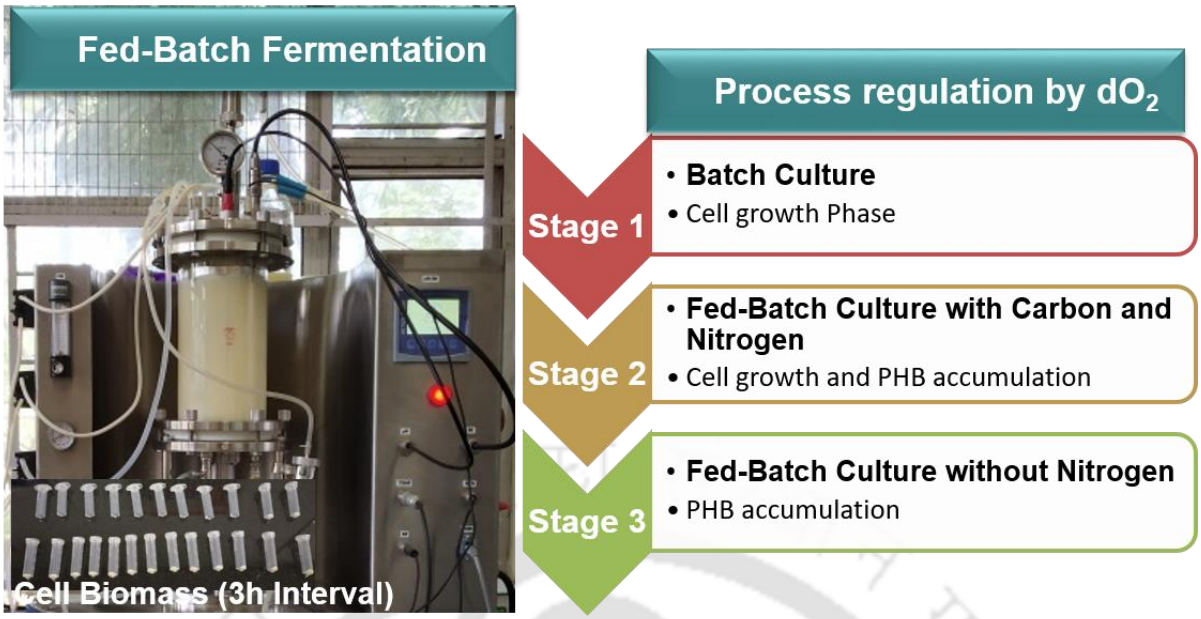

Figure 2.2. Fed-batch process for the production of polyhydroxybutyrate regulated by dissolved oxygen.

2.1.4 Cell harvest, extraction, and purification of PHB

Bacterial cells after fermentation were harvested using Heraeus Megafuge 16 R centrifuge (Thermo Scientific) at 5500 rpm for 10 min at 25 °C. The cell pellets obtained after centrifugation were washed twice with distilled water to remove impurities, followed by freeze-drying in a lyophilizer at -80 °C for 6 h to remove the moisture completely. Cell dry weight obtained after lyophilization was noted for yield calculation. The cell-free supernatant was analyzed for residual sugar content.

The PHB was extracted from lyophilized cells (Figure 2.3) using the reported method with slight modification [89] as follows: First method: 5%, w/v of cells were extracted in chloroform under reflux at 70 °C for 12 h, second method: 5%, w/v of cells were stirred with acetone for 10 min at 100 rpm to remove moisture content and remove the residual antifoaming agent. Then it was extracted using chloroform under reflux at 70 °C for 12 h. The obtained solution was filtered using a 0.2 μm filter to remove the cell debris. Then the solution was concentrated by a rotary evaporator and precipitated by the dropwise addition of polymer solution into five

volumes of chilled methanol (99.8%) with stirring. The white precipitate of the PHB polymer was collected and dried at 65 °C in a vacuum oven for evaporation of any residual solvent. The dried PHB polymer in powder form was used for further characterization.

The concentration of the PHB was determined using the crotonic acid assay [90], by dissolving 5 mg of PHB-enriched cell biomass in 1 mL of concentrated H_2SO_4 at elevated temperature and analyzed at 208 nm. The commercial PHB was used for making the calibration curve.

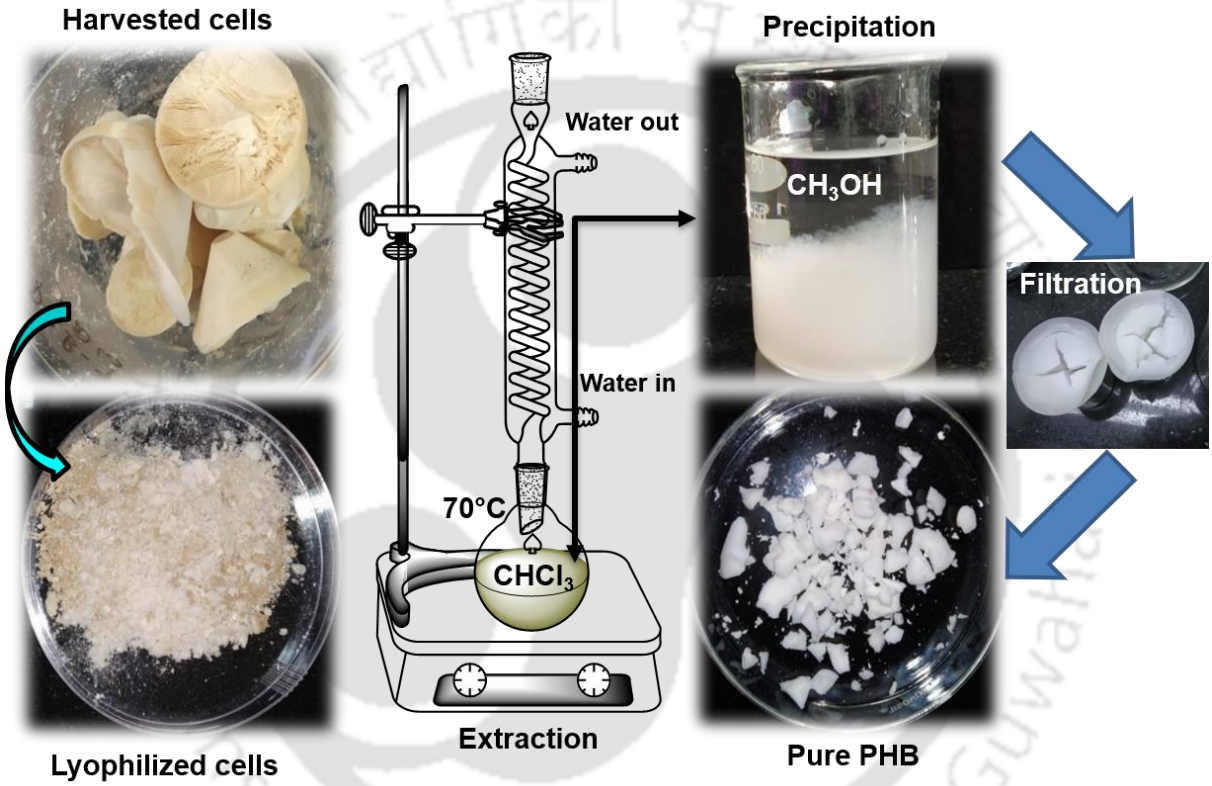

Figure 2.3. Schematic representation of cell harvesting after fermentation and the process of extraction of PHB granules from the dry cell biomass.

Characterization techniques used: Cytotoxicity assay, FESEM, EDX, ^{1}H, and ^{13}C NMR, FTIR, FETEM, TGA, DSC, XRD, Wettability, GPC, POM, MALDI-TOF-MS

2.2 Preparation of PHB microspheres for embolization: *in vitro* study using PLA-based 3d printed hepatic vascular phantom

2.2.1 Materials

Polyhydroxybutyrate (PHB, 99%) was synthesized in the lab using *Bacillus megaterium* NCIM 5472, having a density of 1.24 g/cm^3. Sodium phosphate monobasic dihydrate ($NaH_2PO_4.2H_2O$, 99%) and poly(vinyl alcohol) (PVA, 99% hydrolyzed) with a density of 1.31 g/cm^3 were procured from Sigma Aldrich, India. Dichloromethane (DCM, 99.5%) was from Finar, India. PLA filament was purchased from Tessaract PLA, India, Glycerol (99%) and Sodium chloride (NaCl) were procured from Himedia Laboratories, India, Cathy I.V cannula (22G×1×0.8×25 mm, 38 mL/min capacity) was from Hindustan Syringes & Medical Devices Ltd, India.

2.2.2 Preparation of PHB microspheres

The PHB microspheres were prepared by oil-in-water emulsion technique using a solvent evaporation approach according to the reported literature with slight modifications [91], as shown in Figure 2.4. Briefly, 20 mg/mL of PHB solution was prepared in DCM with gentle heating. 1% w/v of PVA solution was prepared in water at 95 °C for 30 min for complete dissolution and allowed to attain room temperature. Further, 10 mL of PHB solution was added to the PVA solution with stirring at 500 and 300 rpm and allowed to evaporate DCM. Then the obtained solution containing microspheres was centrifuged at 5000 rpm for 5 min to obtain the microspheres at the bottom. The supernatant solution was discarded, and the remaining microspheres were washed thrice with distilled water to remove the adsorbed PVA. The obtained microspheres were dried in an oven at 40 °C for 24 h and stored at an ambient temperature in a desiccator.

The yield of the PHB microspheres was calculated by dividing the weight of the obtained microspheres by the weight of the initial PHB.

$$\text{PHB microsphere yield (\%)} = \frac{Weight\ of\ microspheres}{Weight\ of\ initial\ PHB} \text{ x } 100$$

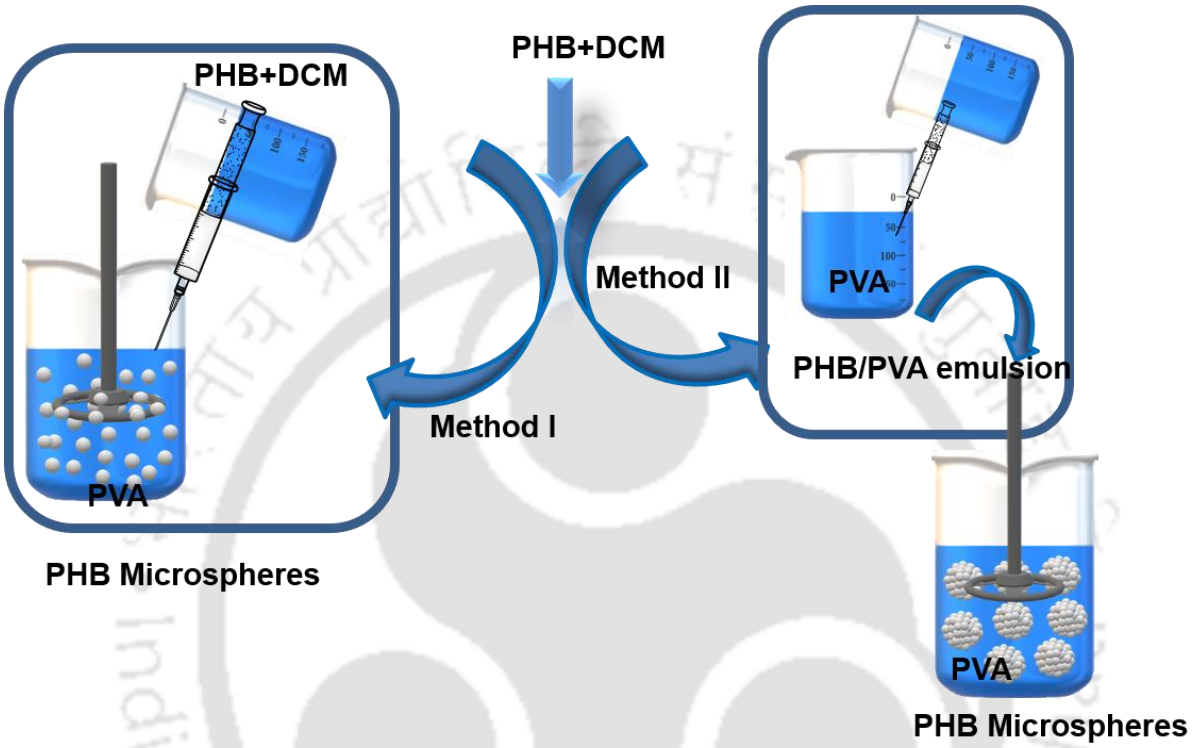

Figure 2.4. Schematic representation of the preparation of PHB microspheres, Method I: PHB in DCM added to PVA solution and Method II: PHB in DCM added to PVA solution followed by second addition to PVA solution.

2.2.3 Three-dimensional (3D) printing of PLA-based hepatic model

The one-dimensional model of the hepatic blood vessels was developed into a 3D model using Computer-Aided Design (CAD) software (Autodesk® Fusion 360). The developed 3D CAD model was exported as a stereolithography (STL) mesh file type and then converted into a machine code (gcode) using open-source slicing software (Ultimaker Cura 4.3). Commercially available PLA filament was used to print the hepatic model with a low-cost Fused Deposition Modeling (FDM) based Printer (Creality CR 10, Shenzhen Creality 3D Technology Co., Ltd).

3D printing was performed at a feed rate of 30 mm/s with 0.1 mm layer height for precision. The nozzle temperature and bed temperature were set to 200 °C and 45 °C, respectively. All the 3D printing parameters were optimized previously for PLA filament of 1.75 mm dia. The printed part was removed from the printer and applied a thin layer of epoxy was on the surface and allowed to dry for 6 h. Then a polyester film was placed on it and allowed to dry for 24 h. Followed by a layer of epoxy poured on the surface of the polyester film. Further, the obtained phantom was allowed to dry for 24 h. Finally, the inlet and outlet pipes were connected to allow the fluid to flow through the hepatic phantom. The 3D printing and the post-processing are depicted in Figure 2.5**.**

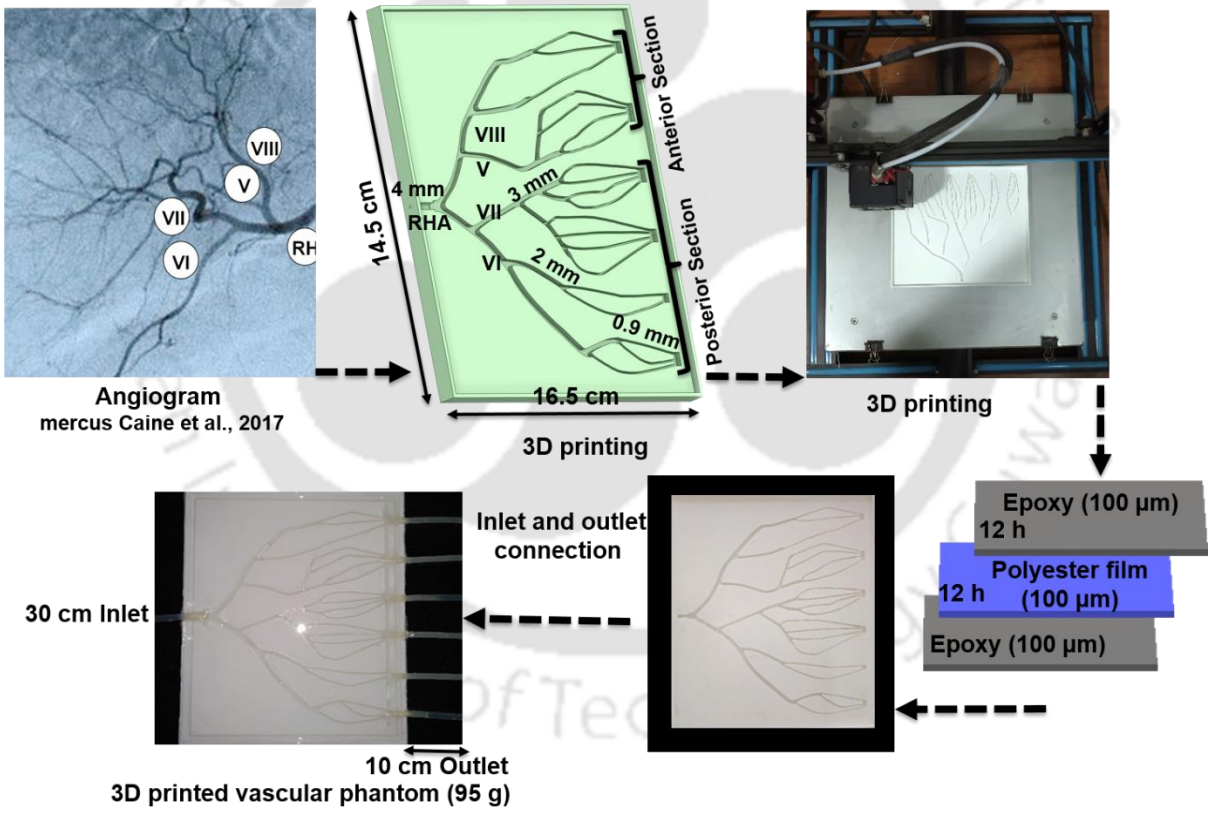

Figure 2.5. The process of 3D printing and post-processing method used in the development of PLA-based hepatic phantom.

2.2.4 Experimental setup

The PLA-based 3D printed hepatic vascular flow model (3D-HVFM) was used in the current study with an inlet channel diameter of 4 mm, first bifurcation channel of 3 mm, second bifurcation channel of 2 mm, and outlet channel diameter of 0.9 mm according to the reported sizes of the right hepatic artery of an angiogram [92]. The experimental setup designed to perform the *in vitro* studies is shown in Figure 2.6. The experimental setup is divided into four sections; the first is the reservoir unit consists of the simulated body fluid and a peristaltic pump to maintain the blood flow similar to that of the right hepatic artery (RHA). The dispensing unit is the second section consisting of the syringe pump along with a syringe filled with carried fluid and microspheres. The third is an experimental unit consisting of a 3D-printed vascular phantom with fluid-collecting tubes at the outlet of each channel and a USB-portable microscope for inline visualization of the microsphere flow. The fourth portion is the data analysis unit which is a computer attached to a USB microscope to record video of simulated body fluid and a flow of microspheres and their embolization effect in the channels.

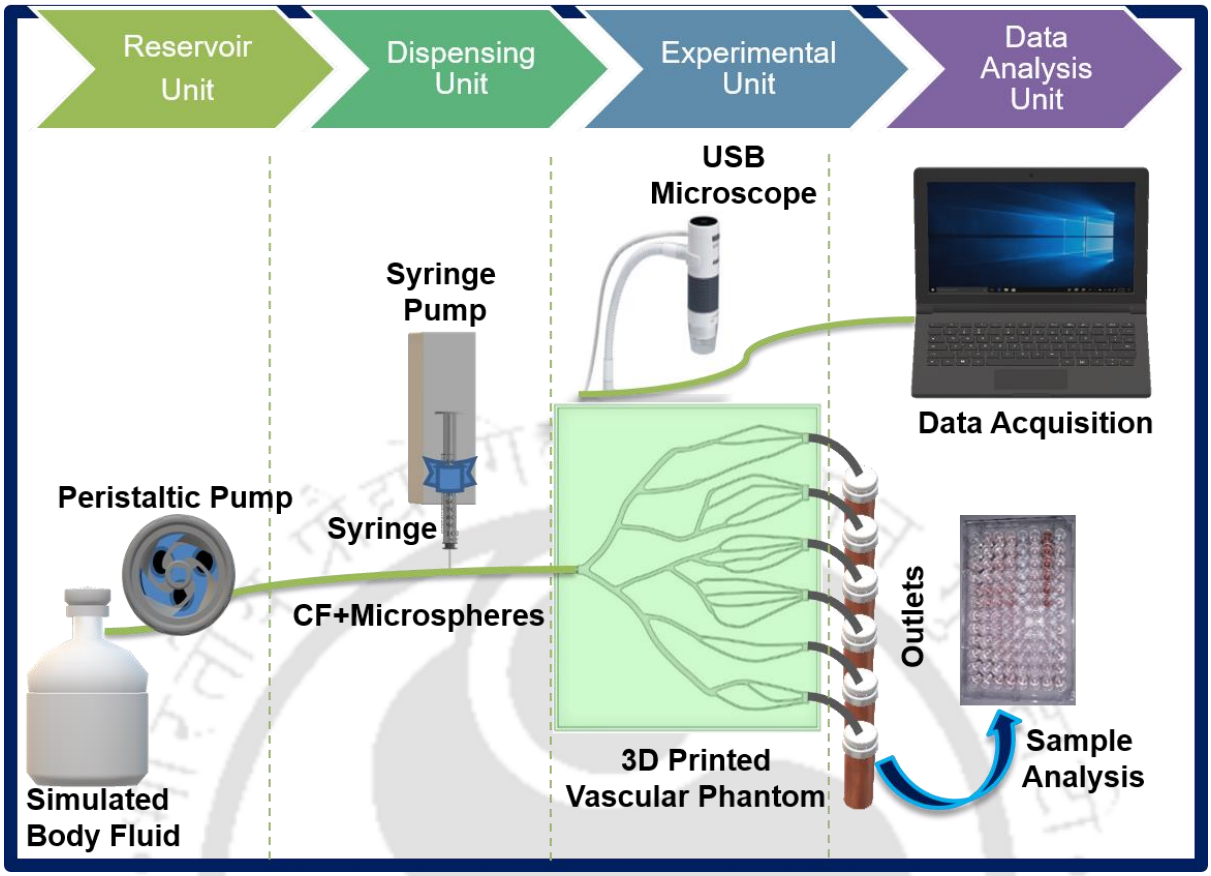

Figure 2.6. Schematic representation of the experimental setup for microsphere delivery.

2.2.5 The viscosity of simulated body fluid (SBF)

The simulated body fluid was formulated to maintain the viscosity ideally matching the dynamic viscosity of the blood (4.40 ± 0.5 cP) [93] at room temperature (25 ± 0.3 °C). An optimally matched SBF was selected further to study the effects in a 3D-printed vascular phantom with a composition of 40% of glycerol, 10% of sodium phosphate, and 0.9% of sodium chloride to get a viscosity equal to 4.5 cP.

Experimental parameters

The viscosity of the SBF: 4.5 cP

The flow rate of injection solution: 20 mL/min

The flow rate of SBF: 60-120 mL/min

Characterization techniques used: FESEM, EDX, TGA, DSC, XRD, Wettability.

2.3 Biosynthesis of prodigiosin from *serratia nematodiphila* for the synthesis of poly(lactic acid)

2.3.1 Materials

Sodium chloride (NaCl), yeast extract, peptone, agar, Luria-Bertani broth, methanol, and spin-column kit were procured from (HiMedia Laboratories, India). Ethanol and chloroform-d ($CDCl_3$, ≥ 99% CP), hydrochloric acid (HCl), chloroform, and silica gel (60-120 mesh size) were from Merck Specialties Pvt Ltd, India. n-hexane (Loba Chemie, India) and ethyl acetate were obtained from Merck Life Sciences Pvt Ltd, India. 2,5-dihydroxybenzoic acid (DHB, HPLC grade) and α-cyano-4-hydroxycinnamic acid (CHCA, HPLC grade) were obtained from Sigma Aldrich, India. All the reagents are analytical grade unless otherwise stated.

2.3.2 Isolation and molecular identification of prodigiosin-producing bacteria

The bacterial strain was isolated from the Brahmaputra river water, Guwahati, Assam, India, by plating the serially diluted samples on nutrient agar consisting of 10 g/L of NaCl, 5 g/L yeast extract, and 10 g/L of peptone with a pH range of 6.5-7.0 [94]. The culture was incubated at 30 °C for 48 h to obtain the red-colored colonies. The obtained colonies were then subcultured to obtain the pure culture. Further, it was distinguished using Grams-staining according to the existing protocol [95]. The 16S ribosomal RNA (rRNA) sequencing was performed by extracting the chromosomal DNA using a spin column kit, and the 16S rRNA gene (1500 bp) was amplified in a thermal cycler. The PCR cleanup was performed using Exonuclease I Shrimp Alkaline Phosphatase (Exo-SAP) [96]. Further, the amplicons were sequenced in a genetic analyzer (ABI 3500Xl, Life Technologies, USA) by the Sanger method. The obtained sequence files were analyzed for the closest sequence using National Centre for Biotechnology Information (NCBI) database. Further, the evolutionary relationship was

predicted by multiple sequence alignment and phylogenetic analysis with the closest similarity index [97]. The analysis involved 14 nucleotide sequences. A total of 1232 positions were obtained in the final data by eliminating the gaps. MEGA6 was used for the evolutionary analyses [98].

2.3.3 Antibiotic susceptibility test

Antibiotic susceptibility of an isolated strain was analyzed using disc diffusion assay for various reference standard antibiotics such as gentamicin (GEN 10 mcg), tetracycline (TE 30 mcg), cephalothin (CEP 30 mcg), amikacin (AK 30 mcg), and chloramphenicol (C 10 mcg) with a disc diameter of 6 mm, and the zone of inhibition was measured after 24 h of incubation [99]. Further, the multiple antibiotic resistance (MAR) was calculated using the existing method (MAR index is a ratio of the number of antibiotics to which the organism is resistant to the total number of antibiotics tested) [100], [101].

2.3.4 Effect of media components on the biosynthesis of prodigiosin

The effect of media components such as peptone, agar, yeast extract, sodium chloride, and glucose (0-10 g/L) was evaluated individually and in combination with the production of prodigiosin. All the experiments were performed on solid-state media with a 1.8 g/L agar concentration. Further, the culture was incubated at a temperature of 30 °C for 48 h for complete biosynthesis and pigment accumulation.

2.3.5 Extraction and purification of prodigiosin

The extraction of the prodigiosin was performed according to the literature [102] with some modifications. Briefly, the cell biomass was scraped out from agar plates and mixed with acidified ethanol (1:10). Then the flask contents were kept on an incubator shaker ORBITEK (Scigenics Biotech Pvt Ltd, India) at 200 rpm at 30 °C for 12 h until the complete discoloration of the cell biomass. The obtained solution, along with biomass, was centrifuged using the cooling centrifuge Heraeus Megafuge 16 R (Thermo Scientific) at 25 °C at 5000 rpm for 15

min to obtain the cell-free prodigiosin solution [103]. The used ethanol was separated by evaporating the pigment solution in a rotary evaporator at 45 °C, 77 mbar pressure (Rotavapor R-3, Buchi®) to obtain the concentrate. Further, it was passed through a silica gel column (hexane, mesh size 60-120) and eluted with n-hexane and ethyl acetate (ratio of mixture 2:1 v/v). Later the elutes were collected and dried at 45 °C in a vacuum [104] to obtain the purified prodigiosin.

The ethanol recovered from the process is calculated by using the following formula:

$$Recovery\ (\%) = \frac{Volume\ of\ ethanol\ recovered}{Initial\ volume} X\ 100$$

2.3.6 Antibacterial activity

The antibacterial activity of prodigiosin was determined against *Staphylococcus aureus* (2.4×10^7 CFU/mL) by measuring the zone of inhibition (mm) using antibiotics cephalothin, gentamicin, and amikacin as reference antibiotics for comparison.

Characterization techniques used: MALDI-TOF MS, FTIR, UV-Vis spectrophotometry, ^{1}H NMR, cytotoxicity assay, color spectrophotometry, and cytotoxicity assay.

2.4 Synthesis of metal-free poly(lactic acid) (PLA) using prodigiosin as a catalyst

2.4.1 Materials

Prodigiosin was synthesized and extracted previously in the lab from *Serratia nematodiphila* CoE-SusPol1 with a GenBank accession number MK968767. Yeast extract, peptone, agar, and methanol were procured from HiMedia Laboratories, India. Benzyl alcohol was procured from Merck Specialties Pvt Ltd, India. Chloroform-d (≥99%, with 0.03% v/v TMS) and 2,5-dihydroxybenzoic acid (DHB, >99.0%) were from Sigma Aldrich, India. 96-well plates (Nunclon Delta Surface) were procured from Thermo Fisher Scientific, India. Pure crystal L-lactide was synthesized in the laboratory from L-lactic acid (99%, PF 90, Purac, India) and

dried under a vacuum for 24 h. Baby hamster kidney fibroblast cells (BHK-21) were obtained from National Centre for Cell Science (Pune, India). Dimethyl sulfoxide (DMSO, ≥99.9%) was from Sigma Aldrich, India, Dulbecco's modified Eagle's medium (DMEM, Gibco^{TM}), trypan blue stain (0.4%, Gibco^{TM}), 96-well cell culture plates (Nunclon^{TM} Delta Surface), 3-(4,5-dimethylthiazol-2-yl)-2,5-diphenyltetrazolium bromide reagent (MTT, Invitrogen^{TM}) were procured from ThermoFisher Scientific, India.

2.4.2 Organocatalytic ring-opening polymerization of L-lactide using bacterial prodigiosin

The L-lactide used in the polymerization experiment was synthesized in the laboratory and has a purity $[\alpha]_{\lambda}^{T}$ of -244.69, moisture content of 0.6 ppm, and an acid value of 13 meq/kg. The prodigiosin was extracted from the *Serratia nematodiphila* CoE-SusPol1 from the existing protocol [105].

The bulk polymerization reaction was performed in a vacuum-sealed glass ampule. The complete process of PLA synthesis in the presence of prodigiosin is depicted (Figure 2.7). The purified crystal L-lactide is loaded into the ampules, and a varying amount of PG is added to maintain the molar ratio [L]/[PG] from 100-10000. The polymerization reactions were carried out using benzyl alcohol (BnOH) as a chain transfer agent, where the composition of the PG and BnOH are maintained equimolar. Further, the ampules were vacuum dried at 60 °C in an oil bath for 2h and were further sealed under vacuum. This mixture is further polymerized by maintaining the temperature of 180 °C in an oil bath for 12 h to get the polymerized poly(lactic acid). After the reaction time, the ampules were cooled immediately by immersing the ampule in ice-cold water. Finally, the sealed ampules were broken to obtain the polymer and were analyzed for their characteristic properties.

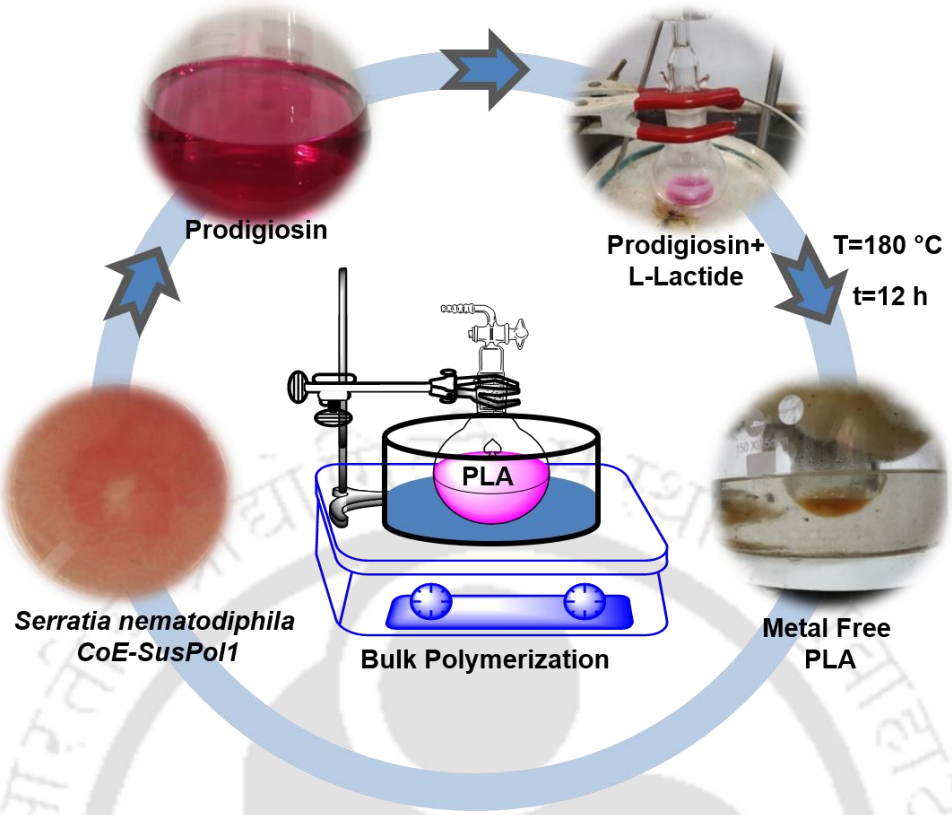

Figure 2.7. Schematic representation of the synthesis of metal-free PLA using prodigiosin as a catalyst.

Characterization techniques used: GPC, MALDI-TOF MS, ^{13}C NMR, FESEM, EDX, FTIR, TGA, cytotoxicity assay

2.5 Prodigiosin-loaded poly(lactic acid) to combat the biofilm-associated infections

2.5.1 Materials

Prodigiosin is synthesized in the lab from *Serratia nematodiphila* CoE-SusPol1 previously isolated from the water sample. Chloroform (Merck Specialties Pvt Ltd, India), 2,5-dihydroxybenzoic acid (DHB) (Sigma Aldrich, HPLC grade, Germany), poly(lactic acid) (PLA) (grade-2003D, NatureWorks, United States), *Staphylococcus aureus* (NCIM-2079), and *Klebsiella aerogenes* (NCIM-2281) were obtained from National Collection of Industrial

Microorganisms (NCIM, Pune), nutrient broth, agar, crystal violet, phosphate buffer (Analytical grade, HiMedia Laboratories, India). The 96 well culture plates Nunclon^{TM} Delta Surface (ThermoFisher Scientific, Denmark) were procured and used in the current study.

2.5.2 Preparation of prodigiosin-loaded poly(lactic acid) films

The current study accessed the suitability of crude and purified prodigiosin. Crude prodigiosin (PG-C) is an ethanol extract obtained after dissolving the *Serratia nematodiphila* CoE-SusPol cells in ethanol, followed by centrifugation at 5500 rpm to remove cell debris and evaporation to get dry prodigiosin powder. Purified prodigiosin (PG-P) involves the additional purification by column chromatography using n-hexane and ethyl acetate (ratio of mixture 2:1 v/v) as eluent followed by drying at 45 °C in a vacuum to get purified powder [106]. Further, the neat PLA (nPLA), PLA with crude prodigiosin (PLA-PG-C), and PLA with purified prodigiosin (PLA-PG-P) polymer films were prepared by adding 0.5 wt.% of crude and purified prodigiosin into the PLA using chloroform as solvent. The solution was mixed at 500 rpm for 12 h to dissolve the components completely. Further, the solution casting method was followed to obtain the films. These films were dried at 60 °C for 24 h to evaporate the solvent completely [107]. The lower concentration of prodigiosin is used in the study by considering the permissible limit of the pyrrole-containing pigments (not exceeding 1% w/w of polymers: according to the code of federal regulations) [108].

2.5.3 *In Vitro* study on biofilm formation using crystal violet staining

The biofilm inhibition [109] by the developed neat PLA, PLA-PG-C, and PLA-PG-P were evaluated in triplicates by immersing the 0.5×0.4 mm films into 2 mL of media consisting of 6×10^7 CFU of *Staphylococcus aureus* and *Klebsiella aerogenes*. The inoculated samples were incubated at 37 °C for 48 h. Further, the films were removed and gently rinsed with phosphate-buffered saline (PBS, pH 7.4) to remove the extracellular metabolites produced by the bacteria along with the planktonic cells. Bacteria attached to the surface of the films were stained with

crystal violet for 5 min. Further, the stained biofilm was washed by soaking it in PBS. The obtained stained biofilm is then treated with ethanol for 15 min. The resulting solution was collected and measured absorbance at 590 nm with a microplate reader.

2.5.4 Influence of the developed films on the pH of synthetic physiological saline (phosphate buffered saline)

The developed polymer samples nPLA, PLA-PG-C, and PLA-PG-P with a weight of 0.1 g were added separately in triplicates to the closed glass container and incubated with 5 mL of phosphate-buffered saline (PBS of pH 7.4) at 37 °C to mimic the physiological conditions [110]. The samples were collected in a particular interval of time and analyzed for the prodigiosin release and change in the pH of the solution. Here the PBS without a sample is used as a control.

2.5.5 *In vitro* biocompatibility study

The biocompatibility study was performed according to the existing protocol [111]. Briefly, the Baby Hamster Kidney Fibroblast (BHK-21) cell lines cultured in Dulbecco's modified Eagles medium (DMEM, Gibco) consisting of fetal bovine serum (10%) and antibiotic-antimycotic cocktail (1%) at 37 °C with 5% CO_2 in a humidified atmosphere for 24 h. The circular polymer samples were placed in the 96-well plate (Nunc) and seeded with DMEM consisting of BHK-21 cells. While 96 well plate without polymer samples was taken as control. After 24, 48, and 72 h of incubation, samples were treated with 100 µL of 3.7% formaldehyde for 10 min to fix the cells. Then it was treated with 100 µL of diamidino-2-phenylindole (DAPI) working solution (1 µg/mL). Further, the plate was incubated in the dark for 15 min. Samples were rinsed with PBS buffer thrice between each step. Finally, the cells were observed under the fluorescent microscope (Nikon H600L) using blue/cyan filter.

Characterization techniques used: UV-Vis spectrophotometry, color spectrophotometry, FTIR, EDX, TGA, TGA hyphenated with FTIR, POM, DSC, and Wettability analysis.

2.6 Fabrication of nanocellulose from waste sorghum bagasse

2.6.1 Materials

Waste sorghum bagasse obtained after juice extraction, sodium hydroxide (NaOH), sulfuric acid (H_2SO_4), hydrogen peroxide (H_2O_2, 30% w/v), lactic acid, sodium acetate, acetic acid, hydrochloric acid, and ethanol were obtained from Merck, India. Cellulase enzyme blend Cellic CTec2 (SAE0020, density ~1.15 g/mL) was obtained from Sigma Aldrich, India.

2.6.2 Sorghum bagasse selection, pretreatment, and characterization

The bagasse obtained after juice extraction was subjected to convection oven drying at 45±5 °C (NREL/TP-510-42620) until the constant weight to remove moisture completely. Further, the obtained biomass was ground and sieved by stacking the sieves in the following order, starting from the bottom: solid catch pan, 80 mesh sieve, and 20 mesh sieve. Then the ground biomass was subjected to sieving in a sieve shaker for 15±1 min. The fraction retained on the 80-mesh sieve (-20/+80 mesh fraction) was selected for compositional analysis. The material in the solid catch pan was the fines (-80 mesh) fraction and was retained for ash analysis. All the -20/+80 mesh batches were combined and weighed the fractions to ~0.1 g. This weight was recorded as $Wt_{20/80}$. The sieved samples were stored in sealable polyethylene bags and kept at -20 °C until further use.

To calculate the fraction percent of -20/80 mesh fraction, the following equation is used:

$$Fraction_{20/80}\% = \left[\frac{(Wt_{20/80})}{(Wt_{20/80} + Wt_{20/80})}\right] \times 100 \quad \ldots\ldots\ldots\ldots\ldots\ldots\ldots\ldots (1)$$

where; $Wt_{20/80}$=Weight of -20/+80 mesh fraction (g), Wt_{80}=Weight of fines fraction (g)

To calculate the fraction percent of -80 mesh fraction, the following equation is used:

$$Fraction_{80}\% = \left[\frac{(Wt_{80})}{(Wt_{20/80} + Wt_{80})}\right] \times 100 \quad \ldots\ldots\ldots\ldots\ldots\ldots\ldots\ldots\ldots\ldots \quad (2)$$

where; $Wt_{20/80}$=Weight of -20/+80 mesh fraction (g); Wt_{80}=Weight of fines fraction (g)

The ash content in the sorghum biomass was determined using the method NREL/TP-510-42622 in a muffle furnace with the following program:

Furnace Temperature Ramp Program: Ramped from room temperature to 105 °C, held at 105 °C for 12 minutes, ramped to 250 °C at 10 °C / minute, held at 250 °C for 30 minutes, ramped to 575 °C at 20 °C / minute, held at 575 °C for 180 minutes, allowed the temperature to drop to 105 °C, held at 105 °C until samples are removed.

Calculation of percentage ash on an oven dry weight (ODW) basis

$$\%Ash = \frac{Weight_{(crucible\ +\ ash)} - Weight_{(crucible)}}{ODW_{(sample)}} \times 100 \quad \ldots\ldots\ldots\ldots\ldots\ldots\ldots\ldots \quad (3)$$

2.6.3 Pretreatment of sorghum bagasse

The processed biomass was pretreated using sodium hydroxide (0.5-2.0 wt.%), followed by hydrogen peroxide (1-4%) treatment, lactic acid (0.5-2% w/v), sulfuric acid (0.5-2% v/v) at 121 °C, 15 lb for 10 min. The obtained mixture was filtered to separate the lignin from the cellulose. Figure 2.8 depicts images of the samples after each step in the alkaline hydrogen peroxide pretreatment (pH 11.5) process.

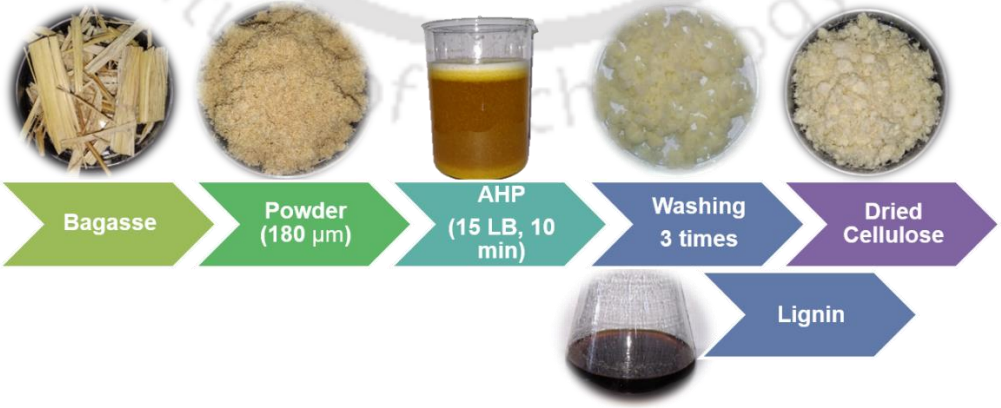

Figure 2.8. Preparation of sorghum powder and pretreatment of bagasse using alkaline hydrogen peroxide treatment.

2.6.4 Acid hydrolysis using sulfuric acid

The pretreated cellulose from the above process is mixed with 1:20 (w/v) of 50% H_2SO_4. Then the hydrolysis was carried out for 15, 30, 45, and 60 min at room temperature. Later the samples were centrifuged at 5000 rpm for 15 min and washed several times to bring the solution pH to ~5. Further, the obtained samples were subjected to dialysis using the cellulose acetate membrane of molecular weight ~14 KDa (Sigma Aldrich) to neutralize the pH. The complete process is shown in Figure 2.9**.**

2.6.5 Enzyme hydrolysis using cellulase

The enzyme hydrolysis was performed in 50 mL sample containers at 50 °C for 5 days. The experiment was performed by incubating the samples at 50 °C with a stirring speed of 100 rpm. 0.1 M sodium acetate buffer at pH 5 was used throughout the experiment. Different (0.1-1 g/g of cellulose) enzyme loadings were used in the experiment to optimize the enzyme loading.

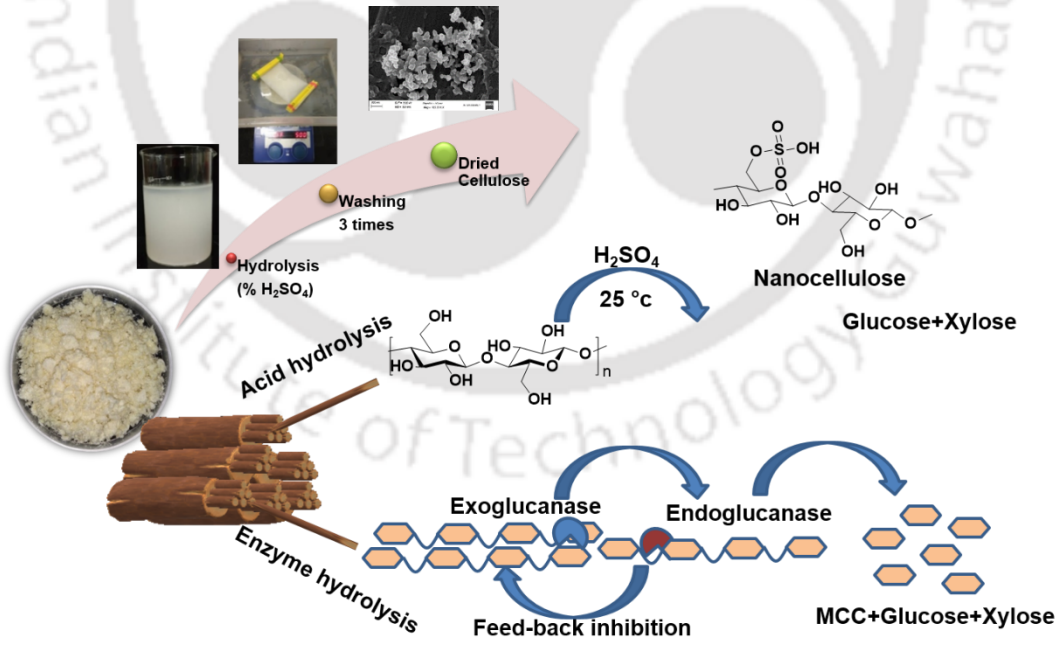

Figure 2.9. The process of sulfuric acid hydrolysis yielding the nanocellulose, and the enzymatic hydrolysis yielding the fermentable sugars glucose and xylose from AHP treated sorghum biomass.

2.6.6 *In vitro* cell cytotoxicity study

Samples analyzed: Prodigiosin, PHB, and metal-free PLA synthesized using prodigiosin as a catalyst.

Dulbecco's modified Eagle's medium (DMEM, Gibco™) was used to culture the Baby Hamster Kidney Fibroblast cells (BHK-21) in T25 flasks. The DMEM is supplemented with fetal bovine serum (10%, FBS) and a 1% antibiotic-antimycotic cocktail. The cells were incubated in a CO_2 incubator at 37 °C with 5% carbon dioxide in a humidified atmosphere. Further, the cells were counted using Countless® II FL cell counter (Thermo Fisher Scientific) after staining with trypan blue. The cells were diluted to the desired concentration and seeded 100 µL (10×10^3/well) into a 96-well plate containing a growth medium. Further, it was incubated for 24 h at the desired growth conditions.

Mitochondrial activity of BHK-21 cells was performed by seeding the cells into 0.25, 0.50, 1.00, and 2.00 mg/mL of prodigiosin samples dissolved in 20% dimethyl sulfoxide (DMSO) and subsequent incubation for 48 h to check the cytotoxicity. 20% DMSO diluted in DMEM was used as solvent control. The 3-(4,5-dimethylthiazol-2-yl)-2,5-diphenyl tetrazolium bromide (MTT) (5 mg/mL in PBS) was added to the plate-containing cells and incubated in a CO_2 incubator at 37 °C for 3 h. Further, the MTT reagent was replaced with DMSO (100 µL), and the resulting cell viability was measured using a 96-well plate reader (Thermo Fisher Scientific) at 570 nm. This optical density was used for the calculation of cell viability.

2.7 Analytical instrumentation and characterization

2.7.1 Ultra-high-performance liquid chromatography (UHPLC)

The sugar content in sorghum juice, residual sugar of the fermentation broth, and hydrolysate after enzyme saccharification was analyzed using a UHPLC system (Dionex Ultimate™ 3000) (ThermoFisher Scientific) equipped with quaternary pump (LPG-3400SDN) and a column oven (HCO-02, PCI Analytics Pvt. Ltd.). Separation was performed using Aminex® HPX-87H

(300 mm × 7.8 mm) (Bio-Rad Laboratories) column with 0.005 N sulfuric acid as eluent. The samples were detected using a refractive index detector (RefractoMax521) supplied with Chromeleon data system (6.80 DU13a). Glucose, fructose, and xylose (500-3000 ppm) were used as standards.

2.7.2 UV-Vis spectroscopy

The concentration of the prodigiosin, crotonic acid, and simulated body fluid containing congo red was determined using a UV-visible spectrometer (PerkinElmer, Lambda 25) at a wavelength of 535 nm, 208 nm, and 498 nm, respectively. The effect of pH on prodigiosin and the transparency of the prodigiosin-loaded films (dimensions 50×20 mm, the average thickness of ~110 µm) were analyzed in the wavelength range of 700-200 nm.

2.7.3 Field emission scanning electron microscopy (FESEM)

The surface morphology of PHB Microspheres, *Bacillus megaterium* with intracellular PHB granules, nanocellulose, and prodigiosin-loaded PLA films were investigated using FESEM. The sample preparation was performed by fixing the samples onto the surface of the aluminum sample holder using carbon tape. Then the samples were sputter-coated in a sputtering unit (Quorum Sc7620, sputtering condition: 10 mA for 180 s at 10^{-1} mbar) with a thin layer of gold and observed under FESEM (Zeiss, Sigma 300). The prodigiosin-loaded PLA films (nPLA, PLA-PG-C and PLA-PG-P), after 48 h of incubation were taken out, washed with PBS buffer and dried at 60 °C to remove the moisture completely, and subjected to imaging.

2.7.4 Field emission scanning electron microscopy-energy dispersive x-ray spectroscopy (FESEM-EDX)

The morphological characterization and compositional analysis of the sorghum juice and prodigiosin-loaded PLA films were performed using FESEM (Zeiss, Sigma) coupled with an energy-dispersive X-ray spectroscopy system (EDX) (Oxford Instruments, UK) at an

accelerating voltage of 20 kV. The sorghum juice was drop casted on aluminum foil and dried in a hot air oven at 60 °C for 24 h to remove moisture completely and analyzed.

2.7.5 Fourier transform infrared spectroscopy (FTIR)

The Fourier transform infrared spectra (FTIR) (PerkinElmer, Frontier spectrometer) of the powdered samples (pelletized with KBr) were analyzed in diffusive reflectance spectroscopy (DRS mode) using neat KBr pellet as background. Whereas the polymer films were analyzed in an attenuated total reflectance (ATR mode) in the spectral range of 4000-500 cm^{-1} at a scan rate of 4 scans/sec.

2.7.6 Thermogravimetric analysis (TGA)

Thermal stability and the degradation behaviors of the obtained prodigiosin, PLA, PHB, prodigiosin-loaded PLA, PHB microspheres, and nanocellulose (7-10 mg) were studied under the nitrogen atmosphere using a thermogravimetric analyzer (TGA 4000, PerkinElmer) with a temperature ramp from 30-700 °C at a heating rate of 10 °C/min. The inert atmosphere was maintained by passing the high-purity nitrogen at 20 mL/min.

2.7.7 Wettability analysis

The surface wettability of the PHB films, prodigiosin-loaded PLA films, and the 3D-printed hepatic vascular phantom was analyzed using a drop shape analyzer (DSA 25, Kruss) equipped with a CCD camera. The hepatic phantom was placed on the stage and dropped with 4 µL of SBF; further, the images were recorded at different time intervals for the determination of wetting behavior/contact angle. For all other samples, water (Millipore®) was used as a wetting agent, and analysis was performed at room temperature. The film samples were prepared by cutting into small pieces (1 cm × 1 cm), pasted onto the glass slide using double-sided tape, and dropped with 4 µL of deionized water

2.7.8 Microscopy

The obtained microspheres were analyzed using polarizing optical microscopy, and the fluorescent microspheres were analyzed using Nikon H600L equipped with fluorescent source Nikon Intenslight C-HGFI using blue/cyan filter.

2.7.9 Viscosity measurement

The viscosity of the SBF was measured using a capillary viscometer having a transparent viscosity thermostat (CT 72/2, SI Analytics) equipped with Pt 100-PID heater connected to a chiller (Siskin profichill) to maintain the temperature of the SBF at 25 ± 0.3 °C.

2.7.10 Antibacterial activity

The antibacterial activity of prodigiosin was determined against *Staphylococcus aureus* (2.4×10^7 CFU/mL) by measuring the zone of inhibition (mm) using antibiotics cephalothin, gentamicin, and amikacin as reference antibiotics for comparison.

2.7.11 Matrix-assisted laser desorption ionization-time-of-flight mass spectrometry (MALDI-TOF-MS)

The extracellular AHL was identified by extracting *Serratia nematodiphila* culture broth twice with acidified ethyl acetate (0.5% acetic acid), and further, it was allowed to dry at 45 °C to remove the solvent completely. The molecular mass of the prodigiosin, gluconic acid, AHL, and metal-free PLA was determined by matrix-assisted laser desorption ionization time-of-flight mass spectrometer (MALDI-TOF-MS) (Bruker, AUTOFLEX SPEED) at an accelerating voltage of 19 Kv with 500 spectrum scans. The samples were prepared by mixing 5 mg/mL of the sample in methanol with 2,5-dihydroxybenzoic acid (10 mg/mL, DHB, methanol). Then the sample solution and matrix were mixed in a ratio of 2:1, and 2 µL of the sample was loaded onto a stainless-steel sample plate, allowed to dry, and analyzed.

2.7.12 Color properties

The characteristic color coordinates (L*, a* and b*) of the prodigiosin solution at different pH and prodigiosin-loaded PLA films were recorded using Datacolor-550 spectrophotometer (Datacolor Technology Co., Ltd.), where L* indicates lightness (+ve is lighter, -ve is darker), a* is red/green coordinate (+ve is reddish, -ve is greener), and b* is yellow/blue co-ordinate (+ve is more yellow, -ve is bluish). ΔL*, Δa*, and Δb* might be either positive (+) or negative (-), but the total difference ΔE is always positive (+), c* is chroma, and h is hue.

2.7.13 Nuclear magnetic resonance (NMR) spectroscopy

The synthesized polymer samples and prodigiosin were analyzed using ^{13}C and ^{1}H nuclear magnetic resonance spectroscopy (NMR). The samples were prepared by dissolving the polymer in the deuterated chloroform ($CDCl_3$) and then filtered through a 0.2 µm syringe filter to remove any undissolved particles. The obtained samples were placed in an NMR tube and analyzed using a 600 MHz nuclear magnetic resonance (NMR) spectrometer (Bruker, Ascend^{TM} 600, Germany).

2.7.14 Gel permeation chromatography (GPC)

Number average [M_n], weight average [M_w] molecular weights, and polydispersity index (PDI) of the synthesized polymers were analyzed using Shimadzu's Prominence GPC (Prominence GPC RID-10A detector). Separation was performed using the PL gel 5 µm (300 × 7.5 mm) columns, and the polystyrene standards in chloroform were used for calibration to get relative molecular weight.

2.7.15 Differential scanning calorimetry (DSC)

The thermal properties of polymers were studied using differential scanning calorimetry (DSC 204 Phoenix®, Netzsch). The following conditions were maintained during the analysis of PLA: temperature ramp from 30-200 °C at a rate of 10 °C/min, isothermal state for 2 min at

200 °C. Further, cooling from 200-30 °C at a rate of 10 °C/min, isothermal state for 2 min at 30 °C, and finally, the second heating from 30-200 °C at a heating rate of 10 °C/min.

The following conditions were used during the analysis of PHB: temperature ramp from 30-190 °C at a rate of 10 °C/min, isothermal state for 2 min at 190 °C. Further, cooling from 190--20 °C at a rate of 10 °C/min, isothermal state for 2 min at -20 °C, and finally the second heating from -20-190 °C at a heating rate of 10 °C/min.

2.7.16 Thermogravimetric analysis hyphenated with Fourier transform infrared spectroscopy (TG-FTIR)

TGA-FTIR analysis was performed for prodigiosin-loaded PLA film to determine the gases released during the thermal degradation process. The thermogravimetric analyzer (TGA 4000, PerkinElmer) coupled with an FTIR spectrophotometer (Frontier, Perkin Elmer) was used for the analysis. The spectrum was collected in the range of 4000-450 cm^{-1} with a temperature from 30-700 °C at a heating rate of 10 °C min^{-1}.

2.7.17 Polarizing optical microscopy (POM)

The POM (Nikon H600L, Japan) was used to study the nucleation behavior and spherulite growth of the developed prodigiosin-loaded films. The samples were mounted on the stage and heated to 200 °C at a rate of 50 °C/min, and thermal history was erased by holding them for 3 min. Further, the samples were cooled to 120 °C at a rate of 50 °C/min and recorded the micrographs for 40 min at 10 min intervals.

Olympus BX 51 polarizing optical microscope equipped with Linkam hot stage was used for the analysis of PHB samples. The films were heated to 190 °C at a heating rate of 10 °C/min held isothermally for 3 min and cooled to 110 °C at 10 °C/min and images were recorded at 110 °C.

The obtained micrographs were used to analyze the morphology and growth rates of the crystals. The number of spherulites per area resulted in the crystal density. The slope obtained

by plotting the spherulite radius (R) v/s time of crystallization (t) resulted in the growth rate of the spherulite (G).

2.7.18 Field emission transmission electron microscopy (FETEM)

The morphological investigations and accumulation of PHB granules in *Bacillus megaterium* during fermentation were confirmed using FETEM (JEOL, JEM 2100F, Japan) at an accelerating voltage of 200 kV. The sample preparation was performed by drop casting of cells onto the carbon-coated grids (Tedpell, USA), followed by drying at 60 °C in a vacuum for 24h.

2.7.19 X-ray diffraction (XRD)

PHB samples were analyzed using a D8 Advance diffractometer (Bruker, Germany), equipped with Cu-Kα radiation (λ=0.1541 nm) X-ray source with an operating voltage of 40 kV. The samples were scanned at a rate of 0.05°/0.5 sec with a 2θ range from 10-80°.

CHAPTER 3

Production of Polyhydroxybutyrate (PHB) from Waste Sorghum Stalks as Raw Material

Graphical Overview

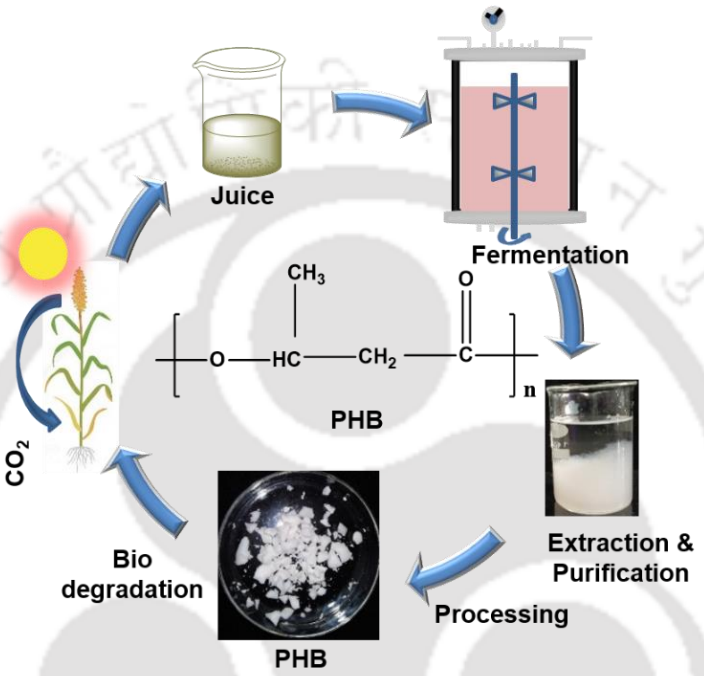

Polyhydroxybutyrate (PHB) is a biodegradable polymer obtained from bacteria as an energy reserve of excess carbon. In the current work, the agricultural waste sorghum stalks were used for the extraction of juice consisting of ~60 g/L of fermentable sugars. Media optimization was performed using JMP statistical software with a sugar concentration of 10-50 g/L, a nitrogen concentration of 2-10 g/L, and 5-10% inoculum of *Bacillus megaterium*.

Patent:

- Vimal Katiyar, Chethana Mudenur, and Amit Kumar. Process of production of polyhydroxybutyrate [PHB] from wild grasses. Indian Patent Application Number: 202131031003

Further, the optimized condition was selected for the scale-up of fed-batch operation using the dissolved oxygen (DO) control strategy. This process yielded up to 8 g/L of PHB within 24 h of cultivation. DO controlled strategy was helpful in the process improvement. Further, the solvent extraction using acetone followed by chloroform yielded 94% recovery. The produced PHB from sorghum biomass exhibited crystallization temperature T_c from 101 to 105 °C, glass transition temperature T_g from -8 to -10 °C, melting temperature from 162-175 °C, maximum degradation temperature (T_{max}) of 318 °C, and wettability from 79-93 °C which are comparable to commercial PHB. Additionally, the produced PHB was subjected to *in vitro* cytotoxicity assay, and the results revealed it does not induce any cytotoxic effects on BHK-21 cells.

3.1 Introduction

Plastics and their products are of global importance, and the quality of life has been improved because of their easy availability and weightlessness with added mechanical properties. However, their residual nature in the environment is preventing its usage due to environmental concerns. These concerns and challenges are the driving forces for the selection of the alternatives such as biodegradable plastics to meet the zero-carbon target. Reducing the carbon emission level is the topmost concern in reducing global warming. Biodegradable plastics, without any impact on the environment, have increased attention as an alternative to conventional plastics [112].

The most investigated plastics in the development of biocompatible plastics are polyhydroxyalkanoates (PHAs). These are polyesters of microbial origin; their elasticity, stiffness, and crystallinity are easily tunable by changing the composition of the monomer [113]. PHAs are such bioplastics regarded as intracellular energy storage material synthesized by bacteria [114]. The major homopolymer of the PHA family is the PHB which is also a widely studied polymer for biomedical applications and is degraded enzymatically by PHB depolymerase. However, the drawback associated with PHB production is the high cost of the

carbon sources used in the production. The cost of PHAs is not competitive enough to the fossil-based plastics. There are wide varieties of carbon sources explored till now at the lab scale, with limited scope for commercialization due to their least availability and cost. The carbon sources which are commercialized include pure glucose, plant oils, camelina seeds, CO_2, sugar beet and sugar cane. Thus, there is a need to explore alternative inexpensive carbon sources which are abundantly available in nature. One such major carbon source that falls under this category is waste sorghum stalks with competitive sugar content in comparison to sugarcane.

The current work is focussed on the utilization of widely available inexpensive waste sorghum biomass for the production of PHB with competitive production yield and product properties. Sorghum is a major crop in many parts of India, and there are two varieties, namely, sweet and grain sorghum. Sweet sorghum is primarily grown for syrup production, whereas grain sorghum is cultivated for grains, and the stems are discarded after harvesting the grains. The main aim here is to efficiently use the stalks of the grain sorghum for the production of PHB. More than 300 microorganisms are capable of producing PHB [115] as intracellular PHB granules as storage of carbon and energy under stress with limited nitrogen and an excess of carbon source [116].

3.2 Results and discussion

3.2.1 Composition of sorghum juice

The HPLC results of sorghum juice indicate the total fermentable sugar content of ~60-70 g/L consisting of fructose and glucose. The FESEM-EDX spectra in Figure 3.1 shows the presence of oxygen (46.8 At%), carbon (46.7 At%), potassium (2.4 At%), nitrogen (2.2 At%), chlorine (1.3 At%), calcium (0.2 At%), magnesium (0.2 At%), manganese (0.1 At%). Trace elements are essential for growth and metabolism that are co-ordinated by a complex metal management

system. The sorghum juice provides all the essential minerals required for *Bacillus megaterium* to grow and produce PHB.

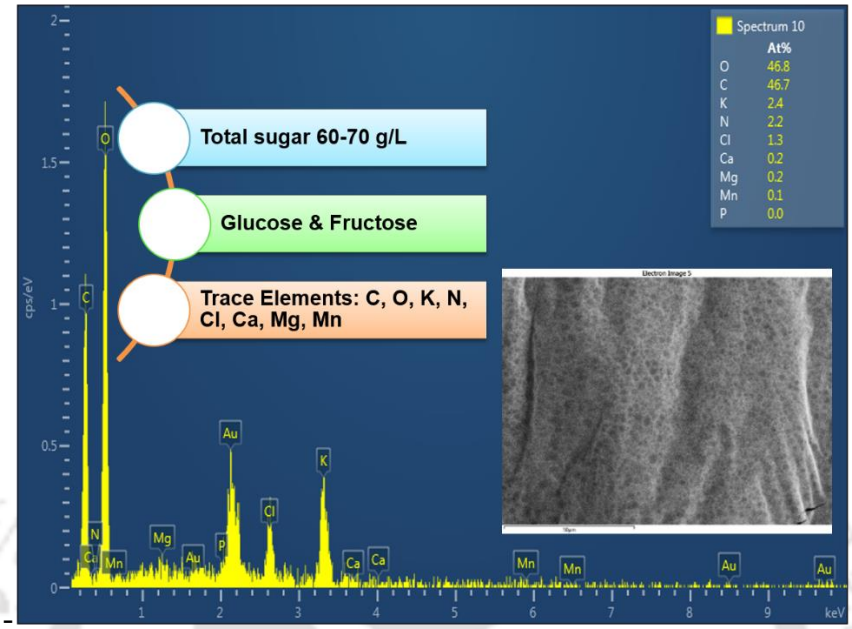

Figure 3.1. FESEM-EDX analysis of the sorghum juice depicting the presence of minerals. The sorghum juice provides all the essential minerals required for *Bacillus megaterium* to grow and produce PHB.

3.2.2 Screening and optimization of the media components using one-factor at a time (OFAT)

The various nitrogen sources affecting cell growth and PHB production were investigated using a one-factor-at-a-time method. The experiments were performed using the shake flask at optimum temperature of 37 °C yielded the PHB in the order of $NaNH_4HPO_4.4H_2O$ (0.98 ± 0.24 g/L) > tryptone (0.73 ± 0.01 g/L) > peptone (0.72 ± 0.04 g/L) > meat extract (0.68 ± 0.11 g/L) > yeast extract (0.55 ± 0.18 g/L). The results indicate that the $NaNH_4HPO_4.4H_2O$ is the most preferred nitrogen source, and it has further opted for the optimization experimental runs.

The central composite design was used to optimize the concentration of carbon, nitrogen, and inoculum by JMP statistical tool. The prediction profiler shown in Figure 3.2 is an interactive profiler, and the red lines in the vertical position correspond to the current values of the factors.

Whereas the horizontal lines refer to the resulting responses. The profiler interactively generates the predictions through a variety of factors at various levels concerning the responses. It finds the optimal settings of carbon, nitrogen, and inoculum concentration for the set response variables such as cell dry weight and the PHB production. Maximizing desirability means the maximization of product formation. The desirability function can be seen for each response. The overall desirability of ~0.745 is a geometric mean of the desirability functions for CDW and PHB. The plot shows the desirability trace for each factor.

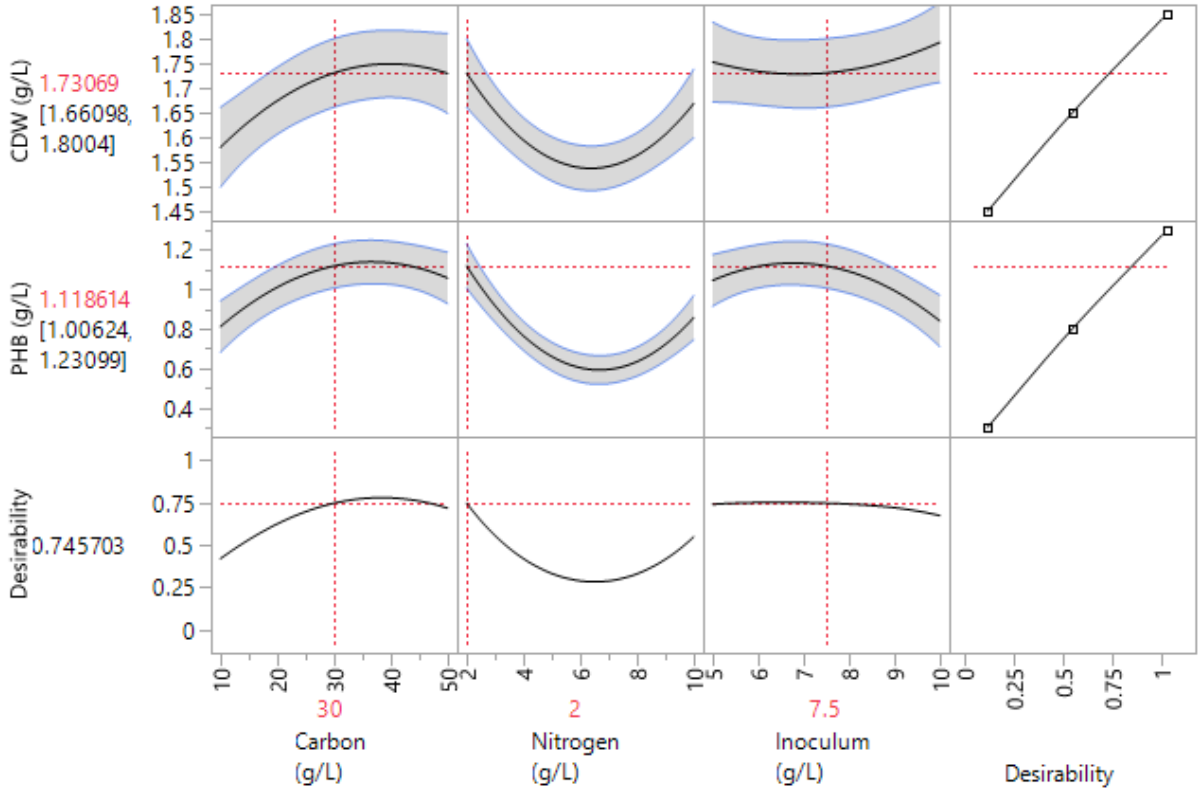

Figure 3.2. The prediction profiler indicates the response against the tested factors.

The product PHB is the main response in the experiment. The prediction against the actual plot shown in Figure 3.3 depicts the effect of the model and its comparison against the null hypothesis. The predicted root mean square error from the model was found to be 0.063, the value of R^2 was found to be 0.97, and the p of 0.0006. The actual values close to the predicted model values show a good fit with a narrow confidence band.

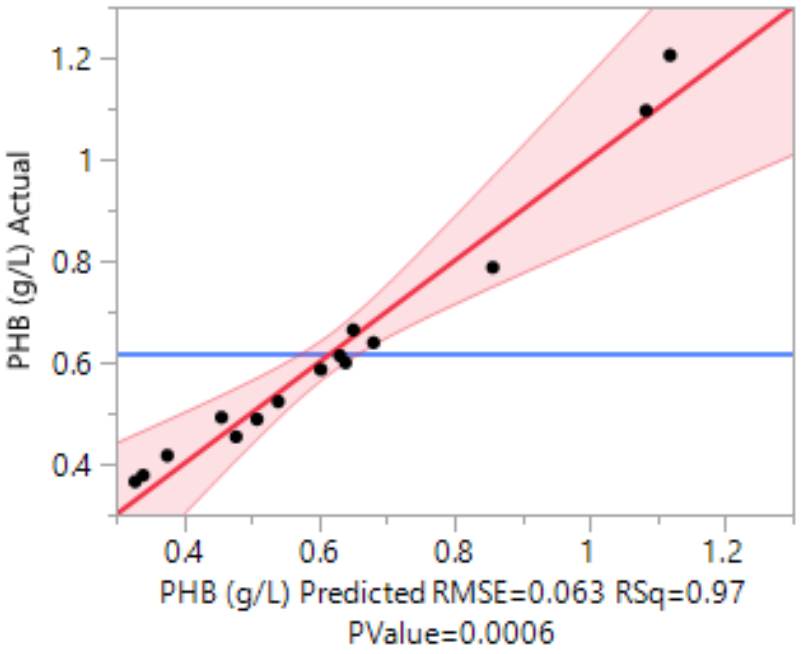

Figure 3.3. The actual by the predicted plot for PHB production.

3.2.3 Enhancement of PHB production by improved fermentation strategies

The batch fermentation of *Bacillus megaterium* was performed to determine the time evolution, cell biomass, consumption of carbon, and formation of PHB granules. Figure 3.4 shows the profile for a minimal medium supplemented with 30 g/L of sorghum juice as a carbon source. The DO was controlled at 60% without additional carbon and nitrogen sources. Here as the cells enters into exponential phase, the PHB started to increase gradually, whereas, the DO and sugar concentration started to fall due to the exponential utilization for cell growth and product formation. When DO fall to 60%, it was controlled throughout the batch to check the effect of DO on product formation. The PHB production in *Bacillus megaterium* is growth associated. PHA production by bacteria is completely dependent on carbon, nitrogen, and other nutrients provided in limited quantities to induce stress, which leads to the formation of intracellular PHA granules. During cell growth, oxygen consumption exceeds the maximum oxygen transfer capacity, which limits cell growth. Thus, a solution to pass an adequate amount of oxygen is by decreasing the specific growth rate. Usually, the DO control strategy helps to control the dissolved oxygen at a constant value using a substrate fed at a specific rate. Once

the carbon source is exhausted in a logarithmic growth phase, the value of O_2 rapidly increases due to hypoxia and cell death. If the carbon and nitrogen sources fed timely, the O_2 value decreases as the cell starts reutilizing the carbon source and restoring its growth. Subsequently, a constant DO level can be maintained by continuous feeding and keeping a balance between oxygen consumption and supply. The DO control strategy experiment has been conducted to increase the yield. This strategy is based on the inline monitoring of DO value, which tends to increase when the substrate was depleted completely. Thus, signals for feeding of sugars into the fermenter.

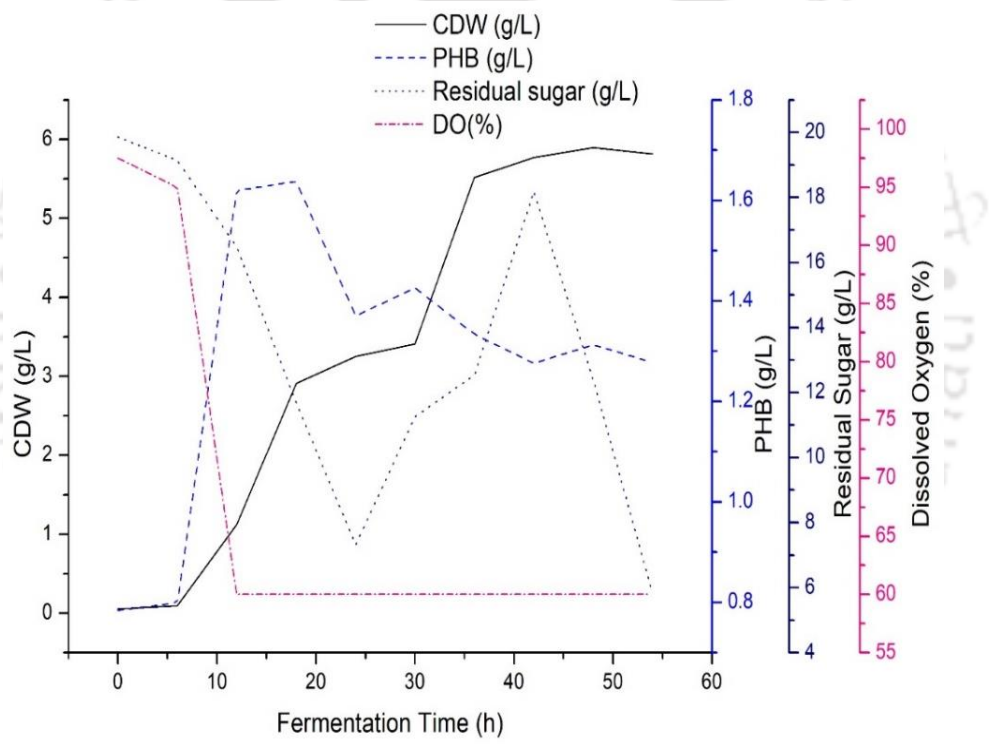

Figure 3.4. Batch fermentation profile of *Bacillus megaterium* in a culture medium supplemented with 30 g/L of sorghum juice with maximum production at 18 h of incubation.

Fed-batch fermentation was performed with different DO strategies. The fed-batch fermentation yielded the higher biomass in which in less than half the time required for the

production of PHB. Figure 3.5 indicates the response obtained for cell biomass and PHB yield using the dissolved oxygen control strategy.

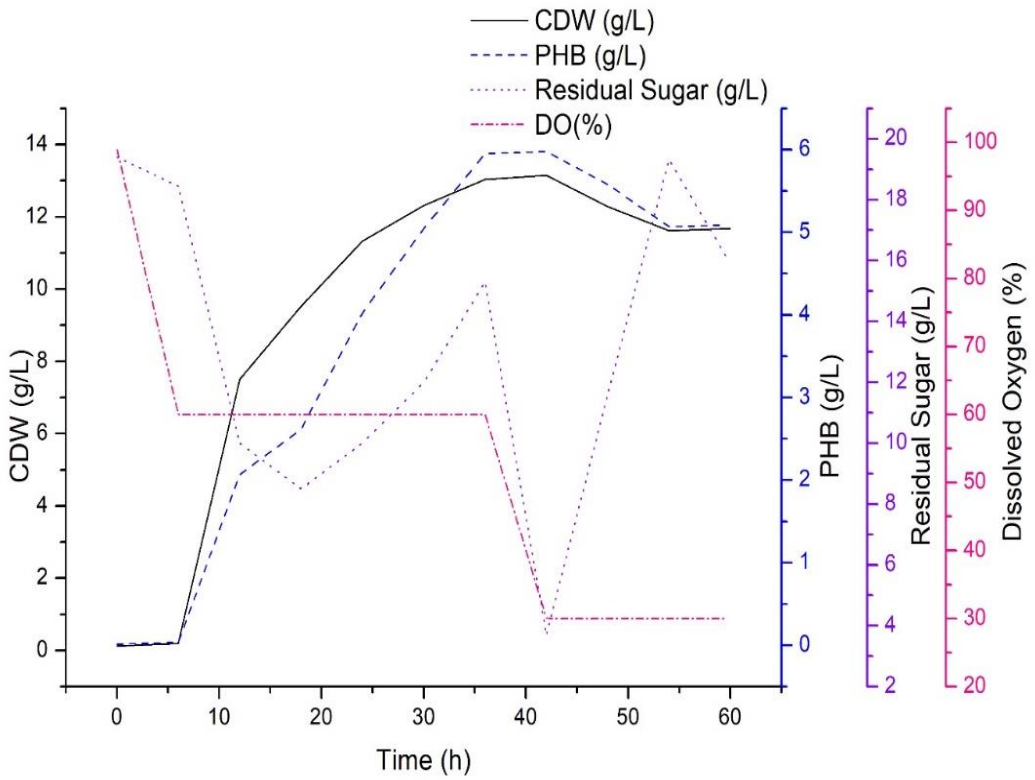

Figure 3.5. Fed-Batch fermentation profile of *Bacillus megaterium* in a culture medium supplemented with sorghum juice with applied DO strategy (i) 100-60% without control (ii) 60-30% after 36 h of incubation.

Table 3.1 depicts an overall summary of the batch and fed-batch operation using the *Bacillus megaterium* as a PHB producer and sorghum juice as a carbon source. The data is compared with *Bacillus aryabhattai* and *Alcaligenes latus* instead of *Bacillus megaterium*, and the carbon source is compared with sweet sorghum juice instead of grain sorghum juice due to the limited data availability.

$$DCW\ (g/L) = \frac{Weight\ of\ dry\ cell\ biomass\ (g)}{Reaction\ volume\ (L)}$$

$$PHB\ (g/L) = \frac{Weight\ of\ PHB\ (g)}{Reaction\ volume\ (L)}$$

$$PHB\ accumulation\ (\%) = \frac{Dry\ weight\ of\ extracted\ PHB\ (g/L)}{DCW\ (g/L)}\ X\ 100$$

Table 3.1. Summary of the PHB production and its comparison with some previous fermentation strategies.

Sl no	Fermentation Strategy	Bacteria/carbon source	Biomass (g/L)	PHB (g/L)	PHB Accumulation (%)	Reference
1	Shake flask	*Bacillus aryabhattai* PKV01 /Sweet sorghum juice	2.8	1.1	39.3	[8]
2	Shake flask	*Bacillus megaterium* /grain sorghum juice	1.7	1.2	**70.6**	This study
3	Batch	*Alcaligenes latus* ATCC 29714/ Sweet sorghum juice	1.73	0.68	39.3	[117]
4	Batch	*Bacillus megaterium* /grain sorghum juice	3.0	1.7	**56.7**	This study
5	Fed-batch	*Cupriavidus necator*/fructose	35.5	17	47.8	[118]
6	Fed-batch	*Bacillus megaterium* /grain sorghum juice	17	8.4	**49.5**	This study

Table 3.2 indicates the overall result for the maximum PHB production of 8.2 g/L using the fed-batch fermentation strategy. The determination of the yield coefficient is important to decide the efficiency of the process, which depicts the conversion of sorghum juice to PHB. It also decides the cost viability of the medium used in the production of PHB, particularly the carbon source. The fed-batch strategy converts used in the current work convert 21% of the

fermentable sugars of the sorghum juice into PHB. The rest is utilized for cell growth and cellular maintenance.

Table 3.2. Summary of the PHB production, yield, and productivity obtained for *Bacillus megaterium* using sorghum as a carbon source.

1	Bacteria used for PHB synthesis	*Bacillus megaterium*
2	Carbon source	Sorghum juice
3	PHB (g/L)	8.4
4	$Y_{P/S}$ (g/g)	0.21
5	Productivity (g/L.h)	0.33

3.2.4 Purification and characterization of PHB

PHB granules are important storage materials of carbon and energy in many bacteria, which permit the cells to survive in the absence of suitable carbon sources [119]. Figure 3.6 represents the various phases involved in PHB biosynthesis. The first phase involves the growth phase, where the cell utilizes the carbon source for cell growth. The second phase involves an exponential phase where the bacteria utilizes the carbon source for cell growth and PHB accumulation. The third phase is only an accumulation phase where the bacteria utilizes the nutrients only for the biosynthesis of PHB, and there is no utilization for its growth.

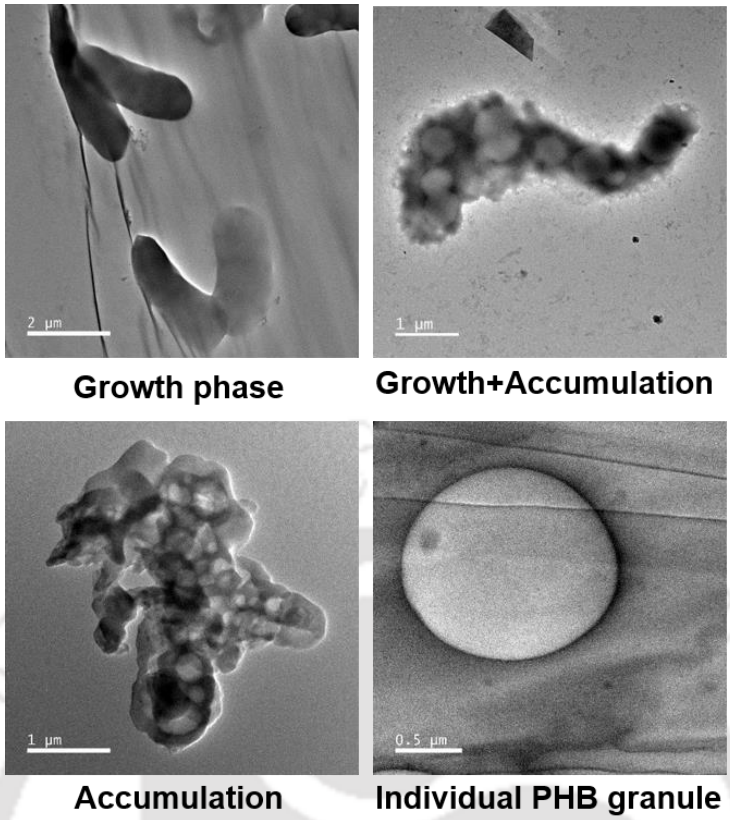

Figure 3.6. The stages involved in the accumulation/formation of PHB granules in *Bacillus megaterium*.

The extraction of PHB was performed with different solvents, in which the acetone pretreatment followed by chloroform extraction yielded the maximum recovery of 94%, shown in Table 3.3. The acetone is considered less toxic and acts as a degreasing agent, and helps in cell permeability by partitioning into the water-free region of the lipid bilayer located near the carbonyl groups of the phospholipids [120]. Thereby increasing the extraction efficiency. Whereas the chloroform yielded less recovery due to less penetration inside the *Bacillus megaterium*. The cell biomass and the effect of solvent on the release of PHB are analyzed through FESEM imaging and are depicted in Figure 3.7.

Table 3.3. Effect of extraction solvents on the recovery of PHB.

Extraction method	Extraction Time (h)	PHB/CDW (g/g)	Recovery (%)
Chloroform (Reflux at -70 °C)	24	0.28	46
Acetone/Chloroform (Reflux at -70 °C)	24	0.56	94
Methanol/Acetone (60 °C)	24	0	0

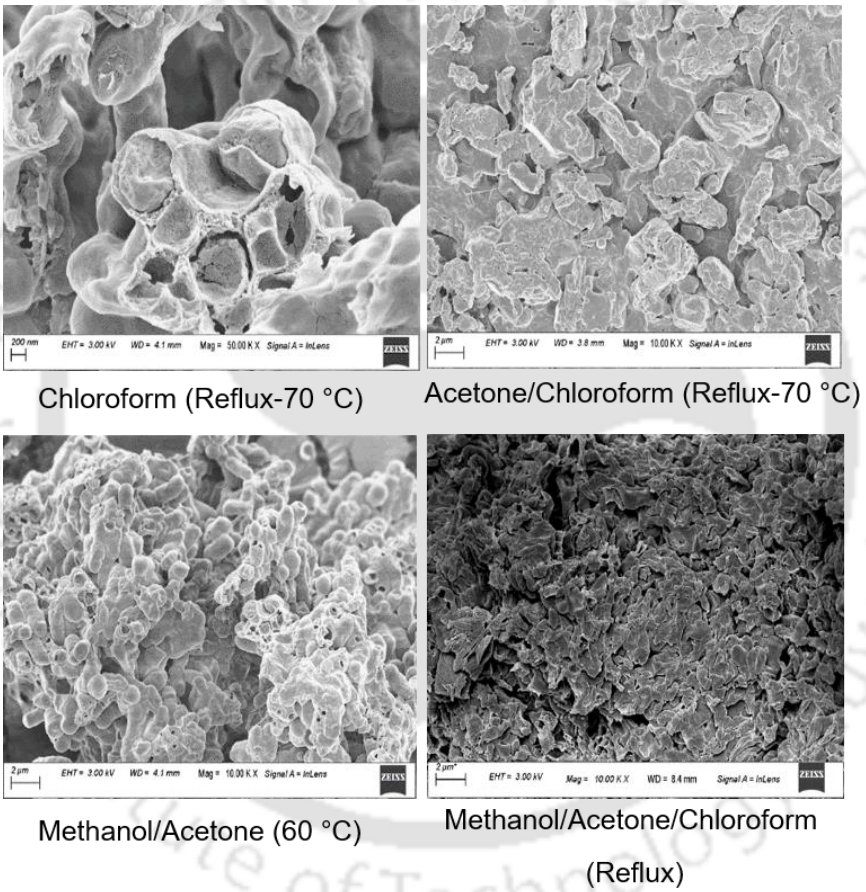

Figure 3.7. Disruption of cells after the treatment with organic solvents.

^{1}H NMR was then carried out. The spectrum given in Figure 3.8 shows the presence of three groups of signals characteristic of the homopolymer PHB. A doublet at 1.29 ppm is attributed to the methyl group coupled to one proton, a doublet of quadruplet at 2.57 ppm is attributed to a methylene group adjacent to an asymmetric carbon atom bearing a single proton, and a multiplet at 5.27 ppm characteristic of the methyne group. ^{13}C NMR spectrum depicts the

chemical shifts at 169 ppm depicts the presence of -CO-, 67.8 ppm for -CH-, 40.2 for -CH_2-, and 19.9 was assigned to -CH_3. Triplet at 77 ppm is due to the solvent $CDCl_3$.

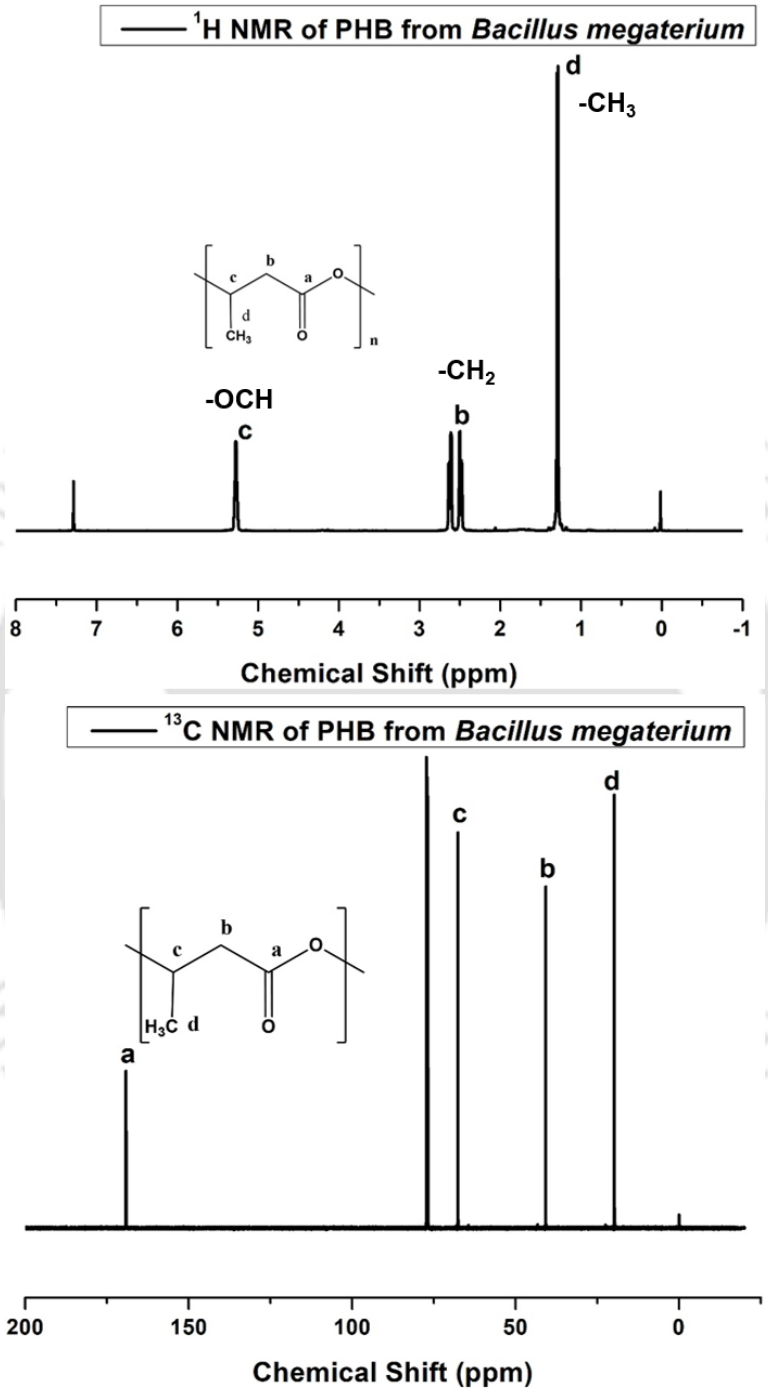

Figure 3.8. ^{1}H NMR and ^{13}C NMR of polyhydroxybutyrate.

The IR spectra shown in Figure 3.9 revealed an intense band at 1720 cm^{-1} associated with the C=O stretching, which corresponds to the characteristic ester carbonyl group of

polyhydroxyalkanoates. At 1181 cm^{-1} is due to asymmetric stretching vibration of the C-O-C group. The C-H stretching at 2900 cm^{-1} is due to the methyl and ethyl groups. The obtained FTIR spectrum of the polymer produced by *Bacillus megaterium* is in good agreement with the corresponding spectrum to the commercial PHB.

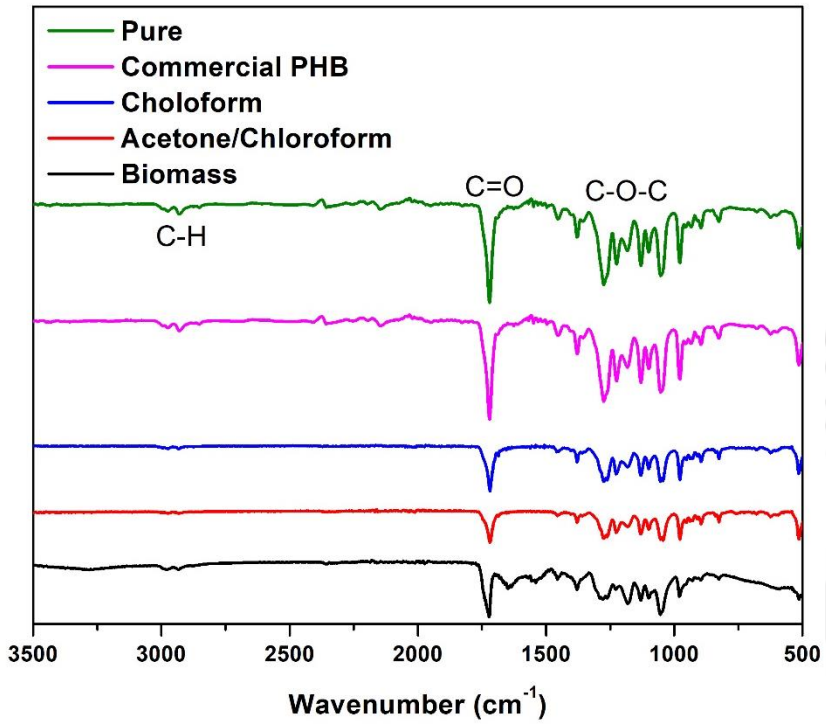

Figure 3.9. FT-IR spectra of *Bacillus megaterium*, extracted PHB, and the commercial PHB.

The microstructure, surface morphology, and chemical composition of PHB samples were studied using field emission scanning electron microscopy coupled with energy dispersive spectroscopy. Figure 3.10 shows the microstructure of the PHB produced from *Bacillus megaterium.* Compositional analysis results in the presence of 81.2% carbon and 18.8% oxygen. The microstructure depicts a fairly porous material with a strong tendency to form aggregates.

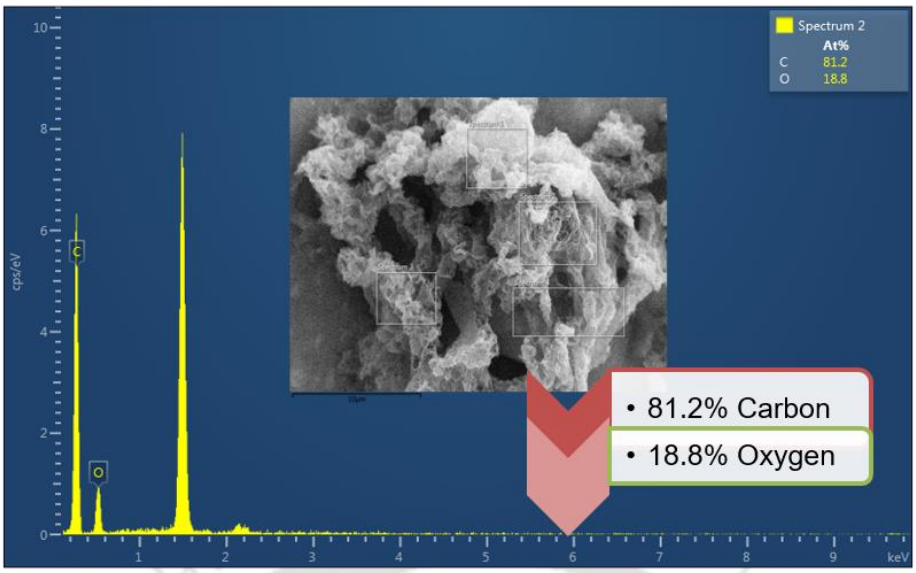

Figure 3.10. FESEM/EDX image of the PHB indicating the elemental composition.

The thermal degradation behavior of the PHB under a nitrogen atmosphere is shown in Figure 3.11. It is apparent from the curve that the PHB exhibits one-step degradation at a temperature with a maximum degradation temperature of 253 °C. Whereas, the PHB-rich *Bacillus megaterium* biomass degraded faster than pure PHB with two-step degradation due to the presence of peptidoglycan layer [121].

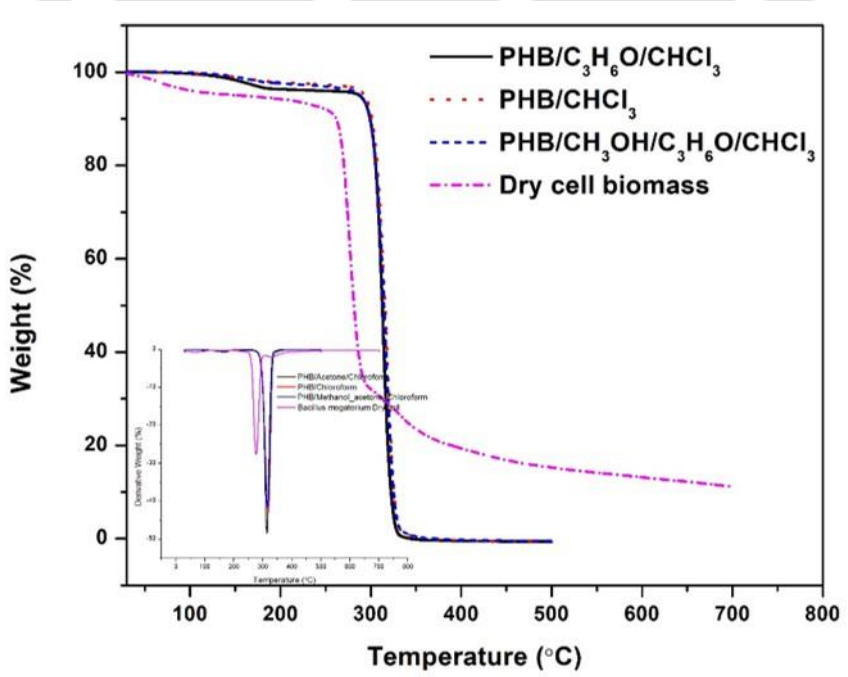

Figure 3.11. TGA and DTG curves of *Bacillus megaterium* and obtained PHB**.**

The thermal properties of PHB were determined using differential scanning calorimetry. The obtained DSC thermograms are shown in Figure 3.12. The melting temperature (T_m), and glass transition temperature (T_g) decide the conditions suitable for polymer processing. The curve obtained from the second heating depicts a melting temperature (T_m) of ~170 °C. Crystallization temperature was observed at (T_c) at 105 °C. The glass transition temperature (T_g) was determined at -8 °C.

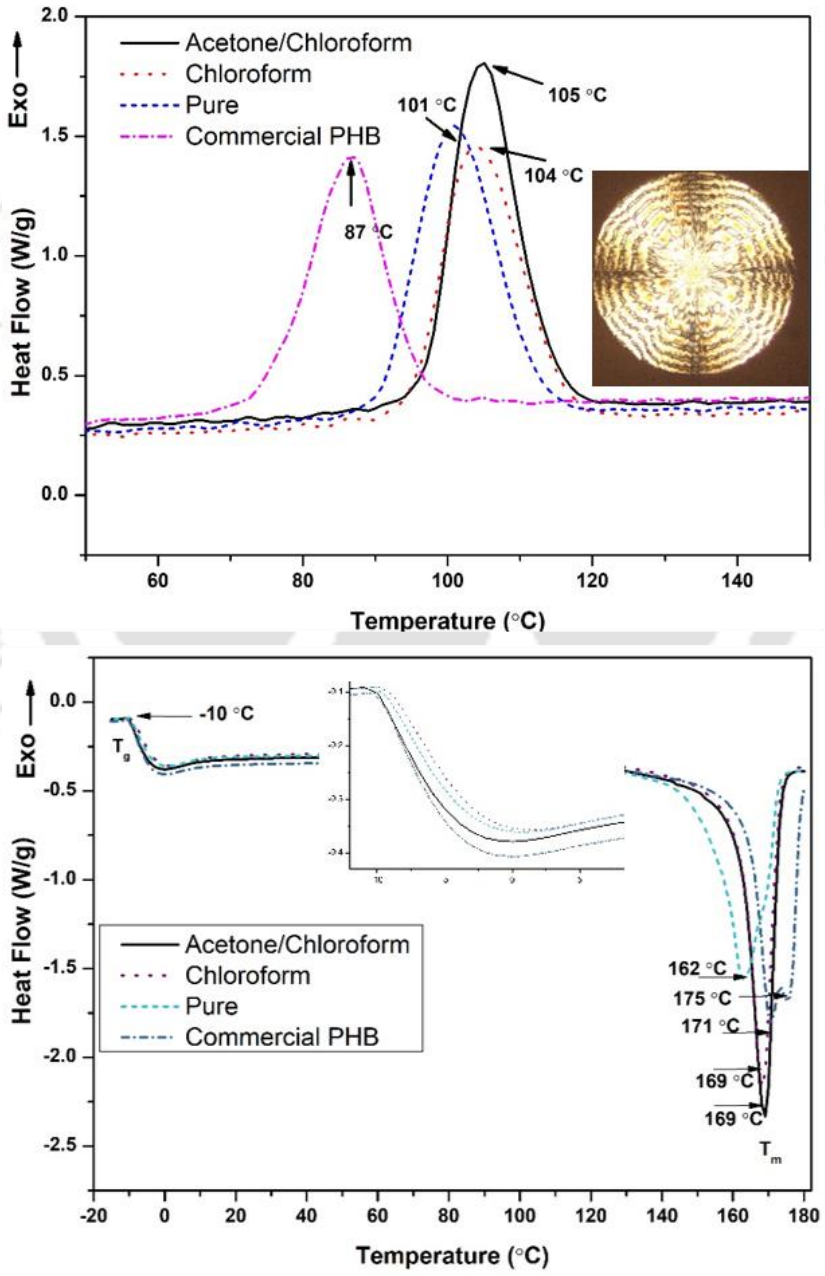

Figure 3.12. DSC thermograms of produced PHB.

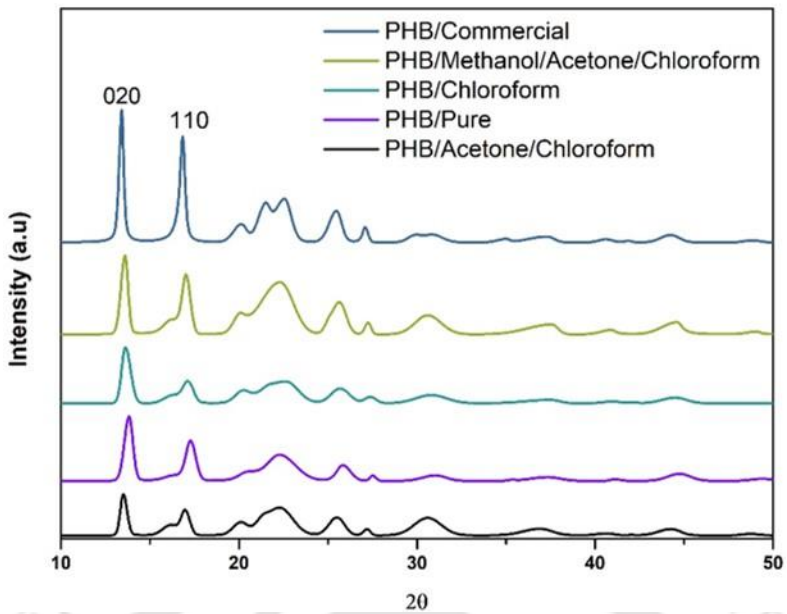

Figure 3.13. X-ray diffraction profiles of PHB extracted using different solvents and commercial PHB.

The X-ray diffraction profiles shown in Figure 3.13 indicates the azimuthal scan of (110) diffraction of the β-form. It shows the repeated intensity change at every 60°. The 020 diffraction of α-form indicates twin structures. Table 3.4 highlights the important properties of the produced PHB.

Table 3.4. Characteristic properties of PHB produced from *Bacillus megaterium* using sorghum juice as carbon source.

Properties	**PHB**
Number Average Molecular Weight M_n (KDa)	400
Density (g/cm^3)	1.25 to 1.45
Melting Point T_m (°C)	170 to180
Glass Transition Temperature T_g (°C)	-8 to -10
Crystallization Temperature T_c (°C)	87-105
Degradation Temperature (T_{onset}) (°C)	253

Wettability analysis of the obtained PHB was performed against the DI water and the images are shown in Figure 3.14. Contact angle (θ) was found to be 98 ± 1.5° for Pure PHB, 93 ± 2° for PHB extracted using acetone/chloroform, 84 ± 1° for commercial PHB and 79 ± 1.5° for PHB extracted using chloroform. Hydrophobic property has increased due to surface modification by solvents. The water contact angle increased for pure PHB in comparison to PHB extracted using other solvents.

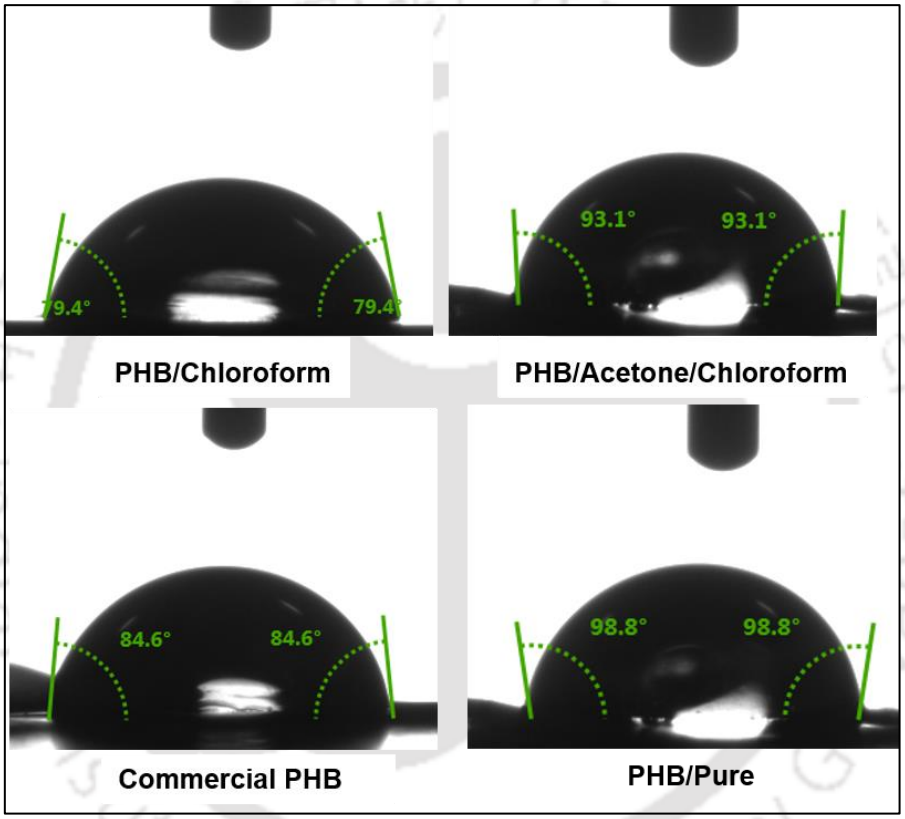

Figure 3.14. The water contact angle of PHB extracted through different solvents.

The formation of spherulite is associated with the crystallization from the melt. The process is controlled by the structure of the polymer molecule and nucleation sites. The time-lapse images of spherulite growth for PHB were captured, and images are shown in Figure 3.15. The formation of spherulite growth and nucleation behavior is compared with commercial PHB. The initial image was taken at $t_0 = 0$ min and then the image after every 1 min was captured to analyze the spherulite growth. Where, nucleation was not observed at 0 min except for purified

PHB, in which it started at 0 min. The size of the spherulites increased gradually with time in all samples.

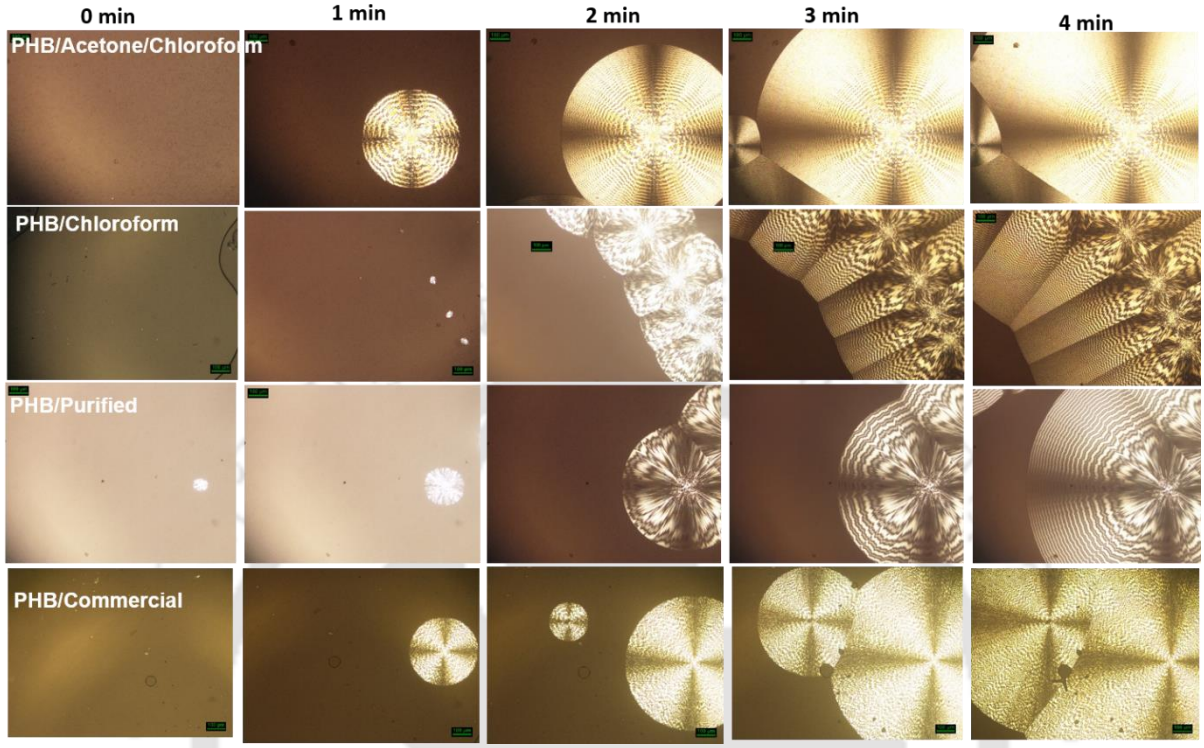

Figure 3.15. Polarizing optical microscopy images of PHB at different time intervals (0-4 min).

3.2.5 End group analysis of PHB using MALDI-TOF-MS

The biosynthesis of PHB is well established in *Bacillus megaterium.* Figure 3.16 shows a typical MALDI-TOF-MS spectrum in a positive reflector mode of PHB polymer. The extended-spectrum from 800 to 1400 in *m*/*z*, shows a distribution of ions in singly charged sodium adduct form. There are four sets of peaks showing a peak-to-peak mass increment of 86 *m*/*z*, which corresponds to the molecular weight of the 3HB repeating unit. Each peak of the higher molecular ion set is larger than the corresponding peak of the lower molecular ion set by 16 *m*/*z*. Fragments derived from the OH side of PHB are capped with an end group having a mass number of 100 or 118 in addition 100 m/z for H_2O. The mass number analysis indicates that the OH group of PHB is succinate for which one carboxyl group is bonded with the PHB hydroxyl terminal, leaving the other carboxyl free.

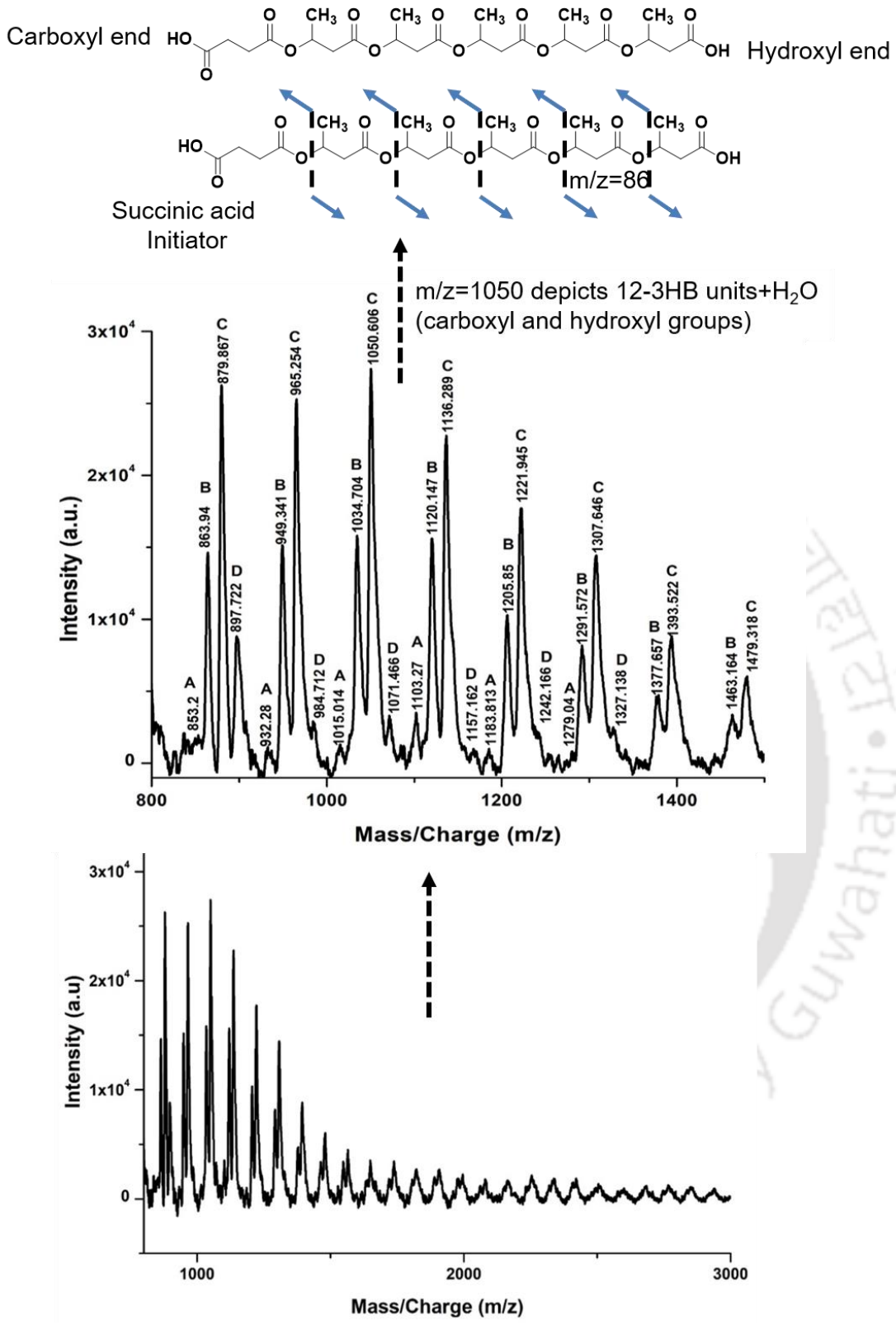

Figure 3.16. MALDI-TOF-MS spectra of PHB depicting the end group analysis.

3.2.6 Cytotoxicity assay of PHB against BHK-21 cell lines

The PHB samples with a concentration of 0.1 g/mL were tested for their cytotoxic effects. The results obtained for the cytotoxicity test of PHB against BHK-21 cells are shown in Figure 3.17. The results of relative cell viability (%) with respect to control show the cell adhesion onto the surface of PHB are similar to that of the control sample, indicating the non-cytotoxic behavior of the PHB produced using sorghum juice as a carbon source. The results show a ~30% reduction in the relative cell viability in the tested sample in comparison to the control even after 48 h of incubation. The results with the least cytotoxicity indicate its promising applications in the field of medicine as a drug carrier for a variety of applications.

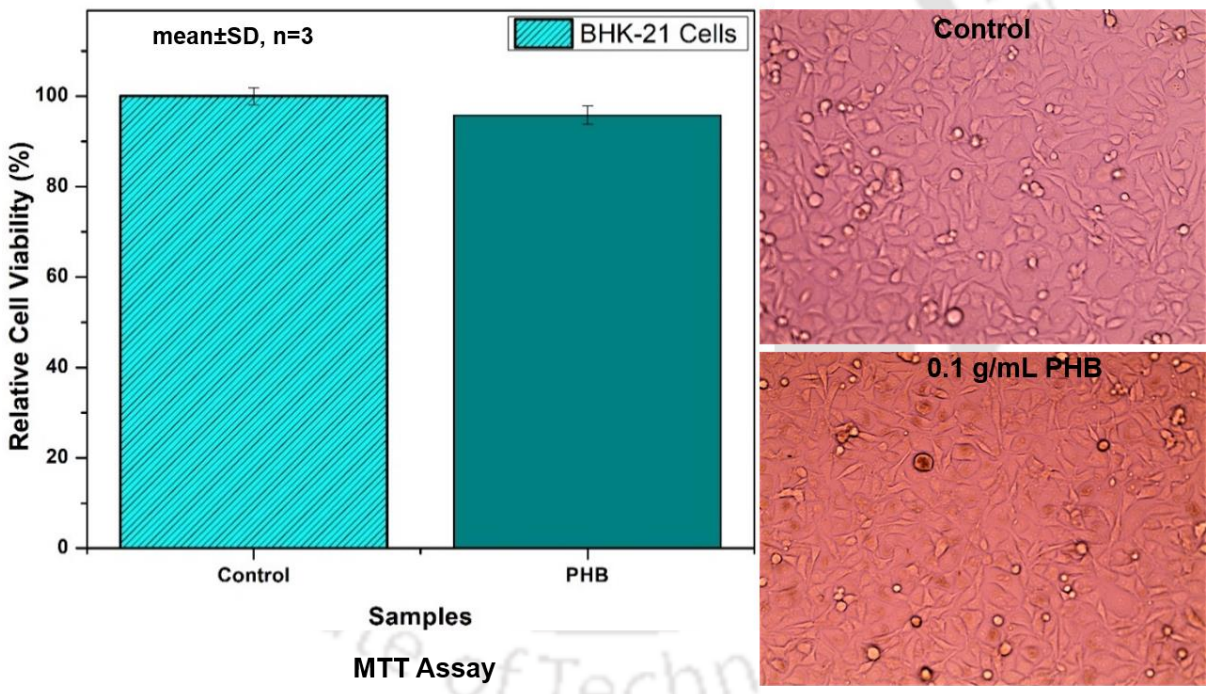

Figure 3.17. Cytotoxicity assay depicting the non-toxic behavior of PHB on BHK-21 cells.

3.3 Conclusions

This work presents the PHB production by fermentation of wild-type *Bacillus megaterium* in a stirred-tank bioreactor. Different fermentation strategies were tested and the experimental results were compared with previously achieved results using shake flask cultures. Variation in fermentation conditions has increased the production of PHB. The PHB productivity obtained by this fed-batch fermentation strategy was 4 and 6 fold higher than in batch strategy and shaken flask cultures. The effect of several parameters such as aeration, agitation mode, and concentrations of carbon and nitrogen sources yield variable productivity. The characterization of the purified PHB by DSC, FTIR, ^{1}H, and ^{13}C NMR techniques confirmed the structure and characteristics of the biopolymer produced by *Bacillus megaterium*. Finally, it was confirmed that the polymer does not induce cytotoxic effects on the BHK-21 cell culture which is one of the features to be fulfilled for biomedical applications. Thus, the following steps of this work will intend to scale up the production of this biopolymer to produce microspheres for drug delivery applications.

CHAPTER 4

Preparation of PHB Microspheres for Embolization: In vitro Study Using PLA-Based 3D-Printed Hepatic Vascular Phantom

Graphical Overview

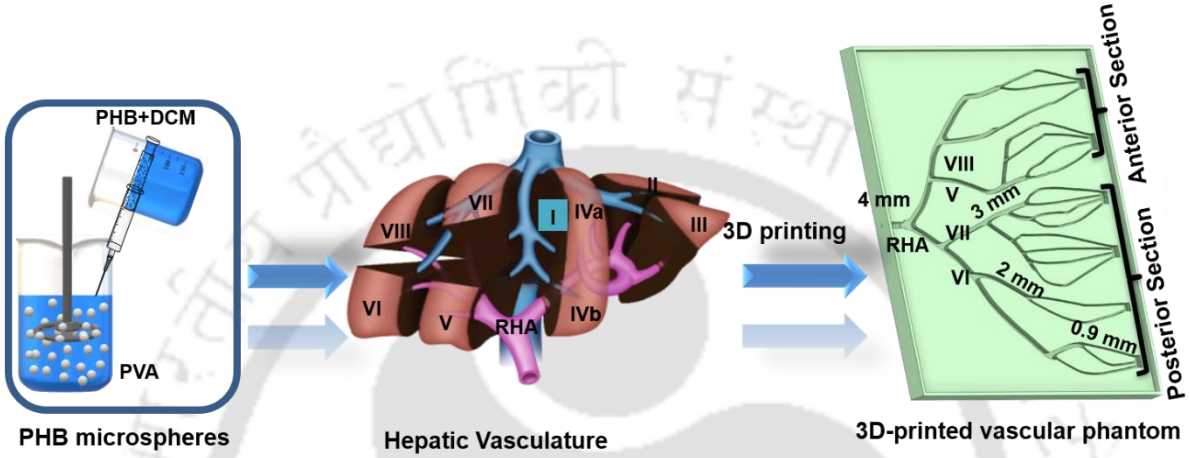

The PHB microspheres were prepared by oil-in-water emulsion technique using 20 mg/mL of PHB solution prepared in DCM with gentle heating. 1% w/v of PVA solution was prepared in water at 95 °C for 30 min. The PHB solution was injected using a syringe into the PVA solution, and solvent evaporation was performed with different stirring speeds resulting in microspheres of 7-300 µm in size. To check its efficacy as an embolizing agent for minimally invasive treatments, a low-cost 3D printed PLA-based hepatic phantom costing 221 INR was developed and evaluated for its suitability as an *in vitro* model for simulating the right hepatic artery. Further, the delivery of the microspheres was tracked inline by a camera. The volume distribution in six-channel outlets was measured with flow rates from 60 to 120 mL/min. The delivery of the microspheres was performed with an injection rate of 20 mL/min. The microscopic tracking revealed the embolization effect in the 0.9 mm channel and the microsphere distribution dependent on the volume distribution.

4.1 Introduction

Liver cancer is the sixth most common cancer and one of the leading health challenges experienced globally, with more than one million estimated cases annually by 2025. The main causes are obesity, radiation, alcohol, and infection [122]. Hepatocellular carcinoma (HCC) is the common form of liver cancer caused by the Hepatitis B virus (HBV), which contributes to ~60% of the cases; other causes include the Hepatitis C virus, long-term heavy alcohol use, and non-alcohol steatohepatitis [123]. Figure 4.1 shows the worldwide statistics of various types of cancers and their values to the total cases

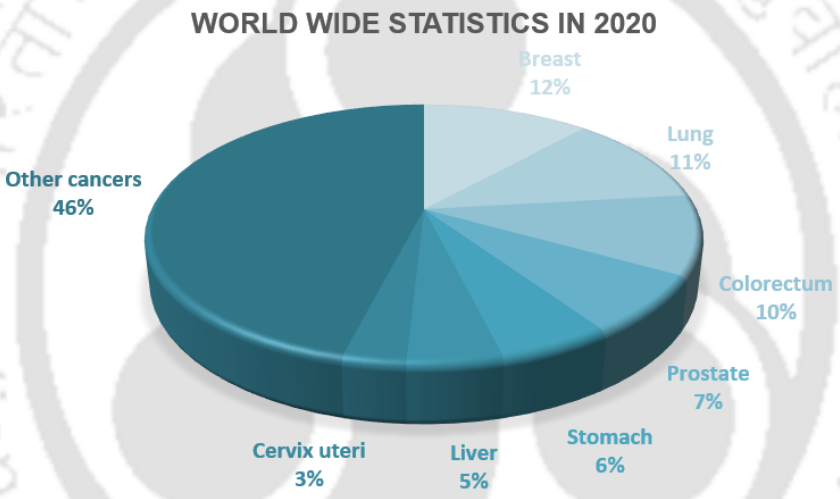

Figure 4.1. Worldwide statistics on various types of cancer.

The possible and available treatments are surgical interventions, including hepatic resection and liver transplantation, image-guided ablation, radiotherapy, trans arterial therapies, and systemic therapies. The treatment is also dependent on the tumor size, location of the tumor, number of tumors, degree of liver function, the extent of the tumor outside the liver, and other medical problems. The most commonly used minimally invasive treatment is embolization therapy. Arterial embolization is a deliberate occlusion of vessels by the injection of substances directly into an artery that blocks or reduces the blood flow to the tumor. Arterial embolization is of two types, namely, chemoembolization and radioembolization [124]. Trans-arterial

chemoembolization is intended for large tumors which cannot be treated with surgery or ablation. It is a combination therapy that includes embolization and chemotherapy. Whereas radioembolization is a combination of embolization and radiation therapy [125]. The commonly used embolizing agents are microspheres. Commercially there are some microspheres available which include SIR spheres (Sirtex Medical, Australia), Embospheres (Merit Medical Systems Inc, USA), and TheraSphere^{TM} (Boston Scientific Corporation, Canada). However, they possess some disadvantages, such as non-degradability and side effects from radioactive elements. To tackle the issue, there is a need to investigate alternative materials which are bioresorbable and biocompatible without any toxic side effects. Polyhydroxybutyrate is a biocompatible and bioresorbable material, also a key player in biomedical applications. It is an intracellular macromolecule receiving scientific attention due to its biocompatibility, and material intrinsic properties with predictable degradation rates [126]. The current chapter explores the fabrication of PHB microspheres as embolizing agents and the fabrication of a 3D-printed PLA-based hepatic model to mimic the dimensions of the right hepatic artery. The objective of the present study is to investigate the material density, flow, viscosity effects, and flow of simulated body fluid on the distribution of microspheres within an *in vitro* vascular flow model, designed by 3D printing to simulate flow conditions of hepatic arteries.

4.2 Results and discussion

4.2.1 Effect of stirring speed and preparation methodology on size and morphology of microspheres

PHB microspheres prepared by solvent evaporation technique using method I at a stirring speed of 300, and 600 rpm yielded microspheres with an average diameter (D) 305 ± 62 µm and 44 ± 32 µm, respectively. The surface morphology of these microspheres was evaluated using

field emission scanning electron microscopy. The obtained microspheres are spherical without any distortion/defective surfaces. The surface of microspheres obtained at 300 rpm possess small particles on the surface, whereas the microspheres obtained at 600 rpm possess a clear surface without any aggregated particles on the surface. The preparation method II yielded microspheres with an average diameter of ~7.6 ± 2.5 µm consisting of millions of aggregated nanospheres. Hence the method of preparation and the stirring speed are key parameters to be considered while preparing the microspheres with tunable sizes. FESEM images of the obtained microspheres are depicted in Figure 4.2.

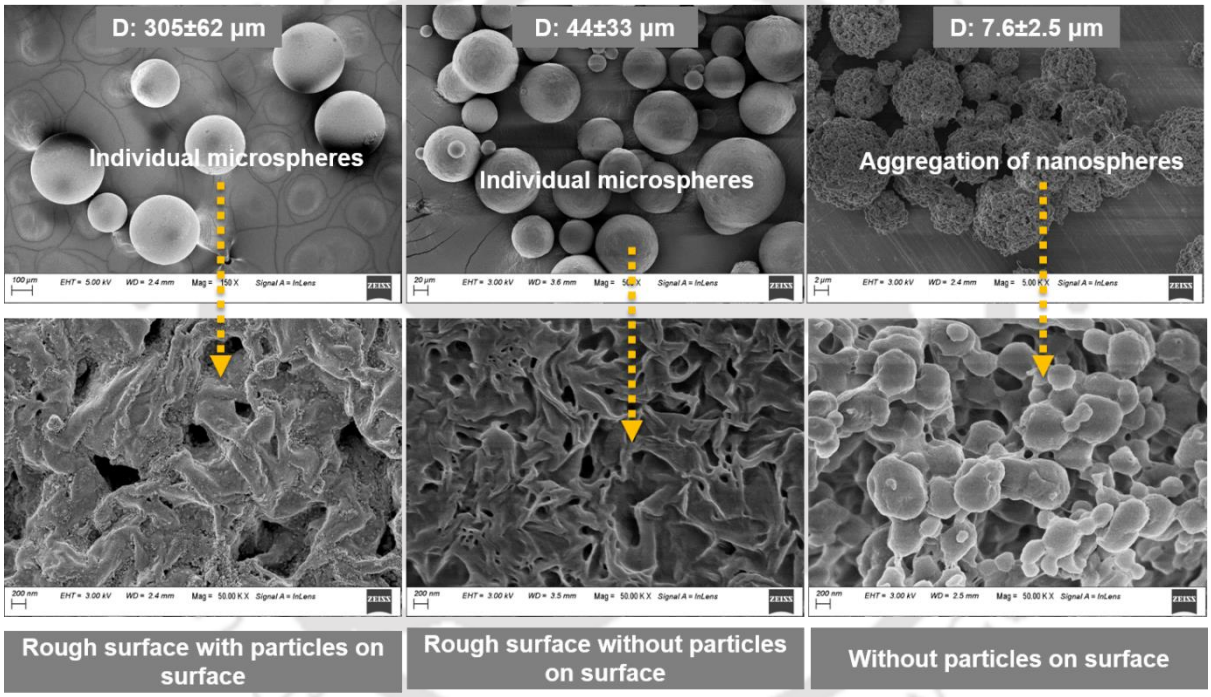

Figure 4.2. FESEM images of produced microspheres and size distribution.

4.2.2. Comparison of properties with commercially available microspheres

To evaluate the applicability of the prepared microspheres, it is compared with the properties of commercially available microspheres and is tabulated in table 4.1. The SIR microspheres produced by Sirtex Medicals are currently used for the treatment of hepatic tumors. However, it exhibits side effects such as radiation hepatitis, and chills due to the radioactive element ^{90}Y. TheraSpheres^{TM} is glass microspheres produced by Boston scientific, and are primarily used

for the treatment of unresectable primary and secondary tumors. In addition to its uses, it poses serious side effects including the radiation effects and its retention at the target delivery site after the treatment [127]. Thus the produced PHB microspheres could be possible alternatives for cancer treatments. PHB microspheres produced in the current study are having a diameter of 44 μm and a density of 1.2 g/cm^3 which is preferable to avoid retention in the catheter while delivery.

4.2.3. Distribution of microspheres in the hepatic model

The delivery of microspheres was carried out using the developed laboratory setup. The developed hepatic vasculature was subjected to the pulsing blood mimicking body fluid and mixing conditions of the right hepatic artery. However, the investigations on drug release kinetics and drug efficacy with PHB as carrier will be of future scope.

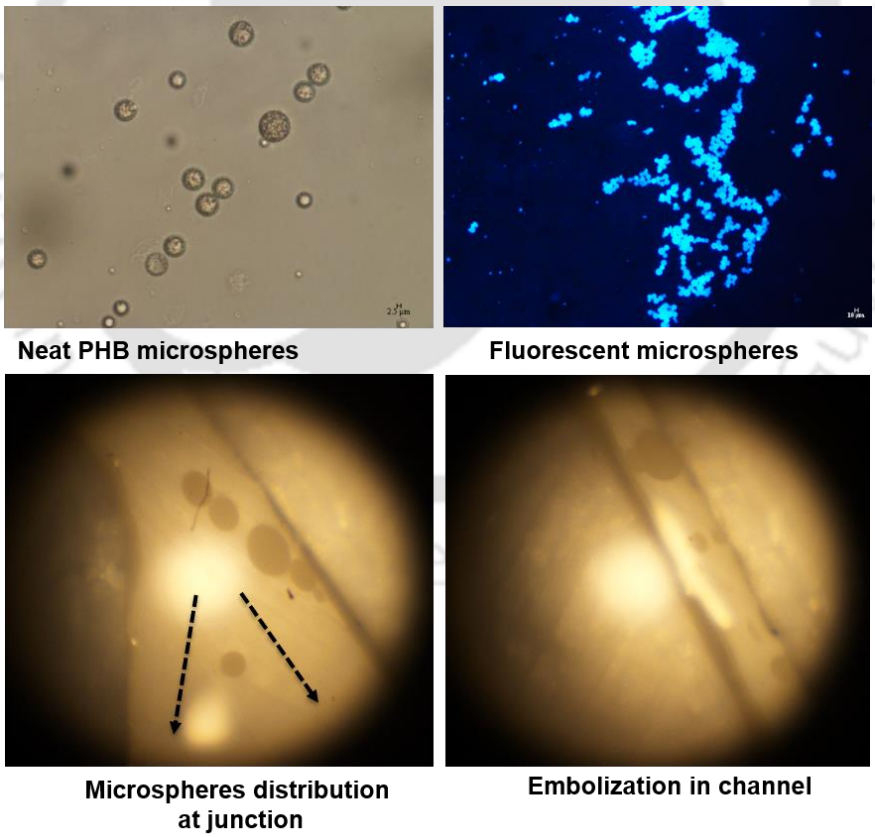

Figure 4.3. Distribution of microspheres in 3D printed PLA-based hepatic vascular phantom, images showing the distribution in channels and junctions.

The pressure was generated at the inlet of the vasculature with a 4 mm channel. The microsphere delivery at 20 mL/min [92] yielded an equal volumetric distribution of the microspheres. The size equal to the diameter of the arteries embolized the channels and it is shown in Figure 1.3. The figure also provides the microscopic images of the neat and fluorescent PHB microspheres and their flow.

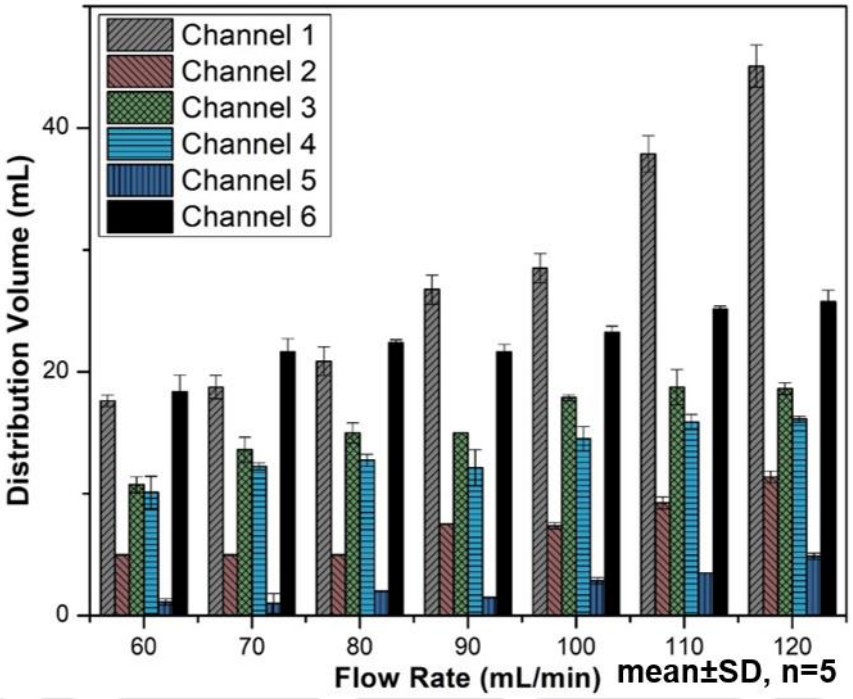

Figure 4.4. Distribution of volume in six outlet channels of the hepatic phantom.

The experiments were performed to analyze the volumetric flow of the body mimicking fluid through the channels of the hepatic phantom with a flow rate ranging from 60 to 120 mL/min to maintain similar to the systolic and diastolic pressure of humans. The flow rate was mentioned using a peristaltic pump at a nominal rate of 120 mL/min, chosen to be quite approximately that of the right hepatic artery. Whereas the study at 60 120 mL/min is suitable for the patient in sedated condition.

Table 4.1. A comparison study on the various microspheres used in the drug delivery

Microspheres	Composition	Drug used	Properties	Application/tumor size	Side effects	Reference
SIR spheres Sirtex Medical, Australia TheraSphere™	Propriatory polymer cross linked with polystyrene	^{90}Y	D=32 μm Density=1.6 g/cm^3	Hepatic tumor	Radiation hepatitis, fever, chills	[128], [129]
Boston Scientific Corporation, Canada	Glass microspheres	^{90}Y	D=32 μm Density=3.3 g/cm^3	Unresectable primary and secondary metastatic liver cancer, Tumor size: 1-8 cm	Glass spheres stay in the liver permanently, and radiation effects	[127]
PHB microspheres	PHB	Neat, 5-FU, Fluorescent (possible drugs)	**D=44 μm Density=1.2 g/cm^3**	*In vitro* delivery through a right hepatic artery using a PLA-based 3D printed model	No residue due to biodegradability	Present study

4.2.4. Wettability analysis of the 3D printed PLA-based hepatic phantom

The surface roughness and the chemical composition of the model play a key role in microsphere delivery. Here the efficacy of the *in vitro* model is also important to decide the actual flow conditions in the hepatic arteries. The wettability of the developed model is checked against three different fluids such as water, simulating body fluid, and the carrier fluid shown in Figure 4.5. It was observed from the study that the contact angle for water was found to be 83 ± 3°, whereas it was not 77 ± 2° for SBF and the carrier fluids, which is due to the viscosity and wetting behavior of the fluids. However, it was observed that after 15 min the wettability is found to be similar for all the samples, and that is due to the 3D printing design, which creates nanochannels, through which blood can easily flow.

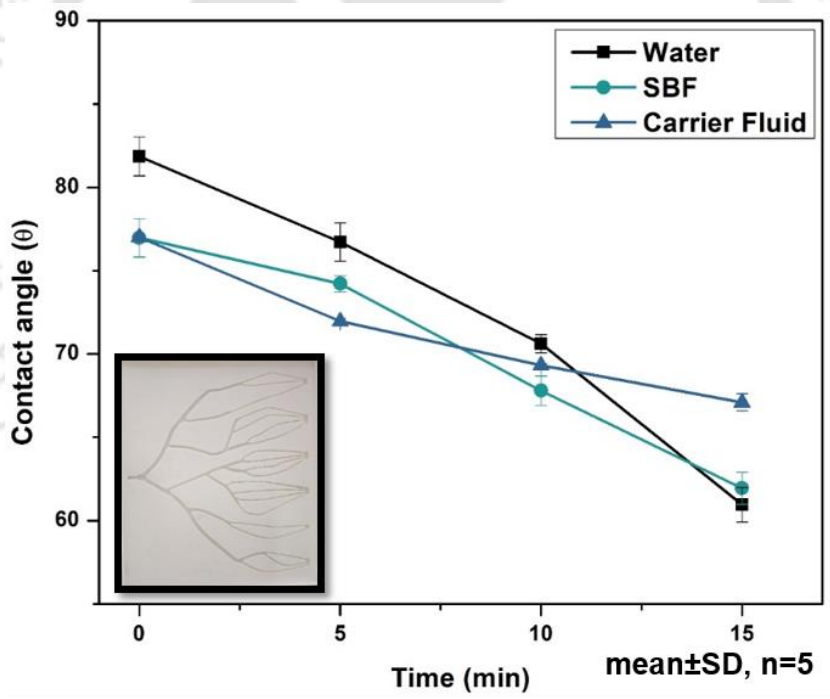

Figure 4.5. Channel wettability of the 3D-printed hepatic vascular phantom

Moving forward, the cost of the 3D-printed hepatic phantom was calculated and it was found to be 221.5 INR when compared to other comparative models. Thus the developed model and the microspheres are promising candidates with beneficial properties

Table 4.2. Cost estimation of the developed PLA based 3D printed hepatic vascular phantom.

3D Printed Phantom	3D-printer	Design Software	Material & Cost (INR)	Print Time (h)	Total cost/model (INR)	Reference
3D-printed abdominal aortic aneurysm	Stratasys Eden 260 printer	Vascular Modeling Toolkit (VMTK) Autodesk MeshMixer	FullCure 930 TangoPlus	13	19, 886	[130]
Patient-specific aortic arch	Delta Wasp 2040 Turbo 2	3D slicer	Formfutura PVA 1.75 mm=3516.46 Ecoflex™ 00-30 silicon=1523	N/A	5039.46	[131]
Right hepatic artery	Creality CR 10 (Power consumption=350 W*6.25h)=13.45 INR	Autodesk® Fusion 360 Ultimaker Cura 4.3	PLA=96 Epoxy=12.3 Tubing=96.12 Polyester film=3.33	6.25	**207.75 +13.4=221.15**	Current work

4.3 Conclusions

The PHB obtained from *Bacillus megaterium* produced using sorghum juice could be used for the preparation of microspheres of variable sizes. The morphology and size of the microspheres are tunable for desired applications. The current study demonstrated that the PHB microspheres obtained using the solvent evaporation technique are suitable for embolization of the hepatic arteries with a diameter of 0.9 mm. It has also explored the novel method of design and development of 3D-printed PLA-based hepatic models for *in vitro* drug delivery studies. PHB microspheres demonstrated a similar distribution within a range of clinically relevant arterial flow conditions with a viscosity of 4.40 ± 0.5 cP mimicking the viscosity of blood. It was also important to notice that the density of the microsphere does not have a significant role in the distribution of the microspheres in the arteries.

CHAPTER 5

Biosynthesis of Prodigiosin from Serratia nematodiphila for the Synthesis of Poly(lactic acid)

Graphical Overview

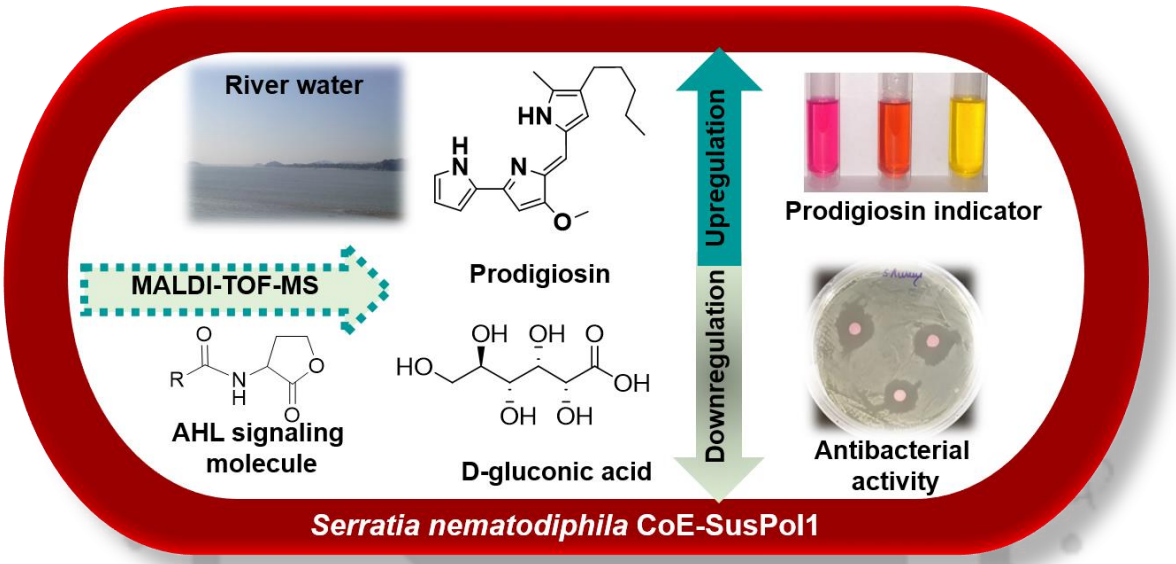

The production of a secondary metabolite prodigiosin is explored in red-pigmented bacteria *Serratia nematodiphila* CoE-SusPol1 isolated from river water. The characterization of bacteria reveals the swarming behavior, cephalothin resistance, and prodigiosin synthesis. The biosynthesis of prodigiosin is found to be substrate-specific, which upregulates in the presence of peptone to yield the prodigiosin and downregulates in the presence of glucose to yield D-gluconic acid. The role of AHL in the synthesis of prodigiosin is proposed based on metabolite identification using MALDI-TOF-MS.

Publication:

- Chethana Mudenur, Amit Kumar and Vimal Katiyar, Acyl-homoserine lactone mediated prodigiosin produced from *Serratia nematodiphila* as an antibacterial wound healing indicator, Advanced Biomaterials (Under review)

The strain yielded a prodigiosin of ~0.37 ± 0.04 g/g of cell biomass at optimum conditions with a molecular mass of (m/z) 323.6 Da, and a characteristic absorption wavelength λ_{max} of 535 nm. Further, the antibacterial activity of prodigiosin against *Staphylococcus aureus* and its non-cytotoxicity results on baby hamster kidney fibroblast cells (BHK-21) support its biocompatibility without any side effects. These properties in addition to the pH-sensitive color-changing behavior are the key elements to exploring prodigiosin as a promising indicator.

5.1 Introduction

Rivers are the reservoirs of various microorganisms, and these microbes produce various primary and secondary metabolites, including antibiotics, pigments, etc. Natural pigments are obtained from various sources such as plants, fungi, and bacteria. Prodigiosin is a tripyrrole and a small organic molecule synthesized by some genera of *Serratia marcescens* [132], *Pseudomonas rubra* [133], *Streptomyces griseoviridis* [134], *Serratia liquefaciens*, etc. [135]. *Serratia sp.* is a Gram-negative and widely studied organism for the production of prodigiosin and the removal of nitrogen [136]. Prodigiosin is an excellent candidate with exceptional medicinal properties such as antiviral, antibacterial, antimalarial, and anticancer properties [137], with negligible or no cytotoxic effects on normal cells [138]. Some studies have suggested that solid-state fermentation yield more prodigiosin in *Serratia marcescens* due to its high nutrient concentrations and easy availability of substrates [139].

The gene expression, synthesis of signaling molecules (auto-inducers), and metabolite production in these bacteria is dependent on cell density. The Gram-negative bacteria use N-acyl-homoserine lactone (AHL) as a communication system [140]. These are the quorum-sensing molecules responsible for intracellular and intercellular bacterial communication [141]. The quorum sensing in this bacteria is regulated by an autoinducer synthase (LuxI) that

is accountable for the generation of AHL signaling molecules with the help of acyl carrier protein [142].

The current investigation aims to isolate, identify, and evaluate the properties exhibited by *Serratia nematodiphila*, and the mechanism of surface motility behavior associated with antibiotic resistance. Further, a systematic assessment has been made on the effect of media components and possible intermediate biochemicals responsible for the regulation of prodigiosin synthesis in bacteria. Here the metabolic products and byproducts have been identified by MALDI-TOF-MS to understand the regulatory mechanism of prodigiosin biosynthesis. Further, the produced prodigiosin is explored for its application as a pH Indicator

5.2 Results and discussion

5.2.1 Isolation of prodigiosin producing bacteria from river water and its characterization

The complete process from strain isolation to extraction of the prodigiosin is depicted in Figure 5.1. The Gram-negative pigment-producing bacterium was isolated from the river water, cultured, and maintained on the nutrient agar media. The detailed method is explained in the methods section. The result obtained from 16S rRNA partial sequencing and phylogenetic analysis shown in Figure 5.2 confirmed that the strain is 99% homology with *Serratia nematodiphila*. The partial genome sequence of the strain is submitted to GenBank and is available from the National Center for Biotechnology Information (NCBI) with GenBank accession number MK968767. The obtained strain has been assigned as the *Serratia nematodiphila* CoE-SusPol1 throughout.

Further, to evaluate such behavior, the antibiotic susceptibility test was performed to check its sensitivity to antibiotics. Bacterial response against five antibiotics Figure. 5.2 (B) and the inhibition pattern and the zone of inhibition of *S. nematodiphila* showed susceptibility to

gentamicin, tetracycline, and amikacin. In contrast, it is resistant to cephalothin without any zone of inhibition. However, cephalothin is a first-generation cephalosporin that consists of a β-lactam ring, reported to be least effective on Gram-negative bacteria capable of producing the β-lactamase that degrades β-lactam ring of cephalothin to make it ineffective [143], [144].

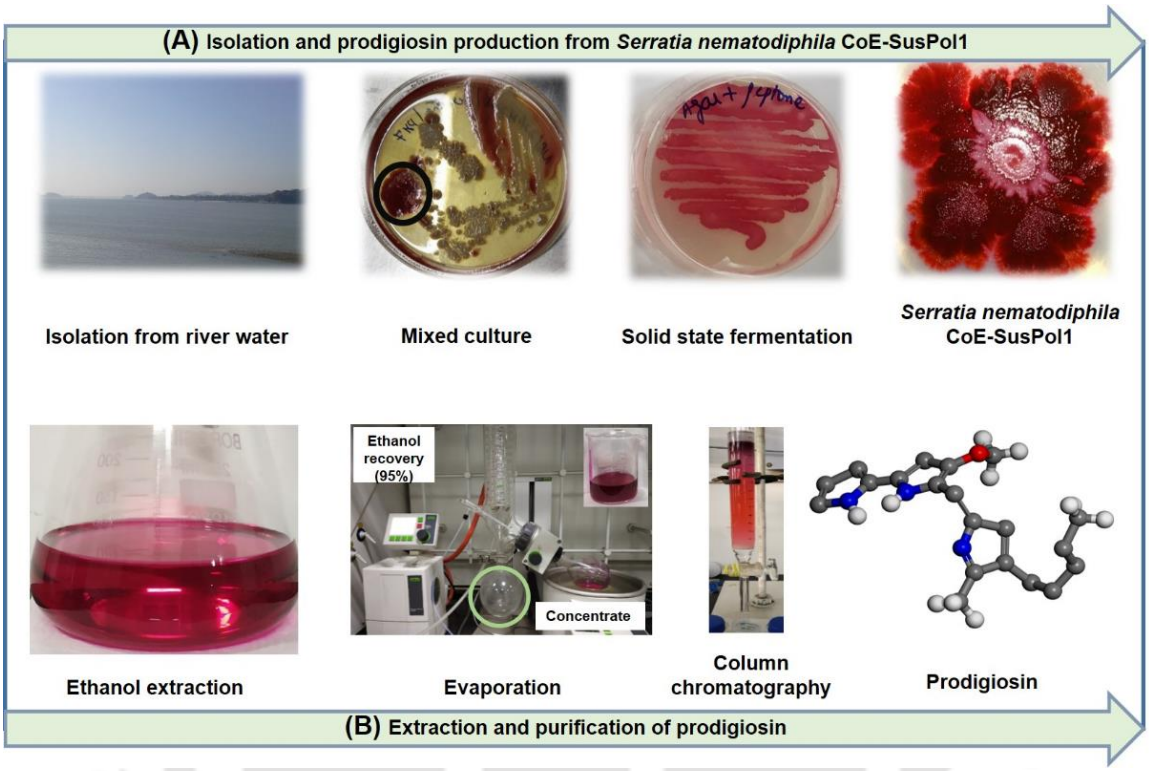

Figure 5.1. (A) Pictorial representation of the process of isolation to prodigiosin production on a solid-state media and (B) Extraction of prodigiosin using ethanol, followed by concentration and purification using column chromatography.

It is observed that no morphological changes in the case of antibiotic resistance, which might be due to the less affinity of penicillin-binding proteins. Whereas bacteriostatic effect and cell damage are observed in case of susceptibility due to the disruption in the synthesis of the peptidoglycan layer leading to cell death at the center. Further, based on the studied antibiotics, the multiple antibiotic resistance (MAR) index obtained is 0.2. MAR greater than 0.2 indicates an increase in the risk factor of pathogenicity [145]. However, results indicated that *S. nematodiphila* is less antibiotic-resistant compared to *Serratia marcescens*, which exhibits

resistance to various antibiotics, including ampicillin, tetracycline, and cephalothin, posing a high risk of pathogenicity [146]. This characteristic susceptibility of *S. nematodiphila* is pragmatic to be considered as a low-risk strain for subsequent work for the production of prodigiosin.

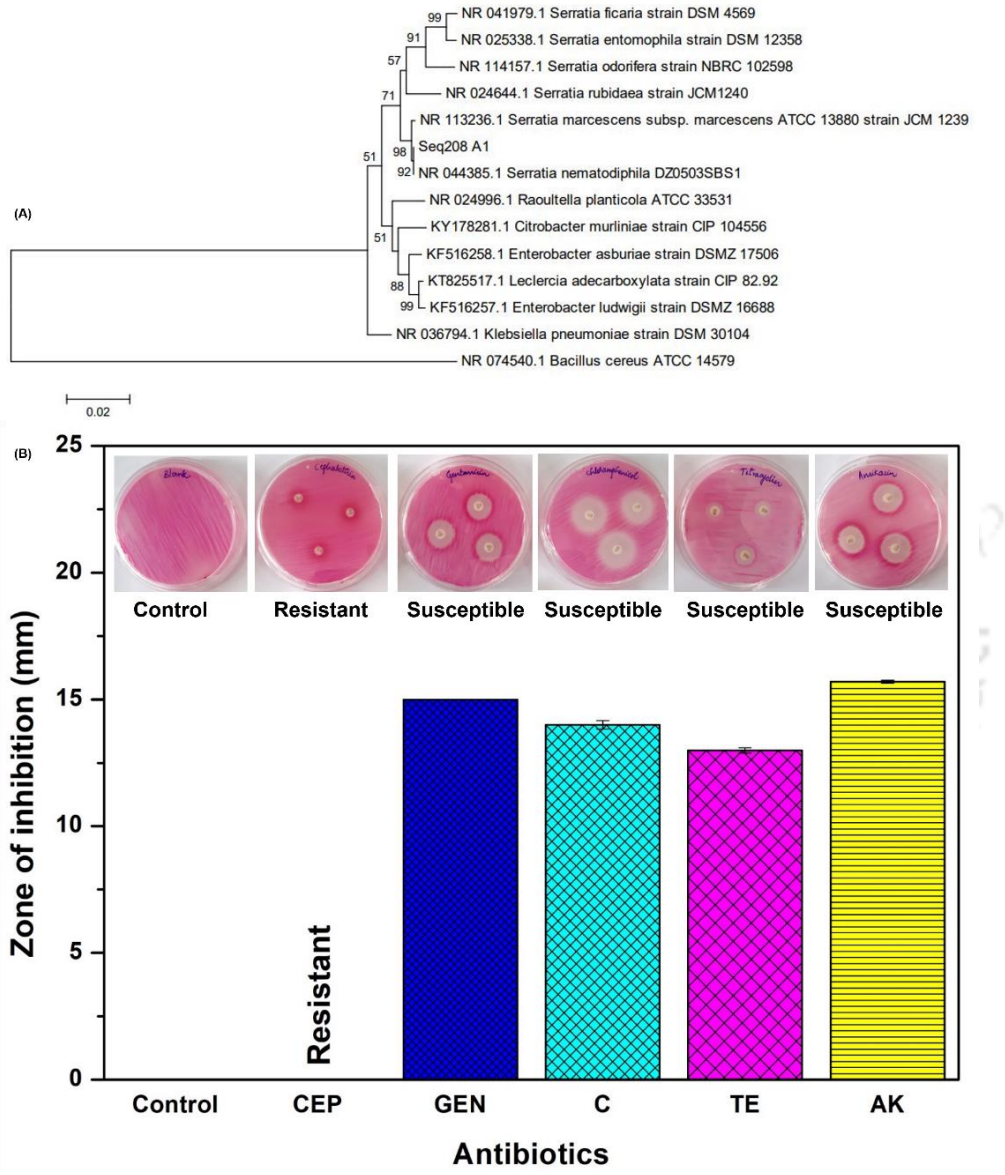

Figure 5.2. (A) Evolutionary relationship of taxa (Neighbor-joining method and (B) Antibiotic susceptibility and inhibition pattern of *Serratia nematodiphila* CoE-SusPol1 against gentamicin (GEN), tetracycline (TE), amikacin (AK) chloramphenicol (C), and cephalothin (CEP) (mean ± SD, n=3).

5.2.2 Effect of media components on the prodigiosin synthesis from *Serratia nematodiphila* CoE-SusPol1

Bacteria need specific nutrient composition for their growth, maintenance, and product formation. Here peptone, glucose, yeast extract, and sodium chloride have been evaluated in different combinations for efficient growth and prodigiosin biosynthesis on solid-state fermentation with agar as a solidifying agent (Figure. 5.3). The maximum prodigiosin obtained is found to be ~0.37 ± 0.04 g/g of cell biomass (DCW) using peptone with a pH value from 7-7.5 at 30 °C, and 48 h of the incubation period. The results obtained are relatively higher than *Serratia marcescens,* yielding ~1.2 ± 0.3 mg/g DWC [147], 8 g/L using brown sugar [148] and *S. nematodiphila* yielding 0.46 mg/mL of broth with lactose as a nutrient [149]. It is observed that the strain is capable of converting peptone to prodigiosin with a high titer of 4 g/L of peptone alone, yielding the prodigiosin of ~0.37 g/g of biomass which may be due to the presence of inherent protease activity. Further, to check the effect of other nutrients, the individual components were studied with optimum concentration of peptone. It was found from the study that glucose concentration beyond 2 g/L inhibited the prodigiosin, whereas the sodium chloride did not show any effect. The response obtained for yeast extract was increasing; however, it has a negative effect on the yield in comparison to peptone alone. Such an interesting behavior triggered to explore more on the mechanism of synthesis of byproducts and their interference in the process of upregulation and downregulation of the prodigiosin synthesis.

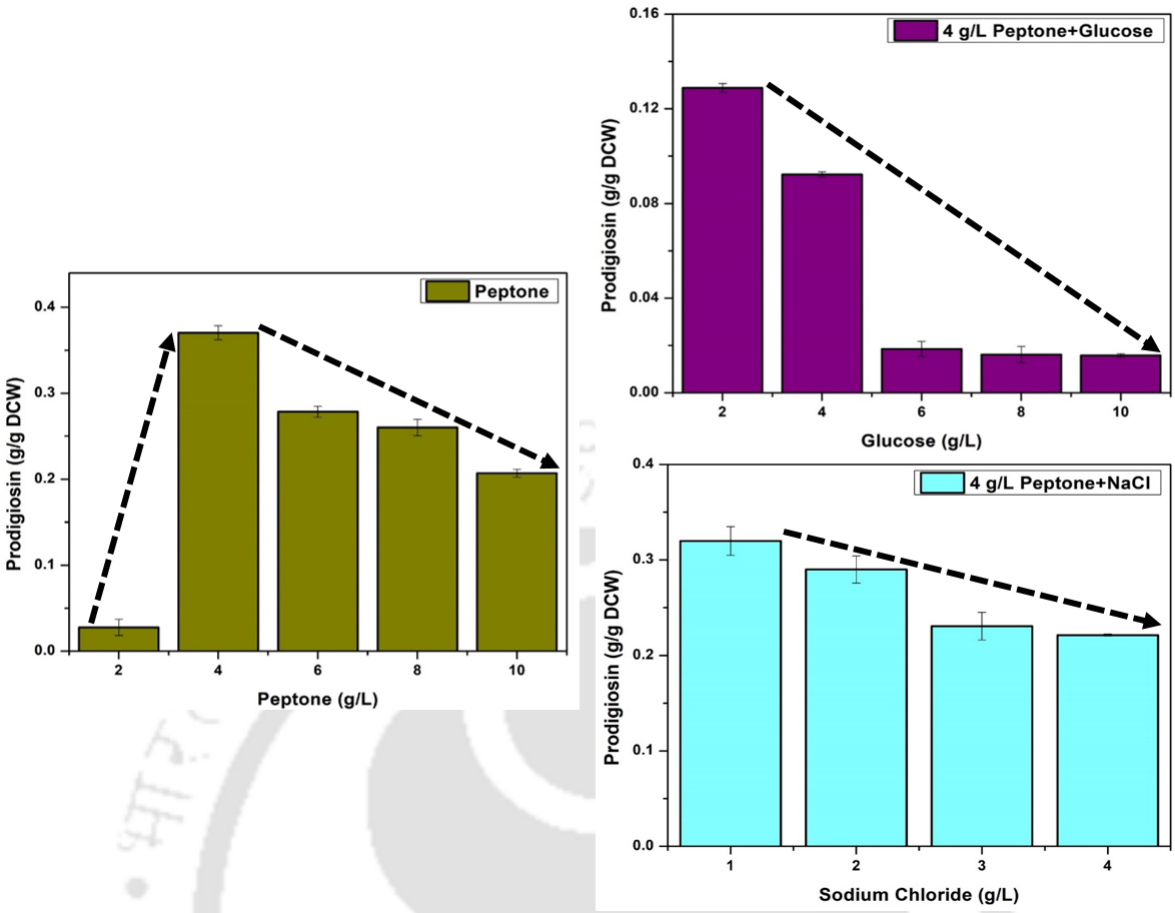

Figure 5.3. Effect of media components peptone, peptone+glucose, and peptone+sodium chloride on the production of prodigiosin (mean ± SD, n=3).

5.2.3 Determination of inducer molecules responsible for prodigiosin synthesis using MALDI-TOF-MS

There is an increasing trend observed in the absence of glucose and decreasing trend (Figure. 5.4) observed in the presence of glucose, and at 8 g/L of glucose, strain lost capacity to produce prodigiosin. Further, this behavior is investigated to determine the molecule responsible for it. The molecules responsible for such a behavior is *N*-Acyl homoserine lactones (AHLs). These are chemical signaling molecules or autoinducers produced in the presence of AHL synthase and used by the bacteria as a secret ballot to show their numerical strength for the production of secondary metabolite prodigiosin. Various bacterial strains produce AHLs with variable acyl chains having a length of C4-C14 with a C3 position as an oxidation point. The type of AHL

responsible for the synthesis of prodigiosin in *Serratia nematodiphila* is assessed by the mass spectra obtained by MALDI-TOF-MS analysis. Some intracellular reactions lead to the formation of homoserine lactone ($C_4H_7NO_2$), *N*-butyryl-L-homoserine lactone ($C_8H_{13}NO_3$) (C4-AHL), and the peak can be seen at m/z of 171 [M], and the peak at 201.3 [$M+H^+$] represents the *N*-hexanoyl-$_L$-homoserine lactone ($C_{10}H_{17}NO_3$) (C4-AHL). When these autoinducer molecules reach the minimal threshold concentration, bacteria detect these signals to alter their gene expression to initiate the synthetic process for prodigiosin production.

5.2.4 AHL-mediated prodigiosin synthesis in *Serratia nematodiphila* CoE-SusPol1

The role of AHL in the synthesis of prodigiosin is significant in the current study. Some studies have shown that the synthesis of prodigiosin, formation of the bacterial biofilm, and their swarming motility are regulated by the AHL-mediated signaling in *Serratia marcescens* [150].

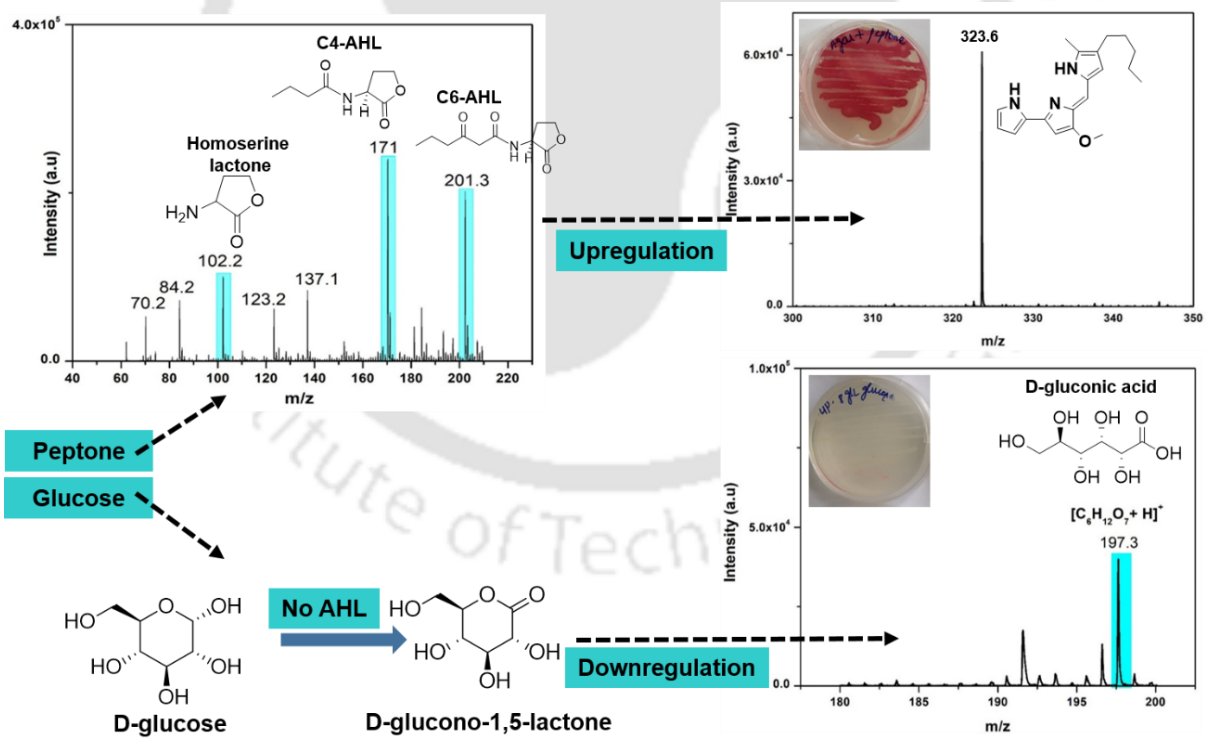

Figure 5.4. Upregulation and downregulation of prodigiosin in the presence and absence of AHL.

In the current study, the presence of signaling molecules such as C4-AHL, and C6-AHL upregulated the synthesis of prodigiosin in Serratia nematodiphila CoE-SusPol1 (Figure. 5.4) when peptone is present as a substrate in the production media. The bacteria sense these signal molecules and trigger the prodigiosin synthesis as a secondary metabolite.

5.2.5 Downregulation of prodigiosin in the presence of glucose

The process of the downregulation of the bioactive prodigiosin takes place with glucose enrichment. Previous studies have suggested that the quinoprotein glucose dehydrogenase is responsible for the downregulation of prodigiosin synthesis [151]. In the current study, the absence of AHLs induces the formation of an inhibitory product D-gluconic acid in the medium and is identified by MALDI-TOF-MS (Figure. 5.4) with a prominent monotonic peak at m/z of 197.3 corresponding to $C_6H_{12}O_7$ $[M+H^+]$. This downregulation effect leads to the inhibition of prodigiosin in the growth medium.

5.2.6 Characterization of the prodigiosin

The produced prodigiosin is characterized using the FTIR and is shown in Figure. 5. 5 (A). The spectra at 2925 cm^{-1} and 1254 cm^{-1} correspond to the methylene ($-CH_2$) and aromatic (-CH) functionality, the peal at 1566 cm^{-1} is due to conjugated aromatic C=C bonds. The pyrrole ring is confirmed by the presence of the amine N-H stretch at 3448 cm^{-1}. The peaks corresponding to 2925 cm^{-1} and 2852 cm^{-1} are due to the methyl groups ($C-O-CH_3$) of prodigiosin. The bands between 1133-1020 cm^{-1} confirmed the attachment of $(-C-O-C-)-O-CH_3$ to the aromatic pyrrole. The peaks at 1410 cm^{-1} and 1125 cm^{-1} correspond to (C-O) and (C-N), respectively [152]. The structure of prodigiosin is further confirmed by ^1H NMR spectroscopy as shown in Figure. 5.5 (B) (600 MHz, $CDCl_3$); the peaks at δ ppm 0.09 (s, 9 H) 0.04 - 0.12 (m, 3 H) 0.84 - 0.92 (m, 2 H) 1.27 (br. s., 4 H) 1.25 - 1.33 (m, 3 H) 1.68 - 1.76 (m, 2 H), and the characteristic N-H peak was found at 4.68 (s, 1 H) and 4.90 (s, 1 H), this data along with the resultant

monoisotopic peak of MALDI-TOF mass spectra (Figure. 5.4) with a molecular weight of 323.6 Da [$M+H^+$], ($C_{20}H_{25}N_3O$) confirmed the prodigiosin molecule.

Further, Figure 5.5 depicts the UV-Vis spectral analysis of prodigiosin with a characteristic absorption peak in the visible region at 535 nm; however, the variation in pH (1-14) leads to the peak shifting towards the UV region, which can be seen along with a gradual change in color from dark pink to dark yellow, while retaining the orange color at neutral pH. Such an effect is mainly due to the protonation effect of prodigiosin (Table 5.1). A similar trend is observed with the bacteria (pink to pale yellow) by changing ion concentration.

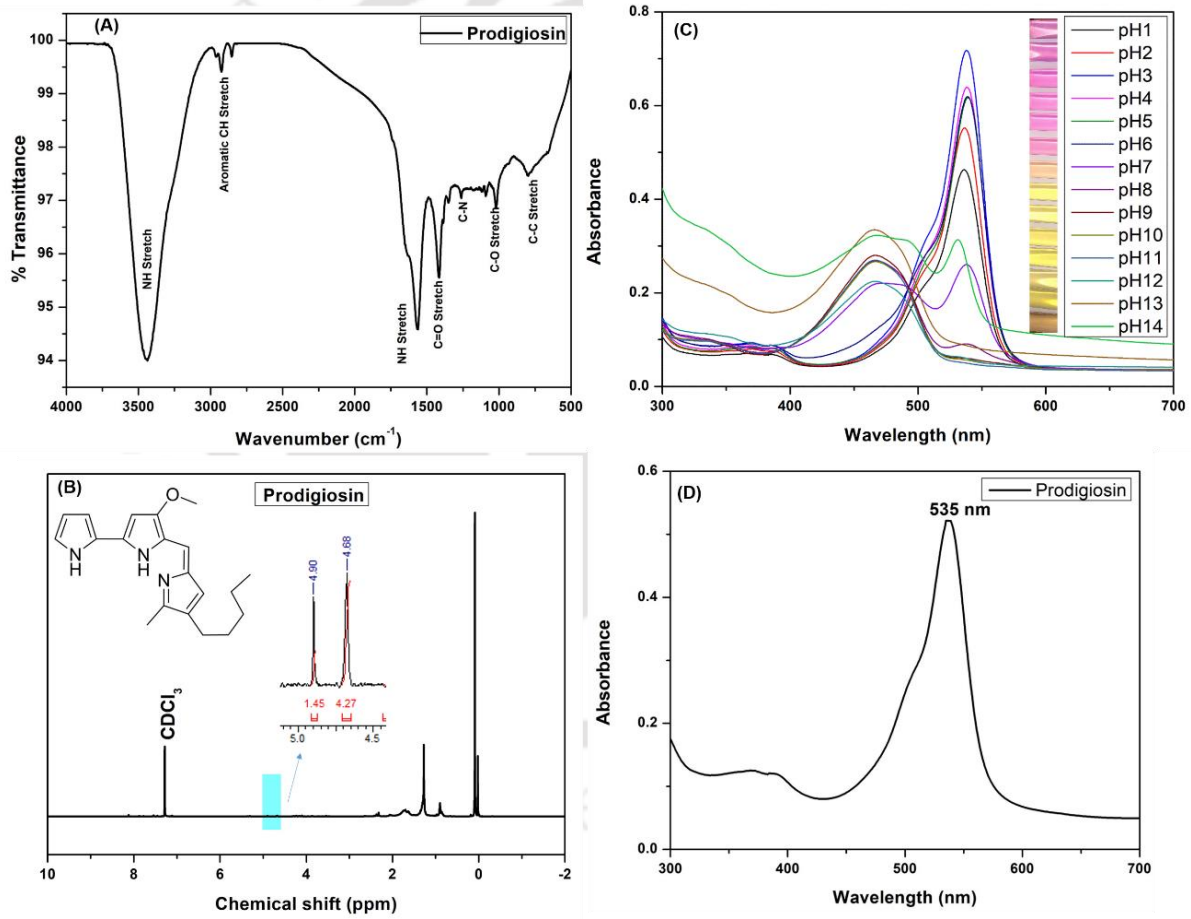

Figure 5.5. (A) FTIR spectrum of the prodigiosin; (B) ^{1}H NMR ($CDCl_3$, 600 MHz) spectrum of prodigiosin; (C) UV-Vis spectra showing the effect of pH on prodigiosin and (D) The characteristic absorption peak of prodigiosin at 535 nm.

5.2.7 Prodigiosin-loaded gel as a pH indicator

The antimicrobial property of the prodigiosin (5 µg/mL) against *Staphylococcus aureus* is depicted in Figure. 5. 6 (A). This indicates that the prodigiosin is antibacterial, exhibiting a diameter of the zone of inhibition of ~20.7 ± 1.2 mm, it showed slightly less activity compared to cephalothin and gentamicin, though it is comparable to amikacin of ~20 ± 0.06 mm. Such an antibacterial property is due to the intracellular leakage of the cellular materials such as amino acids and potassium ions of pathogenic strains [153].

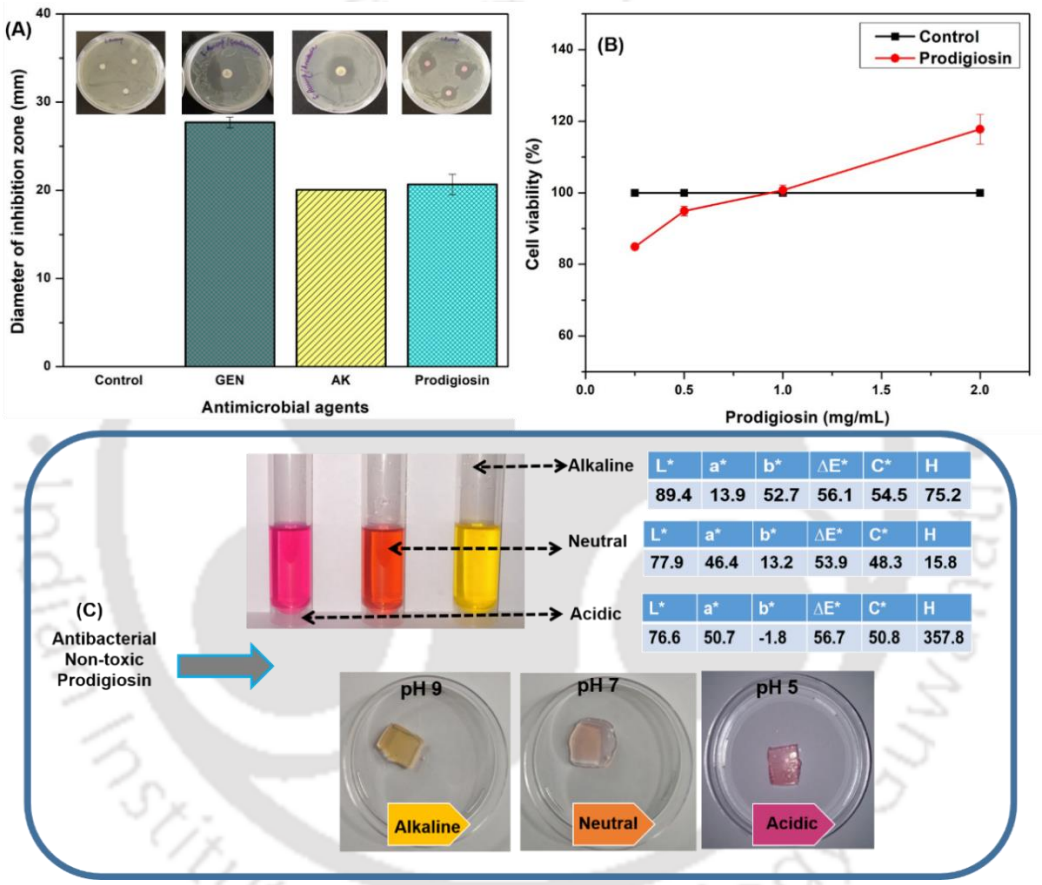

Figure 5.6. (A) Antibacterial activity of prodigiosin represented as the zone of inhibition against *Staphylococcus aureus*; (B) Graph of % cell viability after 48 h of incubation with various concentrations of prodigiosin (mean ± SD) indicating the non-toxic nature of prodigiosin and (C) Pictorial representation of the application of prodigiosin as an antibacterial, non-toxic pH indicator.

Further, the prodigiosin is evaluated for its cytotoxic effects on the BHK-21 cells with concentrations ranging from 0.25-2 mg/mL (Figure. 5. 6 (B)). Fibroblasts like BHK-21

adherent cell lines, and are widely used to study the cytotoxicity and cell adhesion on polymer products. Also play an important role in an immune response to a tissue injury. It was found that the prodigiosin is non-cytotoxic, in which the cell viability is directly proportional to the prodigiosin concentration in healthy cell lines. At 1 mg/mL the cell viability is the same as that of the control, above which the prodigiosin promotes the cell growth, and it has been increased to ~120%. This effect is supported by some previous studies, where the prodigiosin showed a cytotoxic effect against the malignant cells, while it is relatively less toxic on non-cancerous cells [154].

Table 5.1. Color properties of prodigiosin at acidic, alkaline, and neutral pH.

pH	L*	a*	b*	ΔE	C*	H
Alkaline	89.4	13.9	52.7	56.1	54.5	75.2
Neutral	77.9	46.4	13.2	53.9	48.3	15.8
Acidic	76.6	50.7	-1.8	56.7	50.8	357.8

The healing process of the acute or chronic wound progresses in an order of alkaline to neutral state when healing begins and proceeds towards the acidic state on complete healing. Here the prodigiosin exhibits yellow color in chronic wound conditions, an orange color in neutral pH, indicating the onset of the wound healing process, and pink color in the acidic pH indicating the healed skin. Thus it could be an effective wound-healing indicator with antibacterial and non-cytotoxic properties Figure. 5. 6 (C).

Prodigiosin is also compatible with various cellulosic materials as well as gels. The prodigiosin-containing gel was evaluated for its indicator effect with phosphate buffer with alkaline, neutral and acidic pH to mimic the biological fluid. The results obtained are shown in Figure. 5. 6. This characteristic color property of prodigiosin in ethanol solution is quantified at different pH. Indicating the dark colors with rose, orange, and yellow color coordinates with pH acidic, neutral, and alkaline, respectively. The color change was observed with a change in pH. Indicating the applicability of prodigiosin in various other biomedical applications.

5.3 Conclusions

The isolated strain *Serratia nematodiphila* CoE-SusPol1 exhibited swarming motility along with a capacity to initiate the C4-AHL and C6-AHL autoinducer-mediated prodigiosin synthesis. However, the absence of such molecules downregulated the prodigiosin synthesis in the presence of glucose by the formation of inhibitory products. The MALDI-TOF-MS is a potential tool used in the identification of products and byproducts. The obtained prodigiosin, after extraction and purification, possesses excellent antibacterial and non-cytotoxic properties with pH-sensitive color-changing behavior.

CHAPTER 6

Synthesis of Metal-Free Poly(lactic acid) (PLA) using Prodigiosin as a Catalyst

Graphical Overview

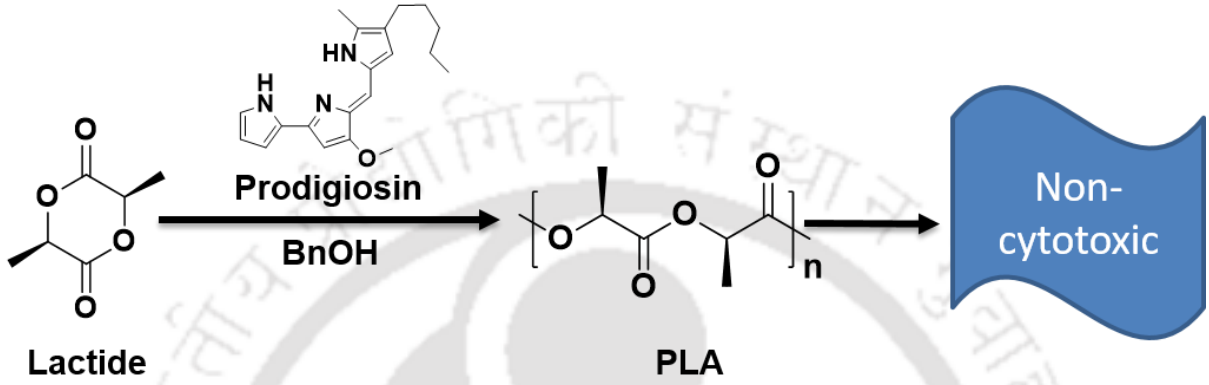

The present study demonstrates the use of prodigiosin (PG) extracted from *Serratia nematodiphila* CoE-SusPol1 isolated from wastewater as a metal-free organic catalyst for ring-opening polymerization (ROP) of L-lactide to produce a metal-free poly(lactic acid) (PLA). Prodigiosin is a tripyrrole small organic molecule synthesized by bacteria with a molecular mass (m/z) of 323.6. The ROP of L-lactide was performed in the presence of benzyl alcohol as a nucleophile and PG as a catalyst. The effect of catalyst concentration in polymerization was evaluated to produce the PLA with a targeted molecular weight (M_n) of 5000 Da at the lactide to PG molar ratio of 2500, which will be useful for drug delivery applications.

Patent:

- Vimal Katiyar, Chethana Mudenur, and Amit Kumar. Metal-free prodigiosin catalyst for lactide polymerization. Indian Patent No (Granted): 419571

Publication:

- Chethana Mudenur, Doli Hazarika, Amit Kumar, and Vimal Katiyar, Ring-opening Polymerization of L-lactide using Metal-free Bacterial Prodigiosin, *ACS Organic Letters* (Under Review)

Further, the synthesized polymer was analyzed by MALDI-TOF-MS, IR, and NMR to access the reacting species involved in the polymerization. Accordingly, the mechanism of PG-based polymerization has been proposed. Further, the synthesized PLA has been assessed for its thermal properties and elemental composition. The cytotoxicity test performed on baby hamster kidney fibroblast cells (BHK-21) confirmed the non-toxicity of the developed PLA, which renders it a potential biomaterial for drug carrier applications.

6.1 Introduction

Wide varieties of biodegradable polymers are currently in use for applications including medicine, pharma, drug delivery, and internal fixation devices, out of which the poly(lactic acid) PLA has received keen attention for its use in bioresorbable products and controlled drug delivery systems due to its biocompatibility and bioresorbable property [155], [66]. PLA is a bio-based aliphatic polymer produced by the condensation polymerization of lactic acid [64] and the ring-opening polymerization (ROP) of cyclic lactide [65]. These are the lactone-based polymers, which polymerize on heating in the presence of catalysts or initiators, and a wide range of metallic and organometallic catalysts have been explored to date for the ROP of lactide. These comprise the compounds of alkoxides, oxides, carboxylates, tin, zinc aluminum, etc. Tin(II) 2-ethyl hexanoate is the most widely used catalyst in the ROP of lactide. Despite its high activity with less reaction time, removing a tin component from the produced product is practically impossible, which leads to a toxic end product [66]. This is the foremost concern that limits its applications in the field of medicine and implant fixation devices. Therefore, there is a need to develop environment-friendly processes and products to tackle such challenging issues. In the current scenario, extensive research has been focused on finding alternative catalysts devoid of heavy metal compounds. Organic catalysts are such promising candidates which could substitute the existing catalysts in an eco-friendly approach.

Organocatalysis is an emerging and environmentally friendly process, and organic catalysts are the potent alternatives for many transition metal catalysts and organometallic catalysts [156] [157]. The organocatalysts are the powerful small organic molecules used to accelerate the chemical transformations in substoichiometric quantities in addition to controlling the selectivity of the reaction of interest [158]. Organic catalysis involves the development of chemical reactions under metal-free conditions with high catalyst stability and robustness without any toxic metals in the produced products [159]. The first investigation on the use of 4-dimethylaminopyridine (DMAP) for ROP of lactide and lactones in the presence of alcohol initiators [160], [161] has encouraged the exploration of more organic catalysts for lactone-based monomers. Indeed, the progress in this field of research has many advantages for metal-based catalysts. Following the DMAP, other organic catalysts were investigated to catalyze the ROP, out of which the N-heterocyclic molecules such as 4-pyrrolidono-pyridine (PDP), 2-methyl-pyridine, pyridine, pyrrole, and imidazole [162], 1-isopropyl-3(4-methoxyphenyl)imidazole-2-carbene [163], acyclic guanidines [164], amino-oxazoline, amino-thiazoline [165] are prominent molecules capable of catalyzing the polymerization reactions. MacMillan catalysts and proline are some other organocatalysts known as universal organic catalysts because of their effectiveness to catalyze a wide range of practical explorations [166]. These are enantioselective, asymmetric imidazolidinone-based organocatalysts used in the fluorination, chlorination, and aldol reactions [167]. The advantages of catalyzing the reaction in metal-free conditions include the insensitive nature to oxygen and moisture, dealing with robust and stable catalysts, and obtaining the final products free of toxic metal leachates [168].

Here the alternative organic molecule from bacteria, such as prodigiosin, is investigated for the synthesis of PLA. Prodigiosin is a red pigment primarily characterized by its tripyrrole structure [169]. Prodigiosin is the class of N-heterocyclic organic molecules and a bioactive

secondary metabolite that exhibit numerous biological activities such as antimalarial [170], antibiotic [171], double-stranded DNA cleavage [172], anticancer [173], and immunosuppressive property [174]. The microorganisms produce assorted pigments and are promising sources of organic pigments. The key microorganisms which produce prodigiosin are *Serratia marcescens* [175], *Vibrio psychroerythrus* [176], *Streptomyces coelicolor* [177], *Alteromonas rubra* [178] *Pseudomonas putida* [179], etc. It demonstrates potent cytotoxic activity against human cancer cell lines with negligible or no cytotoxic effects on normal cells [180]. It consists of tripyrrole rings with a molecular formula of $C_{20}H_{25}N_3O$ [181]. This tripyrrole species is a parent compound for synthetic analogs such as prodigiosenes having diverse biological activity profiles [182]. It has an architype scaffold with tripyrrole moiety which is bridged by the methylene group similar to the heme-group of the blood [183].

The current work demonstrates the development of the nontoxic and metal-free PLA by utilizing the bacterial secondary metabolite prodigiosin as a catalyst. The investigation focused on the development of prodigiosin incorporated PLA. Subsequently characterizing the obtained PLA having a wide range of molecular weights using various characterization techniques such as MALDI-TOF-MS, NMR, and IR to determine the reactive species responsible for the polymerization reaction and determination of the molecular weight of the polymer using gel permeation chromatography. To establish a synthetic approach, the current work adopted the process of ring-opening polymerization, which is used ubiquitously for the development of poly(lactic acid). It is also expected that the lactide monomers could be converted to polymers, which bear various end groups depending on the catalysts used in the process. It also demonstrated the synthetic applicability of bacterial metabolites in the field of sustainable polymers.

6.2 Results and discussion

6.2.1 Effect of PG concentration on the ROP of L-lactide

The variation in M_n, M_w, and PDI with the variation in the [L]/[PG] ratio is shown (Figure 6.1). The behavior of the PG was examined during the bulk ROP of L-lactide in the presence of BnOH as a chain transfer agent. The number average molecular weight increased with an increase in the [L]/[PG] ratio up to the optimum dose. Further, a decreasing trend is observed. The same trend could be observed with the ROP of lactone-based monomer using N-heterocyclic carbene (NHC)-adducts with $SnCl_2$, $Sn(OAc)_2$, $AlCl_3$ as catalysts [184]. With an increase in the ratio, the molecular weight increased and reached to maximum M_n of 5000 Da at a molar ratio of [L]/[PG]=2500, indicating the optimized performance of the PG as an organocatalyst. Beyond this ratio, the molecular weight gradually decreased. The behavior of the PG was examined during the bulk ROP of L-lactide in the presence of benzyl alcohol as a chain transfer agent. Low molecular weight polymers <10000 Da are used in cancer treatment which helps in the plasma clearance to penetrate the drug deeper at the targeted tumor site [185].

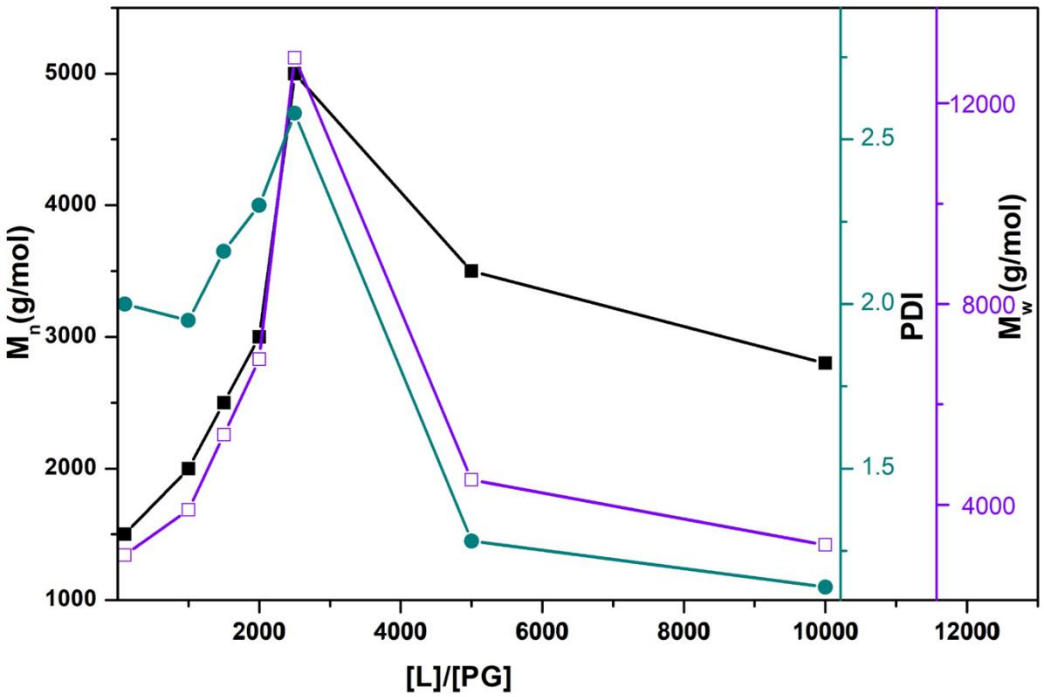

Figure 6.1 Graphical representation of the effect of [L]/[PG] concentration on M_n, M_w, and PDI at 180 °C for 12 h.

6.2.2 Determination of the reacting species involved in the ring-opening polymerization of L-lactide

The MALDI-TOF-MS analysis was performed for prodigiosin, and the obtained mass spectra are depicted (Figure 6.2A). The intense peak at m/z of 323.6 confirmed the molecular mass of prodigiosin bearing a molecular formula of $C_{20}H_{25}N_3O$. The prodigiosin is from *Serratia nematodiphila*. This exhibits a maximum absorbance wavelength of 535 nm.

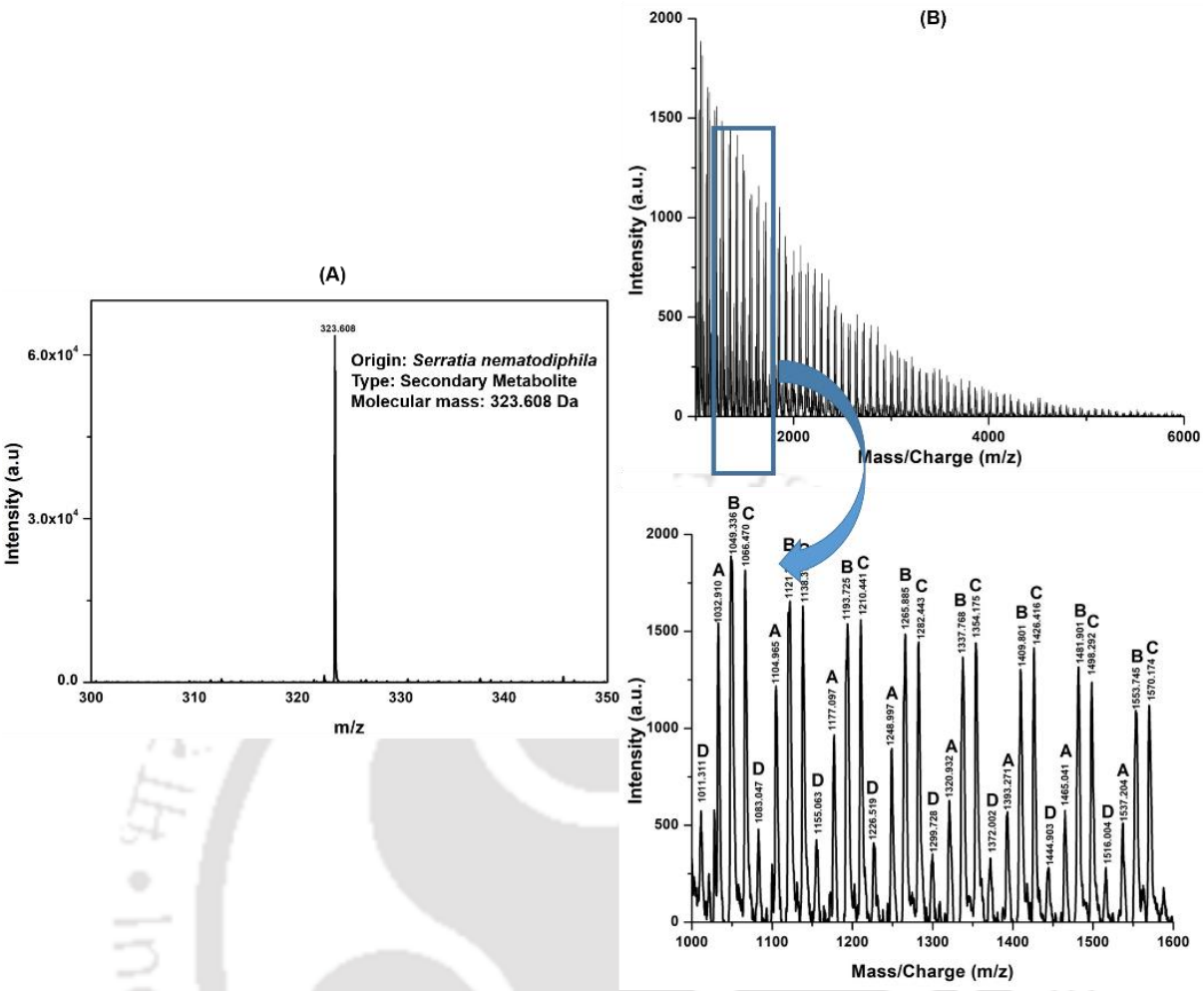

Figure 6.2. (A) MALDI-TOF mass spectra of the bacterial prodigiosin and (B) MALDI-TOF-MS analysis of PLA obtained at a ratio of [L]/[I]=2500 at 180 °C for 12 h. The peaks A, B, C, and D satisfy the equations I, II, III, IV.

The MALDI-TOF mass spectra of the PLA synthesized by PG+BnOH initiated bulk ring-opening polymerization are depicted by the mass spectra (Figure 6.2B), and the portion of the spectra is enlarged and represented below to calculate the mass of each repeating unit. The MALDI-TOF-MS data is corroborated by NMR to find the reacting species involved during the ROP. The plausible end groups of the PLA samples obtained in the current study are indicated by the equations below.

$$M^A = 72x + M_{Na^+}(23) \ldots\ldots\ldots\ldots\ldots\ldots\ldots\ldots\ldots\ldots \text{(I)}$$

$$M^B = 72x + M_{BnOH}(108) + M_{H^+}(1) \ldots\ldots\ldots\ldots\ldots\ldots \text{(II)}$$

$$M^C = 72x + M_{PG}(323) + M_{Na^+}(23) \ldots\ldots\ldots\ldots\ldots\ldots \text{(III)}$$

$$M^D = 72x + M_{H^+}(1) \ldots\ldots\ldots\ldots\ldots\ldots\ldots\ldots\ldots\ldots \text{(IV)}$$

Where, M^B and M^C are the masses of linear PLA, bearing BnOH and PG as end groups with hydrogen and sodium adduct ions. M^A and M^D are the masses of the ring or cyclic form of PLA with sodium and hydrogen adduct ions, and *x* is the number of lactyl repeat units, each having a molecular weight of 72.

The spectra showed four series of peaks exhibiting an interval with a mass-to-charge ratio m/z of 72 corresponding to the lactyl repeating units. The four distinct peaks molecular weights are assigned as A, B, C, and D. The peaks A and D indicate the formation of the macrocyclic chain with even and odd values of *x*, respectively, bearing the Na^+ and H^+ adduct ions without PG or BnOH. This effect may be due to the backbiting of the propagating ions; the same effect was reported in a reaction catalyzed by the 4-pyrrolidino-pyridine [70], or due to the intramolecular trans-esterification reactions occurring during the polymerization reactions [186]. Indicating the function of benzyl alcohol as a chain transfer agent during the polymerization reaction. PLA synthesized by PG+BnOH contains diverse types of PLA chains. The masses of which are represented by equations I, II, and III. These equations are validated with four distinct peak envelopes, A, B, C, and D. Where C confirms the growth of the PLA chain with one prodigiosin terminal group and B with BnOH as a terminal group.

6.2.3 Determination of the functional groups of PLA synthesized using prodigiosin

The ^{13}C NMR spectra of the produced PLA (Figure 6.3) are represented, and the peak at ~68 ppm corresponds to the -CH_2 of BnOH attaching to PLA. Methyl carbon at 16.7 ppm, methyne carbon at 69.1 ppm, and carbonyl carbon at 170 ppm. This indicates the chain transfer to the BnOH by the growing chain occurs efficiently, which leads to the formation of a linear chain of PLA with alcohol terminated and a PG terminated chain. Such structures are correlated with the results obtained by the MALDI-TOF mass spectra.

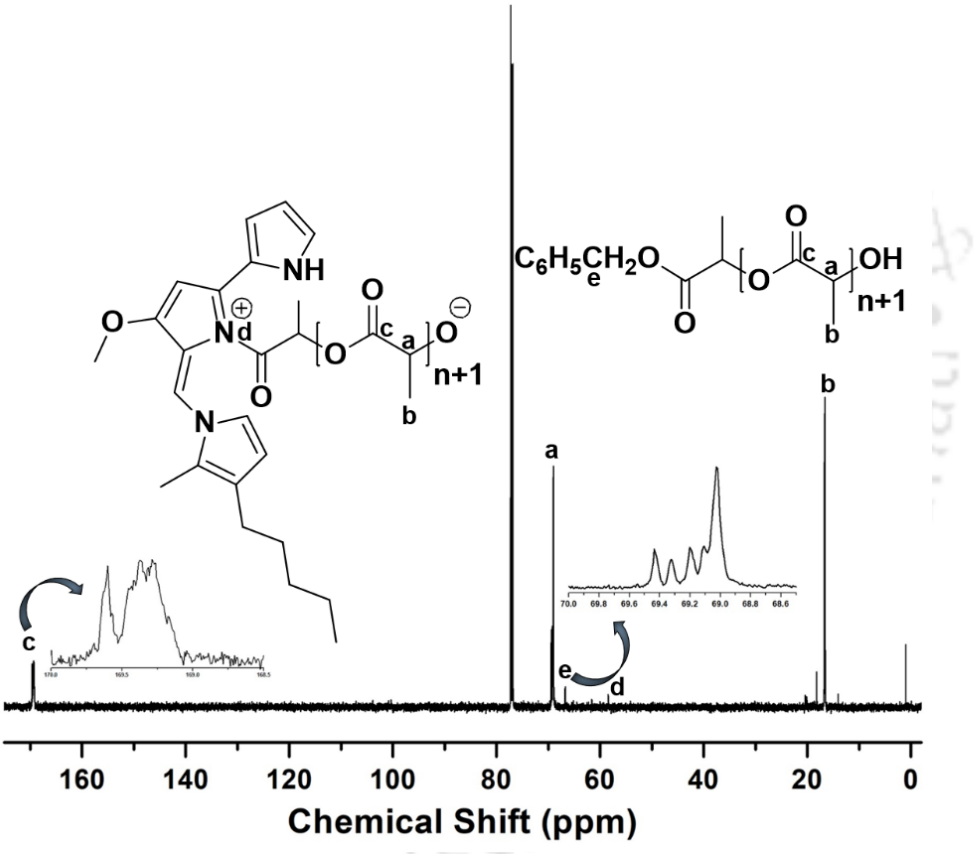

Figure 6.3. ^{13}C NMR spectrum of PLA in chloroform-d synthesized using PG+BnOH with [L]/[PG] ratio of 2500 at 180 °C with a reaction time of 12 h.

6.2.4 Plausible polymerization mechanism

The stability of the prodigiosin has been analyzed first to determine the possibility of the direct participation of the prodigiosin molecule in the polymerization reaction. The degradation temperature of the prodigiosin indicated that it does not undergo a significant mass change at the temperature suitable for polymerization. Further, the reaction was carried out in the presence of PG+BnOH, and the individual reactions involving the BnOH and PG were unsuccessful, which yields the PLA with very few repeating units. Therefore, the presence of both the PG and BnOH is necessary for the polymerization reaction to produce the PLA with a considerable chain length.

The proposed ROP reaction is depicted (Figure 6.4). The L-lactide first reacts with PG to form product A shown in the reaction mechanism.

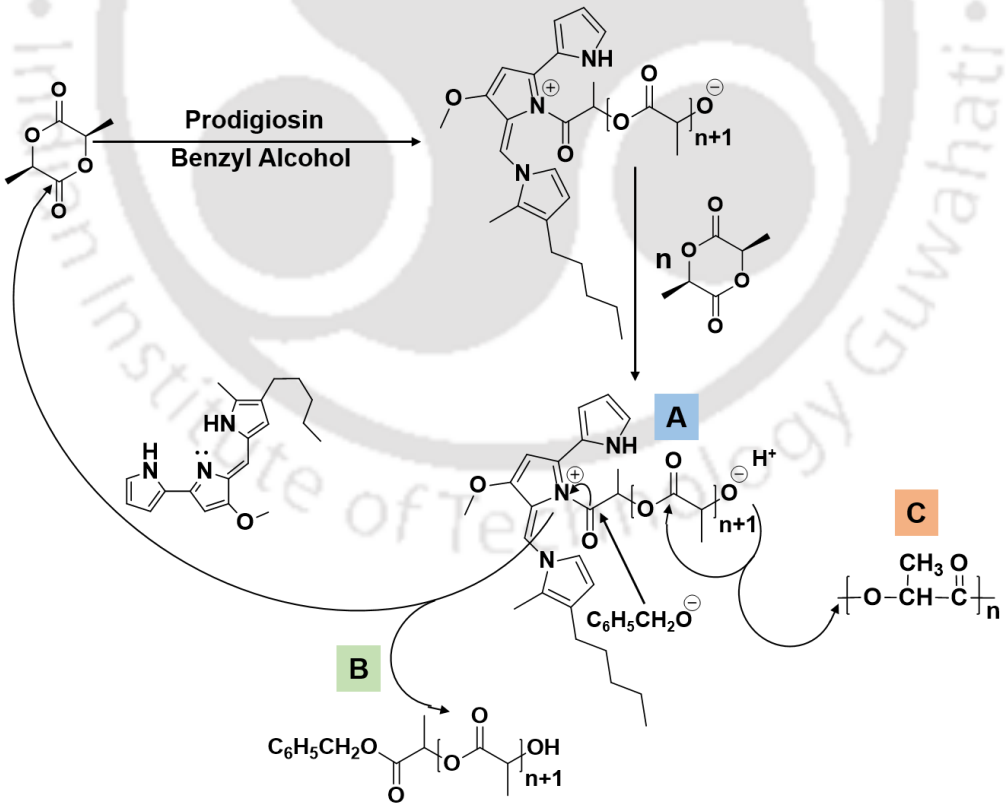

Figure 6.4. The plausible polymerization mechanism for ROP of L-lactide by PG in the presence of BnOH.

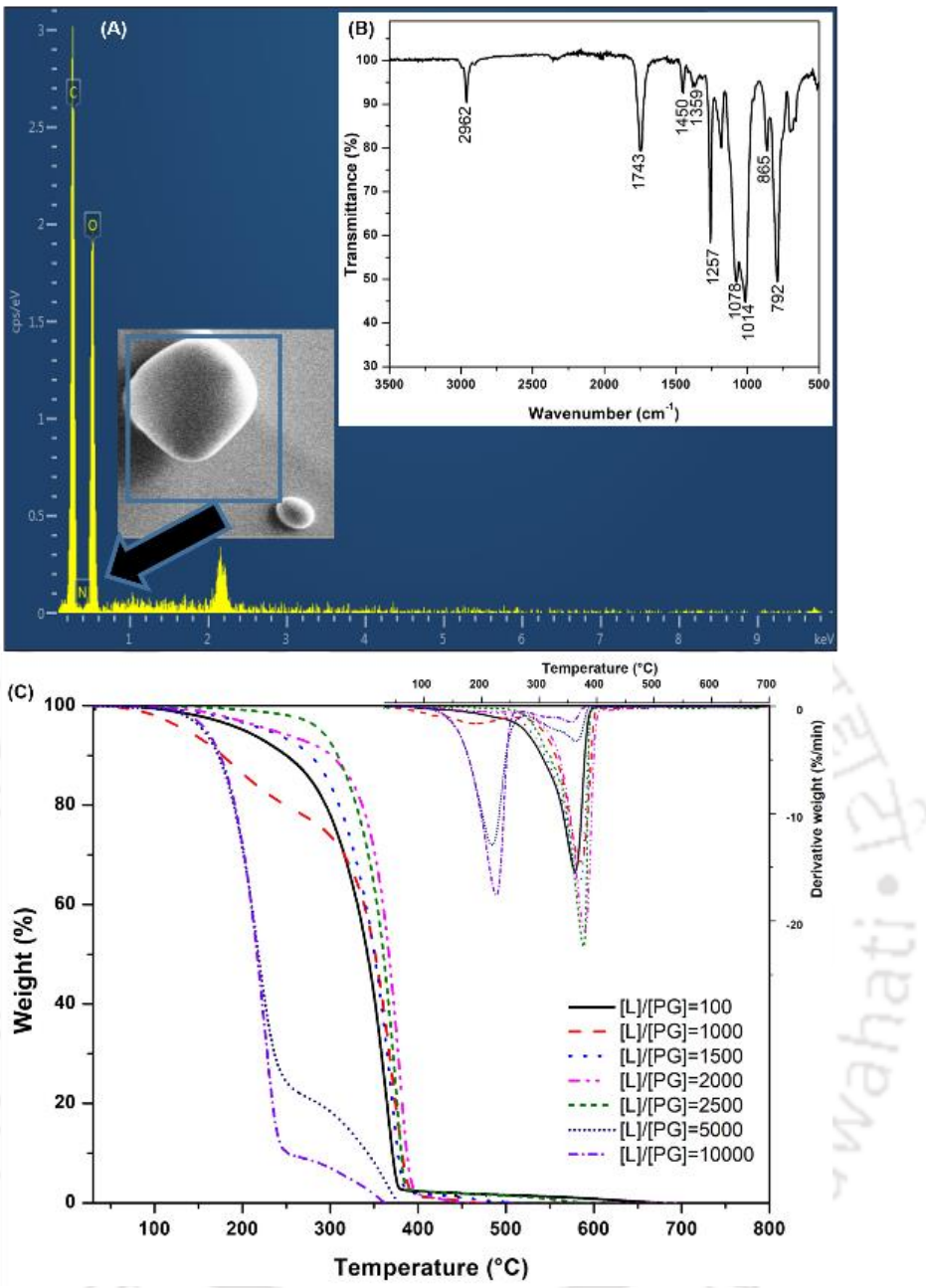

Figure 6.5. (A) FESEM/EDX indicating the insertion of prodigiosin in the PLA chain synthesized using PG+BnOH (B) FTIR spectrum indicating the characteristic functional groups representing the PLA and (C) TGA thermograms of PLA synthesized using PG+BnOH with [L]/[I] from 100 to 10000 at 180 °C for 12 h.

In IR spectra (Figure 6.5B) revealed the characteristic stretching frequency at 2962 cm^{-1} indicates the presence of aromatic -CH stretch of the benzyl group, 1743 cm^{-1} indicates the C=O, 1450 cm^{-1} is due to the $-CH_3$ bend, bending frequencies for $-CH_3$, C=O were identified

at 1359 cm^{-1} and 792 cm^{-1}, 1257 cm^{-1} indicates the formation of C-N bond between PG and lactide, which is also supported by the ^{13}C NMR, peaks between 1078 cm^{-1} and 1014 cm^{-1} are due to the -CH in-plane deformations and 865 cm^{-1} are due to the presence of N-H. The peak at 792 cm^{-1} is due to the presence of C=C of benzyl-terminated PLA chains. The FESEM/EDX spectra (Figure 6.5A) depict the elemental composition of the synthesized PLA. The presence of carbon and oxygen nitrogen groups of the lactide and prodigiosin.

6.2.5 Thermal stability of the synthesized PLA

The thermal stability of the developed PLA is evaluated, and the thermograms (Figure 6.5C) of the weight (%) vs temperature and differential thermogravimetry (DTG) were obtained. It is found that the increase in the [L]/[PG] ratio leads to the increase in the thermal stability of the PLA and reaches a maximum onset degradation temperature of 340 °C for [L]/[PG]=2000 and 2500, whereas the offset degradation temperature of ~390 °C. The maximum degradation was found to be almost the same for [L]/[PG]=2000 and 2500, which is 379 and 377, respectively. Some of the previous studies have reported the degradation temperature of the PLA. Whereas the two-step degradation was observed for the sample[L]/[PG]=5000 and 10000, its effect is due to the inefficient conversion of the L-lactide to PLA, the lower degradation temperature is due to the L-lactide, and the higher degradation temperature is due to the PLA with prodigiosin as an end group. The lower degradation temperature is due to the amorphous form of polymer with very low molecular weight.

6.2.6 Cytotoxicity test against BHK-21 cells

The cytotoxicity test against the BHK-21 cells was performed. The results of relative cell viability (%) with respect to control are depicted (Figure 6.6). The PLA samples with a concentration of 0.25-2.0 mg/mL were tested for their cytotoxic effects. It was found that the PLA supported the cell growth with an increase in the sample concentration. [L]/[PG]=2000

sample was found to be more suitable for cell growth with a 2-fold surge in the cell viability compared to the control experiment. Above this concentration, the cell viability decreased, though cell viability is more than 100% in comparison to control for all the samples. After 48 h of exposure, the PLA samples were demonstrated as supporting materials for cell growth and development without any cytotoxic effects. It is noteworthy that with an increase in the concentration of PLA, the cell viability has increased 2 folds. It is the most promising approach for safer polymeric materials. It is a safer candidate applicable as a carrier for drug delivery applications.

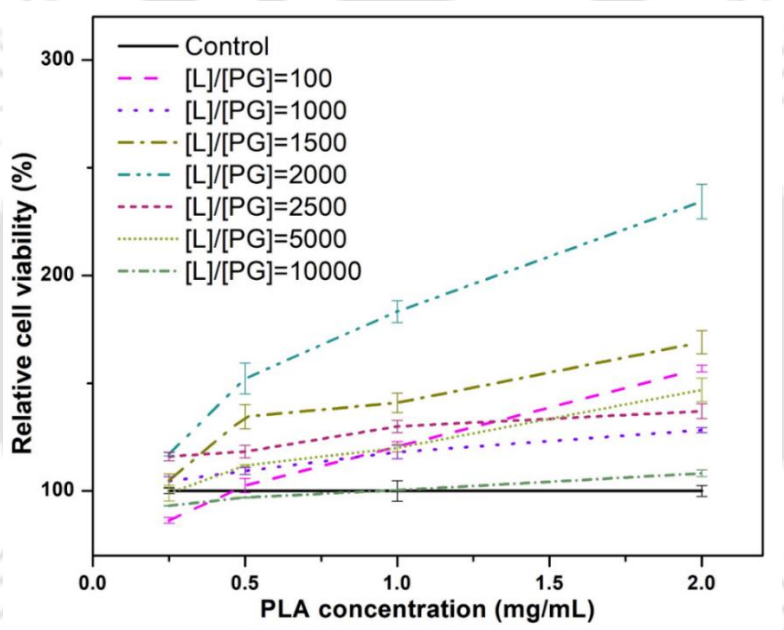

Figure 6.6. The relative cell viability (%) data after 48 h of incubation with synthesized PLA samples.

6.3 Conclusions

The present work demonstrates the utilization of bacterial secondary metabolite prodigiosin as an effective organic catalyst for the ROP of L-lactide. Understanding the mechanism of action of bacterial secondary metabolites as eco-friendly catalysts to create biocompatible polymers. The current investigation also represents the possible side reactions during the ROP to form macrocyclic chains and the possible end groups confirmed from the MALDI-TOF-MS and NMR correlations. Further, the cytotoxicity test indicates the least to no cytotoxic effect on the BHK-21 cell lines, which is an advantage to being used as a drug carrier system without cytotoxic effects.

CHAPTER 7

Prodigiosin-Loaded Poly(lactic acid) to Combat the Biofilm-Associated Infections

Graphical Overview

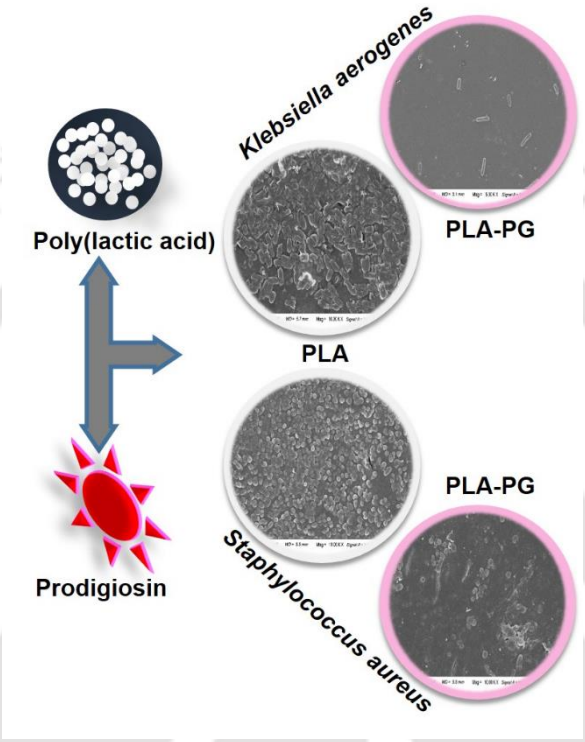

Poly(lactic acid) (PLA) is an emerging bio-based implant material. Despite its biocompatibility and the aseptic procedures followed during orthopedic surgery, bacterial infection remains an obstacle in implementing PLA-based implants. To tackle this issue, prodigiosin incorporated PLA has been developed, which possesses an improved hydrophobicity with a contact angle of 111±1.5°.

Publication:

- **Chethana Mudenur**, Pankaj Boruah, Amit Kumar, and Vimal Katiyar, 2022, Prodigiosin-loaded poly(lactic acid) to combat the biofilm-associated infections, *ACS Applied biomaterials*, 2022 April 25, 5 (5), 2143-2151.

The degradation temperature of the prodigiosin is 215 °C, which is more than the melting temperature of PLA supports the processability and sterilization of the PLA-based implants without any toxic gases. Further, the prodigiosin improved the transparency of the PLA and acted as a nucleation site. The spherulite density increases three times compared to the neat PLA. The inherent methoxy group of the prodigiosin is an active site responsible for the inhibition of bacterial attack and biofilm formation. The *in vitro* study on biofilm formation shows excellent inhibition activity against implant-associated pathogens such as *Klebsiella aerogenes* and *Staphylococcus aureus*.

7.1 Introduction

The advancements in the field of biodegradable internal fixation devices have contributed to the field of medicine due to their biocompatibility and non-toxic nature. The most commonly used bio-based and biocompatible polymers in the manufacturing of implants are poly(lactic acid) (PLA) [187], collagen [188], [189], silk [190], [191], keratin [192], [193], etc. The application of biocompatible polymers in the field of biomedical engineering is growing rapidly due to their effectiveness in substituting defective parts of the body or biological function. These materials are chemically inert and possess properties comparable to the inherent anatomical structures [67]. Despite the advantages, these implant materials are susceptible to bacterial attack and biofilm formation, which account for a greater portion of hospital-acquired infections. These infections are caused by various opportunistic pathogens, depending on the implant site, material composition, and properties. The main reason behind the infection is the surface interactions between the biomaterial and the pathogen in the presence of the immune response of the host [68]. Bacterial adhesion on the polymer surface is the first and most critical period of bacterial colonization on the surface of medical devices [69].

Gram-negative *Klebsiella aerogenes* (*Enterobacter aerogenes*) [194] and, Gram-positive *Staphylococcus aureus* [195] are opportunistic pathogens responsible for nosocomial, and implant-associated infections. These are the key bacteria responsible for up to 60% of implant-associated infections capable of spreading rapidly and initiating the process of biofilm formation. These bacteria invade via intraoperative procedures through direct contact or spread from a wound through the circulatory system [196]. Patients in healthcare settings are susceptible to bacterial infections and biofilm formation at the site of internal fixation devices after orthopedic surgery. Unfortunately, the composition of the implant material, medical tools, and hospital conditions allow pathogenic bacteria to enter the body and develop infections at the site of implants. The prevalence of implant-associated infections is increasing due to the use of extended antibiotic therapy [197], which leads to the development of pan-drug resistance in bacteria. Such infections are further associated with perpetual hospitalization and mortality [198].

Implant-associated infections that develop from microbial contamination are regarded as postoperative infections. The treatment of serious infections associated with surgical implants involves a highly expensive procedure and is associated with uncertainties. Therefore, the prevention of such infections precedes the administration of antibiotics in systemic circulation in post-operative procedures [199]. Gamma radiation and alcohol disinfection are the commonly used sterilization methods to get rid of bacteria adhered to the surface [200]. Some methods also involve the surface coating of the implant using platinum, palladium, gold, titanium, nickel, silver, etc. However, some of the metals are toxic, which affects the various organs of the human body [201].

The main focus of the current study is to develop the prodigiosin-loaded PLA with inherent antibacterial activity and improved material properties. The adhesion and biofilm formation results are correlated with the material functionalization, surface wettability, and bacterial

interaction with the developed surface. The study also verifies the extent of inhibition of implant-associated pathogens such as *Staphylococcus aureus* and *Klebsiella aerogenes.*

7.2 Results and discussion

7.2.1 Effect of prodigiosin on optical transparency and color characteristics

The anatomical structure of each body part and the organ system consists of different tissue layers. The slight variation in these physiological responses leads to the alteration in absorption, refractive index, and spectral features of the light reflected. The conventional cranial prosthesis, such as titanium and acrylic materials, do not provide the desired transparency, which is a major drawback [202]. Pictorial representation indicates (Figure 7.1 A) the process of preparation of the prodigiosin-loaded films by solvent casting method, the film thickness of ~0.12 mm was maintained for all the samples.

The obtained nPLA, PLA-PG-C, and PLA-PG-P films and the respective digital photographs are presented for the visual effect of transparency (Figure 7.1 B). Further, the prodigiosin loading enhanced the optical transparency of the PLA films up to 70% in both ultraviolet and visible regions in comparison to the nPLA films (Figure 7.1 C). A slight dip at 535 nm in prodigiosin-loaded films indicates the presence of a characteristic absorption peak of prodigiosin molecules in polymer films. This unique property could be helpful in wavelength-specific sensing applications in the field of biomedical engineering.

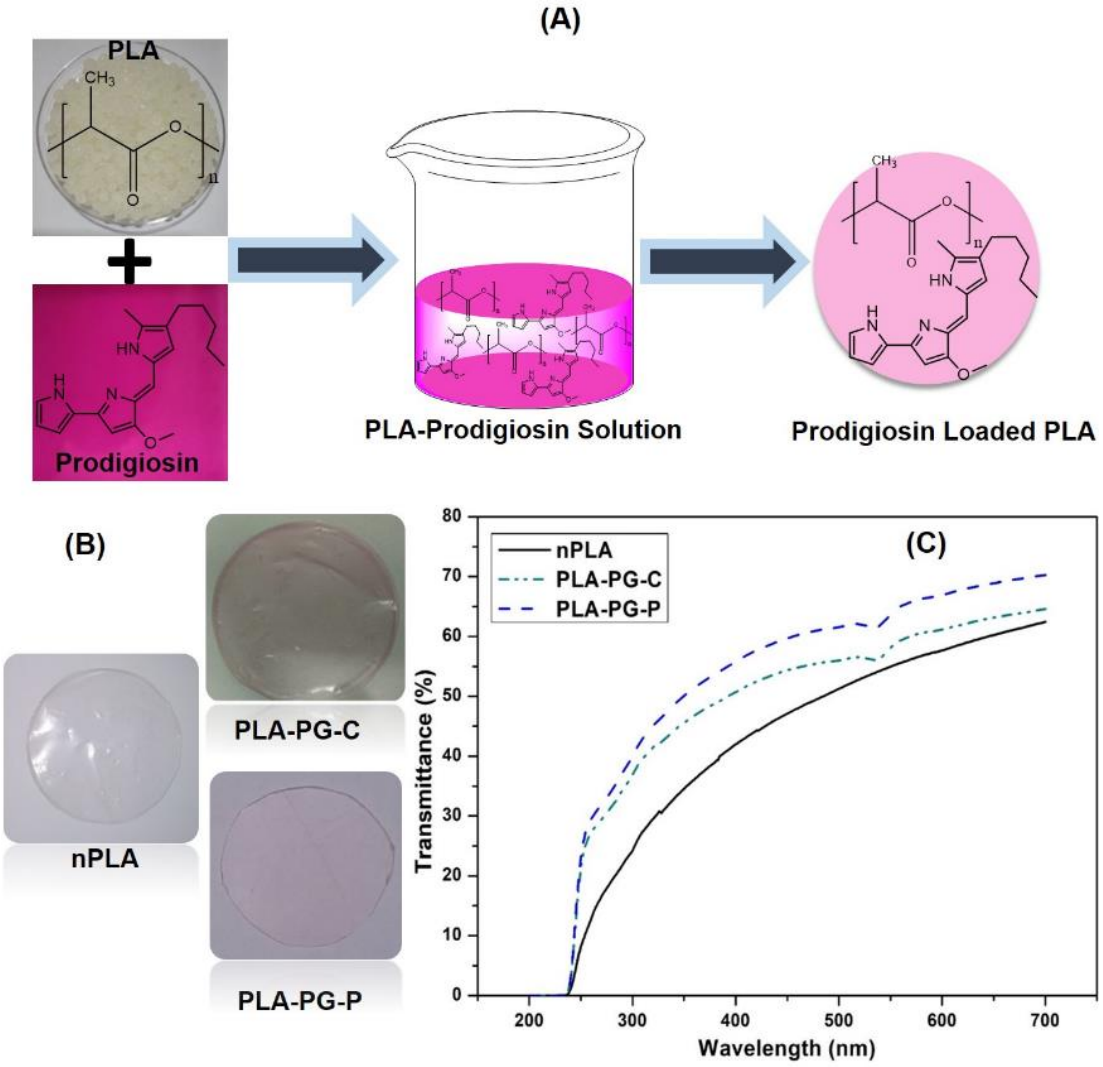

Figure 7.1. (A) Schematic representation of the method of preparation of prodigiosin-loaded PLA films (B) Digital photographs of the developed films and (C) Transparency of the developed neat PLA and prodigiosin-loaded PLA films.

The color characteristics (Table 7.1) indicate the extent of the color change of prodigiosin-loaded PLA in comparison to nPLA. The developed material is light pink in color due to the addition of prodigiosin with a color strength value increasing from 100 to 146 indicating the depth of the colored polymer.

Table 7.1. The color characteristics of the developed nPLA, PLA-PG-C, PLA-PG-P.

Sample	L*	a*	b*	ΔE*	C*	H	Color Strength
nPLA	90.9	1.2	5.1	0.2	5.2	76.5	($K/S_{420\ nm}$ =100)
PLA-PG-C	89.3	4.5	5.6	3.7	7.2	51.6	($K/S_{420\ nm}$ =131)
PLA-PG-P	88.8	4.7	6.0	4.3	7.6	51.6	($K/S_{420\ nm}$ =146)

7.2.2 Determination of functional groups of the developed polymer

The FTIR spectral data of the PLA-PG-C and PLA-PG-P films (Figure 7.2A) are almost similar to those of nPLA showing the characteristic major peaks at 1748 cm^{-1} is due to the C=O stretch, 1452 cm^{-1} due to -CH_3 bend, 2920 cm^{-1} represents asymmetric C-H stretch, and this has shifted to 2994 in case of PLA-PG-P, and 2852 cm^{-1} due to symmetric C-H stretch. In addition, the characteristic peaks of prodigiosin were found in the prodigiosin-loaded films with a slight shift towards the higher wavenumber region from 3443 to 3505 cm^{-1} due to N-H stretch and peaks in the range of 1133-1020 cm^{-1} are due to the aromatic pyrrole group. The energy-dispersive X-ray spectroscopy (Figure 7.2 B-D) confirmed the presence of nitrogen (N), a characteristic component of the pyrrole ring of prodigiosin which is loaded in PLA along with carbon and oxygen of nPLA. Whereas only carbon and nitrogen peaks are seen in nPLA films lacking nitrogen

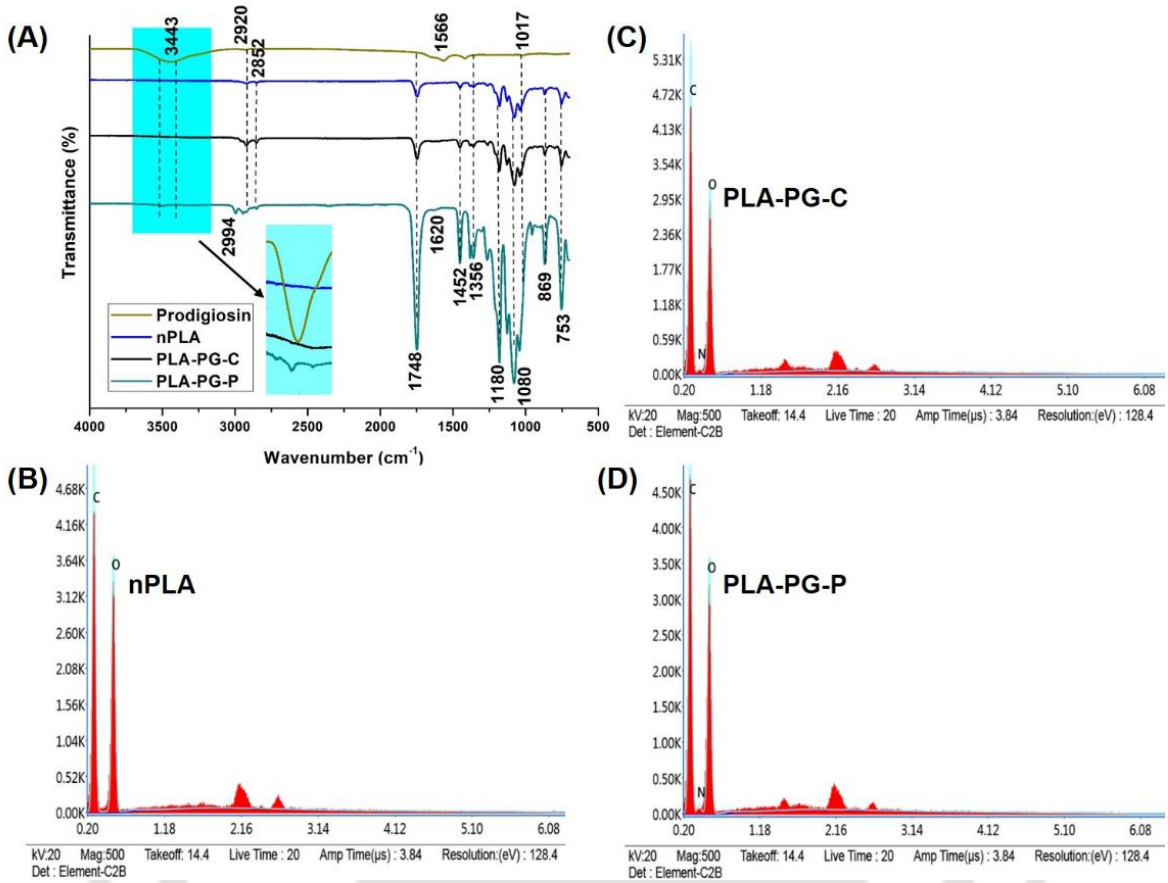

Figure 7.2. (A) FT-IR spectra of the prodigiosin, nPLA, prodigiosin-loaded films (B) FESEM/EDX images of the nPLA (C) PLA-PG-C and (D) PLA-PG-P.

7.2.3 Thermal degradation

The thermal decomposition of the prodigiosin, nPLA, and prodigiosin-loaded films was analyzed in a nitrogen atmosphere (Figure 7.3 A). The decomposition of the prodigiosin started with an onset degradation temperature of (T_{onset}) 170 °C with a weight loss of 5%. The maximum degradation occurs in two steps, the first step at a temperature of 215 °C, and the second degradation step at 296 °C. Further, the complete degradation process continued, and ~45% weight loss is observed between 170-500 °C due to the destabilization of the N-H bonds present in prodigiosin. In contrast, the thermograms obtained for the nPLA and the prodigiosin-loaded PLA reflect a weight loss of ~7% at 150 °C due to the elimination of the moisture content captured in the films. Further, the incorporation of the prodigiosin in PLA did not affect

the degradation temperature of the PLA films. It retains all the unique properties of PLA. Though it has a lower degradation temperature, it did not affect the prodigiosin-loaded films because of its high stability at higher temperatures. However, a slight improvement in the onset degradation temperature of 326 °C, 342 °C, and 358 °C for nPLA, PLA-PG-C, and PLA-PG-P, respectively. Similar results were obtained for the nPLA by the previous studies [203], [201]. This property indicates that the developed PLA can be implemented as an implant material, which can be sterilized to avoid the chances of contamination. It can also be noted that the property of prodigiosin remains the same after the sterilization of the implant materials.

7.2.4 Analysis of the evolved gas components during decomposition

The 3-dimensional graph of TGA-coupled with FTIR indicates (Figure 7.3B) the thermal stability of the prodigiosin-loaded PLA and the release of volatile constituents during the thermal degradation process at different temperatures. It is a very useful technique in which the evolved volatiles help to determine the unique characteristic properties of the samples, which are difficult to identify by TGA alone. Determination of the volatile compounds is important to understand the material properties during sterilization in the case of implant materials. The peak length in this analysis indicates the concentration of the volatile group present in the materials. The stacked IR spectra (Figure 7.3C) obtained for the prodigiosin-loaded PLA exhibit thermal degradation in the temperature range of 30-700 °C.

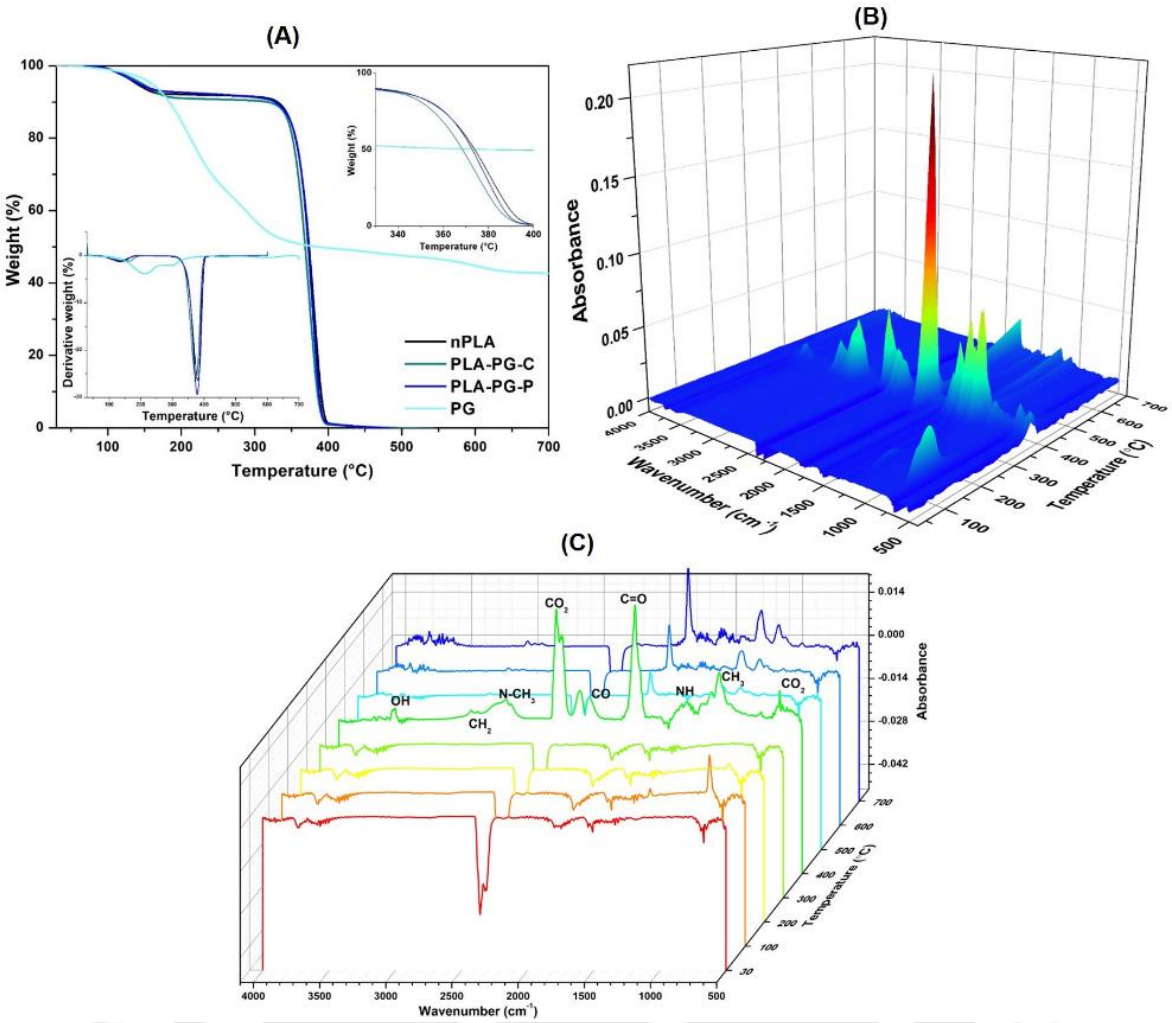

Figure 7.3. (A) TGA and DTG of prodigiosin, nPLA, and prodigiosin loaded films (B) 3-dimensional graph of TGA-FTIR of the prodigiosin-loaded PLA and (C) Stack plot for the characteristic spectra of the degradation products recorded at different temperatures.

The major decomposition starts at 400 °C. The characteristic components evolved at 400 °C are identified, and the bands observed at 824 cm^{-1} are due to the CO_2, 1412 cm^{-1} is due to CH_3, 1512 cm^{-1} is due to N-H, 1766 cm^{-1} is due to C=O, 2384 cm^{-1} is due to CO, 2360 cm^{-1} is due to CO_2, 2752 cm^{-1} is due to N-CH_3, 3004 cm^{-1} is due to CH_2, the peak between 1650-1580 cm^{-1} is due to the N-H stretch, the peak between 3250-3400 cm^{-1} depicts the N-H of prodigiosin

bonded to the water molecule. The peak at 768 cm^{-1} at 100 °C is due to the moisture content captured in the polymer films.

7.2.5 Influence of prodigiosin on spherulite growth rate

Crystallinity refers to the degree of order of the molecules in the polymer. A time-lapse image of the nPLA, PLA-PG-C, and PLA-PG-P was captured to observe the spherulite growth (Figure 7.4C). The comparison of the spherulite growth and the nucleation behavior helps in understanding the bulk crystalline property.

The size of the spherulite was measured in four different time intervals (Figure 7.4A). The initial image was taken at $t_0 = 0$ min, and then the image after every 10 secs was considered for the study. At $t = t_0$ no nucleation was observed for all the samples. However, after 10 min few distinct nucleation points were observed for all the samples. The size of the spherulites increased gradually with time. In comparison to nPLA, the prodigiosin-loaded PLA has more nucleation sites, which originate in the vicinity of the prodigiosin. Therefore, the number of spherulites increased for PLA-PG-P and PLA-PG-C. Distinct-shaped spherulites are observed until t=30 min for all the samples, but at t=40 min the spherulite growth was obstructed by another spherulite for PLA-PG-P and PLA-PG-C. The average diameter of the spherulite is lower for the PLA loaded with prodigiosin compared to nPLA. The growth rate is calculated from the slope obtained by plotting the spherulite radius (μm) vs time (min).

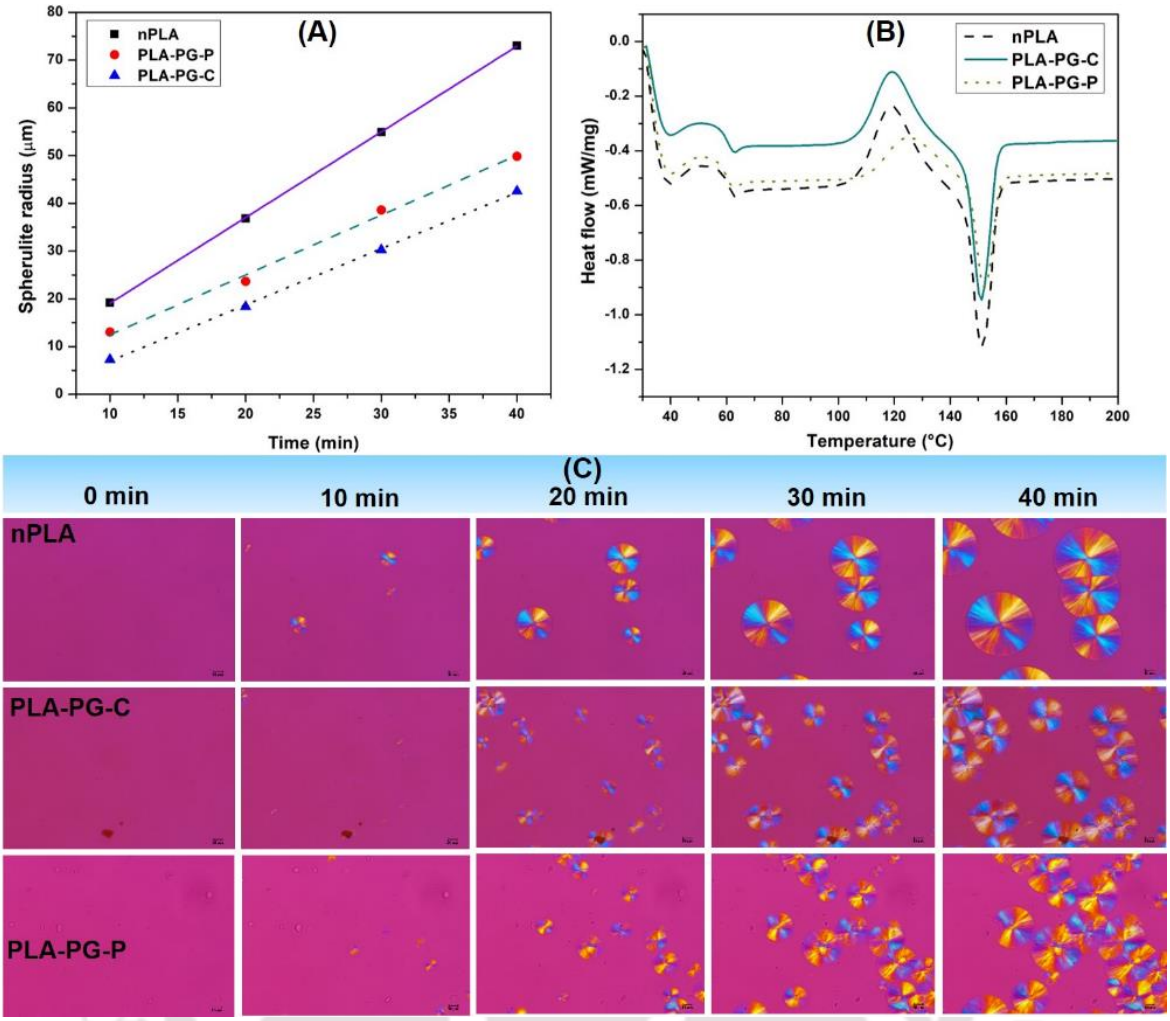

Figure 7.4. (A) Radius and growth rate of spherulite of nPLA, PLA-PG-C, PLA-PG-P; (B) DSC thermograms of the developed films and (C) Polarizing optical microscopy images of nPLA, PLA-PG-C, PLA-PG-P.

The growth rate decreased in the presence of prodigiosin due to the hindering effect. However, the number of spherulites increased due to the action of prodigiosin as a nucleation agent for spherulite formation. The size of the spherulite for nPLA was large relative to the prodigiosin-loaded samples. The growth rate is found to be 1.79, 1.25, and 1.17 for nPLA, PLA-PG-C, and PLA-PG-P, respectively, and the spherulite density increased by 3 times with an appreciable decrease in the size of spherulites with the addition of prodigiosin.

Further, differential scanning calorimetry was performed to check its effect on the crystallization, melting, and thermal behavior of PLA. The obtained data is represented by

thermograms (Figure 7.4B), showing that there is no effect on glass transition, crystallization, and melting temperature (T_g ~60 °C, T_c ~120 °C, T_m ~152 with 30% crystallinity) of PLA with crude prodigiosin. In contrast, slight changes (T_c ~125 °C, ~18% crystallinity) were observed for PLA with purified prodigiosin.

7.2.6 Inhibition of biofilm formation on prodigiosin-loaded PLA

An enormous proportion of healthcare and impact-associated infections are caused due to the presence of *Staphylococcus aureus* [205] and *Klebsiella aerogenes* [206]. These are the common bacteria found in hospital-acquired infections, particularly in surgical site infections. In the current study, the formation of bacterial biofilm is assayed *In vitro* by growing the bacterial cells in the presence of the PLA samples with and without prodigiosin. It is observed that (Figure 7.5A-D) the biofilm formation on the PLA without prodigiosin is more and completely covered the surface of the polymer film, which could be corroborated with the change in the pH of the medium from neutral to acidic in the presence of the nPLA, whereas there was insignificant change in case of prodigiosin loaded PLA films (Figure 7.5) also indicating there is no release of prodigiosin from the developed polymer films. However, the prodigiosin loaded with crude prodigiosin exhibits inhibition activity, but it is less effective than the PLA consisting of pure prodigiosin. The highly effective antibacterial activity was found with the PLA loaded with purified prodigiosin. The effect was similar to both *Staphylococcus aureus* and *Klebsiella aerogenes*. The methoxy group present in the prodigiosin is responsible for the antimicrobial property of the prodigiosin. The methoxy group ($–OCH_3$) is an electron-withdrawing group, and the oxygen here is more electronegative than the carbon. This group will lose the electrons by delocalization of pi electrons due to the lone pairs of electrons on the oxygen atom. In addition, the C-pyrrole ring and the bipyrrole AB-ring of the prodigiosin are responsible for the double-stranded DNA damage, though their

mode of action has not been completely established [207]. However, the developed films are biocompatible without any cytotoxic effects

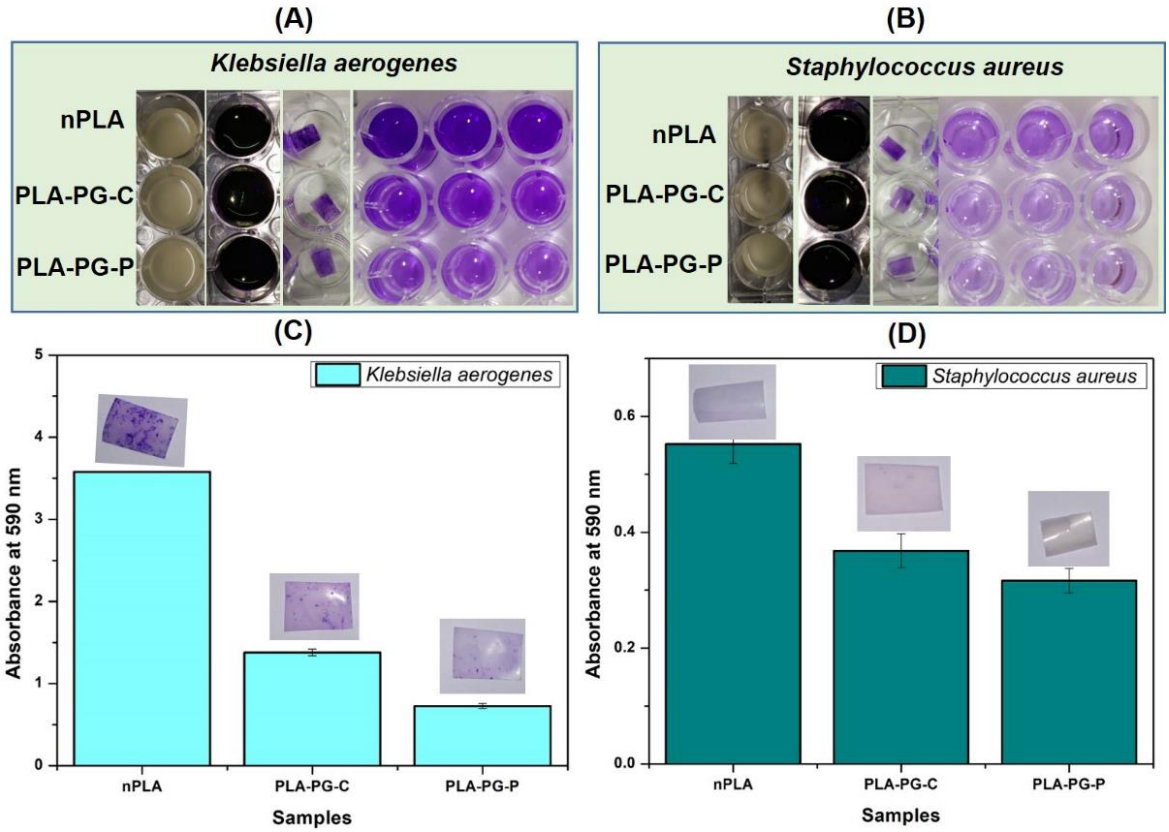

Figure 7.5. (A) Crystal violet staining of the biofilm formed by *Klebsiella aerogenes*; (B) Crystal violet staining of the biofilm formed by *Staphylococcus aureus*; (C) The absorbance of the biofilm formed by *Klebsiella aerogenes* on polymer samples after 48 h and (D) The absorbance of the biofilm formed by *Staphylococcus aureus* on polymer samples after 48 h.

7.2.7 Wettability analysis and morphological study of the biofilm formation

Furthermore, to understand the surface property of the film, the wettability analysis was performed with water. Obtained data represents that the water contact angle (Figure 7.6A) of the prodigiosin-loaded polymers is slightly increased in comparison to neat films. Here the wettability (contact angle θ) of the neat PLA was found to be 68.5° whereas it is elevated to 101° for PLA loaded with crude prodigiosin and 111.55° for PLA loaded with purified

prodigiosin. Such a hydrophobic effect is due to the presence of a long hydrophobic hydrocarbon chain of prodigiosin that makes the polymer more hydrophobic, resisting the water on its surface and bacterial adhesion onto the polymer surface.

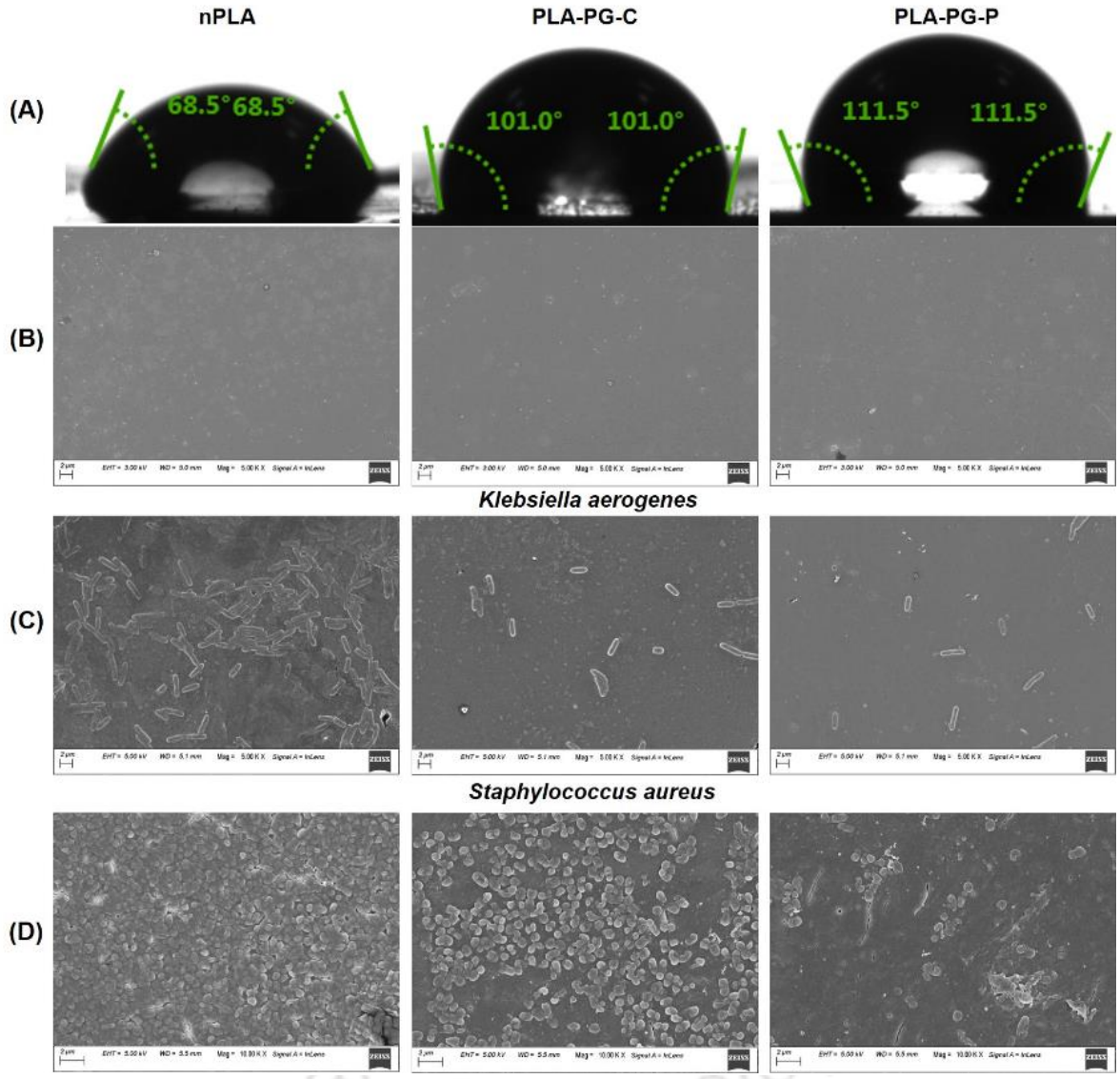

Figure 7.6. (A) Contact angle of water on the nPLA, PLA-PGC, and PLA-PG-P (B) FESEM images of nPLA, PLA-PGC, and PLA-PG-P films before contact with bacteria (C) FESEM images of nPLA, PLA-PGC, and PLA-PG-P films with biofilms of *Klebsiella aerogenes* after 48 h and (D) FESEM images of nPLA, PLA-PGC, and PLA-PG-P films with biofilms of *Staphylococcus aureus* after 48 h.

In addition, the terminal -CH_3 and -OCH_3 hydrophobic groups of the prodigiosin incorporated into the PLA matrix also cause hydrophobicity and oxidative cell damage by attacking the nucleophilic center of the carbonyl group of the peptide bonds present in the bacteria. The peptide bonds of the bacteria are cleaved by the methoxy group of prodigiosin, resulting in the formation of primary amine and carboxylic.

As a result, there is an inhibition in cell multiplication and biofilm formation on the polymer surface. From the morphological analysis using FESEM (Figure 7.6 B-D), it is observed that the prodigiosin is more effective on the *Klebsiella aerogenes* compared to the *Staphylococcus aureus*. It has been observed that there is a formation of a thick layer of biofilm with extracellular matrix material produced by the metabolism of the bacteria in the case of nPLA. However, individual bacterial cells without colonization are observed in the case of the prodigiosin-loaded PLA with few cells on the surfaces. This antibacterial property of the developed PLA is helpful to combat the infections associated with any implants made up of PLA.

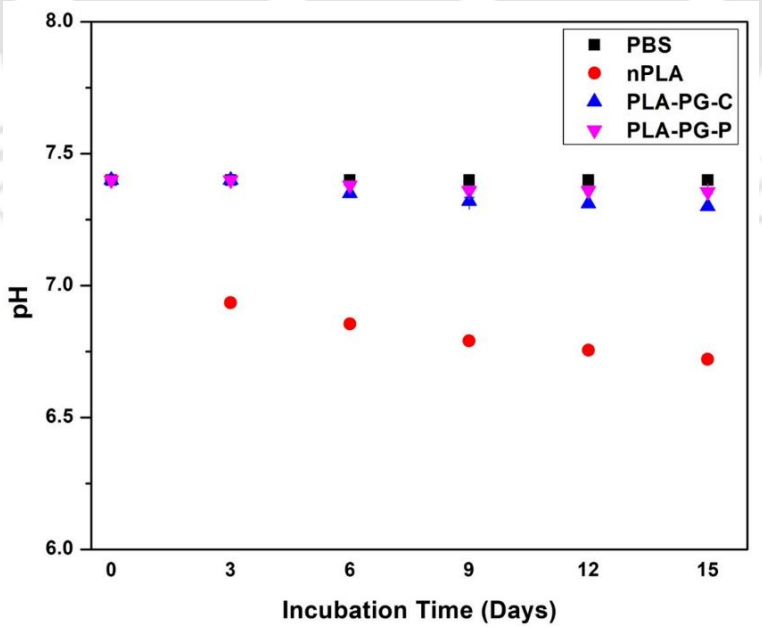

Figure 7.7. Change in the pH of the phosphate-buffered saline solution (PBS) incubated with nPLA, PLA-PG-C, and PLA-PG-P for 15 days.

The change in the pH of the phosphate buffer is observed in Figure 7.7. The solution pH was gradually changed to acidic from 7.4 to ~6.72 after 15 days of incubation. This effect could be due to the hydrolytic degradation of the polymer chains and the release of lactic acid monomers into the solution. However, the change in solution pH is insignificant in the case of the PLA-PG-C, and PLA-PG-P. It indicates that there is no material degradation and there is no release of prodigiosin from the polymer films.

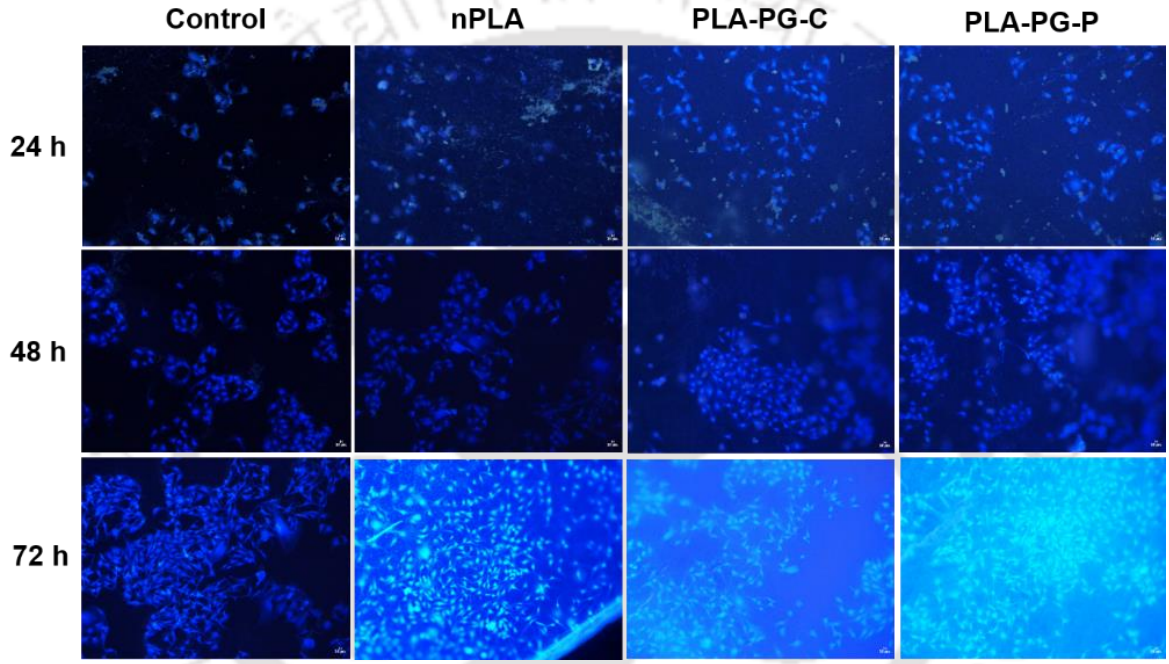

Figure 7.8. BHK-21 cell proliferation on control, without sample, nPLA, PLA-PG-C, and PLA-PG-P at 24, 48, and 72 h of incubation at 37 °C and staining with DAPI.

The nuclei-stained cells indicate that they are intact, and cell adherence to the sample surfaces and cell proliferation (Figure 7.8). The results suggest that developed films are safe to use without any cytotoxic effects.

7.3 Conclusions

PLA-based implants are promising alternatives to many conventional medical implants with proven biocompatibility and non-toxicity. However, PLA-based implants are prone to bacterial adhesion and biofilm formation. Antibiotic therapy has been a widely used method to treat such conditions since its inception. However, there is a risk of bacterial resistance, which leads to severe infections. To combat such a situation, the prodigiosin-loaded PLA with inherent -OCH_3 functionalization can be used as an implant material to inhibit biofilm formation. This method takes advantage of the improved hydrophobicity, thermal stability, and antimicrobial properties of the developed PLA films, with the ability to disrupt the interaction between the surface of the polymer and the bacterial cells. The developed material is effective against both Gram-positive and Gram-negative bacteria to combat biofilm-associated infections.

CHAPTER 8

Fabrication of Nanocellulose from Waste Sorghum Bagasse

Graphical Overview

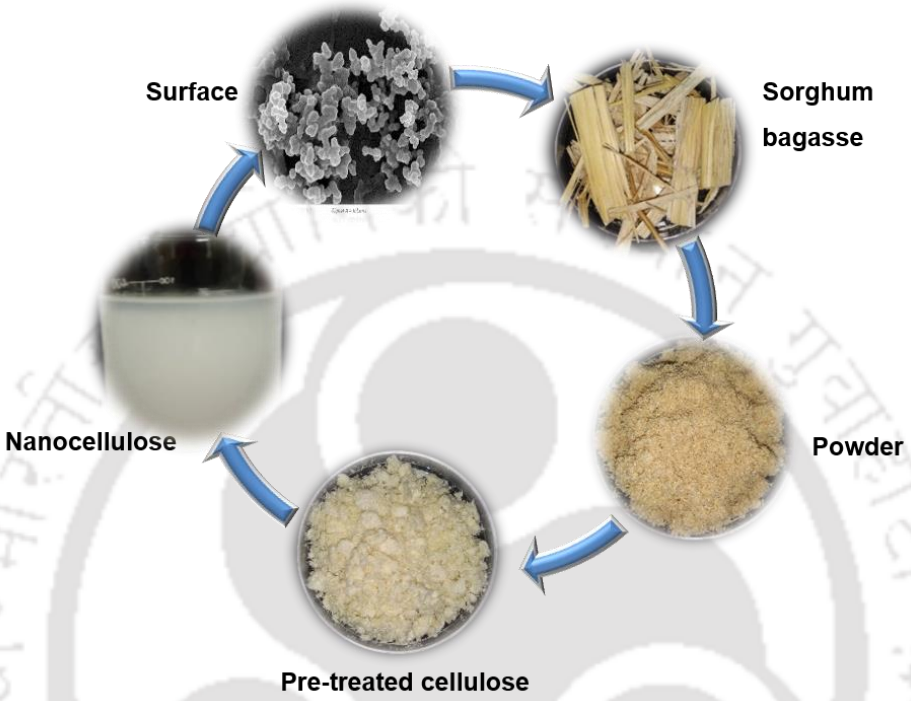

Nanocellulose was fabricated from leftover sorghum bagasse after the extraction of juice. The alkaline hydroxide peroxide is an eco-friendly method effective with alkaline pH of 11.5. The current method utilized the high-pressure treatment at 15 lb. This process could remove ~97% of the lignin. Further, the obtained cellulose hydrolyzed with sulfuric acid at different time intervals was found to be 33 ± 4 nm to 560 ± 126 nm in size. This process also yielded ~50 g/L of xylose and 7 g/L of glucose, indicating the breakdown of hemicellulose and cellulose, respectively. Though the sugar yield is high, the acidity of the medium limits its usage as a fermentable sugar for PHB production. However, the enzymatic hydrolysis yielded microcellulose due to the high saccharification of the cellulose to fermentable sugars with 33 g/L of glucose and 12 g/L of xylose at an optimum dose of Cellic CTec 2. The produced sugars from enzymatic hydrolysis are suitable for the production of PHB.

8.1 Introduction

Cellulose is abundantly available in nature and is a renewable polymer, it is well known for its uses in many fields in the form of fibers or as derivatives in a wide variety of products and materials. Cellulose is the structural parts formed through the manufacturing of the cellular components and biogenesis of cellulose. cellulose fibrils consist of both the amorphous and crystalline regions, which can be easily separated by mechanical, chemical, or enzymatic methods to yield cellulose nanofibers and cellulose nanocrystals [208]. Nanocellulose is derived from renewable resources such as oil-palm biomass [209], wheat straw lignocellulosic hydrolysates [210], paddy straw [211], paper waste, wood chips, and most agricultural biomass. The pretreatment methods include physical, mechanical, chemical, high temperature, and enzymatic methods [212]. Other methods include the steam explosion, in which the lignocellulosic materials are subjected to high-pressure saturated steam to ~160-260 °C temperature with a pressure of 5-50 atm for a very short time duration, followed by rapid system depressurization. The gradual release of pressure will expand the steam through the lignocellulosic matrix. It is a common pretreatment method that uses both chemical and physical techniques for the better breakdown of the lignin materials [213]. Organosolv is another method of extracting lignin from lignocellulosic biomass using organic solvents such as acetone, ethanol, methanol or its aqueous solutions The temperature of the treatment depends on the type of lignocellulosic biomass, which can vary from ~130 °C to ~200 °C [214]. Alkali pretreatment makes easy access of cellulosic surface to the enzymes by intermolecular ester bond saponification. The acid pre-hydrolysis is an alternative method that can achieve high reaction rates within a short interval of time which improves the hydrolysis of the cellulose [215]. The biological process includes the enzymatic saccharification of lignocellulosic biomass. The conversion of cellulose present in lignocellulosic biomass to simple fermentable sugars can be done by using chemical, physical and enzymatic processes. The microbial and

enzymatic pretreatment are considered to be economically viable only if the biomass components can be converted into valuable products [216]. The supercritical CO_2 pretreatment, followed by the enzymatic hydrolysis of the bagasse obtained from the cane sugar, yields a sugar concentration up to 72% [217]. Cellulases obtained from the *Trichoderma viride* from solid-state fermentation show the maximum enzymatic activity of 10 U/g at ~40 °C with a pH sensitivity of 5.2 [218]. The investigation of the treated and untreated cellulosic waste from a date palm tree (4%) under the optimum concentration of the cellulases (30 FPU/g) obtained from the *Geobacter stearothermophilus* at a pH (5) and temperature (50 °C) can yield ~32 mg/mL of glucose with the degree of saccharification of up to 71% with 24 h of incubation [219]. But there are some intermediates produced during the reaction of the enzymes with the lignocellulosic biomass, which include tannic acid, trimesic acid, and gallic acid [220]. Use of roller bottle reactors is used for the proper mixing of the enzymes with biomass having high solid concentration [221].

The current study is focused on the utilization of the waste sorghum bagasse after the extraction of juice from stalks. The juice was previously utilized for the production of PHB by fermentation. Whereas, the leftover bagasse is a waste. Thus here the main aim of the study is to utilize the sorghum bagasse for the fabrication of nanocellulose and possible conversion into fermentable sugars will be explored further.

8.2 Results and discussion

8.2.1 Compositional analysis of sorghum stalks

The sorghum is mainly consisting of cellulose, hemicellulose, and lignin. It was found from the analysis that, the total solid content with % fraction (20/+80) is 58.5%, % fraction (80) is ~ 41.5%, ash content was found to be 4.2% for (–20/80) fraction, and 6% for (-80) fraction.

Further, the lignin content was quantified and was observed ~13% of acid-soluble lignin and 18% of acid-insoluble lignin.

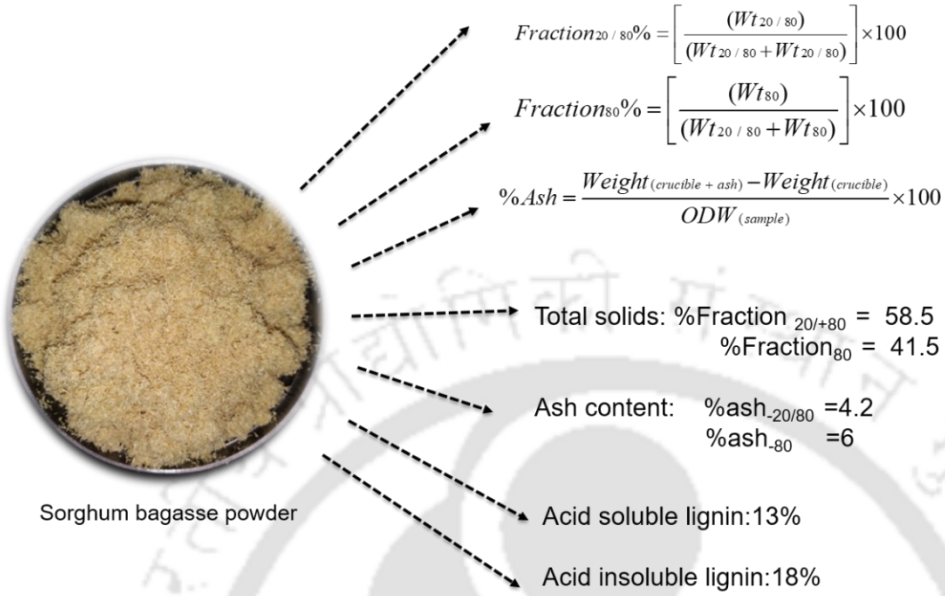

Figure 8.1. The composition of the sorghum biomass.

8.2.2 Effect of different solvents on delignification

The obtained sorghum bagasse powder was subjected to different pretreatment methods such as 2% H_2SO_4, 2% NaOH, 60% ethanol, 2% lactic acid, and alkaline hydrogen peroxide treatment at pH 11.5. The FESEM images obtained after pretreatment methods are shown in Figure 8.2. The raw sorghum biomass is compared with the treated biomass and it was found that there is less lignin release from the weak acid and ethanol pretreatment, whereas ~97 of the lignin has been removed from the sorghum biomass using AHP. Alkaline hydrogen peroxide (AHP) treatment and the 2% NaOH are efficient methods to treat the sorghum biomass with >90% lignin removal efficiency. However, the concentration of NaOH used for the pretreatment limits its usage because it is not an environmentally friendly process. Thus the AHP pretreated biomass is used further for acid hydrolysis to produce nanocellulose.

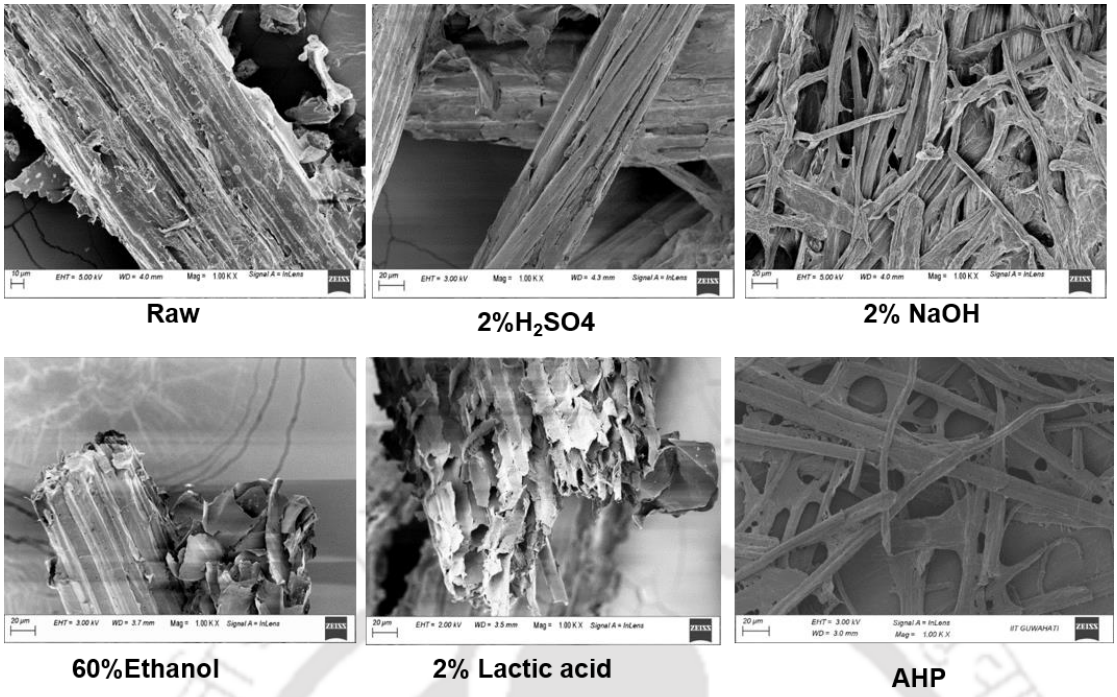

Figure 8.2. Pretreatment of sorghum biomass for the production of nanocellulose.

8.2.3 Fabrication of nanocellulose using the leftover sorghum bagasse

The alkaline pretreated biomass was subjected to acid hydrolysis at the conditions mentioned in the methodology. The FESEM images of the obtained nanocellulose are shown in figure 8.3. The sulfuric acid hydrolysis was carried out at different time intervals at room temperature. The morphological analysis of the four different nanocellulose obtained at different time intervals, which exhibits variations in length, diameter and aspect ratio. The diameters of nanocellulose i.e., average length distribution was calculated from FESEM analysis. The sample hydrolyzed for 15 min yielded a sheet-like morphology with a diameter of 560 ± 126 nm, which is relatively larger due to the less contact time of biomass with acid. The sample obtained at 45 min yielded nanocellulose of a diameter (D) of 33 ± 4 nm, bearing an aspect ratio of 2.0, which is a perfect material for high-performance applications, where such nanocellulose helps in the self-assembly of the matter [222]. The aspect ratio is the length/width. It is an important parameter of nanocellulose or cellulose nanocrystals. The performance of the nanocellulose reinforced polymers, functional materials and suspensions

are dependent on the aspect ratio of the filler [223]. These variations in morphologies are due to the different degree of dissociation. Hence affects the degradation of amorphous part of the cellulose. Here AHP pretreated sorghum biomass is a promising candidate for all the applications where the less aspect ratio is a criterion. The comparison of the various nanocellulose obtained through different fabrication methods and sources is tabulated (Table 8.1). From Table 8.1 it is evident that the nanocellulose obtained in the current work shows superior dimensions compared to the reported methods.

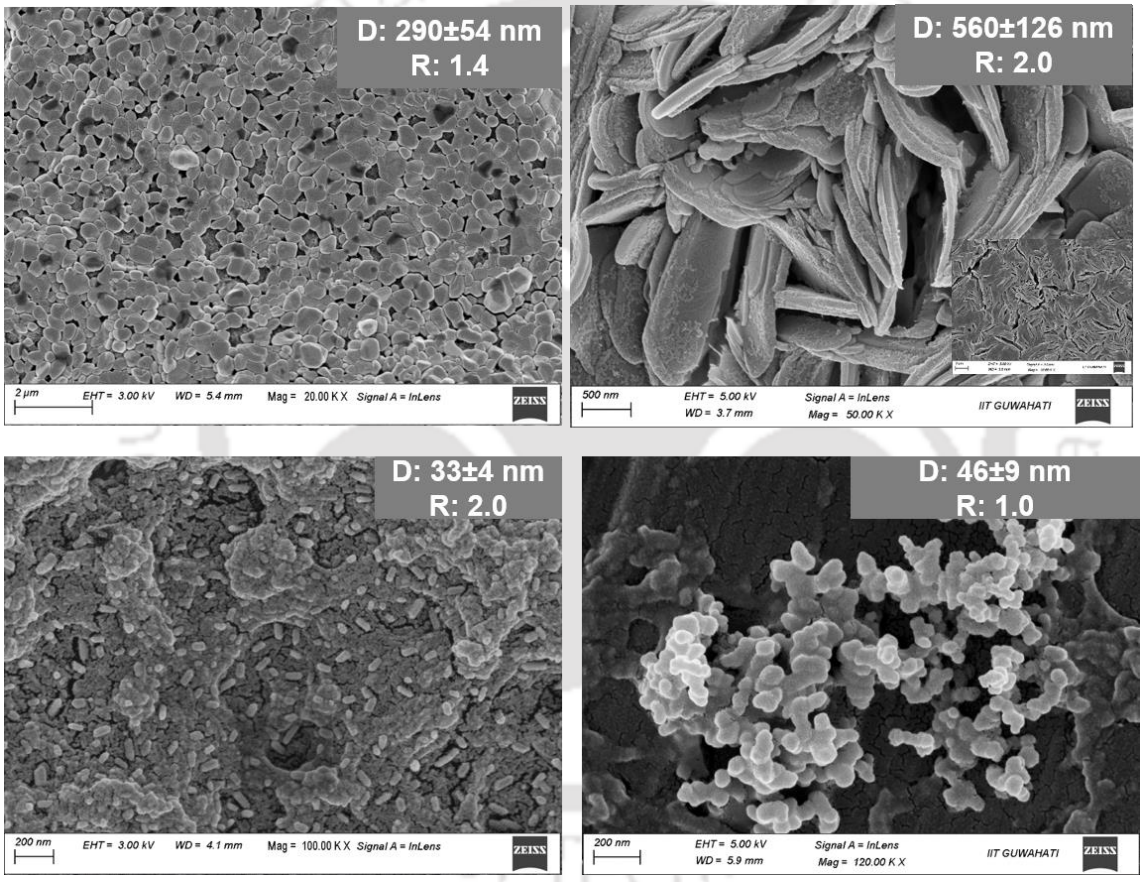

Figure 8.3. The nanocellulose produced at different hydrolysis times yields various aspect ratios.

8.2.4 Enzymatic hydrolysis of the pretreated sorghum biomass using cellulases

The AHP pretreated biomass was subjected to two types of hydrolysis first is sulfuric acid hydrolysis and the second is enzyme hydrolysis, and the sugar yield is shown in Figure 8.4. It was found from the results that sulfuric acid hydrolysis is preferable for the fabrication of the nanocellulose due to the highly acidic nature of the hydrolysate. Though the sugar conversion was quantified and is depicted in Figure 8.4. It was found that ~50 g/L of sorghum cellulose is converted to xylose and ~10 g/L of the cellulose is converted to glucose. The rest of the part has been converted to nanocellulose. Here the main hydrolysis process occurs on the hemicellulose leading to the formation of highly crystalline nanocellulose. On the other hand, the enzyme hydrolysis yielded the maximum glucose concentration of ~32 g/L of sugars at 0.5 g/g of enzyme loading, however, it yielded ~12 g/L of xylose at 0.5 g/g of enzyme loading. The yield of glucose with different enzyme loading, as the enzyme loading increased, the glucose conversion is increased upto 0.5g/g of enzyme loading, this exponential increasing trend is due to the action of enzyme blend used in the study CellicCTec2, which consists of cellulases, β-glucosidase and hemicellulases, that converts carbohydrates to simple sugars at different rates. These catalyzes the hydrolysis of β-1,4 glycosidic bonds in cellulose to yield fermentable sugars. The decreasing trend was observed at an enzyme loading of 0.8 g/g. This could be correlated to slight increase in xylose concentration was observed at the same concentration. Further in-depth investigation is needed in this regard.

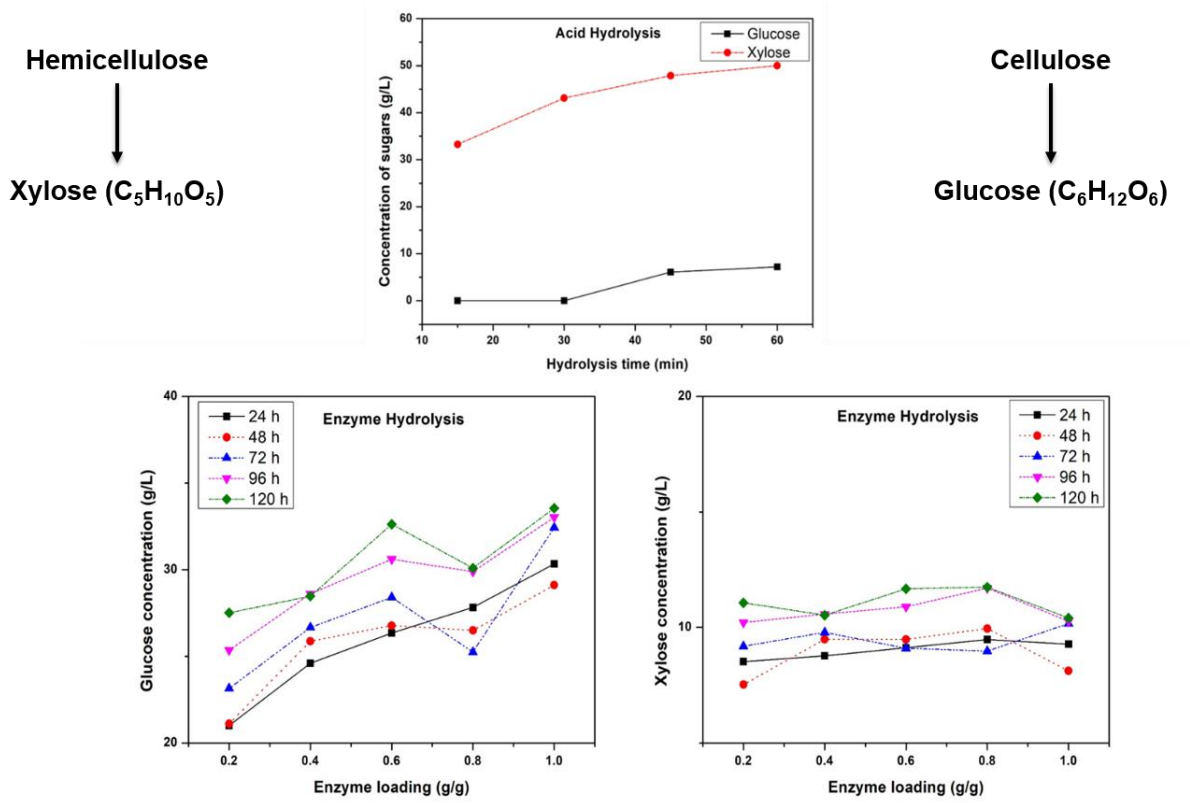

Figure 8.4. The HPLC analysis of the sugar yield on enzymatic hydrolysis.

The production cost of nanocellulose depends on the pretreatment method, acid used for production and feed stock cost. The feed stock material sorghum bagasse used in the preparation of nanocellulose does not have any economic value and is a waste material. This could reduce the feedstock cost and also prevents the environmental damage caused by deforestation for the fabrication of nanocellulose from trees. In case of pretreatment method, the alkaline hydrogen peroxide treatment used in the current research utilized 50% less NaOH compared to conventional alkaline pretretment which utilizes ~20% NaOH. The cost of H_2SO_4 used is almost same as that of other method [6]. The cost related to power consumption and other factors will vary at larger scales, which needs evaluation of production process at pilot scale and industrial scales to predict the accurate costs.

Table 8.1. The fabrication of the nanocellulose using various lignocellulosic biomass and their dimensions.

Feed stock	Fabrication method	Morphology	Dimensions (nm)	Applications	Reference
Cotton fibers	NaOH (2%)/H_2SO_4 (65%)	Rod	D=220	Cross-linking aid for alginate	[224]
bamboo	NaOH/H_2SO_4 (64%) Magnetization	Rod	D=37 ± 8, R= ~20	Filler for PLA to incorporate magnetic property	[225]
Filter paper	NaOH/H_2SO_4 (64%)	Rod	D=30 ± 11, R=~36	Filler for PLA, PHB	[226]
	H_3PO_4 (11 M)	Rice grain	D=21± 5, R= ~44		
	HCl (6 M)	Small rod	D=15 ± 4, R= ~14		
	HNO_3	Thin fibrils	D=24 ± 12, R= ~21		
Filter paper	Endoglucanase Enzymatic method	Needle	D=3-40, R= <100	Biocompatible material for tissue engineering	[227]
Cotton gin motes	NaOH (4%)/$NaClO_2$/H_2SO_4 (62%)	Cylindrical rod	R= ~20.4	NA	[228]
Waste paper	NaOH/H_2SO_4 (95-97%)	Rod	D=18-22, R= ~20	Hydrogel for dye removal	[229]
Sorghum bagasse	AHP/H_2SO_4 (60%)	Rod	**D: 33 ± 4, R= 2.0**	For drug delivery	Current study
		Sphere	**D: 46 ± 9, R=1.0**		

8.3 Conclusions

The sorghum bagasse is an agricultural waste, in which the juice was utilized for the production of the PHB, whereas the leftover bagasse is of no use. Sorghum bagasse is rich in cellulose and hemicellulose more suitable for the fabrication of nanocellulose. However, it consists of lignin, which hinders the acid hydrolysis process for the conversion of cellulose to nanocellulose. The current work utilized sorghum bagasse for the fabrication of nanocellulose. The eco-friendly alkaline hydrogen peroxide at pH of 11.5 employed in the current work could remove ~97% of lignin from the biomass. Further, the acid hydrolysis yields the nanocellulose with exceptional dimensions of 33 ± 4 nm with an aspect ratio of 2.0 and 46 ± 9 nm with an aspect ratio of 1.0. The enzymatic hydrolysis yielded high glucose and xylose concentrations, which are further promising carbon sources for the production of polyhyroxybutyrate. The acid hydrolysis mainly occurs on the hemicellulose to yield more xylose and the enzyme saccharification is more specific on the cellulose region to yield more glucose.

CHAPTER 9

Conclusions and Future Scope

9.1 Conclusions

This chapter presents the major conclusion of the research work carried out in this thesis and also indicates the future direction of the research work. The overall conclusions can be broadly classified into two subsections.

The first part is focused on the utilization of waste sorghum stalks for the production of PHB and nanocellulose. Also, the application of obtained PHB for embolization of the right hepatic artery using low-cost 3D printed PLA-based hepatic phantom.

- Waste sorghum stalks selected for the study consisting of ~60-70 g/L of fermentable sugars and mineral components such as potassium, nitrogen, chlorine, calcium, magnesium, manganese suitable for the growth of *Bacillus megaterium* and PHB production.
- JMP software used for statistical medium optimization and selected parameters for the bioreactor experiment are carbon (30 g/L), nitrogen (2 g/L), and initial inoculum concentration (7.5%), the software helped to get an interactive plot to maximize the yield.
- The fed-batch process operated using the dissolved oxygen control strategy yielded the maximum PHB of ~8.2 g/L which is four folds higher than the batch operations.
- The PHB production in *Bacillus megaterium* is growth associated, thus the fed-batch operation helped in decreasing 1/3rd the time used for batch operations for enhanced productivity.

- The characteristic properties of the obtained PHB are confirmed using various characterization techniques and obtained properties were comparable to commercial PHB.
- The cytotoxicity test of PHB on Baby Hamster Kidney cell (BHK-21) confirmed its non-toxicity.
- The produced PHB with number average molecular weight of ~400 KDa is used for the preparation of microspheres with various tunable sizes.
- The obtained microspheres are demonstrated for their suitability to be used as drug delivery and embolization agent using a 3D-printed hepatic model.
- A low-cost PLA-based 3D printed hepatic phantom was developed, the cost of which is ~22 times less compared to other commercially available *in vitro* 3D printed phantoms.
- The unique experimental setup is demonstrated for conducting the in vitro studies for microsphere delivery and tracking the embolizing agents during delivery.
- The sorghum bagasse left over after the extraction of sorghum juice is further utilized for the fabrication of nanocellulose
- The alkaline hydrogen peroxide pretreatment is the more preferable method for lignin removal of ~97%at a pH of 11.5.
- The sulfuric acid hydrolysis at room temperature yielded the nanocellulose from 33 ± 4 nm to 560 ± 126 nm in size based on the reaction time
- The enzymatic hydrolysis using Cellic CTec2 cellulose enzyme blend yielded ~50 g/L of xylose and 7 g/L of glucose

The second part is focused on the production of prodigiosin from Serratia nematodiphila isolated from river water and its application in the synthesis of metal free-PLA, also for inhibition of biofilm formation in commercial PLA

- The prodigiosin isolated from river water demonstrated a relatively higher yield compared to the literature data, and the mechanism of upregulation and downregulation of prodigiosin is explored.
- Though the produced pigment has been reported as an anticancer agent, it has not been explored its use in polymer processing to date.
- The addition of prodigiosin to PLA has improved its surface properties, and hence the inhibition of biofilm-associated infections.
- Prodigiosin is demonstrated for its applicability as a catalyst for ring-opening polymerization of L-lactide for the first time.
- The molecular weight of PLA obtained by using prodigiosin as a catalyst is ~ 5000 Da
- The produced PLA is metal-free, and exhibited cell proliferation activity without any cytotoxic effects. Thus further it could be applied in the field of drug delivery and tissue engineering applications

9.2 Future scope

Based on the outcomes of this work, some recommendations for future work are presented pictorially (Figure 9.1) as follows:

- The sugar content in sorghum juice and its huge availability are promising. Thus the use of sorghum juice for PHB production using other bacteria will be explored to maximize the yield.
- A preliminary study has been performed on the enzymatic saccharification of sorghum bagasse. Detailed enzyme optimization and scale-up could be carried out further to make the process economically viable.

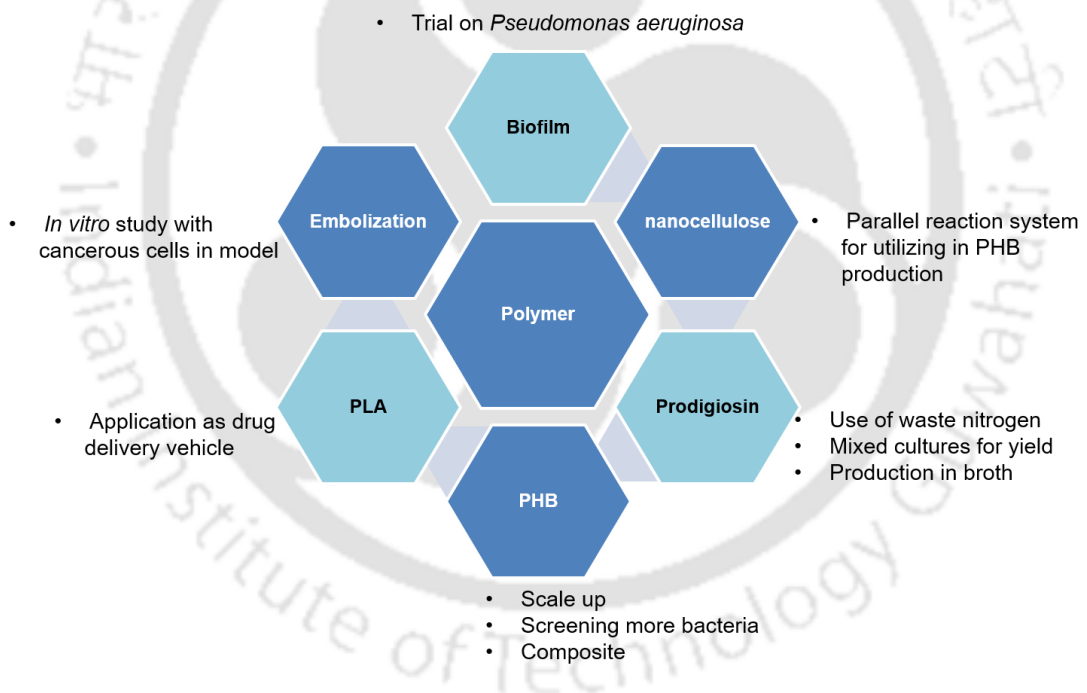

Figure 9.1. Future perspectives.

- A parallel saccharification and PHB production system could be developed.
- The application of produced PHB will be explored further for its use in packing.
- The waste nitrogen source could be used for the production of prodigiosin to achieve improved yield.

- The biofilm inhibition ability of prodigiosin-loaded PLA could be explored for other biofilm-forming bacteria such as *Pseudomonas aeruginosa*
- The 3D-printed model could be used for real-time applications by growing the cells in the channels

References

[1] https://plasticseurope.org/wp-content/uploads/2021/10/2017-Plastics-the-facts.pdf.

[2] L. Nizzetto and S. Sinha, "Top Priority to Curb Plastic Pollution: Empowering Those at the Bottom," *One Earth*, vol. 2, no. 1, pp. 11–15, Jan. 2020.

[3] I. E. Napper and R. C. Thompson, "Environmental Deterioration of Biodegradable, Oxo-biodegradable, Compostable, and Conventional Plastic Carrier Bags in the Sea, Soil, and Open-Air Over a 3-Year Period," *Environ. Sci. Technol.*, vol. 53, no. 9, pp. 4775–4783, May 2019.

[4] http://www.gesamp.org.

[5] B. Slootmaekers *et al.*, "Microplastic contamination in gudgeons (Gobio gobio) from Flemish rivers (Belgium)," *Environ. Pollut.*, vol. 244, pp. 675–684, Jan. 2019.

[6] C. Trakunjae *et al.*, "Enhanced polyhydroxybutyrate (PHB) production by newly isolated rare actinomycetes Rhodococcus sp. strain BSRT1-1 using response surface methodology," *Sci. Rep.*, vol. 11, no. 1, Art. no. 1, Jan. 2021.

[7] C. S. K. Reddy, R. Ghai, null Rashmi, and V. C. Kalia, "Polyhydroxyalkanoates: an overview," *Bioresour. Technol.*, vol. 87, no. 2, pp. 137–146, Apr. 2003.

[8] V. Tanamool, T. Imai, P. Danvirutai, and P. Kaewkannetra, "An alternative approach to the fermentation of sweet sorghum juice into biopolymer of poly-β-hydroxyalkanoates (PHAs) by newly isolated, Bacillus aryabhattai PKV01," *Biotechnol. Bioprocess Eng.*, vol. 18, no. 1, pp. 65–74, Feb. 2013.

[9] R. Rai, T. Keshavarz, J. A. Roether, A. R. Boccaccini, and I. Roy, "Medium chain length polyhydroxyalkanoates, promising new biomedical materials for the future," *Mater. Sci. Eng. R Rep.*, vol. 72, no. 3, pp. 29–47, Apr. 2011.

[10] https://www.researchgate.net/publications/310774120_Recovery and characterization of polyhydroxyalkanoates.

[11] J. G. Lillo and F. Rodriguez-Valera, "Effects of Culture Conditions on Poly(β-Hydroxybutyric Acid) Production by Haloferax mediterranei," *Appl. Environ. Microbiol.*, vol. 56, no. 8, pp. 2517–2521, Aug. 1990.

[12] J. Quillaguamán, S. Hashim, F. Bento, B. Mattiasson, and R. Hatti-Kaul, "Poly(β-hydroxybutyrate) production by a moderate halophile, Halomonas boliviensis LC1 using starch hydrolysate as substrate," *J. Appl. Microbiol.*, vol. 99, no. 1, pp. 151–157, 2005.

[13] B. Panda, P. Jain, L. Sharma, and N. Mallick, “Optimization of cultural and nutritional conditions for accumulation of poly-β-hydroxybutyrate in Synechocystis sp. PCC 6803,” *Bioresour. Technol.*, vol. 97, no. 11, pp. 1296–1301, Jul. 2006.

[14] C. Marangoni, A. jun Furigo, and G. M. F. de Aragão, “Production of poly(3-hydroxybutyrate-*co*-3-hydroxyvalerate) by *Ralstonia eutropha* in whey and inverted sugar with propionic acid feeding,” pp. 137–141, 2002.

[15] W. J. Page, J. Manchak, and B. Rudy, “Azotobacter vinelandii UWD,” *APPL Env. MICROBIOL*, vol. 58, p. 8, 1992.

[16] P. Kanjanachumpol, S. Kulpreecha, V. Tolieng, and N. Thongchul, “Enhancing polyhydroxybutyrate production from high cell density fed-batch fermentation of Bacillus megaterium BA-019,” pp. 1463–1474, 2013.

[17] D. Van-Thuoc, J. Quillaguamán, G. Mamo, and B. Mattiasson, “Utilization of agricultural residues for poly(3-hydroxybutyrate) production by Halomonas boliviensis LC1,” *J. Appl. Microbiol.*, vol. 104, no. 2, pp. 420–428, 2008.

[18] Y. KAWATA and S. AIBA, “Poly(3-hydroxybutyrate) Production by Isolated Halomonas sp. KM-1 Using Waste Glycerol,” *Biosci. Biotechnol. Biochem.*, vol. 74, no. 1, pp. 175–177, Jan. 2010.

[19] J. Han *et al.*, “Complete Genome Sequence of the Metabolically Versatile Halophilic Archaeon Haloferax mediterranei, a Poly(3-Hydroxybutyrate-co-3-Hydroxyvalerate) Producer,” *J. Bacteriol.*, vol. 194, no. 16, pp. 4463–4464, Aug. 2012.

[20] C.-C. Chien and L.-Y. Ho, “Polyhydroxyalkanoates production from carbohydrates by a genetic recombinant Aeromonas sp,” *Lett. Appl. Microbiol.*, vol. 47, no. 6, pp. 587–593, Dec. 2008.

[21] A. Yezza, D. Fournier, A. Halasz, and J. Hawari, “Production of polyhydroxyalkanoates from methanol by a new methylotrophic bacterium Methylobacterium sp. GW2,” *Appl. Microbiol. Biotechnol.*, vol. 73, no. 1, pp. 211–218, Nov. 2006.

[22] A. A. Pantazaki, M. G. Tambaka, V. Langlois, P. Guerin, and D. A. Kyriakidis, “Polyhydroxyalkanoate (PHA) biosynthesis in Thermus thermophilus: purification and biochemical properties of PHA synthase,” *Mol. Cell. Biochem.*, vol. 254, no. 1–2, pp. 173–183, Dec. 2003.

[23] L. E. A. Munoz and M. R. Riley, “Utilization of cellulosic waste from tequila bagasse and production of polyhydroxyalkanoate (PHA) bioplastics by Saccharophagus degradans,” *Biotechnol. Bioeng.*, vol. 100, no. 5, pp. 882–888, 2008.

[24] H. Kimura, T. Yamamoto, and K. Iwakura, “Biosynthesis of Polyhydroxyalkanoates from 1,3-Propanediol by *Chromobacterium* sp.,” *Polym. J.*, vol. 34, no. 9, pp. 659–665, Sep. 2002.

[25] S. Fidler and D. Dennis, “Polyhydroxyalkanoate production in recombinant Escherichia coli,” *FEMS Microbiol. Lett.*, vol. 103, no. 2, pp. 231–235, Dec. 1992.

[26] https://www.sciencedirect.com/topics/engineering/batch-fermentation“Batch Fermentation - an overview | ScienceDirect Topics.

[27] https://getrevising.co.uk/grids/advantages_and_disadvantages_of_batch_cultures “Advantages and disadvantages of batch cultures.

[28] https://www.researchgate.net:Continuous and batch fermentation.

[29] P. J. Senior, G. A. Beech, G. A. Ritchie, and E. A. Dawes, “The role of oxygen limitation in the formation of poly- -hydroxybutyrate during batch and continuous culture of Azotobacter beijerinckii,” *Biochem. J.*, vol. 128, no. 5, pp. 1193–1201, Aug. 1972.

[30] B. A. Ramsay, K. Lomaliza, C. Chavarie, B. Dubé, P. Bataille, and J. A. Ramsay, “Production of poly-(beta-hydroxybutyric-co-beta-hydroxyvaleric) acids.,” *Appl. Environ. Microbiol.*, vol. 56, no. 7, pp. 2093–2098, Jul. 1990.

[31] H. Ishizaki and K. Hasumi, “Chapter 10 - Ethanol Production from Biomass,” in *Research Approaches to Sustainable Biomass Systems*, S. Tojo and T. Hirasawa, Eds., Boston: Academic Press, 2014, pp. 243–258.

[32] M. Koller, P. Hesse, R. Bona, C. Kutschera, A. Atlić, and G. Braunegg, “Potential of Various Archae- and Eubacterial Strains as Industrial Polyhydroxyalkanoate Producers from Whey,” *Macromol. Biosci.*, vol. 7, no. 2, pp. 218–226, 2007.

[33] F. Wang and S. Y. Lee, “Poly(3-Hydroxybutyrate) Production with High Productivity and High Polymer Content by a Fed-Batch Culture of Alcaligenes latus under Nitrogen Limitation.,” *Appl Env. Microbiol*, vol. 63, no. 9, pp. 3703–3706, Sep. 1997.

[34] J. Choi and S. Y. Lee, “High-Level Production of Poly(3-Hydroxybutyrate-co-3-Hydroxyvalerate) by Fed-Batch Culture of Recombinant Escherichia coli,” *Appl Env. Microbiol*, vol. 65, no. 10, pp. 4363–4368, Oct. 1999.

[35] S. Y. Lee, “Bacterial polyhydroxyalkanoates,” *Biotechnol. Bioeng.*, vol. 49, no. 1, pp. 1–14, 1996.

[36] S.-G. Hong, H.-W. Hsu, and M.-T. Ye, “Thermal properties and applications of low molecular weight polyhydroxybutyrate,” *J. Therm. Anal. Calorim.*, vol. 111, no. 2, pp. 1243–1250, Feb. 2013.

[37] M. Koller *et al.*, “Production of Polyhydroxyalkanoates from Agricultural Waste and Surplus Materials †,” *Biomacromolecules*, vol. 6, no. 2, pp. 561–565, Mar. 2005.

[38] T. Keshavarz and I. Roy, “Polyhydroxyalkanoates: bioplastics with a green agenda,” *Curr. Opin. Microbiol.*, vol. 13, no. 3, pp. 321–326, Jun. 2010.

[39] G. Braunegg, G. Lefebvre, and K. F. Genser, “Polyhydroxyalkanoates, biopolyesters from renewable resources: Physiological and engineering aspects,” *J. Biotechnol.*, vol. 65, no. 2, pp. 127–161, Oct. 1998.

[40] S. Nakamura, Y. Doi, and M. Scandola, “Microbial synthesis and characterization of poly(3-hydroxybutyrate-co-4-hydroxybutyrate),” *Macromolecules*, vol. 25, no. 17, pp. 4237–4241, Aug. 1992.

[41] E. Akaraonye, T. Keshavarz, and I. Roy, “Production of polyhydroxyalkanoates: the future green materials of choice,” *J. Chem. Technol. Biotechnol.*, vol. 85, no. 6, pp. 732–743, 2010.

[42] C. Sanhueza, F. Acevedo, S. Rocha, P. Villegas, M. Seeger, and R. Navia, “Polyhydroxyalkanoates as biomaterial for electrospun scaffolds,” *Int. J. Biol. Macromol.*, vol. 124, pp. 102–110, Mar. 2019.

[43] M. Eesaee, P. Ghassemi, D. D. Nguyen, S. Thomas, S. Elkoun, and P. Nguyen-Tri, “Morphology and crystallization behaviour of polyhydroxyalkanoates-based blends and composites: A review,” *Biochem. Eng. J.*, vol. 187, p. 108588, Nov. 2022.

[44] M. Avella, E. Martuscelli, and M. Raimo, “Review Properties of blends and composites based on poly(3-hydroxy)butyrate (PHB) and poly(3-hydroxybutyrate-hydroxyvalerate) (PHBV) copolymers,” *J. Mater. Sci.*, vol. 35, no. 3, pp. 523–545, Feb. 2000.

[45] Ł. Kaniuk and U. Stachewicz, “Development and Advantages of Biodegradable PHA Polymers Based on Electrospun PHBV Fibers for Tissue Engineering and Other Biomedical Applications,” *ACS Biomater. Sci. Eng.*, vol. 7, no. 12, pp. 5339–5362, Dec. 2021.

[46] V. Tanamool, T. Imai, P. Danvirutai, and P. Kaewkannetra, “An alternative approach to the fermentation of sweet sorghum juice into biopolymer of poly-β-hydroxyalkanoates (PHAs) by newly isolated, Bacillus aryabhattai PKV01,” *Biotechnol. Bioprocess Eng.*, vol. 18, no. 1, pp. 65–74, Feb. 2013.

[47] G. Gahlawat and A. K. Srivastava, "Development of a mathematical model for the growth associated Polyhydroxybutyrate fermentation by Azohydromonas australica and its use for the design of fed-batch cultivation strategies," *Bioresour. Technol.*, vol. 137, pp. 98–105, Jun. 2013.

[48] Y. Chen, M. Li, F. Meng, W. Yang, L. Chen, and M. Huo, "Optimal poly (3-hydroxybutyrate/3-hydroxyvalerate) biosynthesis by fermentation liquid from primary and waste activated sludge," *Environ. Technol.*, vol. 35, no. 14, pp. 1791–1801, Jul. 2014.

[49] D. Moorkoth and K. M. Nampoothiri, "Production and characterization of poly(3-hydroxy butyrate-co-3 hydroxyvalerate) (PHBV) by a novel halotolerant mangrove isolate," *Bioresour. Technol.*, vol. 201, pp. 253–260, Feb. 2016.

[50] S. Ghosh, R. Gnaim, S. Greiserman, L. Fadeev, M. Gozin, and A. Golberg, "Macroalgal biomass subcritical hydrolysates for the production of polyhydroxyalkanoate (PHA) by Haloferax mediterranei," *Bioresour. Technol.*, vol. 271, pp. 166–173, Jan. 2019.

[51] N. A. Manikandan, K. Pakshirajan, and G. Pugazhenthi, "A closed-loop biorefinery approach for polyhydroxybutyrate (PHB) production using sugars from carob pods as the sole raw material and downstream processing using the co-product lignin," *Bioresour. Technol.*, vol. 307, p. 123247, Jul. 2020.

[52] K. Zhang, Y. Zhou, T. Song, and J. Xie, "Bioplastic Production from the Microbial Electrosynthesis of Acetate through CO2 Reduction," *Energy Fuels*, vol. 35, no. 19, pp. 15978–15986, Oct. 2021

[53] I. Ali and N. Jamil, "Polyhydroxyalkanoates: Current applications in the medical field," *Front. Biol.*, vol. 11, no. 1, pp. 19–27, Feb. 2016

[54] K. Zhao, Y. Deng, J. C. Chun, and G. Q. Chen, "Polyhydroxyalkanoate (PHA) scaffolds with good mechanical properties and biocompatibility.," *Biomaterials*, vol. 24, no. 6, pp. 1041–1045, Mar. 2003.

[55] L. Drew, A. Scott, B. Morgan, and K. Gruber, "Clinical devices and services: Repair shops," *Nature*, May 17, 2017. https://www.nature.com/articles/545S21a.

[56] W. Zhang, H. Ouyang, C. R. Dass, and J. Xu, "Current research on pharmacologic and regenerative therapies for osteoarthritis," *Bone Res.*, vol. 4, p. 15040, Mar. 2016.

[57] S. F. Williams and D. P. Martin, "Polyhydroxyalkanoate compositions for soft tissue repair, augmentation, and viscosupplementation," US6585994B2, Jul. 01, 2003: https://patents.google.com/patent/US6585994B2/en.

[58] S. F. Williams, D. P. Martin, and F. Skraly, "Medical devices and applications of polyhydroxyalkanoate polymers," EP2305324A1, Apr. 06, 2011. https://patents.google.com/patent/EP2305324A1/en

[59] M. Prasad *et al.*, "Efficient Transformation of Agricultural Waste in India," in *Contaminants in Agriculture: Sources, Impacts and Management*, M. Naeem, A. A. Ansari, and S. S. Gill, Eds., Cham: Springer International Publishing, 2020, pp. 271–287.

[60] S. Bhuvaneshwari, H. Hettiarachchi, and J. N. Meegoda, "Crop Residue Burning in India: Policy Challenges and Potential Solutions," *Int. J. Environ. Res. Public. Health*, vol. 16, no. 5, p. E832, Mar. 2019.

[61] "FAOSTAT." https://www.fao.org/faostat/en/#search/sorghum.

[62] "USDA - National Agricultural Statistics Service - Charts and Maps - A to Z - Sorghum." https://www.nass.usda.gov/Charts_and_Maps/A_to_Z/in-sorghum.php.

[63] R. Madhusudhana, "Chapter 6 - Marker-Assisted Breeding in Sorghum," in *Breeding Sorghum for Diverse End Uses*, C. Aruna, K. B. R. S. Visarada, B. V. Bhat, and V. A. Tonapi, Eds., in Woodhead Publishing Series in Food Science, Technology and Nutrition. Woodhead Publishing, 2019, pp. 93–114.

[64] V. Nagarajan, A. K. Mohanty, and M. Misra, "Perspective on Polylactic Acid (PLA) based Sustainable Materials for Durable Applications: Focus on Toughness and Heat Resistance," *ACS Sustain. Chem. Eng.*, vol. 4, no. 6, pp. 2899–2916, Jun. 2016.

[65] X. Montané *et al.*, "Synthesis and synthetic mechanism of Polylactic acid," *Phys. Sci. Rev.*, vol. 1, no. ahead-of-print, Apr. 2020.

[66] A.-C. Albertsson and I. K. Varma, "Recent Developments in Ring Opening Polymerization of Lactones for Biomedical Applications," *Biomacromolecules*, vol. 4, no. 6, pp. 1466–1486, Nov. 2003.

[67] R. Kuehl *et al.*, "Preventing Implant-Associated Infections by Silver Coating," *Antimicrob. Agents Chemother.*, vol. 60, no. 4, pp. 2467–2475.

[68] C. R. Arciola, D. Campoccia, and L. Montanaro, "Implant infections: adhesion, biofilm formation and immune evasion," *Nat. Rev. Microbiol.*, vol. 16, no. 7, pp. 397–409, Jul. 2018.

[69] M. Lorenzetti *et al.*, "The Influence of Surface Modification on Bacterial Adhesion to Titanium-Based Substrates," *ACS Appl. Mater. Interfaces*, vol. 7, no. 3, pp. 1644–1651, Jan. 2015.

[70] V. Katiyar and H. Nanavati, “Ring-opening polymerization of L-lactide using N-heterocyclic molecules: mechanistic, kinetics and DFT studies,” *Polym. Chem.*, vol. 1, no. 9, pp. 1491–1500, 2010.

[71] M. Mili, A. Gupta, Monika, and V. Katiyar, “Designing of Poly(l-lactide)–Nicotine Conjugates: Mechanistic and Kinetic Studies and Thermal Release Behavior of Nicotine,” *ACS Omega*, vol. 2, no. 9, pp. 6131–6142, Sep. 2017.

[72] A. Gadomska-Gajadhur and P. Ruśkowski, “Biocompatible Catalysts for Lactide Polymerization—Catalyst Activity, Racemization Effect, and Optimization of the Polymerization Based On Design of Experiments,” *Org. Process Res. Dev.*, vol. 24, no. 8, pp. 1435–1442, Aug. 2020.

[73] M. Guadalupe Ortiz-Aldaco, J. E. Báez, and J. O. C. Jiménez-Halla, “Bismuth subsalicylate, a low-toxicity catalyst for the ring-opening polymerization (ROP) of l -lactide (l -LA) with aliphatic diol initiators: synthesis, characterization, and mechanism of initiation,” *RSC Adv.*, vol. 10, no. 51, pp. 30815–30824, 2020.

[74] S. Al-Malaika, F. Axtell, R. Rothon, and M. Gilbert, “Chapter 7 - Additives for Plastics,” in *Brydson’s Plastics Materials (Eighth Edition)*, M. Gilbert, Ed., Butterworth-Heinemann, 2017, pp. 127–168.

[75] P. Kovacic and R. Somanathan, “Toxicity of imine-iminium dyes and pigments: electron transfer, radicals, oxidative stress and other physiological effects,” *J. Appl. Toxicol. JAT*, vol. 34, no. 8, pp. 825–834, Aug. 2014.

[76] “Developmental toxicity and psychotoxicity of FD and C red dye no. 40 (Allura red AC) https://www.sciencedirect.com/science/article/pii/0300483X8390118X?via%3Dihub.

[77] C. for F. S. and A. Nutrition, “Color Additives History,” *FDA*, Mar. 16, 2019. http://www.fda.gov/industry/color-additives/color-additives-history.

[78] “Joint FAOWHO Expert Committee on Food Additives et al. - 2017 - Safety evaluation https://apps.who.int/iris/bitstream/handle/10665/258934/9789241660730.

[79] “Scientific topic: Food ingredients and packaging | European Food.” https://www.efsa.europa.eu/en/topics/topic/food-ingredients-and-packaging.

[80] H. S. Tuli, P. Chaudhary, V. Beniwal, and A. K. Sharma, “Microbial pigments as natural color sources: current trends and future perspectives,” *J. Food Sci. Technol.*, vol. 52, no. 8, pp. 4669–4678, Aug. 2015.

[81] K. Papireddy *et al.*, "Antimalarial Activity of Natural and Synthetic Prodiginines," *J. Med. Chem.*, vol. 54, no. 15, pp. 5296–5306, Aug. 2011.

[82] A. Domröse *et al.*, "Efficient recombinant production of prodigiosin in Pseudomonas putida," *Front. Microbiol.*, vol. 6, p. 972, 2015.

[83] M. Kanelli *et al.*, "Microbial Production of Violacein and Process Optimization for Dyeing Polyamide Fabrics With Acquired Antimicrobial Properties," *Front. Microbiol.*, vol. 9, 2018.

[84] C. Lin *et al.*, "Enhanced production of prodigiosin by Serratia marcescens FZSF02 in the form of pigment pellets," *Electron. J. Biotechnol.*, vol. 40, pp. 58–64, Jul. 2019.

[85] "EVOWARE." https://rethink-plastic.com/home/.

[86] "About Us," *Choose*. https://www.choosepackaging.co.uk/about-us.

[87] "We make packaging disappear," *Notpla*. https://www.notpla.com/.

[88] "Ban on identified Single Use Plastic Items from 1st July 2022." https://pib.gov.in/pib.gov.in/Pressreleaseshare.aspx?PRID=1837518.

[89] M. Koller, R. Bona, E. Chiellini, and G. Braunegg, "Extraction of short-chain-length poly-[(R)-hydroxyalkanoates] (scl-PHA) by the 'anti-solvent' acetone under elevated temperature and pressure," *Biotechnol. Lett.*, vol. 35, no. 7, pp. 1023–1028, Jul. 2013.

[90] D. B. Karr, J. K. Waters, and D. W. Emerich, "Analysis of Poly-β-Hydroxybutyrate in Rhizobium japonicum Bacteroids by Ion-Exclusion High-Pressure Liquid Chromatography and UV Detection," *Appl. Environ. Microbiol.*, vol. 46, no. 6, pp. 1339–1344, Dec. 1983.

[91] K. Chaturvedi, A. R. Kulkarni, and T. M. Aminabhavi, "Blend Microspheres of Poly(3-hydroxybutyrate) and Cellulose Acetate Phthalate for Colon Delivery of 5-Fluorouracil," *Ind. Eng. Chem. Res.*, vol. 50, no. 18, pp. 10414–10423, Sep. 2011.

[92] M. Caine *et al.*, "Impact of Yttrium-90 Microsphere Density, Flow Dynamics, and Administration Technique on Spatial Distribution: Analysis Using an In Vitro Model," *J. Vasc. Interv. Radiol. JVIR*, vol. 28, no. 2, pp. 260-268.e2, Feb. 2017.

[93] M. Y. Yousif, D. W. Holdsworth, and T. L. Poepping, "A blood-mimicking fluid for particle image velocimetry with silicone vascular models," *Exp. Fluids*, vol. 50, no. 3, pp. 769–774, Mar. 2011.

[94] A. M. Abdou, “Purification and Partial Characterization of Psychrotrophic Serratia marcescens Lipase,” *J. Dairy Sci.*, vol. 86, no. 1, pp. 127–132, Jan. 2003.

[95] R. Coico, “Gram Staining,” *Curr. Protoc. Microbiol.*, vol. 00, no. 1, p. A.3C.1-A.3C.2, 2006.

[96] A. C. Darby, S. M. Chandler, S. C. Welburn, and A. E. Douglas, “Aphid-Symbiotic Bacteria Cultured in Insect Cell Lines,” *Appl. Environ. Microbiol.*, vol. 71, no. 8, pp. 4833–4839, Aug. 2005.

[97] S. Karlin and S. F. Altschul, “Methods for assessing the statistical significance of molecular sequence features by using general scoring schemes.,” *Proc. Natl. Acad. Sci.*, vol. 87, no. 6, pp. 2264–2268, Mar. 1990.

[98] K. Tamura, G. Stecher, D. Peterson, A. Filipski, and S. Kumar, “MEGA6: Molecular Evolutionary Genetics Analysis Version 6.0,” *Mol. Biol. Evol.*, vol. 30, no. 12, pp. 2725–2729, Dec. 2013.

[99] P. Greenup and D. J. Blazevic, “Antibiotic Susceptibilities of Serratia marcescens and Enterobacter liquefaciens,” *Appl. Microbiol.*, vol. 22, no. 3, pp. 309–314, Sep. 1971.

[100] P. H. Krumperman, “Multiple Antibiotic Resistance Indexing of Escherichia coli to Identify High-Risk Sources of Fecal Contamination of Foodst,” *APPL Env. MICROBIOL*, vol. 46, p. 6, 1983.

[101] R. Sandhu, S. Dahiya, and P. Sayal, “Evaluation of multiple antibiotic resistance (MAR) index and Doxycycline susceptibility of Acinetobacter species among inpatients,” *Indian J. Microbiol. Res.*, vol. 3, no. 3, p. 299, 2016.

[102] N. M. Elkenawy, A. S. Yassin, H. N. Elhifnawy, and M. A. Amin, “Optimization of prodigiosin production by Serratia marcescens using crude glycerol and enhancing production using gamma radiation,” *Biotechnol. Rep.*, vol. 14, pp. 47–53, Apr. 2017.

[103] N. M. Elkenawy, A. S. Yassin, H. N. Elhifnawy, and M. A. Amin, “Optimization of prodigiosin production by Serratia marcescens using crude glycerol and enhancing production using gamma radiation,” *Biotechnol. Rep.*, vol. 14, pp. 47–53, Apr. 2017.

[104] N. Darshan and H. K. Manonmani, “Prodigiosin inhibits motility and activates bacterial cell death revealing molecular biomarkers of programmed cell death,” *AMB Express*, vol. 6, Jul. 2016.

[105] C. Mudenur, P. Boruah, A. Kumar, and V. Katiyar, “Prodigiosin-Loaded Poly(lactic acid) to Combat the Biofilm-Associated Infections,” *ACS Appl. Bio Mater.*, Apr. 2022.

[106] N. Darshan and H. K. Manonmani, “Prodigiosin inhibits motility and activates bacterial cell death revealing molecular biomarkers of programmed cell death,” *AMB Express*, vol. 6, no. 1, p. 50, Jul. 2016.

[107] A. Bouamer, N. Benrekaa, and A. Younes, “Characterization of polylactic acid ceramic composites synthesized by casting method,” *Mater. Today Proc.*, vol. 42, pp. 2959–2962, Jan. 2021.

[108] “CFR - Code, https://www.accessdata.fda.gov/scripts/cdrh/cfdocs/cfcfr/.

[109] M. E. Skogman, P. M. Vuorela, and A. Fallarero, “Combining biofilm matrix measurements with biomass and viability assays in susceptibility assessments of antimicrobials against Staphylococcus aureus biofilms,” *J. Antibiot. (Tokyo)*, vol. 65, no. 9, pp. 453–459, Sep. 2012.

[110] X. Y. Xiong, K. C. Tam, and L. H. Gan, “Hydrolytic Degradation of Pluronic F127/Poly(lactic acid) Block Copolymer Nanoparticles,” *Macromolecules*, vol. 37, no. 9, pp. 3425–3430, May 2004.

[111] A. Gupta *et al.*, “Multifunctional Nanohydroxyapatite-Promoted Toughened High-Molecular-Weight Stereocomplex Poly(lactic acid)-Based Bionanocomposite for Both 3D-Printed Orthopedic Implants and High-Temperature Engineering Applications,” *ACS Omega*, vol. 2, no. 7, pp. 4039–4052, Jul. 2017.

[112] T. D. Moshood, G. Nawanir, F. Mahmud, F. Mohamad, M. H. Ahmad, and A. AbdulGhani, “Sustainability of biodegradable plastics: New problem or solution to solve the global plastic pollution?,” *Curr. Res. Green Sustain. Chem.*, vol. 5, p. 100273, Jan. 2022.

[113] P. Anbukarasu, D. Sauvageau, and A. Elias, “Tuning the properties of polyhydroxybutyrate films using acetic acid via solvent casting,” *Sci. Rep.*, vol. 5, no. 1, Art. no. 1, Dec. 2015.

[114] J. M. Naranjo, J. A. Posada, J. C. Higuita, and C. A. Cardona, “Valorization of glycerol through the production of biopolymers: The PHB case using Bacillus megaterium,” *Bioresour. Technol.*, vol. 133, pp. 38–44, Apr. 2013.

[115] D. Nygaard, O. Yashchuk, D. G. Noseda, B. Araoz, and É. B. Hermida, “Improved fermentation strategies in a bioreactor for enhancing poly(3-hydroxybutyrate) (PHB) production by wild type Cupriavidus necator from fructose,” *Heliyon*, vol. 7, no. 1, p. e05979, Jan. 2021.

[116] M. Koller, “Polyhydroxyalkanoate Biosynthesis at the Edge of Water Activitiy-Haloarchaea as Biopolyester Factories,” *Bioengineering*, vol. 6, no. 2, p. 34, Apr. 2019.

[117] P. Kaewkannetra, “Production of Poly-β-hydroxybutyric acid (PHB) from sweet sorghum juice by Alcaligenes eutrophus TISTR 1095 and Alcaligenes latus ATCC 29714 via batch …,” *3th Int.* https://www.academia.edu/es/58384995/Production

[118] D. Nygaard, O. Yashchuk, D. G. Noseda, B. Araoz, and É. B. Hermida, “Improved fermentation strategies in a bioreactor for enhancing poly(3-hydroxybutyrate) (PHB) production by wild type Cupriavidus necator from fructose,” *Heliyon*, vol. 7, no. 1, p. e05979, Jan. 2021.

[119] A. Wahl, N. Schuth, D. Pfeiffer, S. Nussberger, and D. Jendrossek, “PHB granules are attached to the nucleoid via PhaM in Ralstonia eutropha,” *BMC Microbiol.*, vol. 12, no. 1, p. 262, Nov. 2012.

[120] Y. O. Posokhov and A. Kyrychenko, “Effect of acetone accumulation on structure and dynamics of lipid membranes studied by molecular dynamics simulations,” *Comput. Biol. Chem.*, vol. 46, pp. 23–31, Oct. 2013.

[121] M. R. J. Salton and K.-S. Kim, “Structure,” in *Medical Microbiology*, S. Baron, Ed., 4th ed.Galveston (TX): University of Texas Medical Branch at Galveston, 1996. http://www.ncbi.nlm.nih.gov/books/NBK8477/.

[122] “Cancer today.” http://gco.iarc.fr/today/home.

[123] J. M. Llovet *et al.*, “Hepatocellular carcinoma,” *Nat. Rev. Dis. Primer*, vol. 7, no. 1, Art. no. 1, Jan. 2021.

[124] “Liver Cancer - Gastrointestinal Cancer | UCLA Health.” https://www.uclahealth.org/medical-services/cancer-services/gi-cancer/conditions/liver-cancer .

[125] “Embolization Therapy for Liver Cancer.” https://www.cancer.org/cancer/liver-cancer/treating/embolization-therapy.html.

[126] S. P. Mohandas *et al.*, “Biocompatibility of polyhydroxybutyrate-co-hydroxyvalerate films generated from Bacillus cereus MCCB 281 for medical applications,” *Int. J. Biol. Macromol.*, vol. 176, pp. 244–252, Apr. 2021.

[127] S. R. Jernigan, J. A. Osborne, C. J. Mirek, and G. Buckner, “Selective Internal Radiation Therapy: Quantifying Distal Penetration and Distribution of Resin and Glass Microspheres in a Surrogate Arterial Model,” *J. Vasc. Interv. Radiol.*, vol. 26, no. 6, pp. 897-904.e2, Jun. 2015.

[128] M. A. Westcott, D. M. Coldwell, D. M. Liu, and J. F. Zikria, “The development, commercialization, and clinical context of yttrium-90 radiolabeled resin and glass microspheres,” *Adv. Radiat. Oncol.*, vol. 1, no. 4, pp. 351–364, Oct. 2016.

[129] A. Al-Kalbani and Y. Kamel, “Y-90 Microshperes in the Treatment of Unresectable Hepatocellular Carcinoma,” *Saudi J. Gastroenterol. Off. J. Saudi Gastroenterol. Assoc.*, vol. 14, no. 2, pp. 90–92, Apr. 2008.

[130] K. M. Meess *et al.*, “3D Printed Abdominal Aortic Aneurysm Phantom for Image Guided Surgical Planning with a Patient Specific Fenestrated Endovascular Graft System,” *Proc. SPIE-- Int. Soc. Opt. Eng.*, vol. 10138, p. 101380P, Feb. 2017.

[131] “Annio et al. - Accepted Manuscript Not Copyedited.pdf.” https://discovery.ucl.ac.uk/id/eprint/10089725/1/jesmdt-19-1037%281%29.pdf.

[132] M. T. Li, L. L. Hao, L. X. Sheng, and J. B. Xu, “Identification and degradation characterization of hexachlorobutadiene degrading strain Serratia marcescens HL1,” *Bioresour. Technol.*, vol. 99, no. 15, pp. 6878–6884, Oct. 2008.

[133] D. Fehér, R. S. Barlow, P. S. Lorenzo, and T. K. Hemscheidt, “A 2-Substituted Prodiginine, 2-(p-Hydroxybenzyl)prodigiosin, from Pseudoalteromonas rubra,” *J. Nat. Prod.*, vol. 71, no. 11, pp. 1970–1972, Dec. 2008.

[134] T. Kawasaki, F. Sakurai, and Y. Hayakawa, “A Prodigiosin from the Roseophilin Producer Streptomyces griseoviridis,” *J. Nat. Prod.*, vol. 71, no. 7, pp. 1265–1267, Jul. 2008.

[135] M. Givskov *et al.*, “Two Separate Regulatory Systems Participate in Control of Swarming Motility of Serratia liquefaciensMG1,” *J. Bacteriol.*, vol. 180, no. 3, pp. 742–745, Feb. 1998.

[136] T. Wang *et al.*, “Heterotrophic nitrogen removal by a newly-isolated alkalitolerant microorganism, Serratia marcescens W5,” *Bioresour. Technol.*, vol. 211, pp. 618–627, Jul. 2016.

[137] N. Stankovic, L. Senerovic, T. Ilic-Tomic, B. Vasiljevic, and J. Nikodinovic-Runic, “Properties and applications of undecylprodigiosin and other bacterial prodigiosins,” *Appl. Microbiol. Biotechnol.*, vol. 98, no. 9, pp. 3841–3858, May 2014.

[138] M. M. Anwar, M. Shalaby, A. M. Embaby, H. Saeed, M. M. Agwa, and A. Hussein, “Prodigiosin/PU-H71 as a novel potential combined therapy for triple negative breast cancer (TNBC): preclinical insights,” *Sci. Rep.*, vol. 10, no. 1, p. 14706, Sep. 2020.

[139] A. Bhagwat and U. Padalia, "Optimization of prodigiosin biosynthesis by Serratia marcescens using unconventional bioresources," *J. Genet. Eng. Biotechnol.*, vol. 18, p. 26, Jul. 2020.

[140] F. Verbeke *et al.*, "Peptides as Quorum Sensing Molecules: Measurement Techniques and Obtained Levels In vitro and In vivo," *Front. Neurosci.*, vol. 11, p. 183, Apr. 2017.

[141] S.-H. Dong, M. Nhu-Lam, R. Nagarajan, and S. K. Nair, "Structure-Guided Biochemical Analysis of Quorum Signal Synthase Specificities," *ACS Chem. Biol.*, vol. 15, no. 6, pp. 1497–1504, Jun. 2020.

[142] C. D. Sifri, "Quorum Sensing: Bacteria Talk Sense," *Clin. Infect. Dis.*, vol. 47, no. 8, pp. 1070–1076, Oct. 2008.

[143] J. C. Tsang, G. A. Sansing, and M. A. Miller, "Relation of Beta-Lactamase Activity to Antimicrobial Susceptibility in Serratia marcescens," *Antimicrob. Agents Chemother.*, vol. 8, no. 3, pp. 277–281, Sep. 1975.

[144] T. Nishiura, Y. Kawada, Y. Shiomi, K. O'Hara, and M. Kono, "Microbial Degradation of Cephalothin by Cephalothin-Susceptible Escherichia coli," *Antimicrob. Agents Chemother.*, vol. 13, no. 6, pp. 1036–1039, Jun. 1978.

[145] M. P. Chitanand, T. A. Kadam, G. Gyananath, N. D. Totewad, and D. K. Balhal, "Multiple antibiotic resistance indexing of coliforms to identify high risk contamination sites in aquatic environment," *Indian J. Microbiol.*, vol. 50, no. 2, pp. 216–220, Jun. 2010.

[146] R. C. Cooksey, E. R. Bannister, and W. E. Farrar, "Antibiotic Resistance Patterns of Clinical Isolates of Serratia marcescens," *Antimicrob. Agents Chemother.*, vol. 7, no. 4, pp. 396–399, Apr. 1975.

[147] A. Domröse *et al.*, "Efficient recombinant production of prodigiosin in Pseudomonas putida," *Front. Microbiol.*, vol. 6, 2015.

[148] C. A. Aruldass, C. K. Venil, Z. A. Zakaria, and W. A. Ahmad, "Brown sugar as a low-cost medium for the production of prodigiosin by locally isolated Serratia marcescens UTM1," *Int. Biodeterior. Biodegrad.*, vol. 95, pp. 19–24, Nov. 2014.

[149] V. S. Gondil, M. Asif, and T. C. Bhalla, "Optimization of physicochemical parameters influencing the production of prodigiosin from Serratia nematodiphila RL2 and exploring its antibacterial activity," *3 Biotech*, vol. 7, no. 5, p. 338, Sep. 2017.

[150] T. Morohoshi *et al.*, "Inhibition of Quorum Sensing in Serratia marcescens AS-1 by Synthetic Analogs of N-Acylhomoserine Lactone," *Appl. Environ. Microbiol.*, vol. 73, no. 20, pp. 6339–6344, Oct. 2007.

[151] J. E. Fender, C. M. Bender, N. A. Stella, R. M. Lahr, E. J. Kalivoda, and R. M. Q. Shanks, "Serratia marcescens Quinoprotein Glucose Dehydrogenase Activity Mediates Medium Acidification and Inhibition of Prodigiosin Production by Glucose," *Appl. Environ. Microbiol.*, vol. 78, no. 17, pp. 6225–6235, Sep. 2012.

[152] K. V. Arivizhivendhan *et al.*, "Synthesis of Surface-Modified Iron Oxides for the Solvent-Free Recovery of Bacterial Bioactive Compound Prodigiosin and Its Algicidal Activity," *J. Phys. Chem. B*, vol. 120, no. 36, pp. 9685–9696, Sep. 2016.

[153] R. K. Suryawanshi, C. D. Patil, S. H. Koli, J. E. Hallsworth, and S. V. Patil, "Antimicrobial activity of prodigiosin is attributable to plasma-membrane damage," *Nat. Prod. Res.*, vol. 31, no. 5, pp. 572–577, Mar. 2017.

[154] I. Guryanov *et al.*, "Selective Cytotoxic Activity of Prodigiosin@halloysite Nanoformulation," *Front. Bioeng. Biotechnol.*, vol. 8, p. 424, 2020.

[155] M. Singhvi and D. Gokhale, "Biomass to biodegradable polymer (PLA)," *RSC Adv.*, vol. 3, no. 33, pp. 13558–13568, Jul. 2013.

[156] N. E. Kamber, W. Jeong, R. M. Waymouth, R. C. Pratt, B. G. G. Lohmeijer, and J. L. Hedrick, "Organocatalytic Ring-Opening Polymerization," *Chem. Rev.*, vol. 107, no. 12, pp. 5813–5840, Dec. 2007.

[157] M. K. Kiesewetter, E. J. Shin, J. L. Hedrick, and R. M. Waymouth, "Organocatalysis: Opportunities and Challenges for Polymer Synthesis," *Macromolecules*, vol. 43, no. 5, pp. 2093–2107, Mar. 2010.

[158] J. Franzén, M. Marigo, D. Fielenbach, T. C. Wabnitz, A. Kjærsgaard, and K. A. Jørgensen, "A General Organocatalyst for Direct α-Functionalization of Aldehydes: Stereoselective C−C, C−N, C−F, C−Br, and C−S Bond-Forming Reactions. Scope and Mechanistic Insights," *J. Am. Chem. Soc.*, vol. 127, no. 51, pp. 18296–18304, Dec. 2005.

[159] M. Benaglia, A. Puglisi, and F. Cozzi, "Polymer-Supported Organic Catalysts," *Chem. Rev.*, vol. 103, no. 9, pp. 3401–3430, Sep. 2003.

[160] F. Nederberg, E. F. Connor, M. Möller, T. Glauser, and J. L. Hedrick, "New Paradigms for Organic Catalysts: The First Organocatalytic Living Polymerization," *Angew. Chem. Int. Ed.*, vol. 40, no. 14, pp. 2712–2715, 2001.

[161] E. F. Connor, G. W. Nyce, M. Myers, A. Möck, and J. L. Hedrick, "First Example of N-Heterocyclic Carbenes as Catalysts for Living Polymerization: Organocatalytic Ring-Opening Polymerization of Cyclic Esters," *J. Am. Chem. Soc.*, vol. 124, no. 6, pp. 914–915, Feb. 2002.

[162] V. Katiyar and H. Nanavati, "Ring-opening polymerization of L-lactide using N-heterocyclic molecules: mechanistic, kinetics and DFT studies," *Polym. Chem.*, vol. 1, no. 9, pp. 1491–1500, Oct. 2010.

[163] Y. Wang, L. Zhang, X. Guo, R. Zhang, and J. Li, "Characteristics and mechanism of L-lactide polymerization using N-heterocyclic carbene organocatalyst," *J. Polym. Res.*, vol. 20, no. 3, p. 87, Feb. 2013.

[164] L. Zhang *et al.*, "Acyclic Guanidines as Organic Catalysts for Living Polymerization of Lactide," *Macromolecules*, vol. 43, no. 3, pp. 1660–1664, Feb. 2010.

[165] J. M. Becker, S. Tempelaar, M. J. Stanford, R. J. Pounder, J. A. Covington, and A. P. Dove, "Development of Amino–Oxazoline and Amino–Thiazoline Organic Catalysts for the Ring-Opening Polymerisation of Lactide," *Chem. – Eur. J.*, vol. 16, no. 20, pp. 6099–6105, 2010.

[166] B. List, R. A. Lerner, and C. F. Barbas, "Proline-Catalyzed Direct Asymmetric Aldol Reactions," *J. Am. Chem. Soc.*, vol. 122, no. 10, pp. 2395–2396, Mar. 2000.

[167] K. A. Ahrendt, C. J. Borths, and D. W. C. MacMillan, "New Strategies for Organic Catalysis: The First Highly Enantioselective Organocatalytic Diels−Alder Reaction," *J. Am. Chem. Soc.*, vol. 122, no. 17, pp. 4243–4244, May 2000.

[168] M. Benaglia, A. Puglisi, and F. Cozzi, "Polymer-Supported Organic Catalysts," *Chem. Rev.*, vol. 103, no. 9, pp. 3401–3430, Sep. 2003.

[169] H. H. Wasserman, G. C. Rodgers, and D. D. Keith, "Metacycloprodigiosin, a tripyrrole pigment from Streptomyces longisporus ruber," *J. Am. Chem. Soc.*, vol. 91, no. 5, pp. 1263–1264, Feb. 1969.

[170] A. J. Castro, "Antimalarial Activity of Prodigiosin," *Nature*, vol. 213, no. 5079, pp. 903–904, Mar. 1967.

[171] J. Hage-Hülsmann *et al.*, "Natural biocide cocktails: Combinatorial antibiotic effects of prodigiosin and biosurfactants," *PLOS ONE*, vol. 13, no. 7, p. e0200940, Jul. 2018.

[172] M. S. Melvin, J. T. Tomlinson, G. R. Saluta, G. L. Kucera, N. Lindquist, and R. A. Manderville, "Double-Strand DNA Cleavage by Copper·Prodigiosin," *J. Am. Chem. Soc.*, vol. 122, no. 26, pp. 6333–6334, Jul. 2000.

[173] Z. Wang *et al.*, "Prodigiosin inhibits Wnt/β-catenin signaling and exerts anticancer activity in breast cancer cells," *Proc. Natl. Acad. Sci.*, vol. 113, no. 46, pp. 13150–13155, Nov. 2016.

[174] R. F. Tsuji *et al.*, "Selective immunosuppression of prodigiosin 25-C and FK506 in the murine immune system," *J. Antibiot. (Tokyo)*, vol. 43, no. 10, pp. 1293–1301, Oct. 1990.

[175] R. P. Williams, "Biosynthesis of Prodigiosin, a Secondary Metabolite of Serratia marcescens," *Appl. Microbiol.*, vol. 25, no. 3, pp. 396–402, Mar. 1973.

[176] J. Y. D'Aoust and N. N. Gerber, "Isolation and Purification of Prodigiosin from Vibrio psychroerythrus," *J. Bacteriol.*, vol. 118, no. 2, pp. 756–757, May 1974.

[177] S. W. Tsao, B. A. Rudd, X. G. He, C. J. Chang, and H. G. Floss, "Identification of a red pigment from Streptomyces coelicolor A3(2) as a mixture of prodigiosin derivatives," *J. Antibiot. (Tokyo)*, vol. 38, no. 1, pp. 128–131, Jan. 1985.

[178] N. N. Gerber and M. J. Gauthier, "New prodigiosin-like pigment from Alteromonas rubra.," *Appl. Environ. Microbiol.*, vol. 37, no. 6, pp. 1176–1179, Jun. 1979.

[179] A. S. Klein *et al.*, "New Prodigiosin Derivatives Obtained by Mutasynthesis in Pseudomonas putida," *ACS Synth. Biol.*, vol. 6, no. 9, pp. 1757–1765, Sep. 2017.

[180] Z. Wang *et al.*, "Prodigiosin inhibits Wnt/β-catenin signaling and exerts anticancer activity in breast cancer cells," *Proc. Natl. Acad. Sci.*, vol. 113, no. 46, pp. 13150–13155, Nov. 2016.

[181] R. P. Williams and W. R. Hearn, "Prodigiosin," in *Biosynthesis*, D. Gottlieb and P. D. Shaw, Eds., in Antibiotics. Berlin, Heidelberg: Springer Berlin Heidelberg, 1967, pp. 410–432.

[182] T. M. Chang, S. Sinharay, A. V. Astashkin, and E. Tomat, "Prodigiosin Analogue Designed for Metal Coordination: Stable Zinc and Copper Pyrrolyldipyrrins," *Inorg. Chem.*, vol. 53, no. 14, pp. 7518–7526, Jul. 2014.

[183] S. Garneau-Tsodikova, P. C. Dorrestein, N. L. Kelleher, and C. T. Walsh, "Protein Assembly Line Components in Prodigiosin Biosynthesis: Characterization of PigA,G,H,I,J," *J. Am. Chem. Soc.*, vol. 128, no. 39, pp. 12600–12601, Oct. 2006.

[184] S. Naumann, P. B. V. Scholten, J. A. Wilson, and A. P. Dove, "Dual Catalysis for Selective Ring-Opening Polymerization of Lactones: Evolution toward Simplicity," *J. Am. Chem. Soc.*, vol. 137, no. 45, pp. 14439–14445, Nov. 2015.

[185] "Low-molecular-weight polymer–drug conjugates for synergistic anticancer activity of camptothecin and doxorubicin combinations." https://www.ncbi.nlm.nih.gov/pmc/articles/PMC4910946/.

[186] C. Hu, E. Louisy, G. Fontaine, and F. Bonnet, "Cyclic versus linear polylactide: Straightforward access using a single catalyst," *J. Polym. Sci. Part Polym. Chem.*, vol. 55, no. 19, pp. 3175–3179, 2017.

[187] A. Prasad, S. Bhasney, V. Katiyar, and M. Ravi Sankar, "Biowastes Processed Hydroxyapatite filled Poly (Lactic acid) Bio-Composite for Open Reduction Internal Fixation of Small Bones," *Mater. Today Proc.*, vol. 4, no. 9, pp. 10153–10157, Jan. 2017.

[188] A. Tampieri *et al.*, "Magnetic Bioinspired Hybrid Nanostructured Collagen–Hydroxyapatite Scaffolds Supporting Cell Proliferation and Tuning Regenerative Process," *ACS Appl. Mater. Interfaces*, vol. 6, no. 18, pp. 15697–15707, Sep. 2014.

[189] X. Li, Q. Feng, X. Liu, W. Dong, and F. Cui, "Collagen-based implants reinforced by chitin fibres in a goat shank bone defect model," *Biomaterials*, vol. 27, no. 9, pp. 1917–1923, Mar. 2006.

[190] B. Mehrjou, S. Mo, D. Dehghan-Baniani, G. Wang, A. M. Qasim, and P. K. Chu, "Antibacterial and Cytocompatible Nanoengineered Silk-Based Materials for Orthopedic Implants and Tissue Engineering," *ACS Appl. Mater. Interfaces*, vol. 11, no. 35, pp. 31605–31614, Sep. 2019.

[191] M. Tesfaye, R. Patwa, P. Dhar, and V. Katiyar, "Nanosilk-Grafted Poly(lactic acid) Films: Influence of Cross-Linking on Rheology and Thermal Stability," *ACS Omega*, vol. 2, no. 10, pp. 7071–7084, Oct. 2017.

[192] J. Ko, L. T. H. Nguyen, A. Surendran, B. Y. Tan, K. W. Ng, and W. L. Leong, "Human Hair Keratin for Biocompatible Flexible and Transient Electronic Devices," *ACS Appl. Mater. Interfaces*, vol. 9, no. 49, pp. 43004–43012, Dec. 2017.

[193] G. J. Dias, P. Mahoney, M. Swain, R. J. Kelly, R. A. Smith, and M. A. Ali, "Keratin-hydroxyapatite composites: biocompatibility, osseointegration, and physical properties in an ovine model," *J. Biomed. Mater. Res. A*, vol. 95, no. 4, pp. 1084–1095, Dec. 2010.

[194] B. G. Pfang *et al.*, "Orthopedic Implant-Associated Infection by Multidrug Resistant Enterobacteriaceae," *J. Clin. Med.*, vol. 8, no. 2, p. 220, Feb. 2019.

[195] C. R. Arciola, D. Campoccia, and L. Montanaro, “Implant infections: adhesion, biofilm formation and immune evasion,” *Nat. Rev. Microbiol.*, vol. 16, no. 7, pp. 397–409, Jul. 2018.

[196] R. Kuehl *et al.*, “Preventing Implant-Associated Infections by Silver Coating,” *Antimicrob. Agents Chemother.*, vol. 60, no. 4, pp. 2467–2475.

[197] A. Davin-Regli and J.-M. Pagès, “Enterobacter aerogenes and Enterobacter cloacae; versatile bacterial pathogens confronting antibiotic treatment,” *Front. Microbiol.*, vol. 6, p. 392, May 2015.

[198] Y. Zhi-Wen, Z. Yan-Li, Y. Man, and F. Wei-Jun, “Clinical treatment of pandrug-resistant bacterial infection consulted by clinical pharmacist,” *Saudi Pharm. J. SPJ*, vol. 23, no. 4, pp. 377–380, Sep. 2015.

[199] A. J. Tande and R. Patel, “Prosthetic Joint Infection,” *Clin. Microbiol. Rev.*, Apr. 2014.

[200] W. A. Rutala, “Guideline for Disinfection and Sterilization in Healthcare Facilities, 2008,” p. 163, 2008.

[201] V. Sansone, D. Pagani, and M. Melato, “The effects on bone cells of metal ions released from orthopaedic implants. A review,” *Clin. Cases Miner. Bone Metab.*, vol. 10, no. 1, pp. 34–40, 2013.

[202] M. S. Cano-Velázquez *et al.*, “Enhanced near infrared optical access to the brain with a transparent cranial implant and scalp optical clearing,” *Biomed. Opt. Express*, vol. 10, no. 7, pp. 3369–3379, Jun. 2019.

[203] M. Tesfaye, R. Patwa, P. Dhar, and V. Katiyar, “Nanosilk-Grafted Poly(lactic acid) Films: Influence of Cross-Linking on Rheology and Thermal Stability,” *ACS Omega*, vol. 2, no. 10, pp. 7071–7084, Oct. 2017.

[204] A. K. Pal and V. Katiyar, “Thermal degradation behaviour of nanoamphiphilic chitosan dispersed poly (lactic acid) bionanocomposite films,” *Int. J. Biol. Macromol.*, vol. 95, pp. 1267–1279, Feb. 2017.

[205] H. Humphreys *et al.*, “Staphylococcus aureus and surgical site infections: benefits of screening and decolonization before surgery,” *J. Hosp. Infect.*, vol. 94, no. 3, pp. 295–304, Nov. 2016.

[206] A. Wesevich *et al.*, “Newly Named Klebsiella aerogenes (formerly Enterobacter aerogenes) Is Associated with Poor Clinical Outcomes Relative to Other Enterobacter

Species in Patients with Bloodstream Infection," *J. Clin. Microbiol.*, vol. 58, no. 9, pp. e00582-20.

[207] M. S. Melvin, M. W. Calcutt, R. E. Noftle, and R. A. Manderville, "Influence of the A-Ring on the Redox and Nuclease Properties of the Prodigiosins: Importance of the Bipyrrole Moiety in Oxidative DNA Cleavage," *Chem. Res. Toxicol.*, vol. 15, no. 5, pp. 742–748, May 2002.

[208] C. Salas, T. Nypelö, C. Rodriguez-Abreu, C. Carrillo, and O. J. Rojas, "Nanocellulose properties and applications in colloids and interfaces," *Curr. Opin. Colloid Interface Sci.*, vol. 19, no. 5, pp. 383–396, Oct. 2014.

[209] M. A. Hassan *et al.*, "Sustainable production of polyhydroxyalkanoates from renewable oil-palm biomass," *Biomass Bioenergy*, vol. 50, pp. 1–9, Mar. 2013.

[210] M. T. Cesário, R. S. Raposo, M. C. M. D. de Almeida, F. van Keulen, B. S. Ferreira, and M. M. R. da Fonseca, "Enhanced bioproduction of poly-3-hydroxybutyrate from wheat straw lignocellulosic hydrolysates," *New Biotechnol.*, vol. 31, no. 1, pp. 104–113, Jan. 2014.

[211] M. Sandhya, J. Aravind, and P. Kanmani, "Production of polyhydroxyalkanoates from Ralstonia eutropha using paddy straw as cheap substrate," *Int. J. Environ. Sci. Technol.*, vol. 10, no. 1, pp. 47–54, Jan. 2013.

[212] J. J. Cheng and G. Timilsina, "Status and barriers of advanced biofuel technologies: A review," *Renew. Energy*, vol. 36, no. 12, pp. 3541–3549, 2011.

[213] G. Brodeur, E. Yau, K. Badal, J. Collier, K. B. Ramachandran, and S. Ramakrishnan, "Chemical and Physicochemical Pretreatment of Lignocellulosic Biomass: A Review," *Enzyme Research*, 2011. https://www.hindawi.com/journals/er/2011/787532/.

[214] A. R. G. da Silva, M. Errico, and B.-G. Rong, "Evaluation of organosolv pretreatment for bioethanol production from lignocellulosic biomass: solvent recycle and process integration," *Biomass Convers. Biorefinery*, vol. 8, no. 2, pp. 397–411, Jun. 2018.

[215] L.-A. T, R. P, R.-M. E, and S.-C. M, "Acid pretreatment of lignocellulosic biomass: steady state and dynamic analysis," *Chem. Eng. Trans.*, pp. 445–450, Sep. 2010.

[216] M. Ayyachamy, V. K. Gupta, F. E. Cliffe, and M. G. Tuohy, "Enzymatic Saccharification of Lignocellulosic Biomass," in *Laboratory Protocols in Fungal Biology: Current Methods in Fungal Biology*, V. K. Gupta, M. G. Tuohy, M. Ayyachamy, K. M. Turner, and A. O'Donovan, Eds., in Fungal Biology. New York, NY: Springer New York, 2013, pp. 475–481.

[217] A. L. F. Santos, K. Y. F. Kawase, and G. L. V. Coelho, "Enzymatic saccharification of lignocellulosic materials after treatment with supercritical carbon dioxide," *J. Supercrit. Fluids*, vol. 56, no. 3, pp. 277–282, Apr. 2011.

[218] T. Sartori, H. Tibolla, E. Prigol, L. M. Colla, J. A. V. Costa, and T. E. Bertolin, "Enzymatic Saccharification of Lignocellulosic Residues by Cellulases Obtained from Solid State Fermentation Using Trichoderma viride," *BioMed Research International*, 2015.

[219] S. A. Alrumman and S. A. Alrumman, "Enzymatic saccharification and fermentation of cellulosic date palm wastes to glucose and lactic acid," *Braz. J. Microbiol.*, vol. 47, no. 1, pp. 110–119, Mar. 2016.

[220] "Improvement of Saccharification and Fermentation by Removal of Endogenous Chemicals from Pretreated Lignocellulosic Biomass (1). Effect of Ion-Exchange Resin Treatment." https://www.omicsonline.org/open-access/improvement-of-saccharification-and-fermentation-by-removal-of-endogenouschemicals-from-pretreated-lignocellulosic-biomass.

[221] C. M. Roche, C. J. Dibble, and J. J. Stickel, "Laboratory-scale method for enzymatic saccharification of lignocellulosic biomass at high-solids loadings," *Biotechnol. Biofuels*, vol. 2, no. 1, p. 28, Nov. 2009.

[222] A. Babaei-Ghazvini and B. Acharya, "Influence of cellulose nanocrystal aspect ratio on shear force aligned films: Physical and mechanical properties," *Carbohydr. Polym. Technol. Appl.*, vol. 3, p. 100217, Jun. 2022.

[223] Q. Wu, X. Li, Q. Li, S. Wang, and Y. Luo, "Estimation of Aspect Ratio of Cellulose Nanocrystals by Viscosity Measurement: Influence of Aspect Ratio Distribution and Ionic Strength," *Polymers*, vol. 11, no. 5, p. 781, May 2019.

[224] N. Lin, C. Bruzzese, and A. Dufresne, "TEMPO-Oxidized Nanocellulose Participating as Crosslinking Aid for Alginate-Based Sponges," *ACS Appl. Mater. Interfaces*, vol. 4, no. 9, pp. 4948–4959, Sep. 2012.

[225] P. Dhar, A. Kumar, and V. Katiyar, "Magnetic Cellulose Nanocrystal Based Anisotropic Polylactic Acid Nanocomposite Films: Influence on Electrical, Magnetic, Thermal, and Mechanical Properties," *ACS Appl. Mater. Interfaces*, vol. 8, no. 28, pp. 18393–18409, Jul. 2016.

[226] Monika, P. Dhar, and V. Katiyar, "Thermal degradation kinetics of polylactic acid/acid fabricated cellulose nanocrystal based bionanocomposites," *Int. J. Biol. Macromol.*, vol. 104, pp. 827–836, Nov. 2017.

[227] B. Alonso-Lerma *et al.*, “High performance crystalline nanocellulose using an ancestral endoglucanase,” *Commun. Mater.*, vol. 1, no. 1, Art. no. 1, Aug. 2020.

[228] J. H. Jordan, M. W. Easson, and B. D. Condon, “Cellulose hydrolysis using ionic liquids and inorganic acids under dilute conditions: morphological comparison of nanocellulose,” *RSC Adv.*, vol. 10, no. 65, pp. 39413–39424, 2020.

[229] R. M. Abdelaziz, A. El-Maghraby, W. A.-A. Sadik, A.-G. M. El-Demerdash, and E. A. Fadl, “Biodegradable cellulose nanocrystals hydrogels for removal of acid red 8 dye from aqueous solutions,” *Sci. Rep.*, vol. 12, no. 1, Art. no. 1, Apr. 2022.

Patents

1. Vimal Katiyar, Chethana Mudenur, and Amit Kumar. Metal-free prodigiosin catalyst for lactide polymerization. Indian Patent No (Granted): 419571
2. Vimal Katiyar, Chethana Mudenur, and Amit Kumar. Process of production of polyhydroxybutyrate [PHB] from wild grasses. Indian Patent Application Number: 202131031003

Publications

1. **Chethana Mudenur**, Pankaj Boruah, Amit Kumar, and Vimal Katiyar, 2022, Prodigiosin-loaded poly(lactic acid) to combat the biofilm-associated infections, *ACS Applied biomaterials*, 2022 April 25, 5 (5), 2143-2151.
1. **Chethana Mudenur**, Amit Kumar and Vimal Katiyar, Acyl-homoserine lactone mediated prodigiosin produced from *Serratia nematodiphila* as an antibacterial wound healing indicator, Advanced Biomaterials (Under review)
2. **Chethana Mudenur**, Doli Hazarika, Amit Kumar, and Vimal Katiyar, Ring-opening Polymerization of L-lactide using Metal-free Bacterial Prodigiosin, *ACS Organic Letters* (Under Review)
3. **Chethana Mudenur**, Riddhi Mahansaria, Amit Kumar, and Vimal Katiyar, production of polyhydroxybutyrate using sorghum juice: batch and fed-batch approach (Under Preparation)
4. **Chethana Mudenur**, Narendren Soundarajan, Pankaj Boruah, Amit Kumar, and Vimal Katiyar, 3Dprinted PLA-based hepatic vascular phantom for *invitro* drug delivery applications (Under Preparation)

Publications (Co-author)

2. Das, Munmi; Zandraa, Oyunchimeg; **Mudenur, Chethana**; Saha, Nabanita; Saha, Petr; Mandal, Bishnupada; Katiyar, Vimal., Composite Scaffolds Based on Bacterial Cellulose for Wound Dressing Application, *ACS Applied biomaterials*, 2022 July 19, 5 (8), 3722-3733.
3. Mondal K, Bhattacharjee SK, **Mudenur C**, Ghosh T, Goud VV, Katiyar V. Development of antioxidant-rich edible active films and coatings incorporated with de-oiled ethanolic green algae extract: a candidate for prolonging the shelf life of fresh produce. *RSC Adv.* 2022 Apr 28;12(21):13295–313.
4. Kalita, N.K., Bhasney, S. M., **Mudenur, C**., Kalamdhad, A., and Katiyar, V. End-of-life evaluation and biodegradation of poly(lactic acid) (PLA)/poly(caprolactone) (PCL)/microcrystalline cellulose (MCC) polyblends under composting conditions, *Chemosphere*, 2020, 125875.
5. Naba Kumar Kalita, Mukesh Kumar Nagar, **Chethana Mudenur**, Ajay Kalamdhad, Vimal Katiyar., Biodegradation of modified poly(lactic acid) based biocomposite films under thermophilic composting conditions, *Polym. Test.*, vol. 76, pp. 522–536, Jul. 2019.

Book Chapters

1. **Chethana Mudenur,** Prodyut Dhar and Vimal Katiyar, 2020, Nanocellulose: surface modification strategies, cellulose nanocrystals: an emerging nanocellulose for numerous chemical processes, Walter de Gruyter GmbH. pp 81-118.
2. **Chethana Mudenur,** Tabli Ghosh and Vimal Katiyar, 2021, Nanodelivery system of bioactive compounds in edible food packaging, Springer Singapore. pp 273-298.

3. **Chethana Mudenur,** Kona Mondal, Urvashi Singh, and Vimal Katiyar, 2019, Production of polyhydroxybutyrate and its potential applications, Advances in sustainable polymers., Springer, pp 131-164.
4. Prodyut Dhar, **Chethana Mudenur** and Vimal Katiyar, 2018, Cellulose nanocrystals: food packaging, encyclopedia of polymer applications., Taylor & Francis.

Presentations at International/National Conferences

1. **Chethana Mudenur,** Amit Kumar and Vimal Katiyar, "Prevention of biofilm associated infections using prodigiosin-loaded poly(lactic acid)" North-East research conclave, May 20-22, 2022, IIT Guwahati, Assam.
2. 'Budding Entrepreneur Program', a flagship program of Eximus 2020, the entrepreneurship summit of IIM Bangalore, 17-18 October 2020.
3. Conference on Polymer Processing and Emerging Technologies, Polymer Processing Academy in Association with IIT Alumni Centre Bangalore., November 2020.
4. **Chethana Mudenur,** Amit Kumar and Vimal Katiyar., "Isolation and characterization of biological pigment prodigiosin from *Serratia nematodiphila CoE-SusPol1* and its novel application as colorant for polymers" in an International Symposium on sustainable polymers & launch of SPSI-Northeast chapter, August 23-25, 2019, IIT Guwahati, Assam.
5. Pankaj Boruah, Chethana Mudenur, Akhilesh Kumar Pal, Vimal Katiyar., "Modified biopolymer as an environmentally friendly dispersant for treatment of oil spills" in International Symposium on Advances in Sustainable Polymers, ASP-17, January 8-11th 2018, IITG, India.

भारतीय प्रौद्योगिकी संस्थान गुवाहाटी
Indian Institute of Technology Guwahati